# EXPERIMENTAL AND SIMULATION STUDIES TO EVALUATE THE IMPROVEMENT OF OIL RECOVERY BY DIFFERENT MODES OF CO2 INJECTION IN CARBONATE RESERVOIRS

A Dissertation

by

AHMED ABDULAZIZ S. ALEIDAN

Submitted to the Office of Graduate Studies of
Texas A&M University
in partial fulfillment of the requirements for the degree of

DOCTOR OF PHILOSOPHY

December 2010

Major Subject: Petroleum Engineering

Experimental and Simulation Studies to Evaluate the Improvement of Oil Recovery by Different Modes of $CO_2$ Injection in Carbonate Reservoirs

# EXPERIMENTAL AND SIMULATION STUDIES TO EVALUATE THE IMPROVEMENT OF OIL RECOVERY BY DIFFERENT MODES OF CO2 INJECTION IN CARBONATE RESERVOIRS

A Dissertation

by

AHMED ABDULAZIZ S. ALEIDAN

Submitted to the Office of Graduate Studies of
Texas A&M University
in partial fulfillment of the requirements for the degree of

DOCTOR OF PHILOSOPHY

Approved by:

| | |
|---|---|
| Chair of Committee, | Daulat D. Mamora |
| Committee Members, | David S. Schechter |
| | Jerome J. Schubert |
| | Luc T. Ikelle |
| Head of Department, | Stephen A. Holditch |

December 2010

Major Subject: Petroleum Engineering

# ABSTRACT

Experimental and Simulation Studies to Evaluate the Improvement of Oil Recovery by Different Modes of $CO_2$ Injection in Carbonate Reservoirs. (December 2010)

Ahmed Abdulaziz S. Aleidan, B.S., Louisiana State University;

M.Eng., University of Adelaide, Australia

Chair of Advisory Committee: Dr. Daulat D. Mamora

Experimental and numerical simulation studies were conducted to investigate the improvement of light oil recovery in carbonate cores during $CO_2$ injection. The main steps in the study are as follows. First, the minimum miscibility pressure of 31ºAPI west Texas oil and $CO_2$ was measured using the slimtube (miscibility) apparatus. Second, miscible $CO_2$ coreflood experiments were carried out on different modes of injection such as CGI, WF, WAG, and SWAG. Each injection mode was conducted on unfractured and fractured cores. Fractured cores included two types of fracture systems creating two shape models on the core. Also, runs were made with different salinity levels for the injected water, 0 ppm, 60,000 ppm, and 200,000 ppm. Finally, based on the experimental results, a 2-D numerical simulation model was constructed and validated. The simulation model was then extended to conduct sensitivity studies on different parameters such as permeability variations in the core, WAG ratio and slug size, and SWAG ratio.

The results of this study indicate that injecting water with $CO_2$ either simultaneously or in alternating cycles increases the oil recovery by at least 10% and reduces the $CO_2$ requirements by 50%. The salinity of the injected water has shown a detrimental effect on oil recovery only during WAG and SWAG injections. Lowering injected water salinity, which increases the $CO_2$ solubility in water, increases oil recovery by up to 18%. Unfractured cores resulted in higher recovery than all fractured ones. CGI in fractured cores resulted in very poor recovery but WAG and SWAG injections improved the oil recovery by at least 25% over CGI. This is because of the better conformance provided by the injected water, which decreased $CO_2$ cycling through the fracture.

$CO_2$ injection in layered permeability arrangements showed significant decrease in oil recovery (up to 40%) compared to the homogenous case. For all injection modes during the layered permeability arrangements, the best oil recovery was obtained when the flow barrier is in the middle of the core. When the permeability was arranged in sequence, each injection mode showed different preference to the permeability arrangements. The WAG ratio study in the homogenous case showed that a 1:2 ratio had the highest oil recovery, but the optimum ratio was 1:1 based on the amount of injected $CO_2$. In contrast, layered permeability arrangements showed different WAG ratio preference depending on the location of the flow barrier.

# DEDICATION

*I wish to dedicate this dissertation to:*

*My mother, to whom I owe everything in my life;*

*My father, for believing in me.*

*Special dedication is due to:*

*My wife, Fatimah Alobaid, for the love and support she has given me throughout my studies at Texas A&M.*

*Finally,*

*To my lovely daughters, Nourah and Renad,*

*And my soon expected son, Abdulaziz.*

## ACKNOWLEDGEMENTS

I am heartily thankful to my committee chair, Dr. Mamora, for his encouragement, guidance and support from the initial to the final level, which gave me the confidence and interest to complete this work.

I would like to extend special thanks to Dr. Schechter whose office door has always been open for my questions. I really appreciate his invaluable advice and consultation.

I also would like to thank my committee members Dr. Schubert and Dr. Ikelle for serving on my committee and for their support and interest in my research.

Thanks also go to my friends and colleagues and the department faculty and staff for making my time at Texas A&M University a great experience. Special thanks to John Maldonado, facilities coordinator, for his support with my experimental work.

Thanks to my siblings for their encouragement and motivation. Finally, I want to extend my gratitude to Saudi Aramco for sponsoring my PhD studies at Texas A&M University.

# TABLE OF CONTENTS

# LIST OF FIGURES

FIGURE Page

FIGURE Page

FIGURE Page

FIGURE Page

FIGURE Page

FIGURE Page

FIGURE Page

FIGURE Page

FIGURE Page

FIGURE Page

# LIST OF TABLES

# CHAPTER I

# INTRODUCTION

Oil production from mature fields decreases with time and a significant amount of oil is left behind. Also, large economical hydrocarbon discoveries have become increasingly rare. Therefore, the need to increase the reserves by improving recovery techniques has become essential. Water alternating gas (WAG) and simultaneous water and gas injection (SWAG) have been proposed and applied with varying results. However, extensive studies to examine the latter have not been carried out, especially in fractured carbonate reservoirs. Carbon dioxide ($CO_2$) has been successfully used for enhanced oil recovery (EOR) methods for many years. The availability of $CO_2$ and the industry's knowledge to employ it have made it a very attractive option. Nowadays, the increase in environmental awareness and the desire to sequester $CO_2$ have added an extra advantage to use it as an injection scheme. $CO_2$ has been known as a successful injectant because of its ability to swell oil and reduce its viscosity as well as its high solubility in oil and water that can have a positive impact on ultimate oil recovery.

The majority of $CO_2$ EOR projects focus on supercritical $CO_2$ especially at high pressures because it enables miscibility with the reservoir oil and achieves higher recoveries. Supercritical $CO_2$ has the advantage of higher densities that are close to liquid densities while having a very low viscosity that is similar to gas viscosities.

---

This dissertation follows the style of *SPE Reservoir Evaluation & Engineering*.

Therefore, supercritical $CO_2$ has a very good displacement for the oil it contacts, but the overall volumetric sweep is considered poor because it tends to segregate or cycles very quickly (Kulkarni and Rao 2005). To overcome this problem, other injection techniques have been proposed and developed over the years.

## 1.1 Background

Primarily, there are five basic methods to inject $CO_2$ into the reservoir (Jarrell et al. 2002).

*Continuous injection:* this method is suitable for gravity-drainage reservoirs. It is usually applied to reservoirs where waterflooding is not applicable, and therefore $CO_2$ injection takes place immediately after primary depletion.

*Continuous $CO_2$ chased with water:* this method is suitable for homogenous reservoirs. It is similar to continuous injection except that waterflood follows the continuous injection of $CO_2$.

*Conventional alternating $CO_2$ and water chased with water:* this method is commonly known as water alternating gas (WAG), where gas is injected in alternating cycles with water. The ratio of fluid injections is kept constant and is known as the WAG ratio. This method is meant for reducing gas segregation and is usually applied in highly stratified heterogeneous reservoirs.

*Tapered alternating $CO_2$ and water:* this method differs from the conventional WAG in that the WAG ratio is changing with increasing water volumes. Sometimes,

chase water is injected after the total $CO_2$ volume has been injected. Operators inject $CO_2$ followed by increasing water volumes to reduce the $CO_2$ utilization factor and hence improve the field's economics.

*Alternating $CO_2$ and water chased with gas:* in this method, $CO_2$ is injected in a manner very similar to the conventional WAG except that it is chased with a cheaper gas after the total $CO_2$ volume has been injected. Water injection sometimes follows the injection of chase gas or alternates with it. Again, the main objective behind this method is to reduce $CO_2$ utilization factor and improve the project economics.

The *hybrid WAG* is another variation of the previous five basic methods that has been reported in the literature (Christensen et al. 2001). This method suggests injecting a large slug of $CO_2$ followed by alternating cycles of water and gas.

All these methods, which are considered basic, suggest that $CO_2$ is injected either alone or alternating with water in different combinations. In contrast, simultaneous water and gas (SWAG) injection (Barnawi 2008; Christensen et al. 2001) suggests that both $CO_2$ and water are injected together. This method has been developed to improve both volumetric sweep efficiency and the project economics. SWAG injection is broken into two major injection methods, conventional SWAG and selective simultaneous water and gas (SSWAG). In conventional SWAG, water and gas are mixed at the surface and injected into the reservoir as one phase. On the other hand, SSWAG uses dual completion to inject water and gas separately into one formation.

Most of these methods have been implemented in the field with varying results (Christensen et al. 2001). Failed projects have been attributed to different causes such as

injectivity decline, fast gas segregation, and early breakthrough. Field challenges, therefore, indicate that further studies should be carried out to evaluate certain parameters such as rock type, reservoir heterogeneity, fluid characteristics, and injection modes in certain reservoirs.

Previous research on conventional WAG injection (Kulkarni and Rao 2005; Nezhad et al. 2006) has shown that WAG in the secondary recovery stage is more effective than waterflooding and continuous gas injection. Also, it is more effective and feasible than its application in the tertiary recovery stage.

Additionally, SWAG injection has been studied briefly on sandstone rocks at a laboratory scale. For example, Sohrabi et al. (2005) concluded that a significant oil recovery by SWAG can be achieved where almost all oil contacted by gas is recovered because of the oil and gas cross flow. This project showed that water/gas ratio has negligible effect on recovery as long as sufficient gas is available to recover bypassed oil.

The effects of $CO_2$ on the reservoir rock and the interaction between $CO_2$ and reservoir fluids have also been experimentally studied (Aguilera and de Ramos 2004; Zekri et al. 2007). The studies showed that the alteration of the rock petrophysical properties is imminent. However, the effects on oil composition, wettability, and interfacial tension (IFT) are favorable.

Injectivity abnormality is the most frequent problem caused by any mode of $CO_2$ injection that encouraged researchers (Christensen et al. 2001; Svec and Grigg 2001) to investigate the possible causes. They have attributed these abnormalities to mineral

dissolution and deposition. Svec, R.K. and Grigg, R.B. (2001) reported that high velocity gas near wellbore creates dissolution or precipitation, whereas further in the reservoir, long-term reactions may occur because multiphase flow takes place.

Reservoir heterogeneity is a detrimental factor on oil recovery, especially during $CO_2$ injection. It can greatly change the field reservoir management if found to be adversely affecting the production. Heterogeneity can take different forms, either different layers with different permeabilities or the presence of vugs and fractures. The presence of fractures has been investigated in the laboratory by creating an artificial fracture in the core plug (Fjelde et al. 2008; Shedid 2009). Researchers concluded that unfractured cores result in higher recovery than fractured ones during $CO_2$ injection. For layered reservoirs, Shedid, S. A. (2009) showed that the highest recovery was obtained from medium-high-low permeability sequence (from top to bottom).

This study aims to investigate the improvement of light oil recovery during simultaneous water and gas (SWAG) injection in homogenous and heterogeneous carbonate reservoirs. Then, it compares the results to the other basic injection methods: continuous gas injection (CGI), water alternating gas (WAG), and waterflooding (WF). The optimal injection method will be selected as the one that yields higher oil production with an optimum $CO_2$ efficiency.

## 1.2 Research Objectives

This research project will study four injection modes: continuous gas (CGI), waterflooding (WF), water alternating gas (WAG), and simultaneous water and gas (SWAG). These injection modes will be conducted in two different sets of carbonate cores, fractured and unfractured. The study aims to examine the influence of these different modes of injection on incremental light oil recovery. The experiments will utilize a coreflood with an auto data logging system and a DBR model Jefri slimtube miscibility apparatus.

Main objectives of my research project are as follows:

1. Evaluate the improvement of displacement efficiency, recovery of light oil, and $CO_2$ efficiency in carbonate reservoirs during four different $CO_2$ injection modes.
2. Compare simultaneous water and $CO_2$ injection (SWAG) to continuous gas injection, waterflooding (WF), and water alternating gas (WAG) for both fractured and unfractured carbonate cores.
3. Evaluate the effect on oil recovery by altering the injected water salinity.

Comparison parameters would be as follows.

- Oil, water, and $CO_2$ cumulative recovery.
- Differential pressure (DP) across the core.
- Oil and water production rates.

# CHAPTER II

# LITERATURE REVIEW

## 2.1 Experimental Studies

The first SWAG studies were carried out by (Caudle and Dyes 1958). They found that one way to improve the miscible displacement sweep efficiency is to lower the mobility behind the flooding front by injecting water with the miscible gas. This will result in reduced relative permeability to gas and hence the total mobility is lowered. The laboratory studies have shown that the increase in the sweep efficiency for a five-spot pattern can reach 90% with SWAG whereas, if continuous gas injection is implemented, only 60% of oil is recovered. Using Darcy's law, they presented a new method to calculate the optimum water/gas ratio from gas-oil relative permeability curves. They found that when gas and water flow at the same velocity, flow is proportional to the mobility of fluids. Therefore, the linear velocity of a fluid is proportional to its mobility divided by the porosity.

Blackwell et al. (1960) presented a laboratory study on a sand packed model to investigate the applicability of simultaneous water and solvent injections in different oil reservoirs. A number of experiments were run to investigate the effect of oil viscosity and water-solvent mixtures ratios on the displacement efficiency. In addition, the effect of gravity segregation and permeability variations were studied. Furthermore, the effective mobility of the mixture in homogenous and steeply deepening reservoirs was calculated using the simultaneous flow of water and solvent. The study showed that the

flow of the mixture in sandstone segregates into solvent at the top and water at the bottom rather than flowing as one phase. However, higher recoveries were obtained with injection of water-solvent mixtures as compared to injection of water or solvent alone.

Holm and Josendal (1974) experimentally discussed the mechanisms of oil recovery by $CO_2$ flooding and how they vary from displacements by other fluids. The study included the well-known $CO_2$ displacement mechanisms such as: solution gas drive, immiscible $CO_2$ drive, $CO_2$ miscible drive, hydrocarbon vaporization, and multiple contact dynamic miscible drive which is emphasized in this study. All displacement methods were carried out using a slimtube and Brea sandstone cores. Using solution gas drive, 14% of the oil was recovered when the pressure was lowered 500 psi and an additional 4.5% was recovered when the pressure was further reduced by 700 psi. The immiscible $CO_2$-hydrocarbon displacement was studied using both secondary and tertiary modes. The $CO_2$ secondary recovery resulted in around 10 % residual oil saturation whereas the tertiary recovery resulted in about 20 % residual oil saturation which showed that the secondary recovery mode is more favorable for this displacement. The dynamic miscible drive (multiple contacts) resulted in a 93% oil recovery with great extraction of the middle range ($C_7$-$C_{30}$) hydrocarbon components. **Fig. 2.1** shows the mechanisms suggested by Holm and Josendal of the $CO_2$ miscible and near miscible displacements at various pressures using synthetic oil.

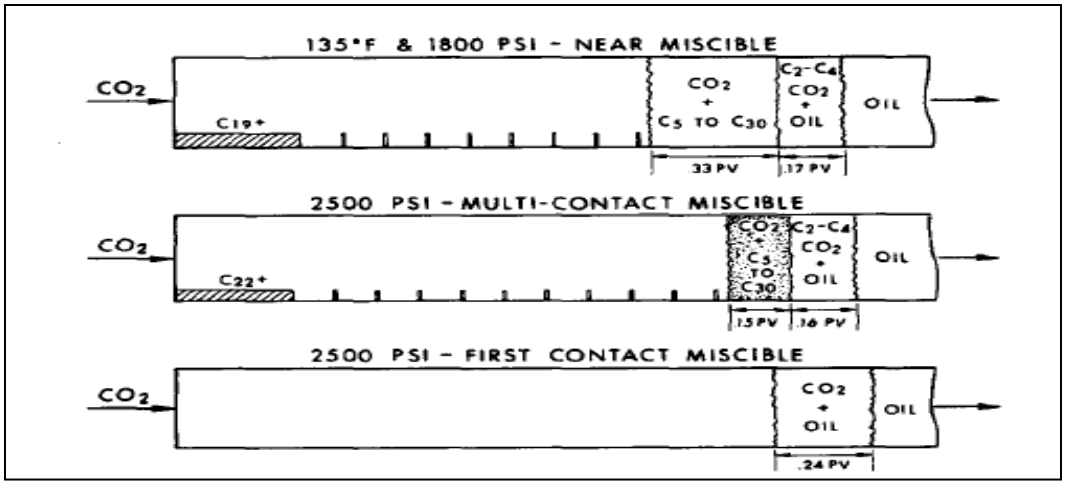


Fig. 2.1— Schematic of $CO_2$ displacement at miscible and near miscible conditions (Holm and Josendal 1974)

**Fig. 2.1** shows that when $CO_2$ was injected at 1800 psi, it saturated the oil in the front part and light ends were vaporized. When more $CO_2$ was injected, it formed a transition zone between the oil and the gas by extracting the middle range ($C_5$-$C_{30}$) hydrocarbon components which lowered the residual oil saturation. On the other hand, at higher pressure of 2500 psi, no transition zone was present. Instead, the oil and $CO_2$ formed a one phase mixture, no extractions occurred, and $CO_2$ was completely miscible with oil (lower part of the figure). The authors also studied the effects of temperature, oil composition, hydrocarbon gas, and high water saturations on dynamic miscible floods. They found that the temperature had a great effect on the pressure at which hydrocarbon extraction took place. Moreover, the hydrocarbon composition was found to have a significant effect on the minimum miscibility pressure (MMP) requirements. The study also highlighted the difference and the similarity between $CO_2$ floods and dry gas. They

were similar in that they occur in multiple contacts but different in that $CO_2$ caused hydrocarbon extraction. The presence of hydrocarbon such as methane in the oil composition or in the injected $CO_2$ had a detrimental effect on both the recovery efficiency and mobility ratio. Watered-out sands were also investigated for the applicability of $CO_2$ floods. It was found that watered-out sands that were water wet had no negative effect on $CO_2$ floods. On the other hand, oil wet sands had lower recovery at breakthrough as well as lower ultimate oil recovery.

A comprehensive study to determine the mechanisms of Levelland oil displacement by continuous $CO_2$ injection was conducted by Yellig (1982). It was intended to evaluate the implication of pilot $CO_2$ injection in the Levelland reservoir. He used a slimtube apparatus to determine the MMP for the Levelland oil while two coreflood systems, using 8 ft and 16 ft long cores, were used to study the flow tests based on previous phase equilibria studies. The study focused on the effects of pressure, core length, and $CO_2$ rate on the displacement efficiency. It concluded that $CO_2$ displaces Levelland oil by multi-contact miscible process and the process is very pressure dependent where miscible floods results in higher ultimate recovery. Also, $CO_2$ injection rate has no effect on ultimate recovery whereas the length is detrimental in developing miscibility especially in linear coreflood systems. He suggested that the displacement length is directly related to the phase equilibria of $CO_2$ and oil.

Potter (1987) conducted an experimental study to test possible wettability alteration after $CO_2$ flooding in west Texas dolomitic formations after injectivity abnormalities were noticed. The wettability changes were inferred by calculating

water/oil relative permeabilites. Fresh state dolomite cores were collected from San Andres and Grayburg fields and relative permeability calculations were carried out before and after $CO_2$ flooding. X-Ray fluoroscope was used to scan the cores and select the most homogeneous ones. Then the cores were mounted in a coreflood apparatus to conduct miscible $CO_2$ injection displacements. Fluid saturations were calculated using X-ray absorption after doping the oil phase where intensities are recorded at each position along the axis of the core. Then, semi-log interpolation using Lambert's law was used to calculate the saturation. The study concluded that a slight change in wettability towards water-wet state was evident. The change in wettability was attributed to rocks' dissolution after contacting $CO_2$. However, this change was not remarkable as reported in other studies. Also, deposition after oil and $CO_2$ flooding was not noticeable.

Wu and Batycky (1990) demonstrated a comprehensive evaluation of minimum miscibility pressure (MMP) measurements from slimtube tests. This study promotes analyzing more data during a slimtube test to confirm miscibility such as produced gas composition, sight glass visual inspection, and pressure drop. Also, accurately tuned equation of state (EOS) is suggested to be used to reduce slim tube experimental runs.

In this study, five examples were analyzed to demonstrate the importance of the suggested measurements to identify MMP using slimtube. The study demonstrated that the standard method of relying on oil recovery alone during slimtube tests is not sufficient to determine MMP. Rather, produced gas composition, visual inspection of sight glass during the test, and pressure drop along with oil recovery are all necessary data to accurately determine MMP. The study also showed that the use of accurately

tuned EOS can reduce the number of slim tube tests. Finally, the tests proved that the physics behind the miscibility phenomenon is a combination of condensing and vaporizing mechanism.

Shyeh-Yung (1991) presented a laboratory study investigating the effect of pressure, initial water saturation, and volume of $CO_2$ injected during miscible and near miscible $CO_2$ floods. The study uses a slimtube, coreflood, and a 16-ft slimtube in combination with a coreflood. The slimtube was placed ahead of the core holder to ensure miscibility by pre-equilibrating the crude oil and $CO_2$. It was concluded that when corefloods are used instead of the slimtube, near miscible injection is feasible. Therefore, it was recommended to use corefloods instead of the slimtube to obtain more representative results. It was also indicated that 18-in long cores are enough to create miscibility during tertiary floods. Finally, secondary floods recover more oil than tertiary floods because of the less water shielding effect.

Van Lingen et al. (1996) presented an experimental study of reducing small scale oil capillary entrapment by water alternating gas injection (WAG) and simultaneous water and gas injection (SWAG). The experimental results were then demonstrated by a one dimensional numerical simulation using Brooks Corey type capillary curves and Stone II three phase relative permeability. To represent the wettability state in this model, glass beads were selected to be the water wet rock whereas resin coated sand was selected to represent oil wet rocks. The whole model was constructed by the glass plates glued together to create a void and fitted at the ends with aluminum plates to create constant pressure boundaries. A number of experiments were conducted to study the

effect of wettability and different types of heterogeneities (perpendicular, parallel, and arbitrary). The results of this study showed that SWAG resulted in twice the recovery of waterflood. In addition, SWAG displacement efficiency depends greatly on the reservoir's wettability and the capillary entrapment.

Bagci and Tuzunoglu (1998) conducted a laboratory study to investigate the feasibility of injecting $CO_2$ to recover heavy oil. The experiments used a three dimensional model, 18° API oil, and crushed limestone with 38% porosity and 8 Darcy permeability. Three well configurations were investigated: vertical producer and vertical injector (VP-VI), horizontal producer and vertical injector (HP-VI), and horizontal producer and injector (HP-HI). Four injection modes were implemented on these configurations: waterflooding, continuous gas injection, simultaneous water and gas injection (SWAG), and water alternating gas injection (WAG). A total of twenty runs were conducted to study the effect of different injection scenarios and different well configurations on oil recovery. Moreover, different gas rates as well as different water/gas ratios were studied to observe their effect on oil recovery. In summary, different well configurations ranked the injection scenarios differently. However, waterflooding using VI-VP resulted in the overall highest oil recovery of 37.2% OOIP while WAG was second best with the same configuration yielding 34.5% OOIP.

Siregar et al. (1999) tested three injection modes in their research: $CO_2$ dissolved in water, $CO_2$ slug followed by water, and finally $CO_2$, surfactant flood and water injection. For the first two injection modes, artificial cores were used while the third mode used loose sand in the form of a sandpack. The cores outperformed the sandpack

because the latter showed inconsistent results. The study was intended to investigate the oil recovery sensitivity to the reservoir dipping angle, $CO_2$ concentration in water, $CO_2$ slug size, and surfactant concentration. The study concluded that an increase in oil recovery can be achieved by adding $CO_2$ because of the positive interaction between the oil, the sand and $CO_2$. Moreover, there is an optimum value of the amounts of $CO_2$ and surfactants after which no extra oil can be obtained and the dip angle plays a major role in oil recovery because of gravity.

Svec and Grigg (2001) focused on the injectivity abnormalities in the field during water alternating gas injections (WAG). They attributed these abnormalities to mineral dissolution and deposition. The claim is that these phenomena occur shortly during $CO_2$ injection (either CGI or WAG) as compared to geological time (millions of years) for normal circumstances. Both increase and decrease in injectivity have been reported in the field, sometimes in the same reservoir but at different wells. In this work, a coreflood apparatus was used with two different kinds of carbonate cores; Indiana limestone and Seminole San Andres dolomite. Backscatter electron imaging was used to look into microscopic images of the cores. Pre-flood and post-flood images were compared to find evidence of mineral changes. The conclusions were inconclusive to injectivity changes. However, dissolution occurred in both types of carbonate rocks but due to different fluids while only limestone experienced significant carbonate deposition.

Aguilera and de Ramos (2004) studied the effect of $CO_2$ diffusion on wettability in different hydrocarbon and water systems. They used three fluid systems with different hydrocarbons, two experimental set ups, and two procedures to visualize different $CO_2$-

fluid interactions. In the experiments, square and cylindrical pyrex capillary tubes are used where the square tubes are to provide wetting corners. The hydrocarbons are represented by n-decane, 2,2,4-trimethylpentane, and decyl alcohol. The water phase is distilled water whereas gas is $CO_2$. The first procedure involves placing hydrocarbon first then water is introduced to visualize $CO_2$ diffusion in water. The second procedure places water first and then oil is introduced to note any changes in water/oil IFT in square tubes. The study concluded that both a decrease in contact angle and displacement of water/oil interphase were observed which confirms the $CO_2$ diffusion. Also, it was observed that $CO_2$ diffuses first through water and then transfers to oil. Water/oil interphase behavior depends on contact angle and surface tension while the displacement changes and the increase in contact angle is greater when IFT decreases.

Egermann et al. (2005) presented an experimental study to investigate different situations where $CO_2$ comes in contact with the reservoir rock and fluids. Different physical and chemical processes may occur when $CO_2$ is injected downhole with various results. For example, near wellbore, where it is subjected to high velocity gas injection, dissolution or precipitation may occur. On the other hand, further in the reservoir long term reactions may occur when multiphase flow takes place. This study used limestone outcrop cores where supercritical $CO_2$ along with brine are injected at reservoir pressure and temperature. The core properties are measured using nuclear magnetic resonance (NMR) and computer tomography (CT) scanner to avoid damage on the cores. Also, chemical analyses of both injected and produced brine are carried out in addition to visual inspection of the cores after the experiments. It was concluded that the fluid-rock

interaction is greatly affected by injection flow rate and brine composition that initially exist in the core. For example, the density of the dissolution increases with higher flow rates. Also, the permeability decreases when the core's brine contains $SO_4^{2-}$.

Kulkarni and Rao (2005) presented an experimental investigation of two different modes of gas injection to improve the sweep efficiency and consequently the amount of contacted hydrocarbon. The main objective of this study is to evaluate the effect of brine composition and miscibility state on ultimate recovery. The two modes considered are continuous gas injection (CGI) and water alternating gas (WAG) on which the sensitivity of two brine compositions and to different pressures (miscible and immiscible) were studied. The study found the 'optimum' mode to inject gas to be 0.7 pore volume of CGI followed by 1:1 WAG injection. They found that WAG injection mode is more successful than CGI based on the tertiary recovery factor. Miscible flood recovered more residual oil than immiscible floods. Also, unlike CGI, WAG floods show great dependence on brine composition since the recoveries due to WAG injection significantly decreased when multi-component brine was used instead of 5% NaCl. They attributed the decrease in recovery to $CO_2$ solubility in multi-component brine.

Sohrabi et al. (2005) conducted flow experiments of a pore-scale simultaneous water and gas injection (SWAG) to recover residual oil. The conditions of the experiments include: very low gas-oil interfacial tension (IFT), negligible gravitational effect, temperature of 100° F and a very high pressure of 5100 psi. The experiments were carried out in a high pressure glass micro-model where water and gas were simultaneously injected at constant rate. Two different water/gas ratios where

considered, 1:1 and 5:1. The oil was initially waterflooded and hence the SWAG injection was meant to recover the residual oil in a tertiary recovery mode. The experimental study concluded that a significant oil recovery by SWAG can be achieved where almost all oil contacted by gas is recovered. This high recovery of residual oil is because a cross flow between oil and gas took place. This experimental study also showed that water/gas ratio has negligible effect on recovery as long as there is sufficient gas to recover bypassed oil.

Yang et al. (2005) showed a new technique to measure the interfacial tension (IFT) and visualize the interactions between $CO_2$ and reservoir brine under reservoir conditions. It investigates both dynamic and equilibrium IFT's, swelling and shrinkage effects, and wettability alterations. It uses axisymmetric drop shape analysis (ADSA) system using pendant drop to measure the IFT while the solubility of $CO_2$ in brine is measured using a PVT system. The ADSA has the ability to measure IFT's at a large range of pressures and temperatures on which the tests were conducted at different pressures and two temperatures. This study concluded that dynamic IFT decreases until it reaches the equilibrium IFT (constant value) and the rate of reduction is dependent on temperature. The equilibrium IFT is inversely proportional to the pressure. It also noted that both swelling and shrinkage occur during the $CO_2$-water interactions interpreted as a two way mass transfer. The swelling is due to $CO_2$ diffusion in water which decreases as the temperature increases and increases with the increase in pressure. The shrinkage takes place when water permeates $CO_2$ as temperature increases. Finally, the change in wettability is because at high pressures, hydrates form at the $CO_2$ and brine interface.

Chakravarthy et al. (2006) performed experiments to measure oil saturations along a fractured core using X-Ray CT scans after $CO_2$ injection. The base case was homogeneous Brea sandstone where two injection rates were considered: high injection rate of $CO_2$ at 1.0 $cm^3$/min and low injection rate of 0.03 $cm^3$/min. It was found that lower rates resulted in a better displacement as it allowed $CO_2$ to diffuse evenly in the core. However, the ultimate recovery for this case was significantly delayed. Following this experiment, another continuous $CO_2$ injection experiment was conducted using a fractured core with the two different rates to study the bypassed oil mechanisms. At a low $CO_2$ injection rate of 0.03 $cm^3$/min, a very small quantity of oil was recovered after 1.5 PV had been injected with instantaneous breakthrough from the fracture. In order to mitigate early $CO_2$ breakthrough, WAG process was tested on the fractured core where brine was injected at 0.1 cc/min. it was found that brine had high mobility especially in the presence of the fracture when the breakthrough took place at about 0.12 PV of injection. Therefore, Xanthan polymer was added to the brine to increase its viscosity and hence delay the breakthrough. Xanthan resulted in water leak-off leaving the fracture open for $CO_2$ to cycle. The $CO_2$ injection following viscofied water resulted in a 4.5% incremental recovery (80% total recovery); however, most of the recovery was attributed to the viscofied water which significantly delayed $CO_2$ breakthrough to 0.44 PV. Finally, in order to further delay $CO_2$ breakthrough, Guar Gum cross linked gel was added to the brine to improve recovery by hindering $CO_2$ breakthrough. The gel resulted in a 95% total oil recovery after almost 2.5 PV of injection with an excellent displacement compared to previous cases.

Nezhad et al. (2006) presented a laboratory study on the feasibility of water-alternating $CO_2$ ($WACO_2$) in secondary and tertiary recovery after waterflood. The study also included a comparison with continuous gas injection. For this experimental study, five injection techniques were conducted: waterflooding in the secondary recovery stage, immiscible water alternating $CO_2$ ($WACO_2$) injection in the tertiary recovery stage, continuous immiscible $CO_2$ injection in the secondary recovery stage, immiscible water alternating $CO_2$ injection in the tertiary recovery stage after continuous gas injection, and immiscible water alternating $CO_2$ injection in the secondary recovery stage. All experiments were conducted at a constant temperature of 190° F and constant pressure of 1500 psig which is below the minimum miscibility pressure (MMP). A sand packed model (37 % porosity and 501 mD permeability) was used in the experiments with dead oil from the southern Iranian reservoir. It was concluded that $WACO_2$ in the secondary recovery stage is more effective than waterflood and continuous gas injection. It is also more effective and more feasible than its application in the tertiary recovery stage since it reduces the amount of required injection fluids.

Zekri et al. (2007) investigated some of the effects of supercritical $CO_2$ flooding on tight limestone. The study analyzed the following: produced oil composition, permeability and porosity changes, relative permeability, water/oil interfacial tension, and the effect of higher water saturation on oil recovery during $CO_2$ floods. It was concluded that the presence of water saturation lowers oil recovery during $CO_2$ flooding and carbonate rocks' porosity and permeability change when contacted by $CO_2$. Also,

$CO_2$ flooding alters the rock wettability to the favorable water-wet condition and water/oil interfacial tension is reduced after $CO_2$ flooding.

Fjelde et al. (2008) experimentally studied the effect of $CO_2$-foaming agent on oil recovery and the transport of $CO_2$ in fractured carbonate oil reservoirs. The experiments were conducted at reservoir conditions using stainless steel cells. The fractures were artificially created and flooded by $CO_2$, $CO_2$- foaming agent plus $CO_2$ gas, and injection of $CO_2$-foaming agent aqueous solution outside the core. The experiments used outcrop chalk cores, synthetic seawater and formation brine, and North Sea reservoir stock tank oil. The main purpose of this experimental work was to measure the $CO_2$ bulk diffusion coefficients and to determine the effect of foaming agents on $CO_2$ diffusion at reservoir conditions. Therefore, bulk $CO_2$ diffusion coefficients were measured both in synthetic seawater and $CO_2$-foaming agents using the pressure decay method. It was concluded that the bulk $CO_2$–foaming agent had no major effect on $CO_2$ diffusion since the diffusion coefficients in seawater and foaming agents were in the same range. Also, the incremental oil recovery due to the addition of foaming agent was only 3.3% higher than injecting $CO_2$ alone.

Shedid (2009) presented an experimental study to investigate the effect of different reservoir heterogeneities on oil recovery during miscible $CO_2$ injection. The heterogeneities were represented by a single fracture with different inclination angles, layered reservoir with different permeabilites, and composite cores. This study aims to determine the performance of $CO_2$ flooding in a Middle Eastern carbonate reservoir that has different heterogeneity and is currently produced by a gas cap and peripheral water injection. The study used actual reservoir rocks in a typical core flood apparatus. The cores were cut individually at different angles to represent a single fracture. For composite and layered reservoir conditions, the cores with different permeabilities were aligned in different sequences. The brine and oil are taken from the Middle Eastern field. The study concluded that unfractured cores resulted in higher recovery than fractured ones during $CO_2$ injection. For layered reservoirs, the highest recovery was obtained from medium-high-low permeability sequence (from top) whereas low-medium-high permeability sequence resulted in the highest recovery in the composite reservoir. The latter permeability sequence showed highest recovery because of the gradual increase in pressure gradient. Finally, among fractured cores, a fracture of 30° inclination showed the highest oil recovery.

## 2.2 Numerical Simulation

Warner (1977) presented a simulation study to investigate the viability of a miscible $CO_2$ flood in hypothetical reservoirs similar to those watered out mid-continent sandstone reservoirs. The objectives of his study was to determine the tertiary oil recovery due to $CO_2$ flood, the best process to inject $CO_2$ in the field, and the sensitivity of $CO_2$ miscible flood to reservoir parameters. Warner is believed to be the first to look into the selective simultaneous water and gas injection (SSWAG). He considered four injection techniques for his study, namely, continuous $CO_2$ injection, slug of $CO_2$, water alternating $CO_2$, and simultaneous water and $CO_2$ injection. For his study, a two dimensional compositional model (25 X 1 X 5) was used to represent a quarter of 5-spot pattern. The three parameters to compare the four tertiary recovery processes are: highest oil recovery, shortest time, and lowest $CO_2$ usage. As for the highest oil recovery, the simultaneous water and $CO_2$ injection was the best recovering 50% of the potential tertiary oil, water alternating $CO_2$ was second recovering 38% and the other two processes were equally poor recovering only 20-25% each. Simultaneous injection also resulted in higher production rate which indicated shorter production time. Moreover, nearly 50% of $CO_2$ injected was produced during the simultaneous injection while 80% was produced during the continuous injection. In all cases, segregation was complete before half of the reservoir rock had been swept by the two phases. The study showed that oil recovery is a function of gravity segregation, i.e., the faster the segregation the lower the oil recovery. Furthermore, the study showed that $k_v/k_h$ had the strongest effect

on gravity segregation. It suggested that the lower the $k_v/k_h$ value, the slower the segregation and hence the higher the oil recovery. Other parameters studied were water/$CO_2$ ratio and well spacing. Three different water/$CO_2$ ratios were investigated in the simulation study (1:1, 1:2 and 1:3). The results showed that water/$CO_2$ ratio during the simultaneous injection affected the oil recovery and recovery speed. Among all ratios, 1:2 resulted in the highest oil recovery and faster recovery. Finally, it was found that well spacing had a more pronounced effect on simultaneous injection than the other processes. The results showed that reducing well spacing increased tertiary oil recovery.

Slack and Ehrlich (1981) presented a numerical simulation study of a simultaneous water and nitrogen injection to displace oil in watered out reservoirs. The study focused on the effects of water-nitrogen ratio, $k_v/k_h$ variation, and changing permeability profile. A number of simultaneous water and nitrogen experiments were conducted to determine the oil saturation changes. The experimental data was then used to test Stone's model of three phase permeability for this simulation study on a five-spot pattern. Water-nitrogen ratios ranging from 0 to 6, different $k_v$ values, and three different permeability profiles were investigated in the study. It was found that residual oil recoveries of 5% to 7% pore volume were obtained at a ratio of 2 and higher with an optimum value around 2. The incremental recovery was obtained with cumulative injection of 4.5 to 8.0 MSCF/STB nitrogen over 3.5 to 6 years. Reduced vertical permeability resulted in higher recovery in a shorter time at lower cumulative injected nitrogen and produced oil. Permeability variation showed different results based on the location of higher permeability. When higher permeability was placed at the bottom,

higher recoveries with lower nitrogen-oil ratios were achieved. On the contrary, lower recoveries and higher nitrogen-oil ratios were obtained when the higher permeability was at the top. Slightly lower recoveries were observed when higher permeability was in the middle of the pay zone. Finally, the study proved that a considerable amount of waterflood residual oil can be recovered with reasonable nitrogen ratio by this technique despite gravity segregation.

Surguchev et al. (1996) presented a comparison study of different IOR methods on a Norwegian field which is characterized by extreme heterogeneity. Waterflooding, gas injection as well as the traditional EOR methods such as polymer and surfactant flooding were not fully effective in this field. Therefore, a three dimensional reservoir simulator (STARS) was used to compare the applicability of three advanced IOR methods: Water alternating gas injection (WAG), foam assisted WAG or surfactant alternated gas injection (FAWAG or SAG) and separate-simultaneous water/gas injection (SWG). Also, the study included different combinations of horizontal and vertical wells, with and without fracturing of injection and production wells. According to this study, the most effective injection strategies were found to be water alternating gas (WAG) and simultaneous injection of water in the upper injectors and gas at the lower injectors (SWG). It was shown that the increase in oil recovery due to WAG process can be as high as 28% of OOIP if there is no permeability barrier. However, if permeability barrier was introduced, SWG is more effective with almost 34% of OOIP can be recovered. Also, the highest recovery was obtained with vertical injectors at the

top of the reservoir and horizontal injectors at the bottom with a combination of IOR methods.

Akin (2001) presented a new approach to measure the oil/water fractures relative permeability curves when the matrix relative permeability is known. The method uses unsteady state corefloods where Brea sandstone cores are artificially fractured. It is then numerically tested by CMG, Computer Modeling Group, black oil simulator, IMEX. The simulator uses the matrix relative permeability data derived from the core floods whereas the relative permeability curves for the fractures are adopted from Romm (1966) linear data. The study investigated five cases: (1) zero capillary pressure in the matrix and fracture, (2) equal capillary pressure in both matrix and fracture, (3) greater capillary pressure in the matrix than in the fracture, (4) fracture capillary pressure greater than the matrix, and (5) zero fracture capillary pressure and finite capillary pressure in the matrix. He concluded that fracture relative permeability curves are power law functions rather than linear as commonly assumed. Also, the sum of fracture relative permeabilities is less than one at intermediate saturations. Finally, the power law exponent (n) decreases when the matrix capillary pressure is accounted for overburden pressure.

Gharbi (2003) conducted a screening study to find the best EOR strategy for a mature field using a three-dimensional, finite-difference simulator. The study included three possible strategies: water alternating gas (WAG), simultaneous water and gas injection (SWAG), and injecting water at the top and gas at the bottom. The field was discovered in 1972 and was produced by expansion drive with a weak aquifer followed

by water injection which started in the early 1980's. The reservoir is a typical Middle Eastern carbonate classified as a structural trap (360 ft thick, 22 % porosity, 115 mD permeability, 29° API oil). The preliminary small scale simulation results using expert system were in favor of miscible $CO_2$ injection. However, the inherited characteristics of injecting $CO_2$ alone such as unfavorable gas-water mobility ratio, poor sweep efficiency, and early breakthrough prevented this application and necessitated studying the alternatives. Therefore, an economic optimization was conducted to find the best EOR design which included different simulation runs. It was concluded that the best EOR strategy for this field was injecting water at the top and gas at the bottom using horizontal injectors and vertical producer. The water injector would be placed 50 ft from the top of the reservoir while the gas injector would be 50 ft from the bottom. This strategy resulted in the highest sweep efficiency and oil recovery at a shorter project life than the other methods.

Stone (2004) introduced a unique completion technique to simultaneously inject water and gas that will result in prolonged reservoirs' lives. The new technique suggests that, in two different sites, the water is injected at the top of the reservoir at high rate while gas is injected simultaneously at the bottom in the same vertical plane. High water injection rates help to increase the vertical sweep up to 3-4 times and allow the two phase mixture to propagate further in the formation. Also, the benefits of this technique are maximized when combined with horizontal wells. It was shown that water and gas injection rates are independent of the reservoir thickness and the only limiting factor is the frac pressure. This is because injection pressure is proportional to the length of the

interval and for horizontal wells, it is the length of the pattern rather than the reservoir thickness. Therefore, the use of horizontal wells for simultaneous water and gas injection is more favorable since it provides higher injection rates and hence higher recovery. Moreover, fields developed with vertical wells, simultaneous water and gas injection will still yield higher recovery than WAG without the need of additional drilling. Throughout the study, Stone used a quasi-steady state reservoir simulator to verify the applicability of this technique.

Algharaib, M.K. et al. (2007a) continued the reservoir management study on the same field used by Gharbi (2003) using the same well configuration, injection strategy and reservoir simulator. They extended the simulation to carry out a sensitivity study on the simultaneous water and gas injection (SWAG). The sensitivity parameters included effective water to oil mobility ratio, viscosity ratio between gas and oil, water and gas injection locations, and injection rates. For gas to oil viscosity ratio, it was found that the higher the ratio, the higher the oil recovery. This was because heterogeneity and viscous forces dominated the flow regime and resulted in lower recovery in the case of lower gas to oil viscosity ratios. Also, the increase in water to oil mobility ratio resulted in lower recovery since most of the oil was bypassed. The study showed that the water injector location is very critical and there existed an optimized location that yielded the highest oil recovery. On the hand, the highest oil recovery was achieved when the gas injector was placed at the lower most part of the reservoir in order to take advantage of gravity segregation. As for injection rates, it was found that higher water injection rates blocked gas segregation and hence resulted in higher oil recovery. However, unstable

displacement and early water breakthrough was noticed during higher water injection rates. Higher gas injection rates also resulted in higher oil recoveries.

Nasir and Amiruddin (2008) presented the results of a numerical simulation study with the emphasis on fluid properties. The main objective of this work is to numerically determine the fluid properties that have major impact on oil recovery during miscible $CO_2$ injection. Using an extended black oil simulator, the effect of varying oil and injected gas density, viscosity, and formation volume factor, on the flood performance is assessed. The effect is quantified using an index called normalized root-mean-square deviation and a fractional change index. From the results of the simulation, the model is found to be most sensitive to fluid formation volume factor, followed by their densities and least sensitive to the fluid's viscosities. Thus, it is recommended that these data must be properly selected and analyzed beforehand in order to minimize their uncertainty prior to any simulation works.

## 2.3 Field Applications

Walker and Turner (1968) reported field results regarding the enriched-gas-drive program in Seeligson field. The program was intended to examine the improvement of displacement and sweep efficiencies as well as the effects of changing the injectant fluids for future applications. The program started with an injection of enriched gas residue mixture (50 percent propane and 50 percent residue gas) to which the reservoir responded quickly until the gas breakthrough was noted in approximately seven months. The evaluation of the enriched gas injection revealed poor vertical and volumetric sweep efficiencies. It was observed that gas produced oil mostly from the top stringers and very little from the bottom layer. Therefore, simultaneous water and enriched gas injection (SWAG) was implemented to improve the volumetric sweep efficiency. Simultaneous injection resulted in low injection rates at high pressure and a drop in reservoir pressure which led to switching to injection of alternating cycles (WAG). The alternating cycles of water and gas did not solve the problem either. It was believed that the water cycles caused a large water saturation zone around the well which lowered the permeability to gas. Finally, the whole project, which lasted ten years, was terminated. A less than anticipated recovery of 50 percent was reported but is considered higher than the average waterflood recoveries from similar fields.

Harjadiwinangun (1984) presented a pressure maintenance feasibility study on Ardjuna field, offshore Northwest Java. For this study, four recovery methods were considered: natural depletion, continuous gas injection, waterflooding, and simultaneous

water and gas injection (SWAG). Those methods were compared in terms of recovery efficiency and cost. A three-dimensional, three-phase black oil simulator was used to monitor the field production since 1972. Then, a compositional reservoir simulator was prepared to include the sales of LPG and residue gas in the pressure maintenance study. It was concluded that continuous gas injection is the most efficient and cost effective method since the facilities already exist. The ultimate recovery using this method is estimated to be 51 % OOIP compared to 41 % using natural depletion. SWAG injection resulted in the highest ultimate oil recovery (57 %) but was not economically attractive because of the higher investment required for the facilities.

Attanucci et al. (1993) discussed the optimization process on the miscible $CO_2$ project in Rangely field, Colorado, USA. It was noted that as the field matured, water alternating gas (WAG) has become more favorable than adding new $CO_2$ injection wells. Additionally, WAG half cycle was further optimized and has become the main focus of the field's optimization study. The simulation study and field trial showed that the production and operational costs can be lowered by decreasing the half cycle. It resulted in the application of tapered WAG which implies reducing $CO_2$ slug size followed by increasing water slugs. The field trial concluded that the optimum tapering strategy was from 1:1 to 2:1 WAG at 30% HCPVI, from 2:1 to 3:1 WAG at 40% HCPVI, and converting to chase waterflood at 50% HCPVI. This achieved a significant reduction of $CO_2$ production at the producing wells with a marginal effect on oil production. Furthermore, the field economics were improved since tapering would reduce $CO_2$ purchase and recompression costs.

Stephenson et al. (1993) reported the first miscible $CO_2$ injection in Canada by Vikor resources, Ltd., in Joffre Viking pool. The field was abandoned in 1960's but simulation results as well as laboratory tests showed that the field is a good candidate for $CO_2$ flood in 1980 which allowed the commercial development of the field in 1991. Different injection strategies were tested in the laboratory and in the field. These strategies include continuous $CO_2$ injection (CGI), water alternating $CO_2$ ($WACO_2$), and simultaneous water and $CO_2$ injection ($SWACO_2$). Also, controlling mobility with surfactants to produce foam was tested in the field and the laboratories. $CO_2$/surfactants simultaneous injection was initially conducted on a short duration on one pattern then; it was extended to the whole field. The results of this test showed a less than expected $CO_2$ mobility control but with higher oil recovery of 21% OOIP. However, the increase in oil recovery was attributed to the additional $CO_2$ injection because the foam did not propagate far in the reservoir. Continuous $CO_2$ injection was then implemented in another pattern which consisted of 30% HCPV of injected $CO_2$. A decline in oil production was observed when the pattern was switched to waterflood indicating the need for more $CO_2$ injection. Therefore, simultaneous water and $CO_2$ injection was implemented and an increase in oil production was realized. An estimated 41 % HCPV of $CO_2$ was injected in the same pattern with a recovery of 13 % OOIP. The field tests and simulation results suggested that simultaneous water and $CO_2$ injection is the optimum strategy in the Viking sand. Hence, $SWACO_2$ was implemented in a third pattern after a short period of continuous $CO_2$ injection to improve injectivity. The forecasted oil recovery in the third pattern is 14 % OOIP after 45 % HCPV of $CO_2$

injection. The lower recovery in this pattern compared to the previous one is due to the lower residual oil saturation after previous waterfloods. The overall injection results of the Viking sand suggest that simultaneous water and $CO_2$ injection had a better sweep and mobility control than the other strategies.

Several publications were documented in the literature on Kuparuk field in Alaska which was initially managed by WAG and then converted to SWAG to reduce operational costs, increase oil rate, and improve sweep efficiency. The following paragraphs include a summary of these publications.

Ma and Youngren (1994) reported their field experience on immiscible water-alternating-gas (IWAG) injection at Kuparuk River Unit, North Slope, Alaska. Also, laboratory tests as well as simulation studies were included. The field was mainly managed by IWAG with 17 out of 42 drill sites had been converted to IWAG where a typical Kuparuk's drill site had 8 injectors and 8 producers with 160 acre well-spacing. A number of coreflooding tests were carried out to investigate the effect of trapped gas on oil saturation and relative permeability. The results of all tests were in favor of IWAG. Furthermore, a compositional reservoir simulator was used to test the applicability of both IWAG and miscible WAG. With a 3 year waterflood as a base line case, many reservoir simulation runs were conducted which included different sensitivities to get representative results. The simulation results concluded at least 1-3% incremental oil recovery due to IWAG over waterflooding. IWAG was successfully implemented in the field with varying ratios and slug sizes depending on the field's gas-oil-ratio (GOR) and pattern maturity. The main objectives of IWAG process were to

manage the field's produced GOR and increase oil recovery. However, other benefits of this technique were also observed such as improved injectivity, better understanding of well interactions, in-situ gas lifting, voidage replacement, and lower water production. The field results agreed to a great extent with the reservoir simulation forecasts in terms of oil recovery and breakthroughs. The overall field results were very promising with higher oil recoveries over waterfloods and managed produced GOR due to the presence of trapped gas.

Stoisits et al. (1995) reported on the effect of surface line impact during a simultaneous water and gas (SWAG) injection pilot in Kuparuk field, Alaska, U.SA. The field is a sandstone with two independent formations, A and C. It has been through many development processes such as primary production, waterflooding, gas storage, immiscible water alternating gas (WAG), miscible water alternating gas, infill drilling, and peripheral development. WAG injection required a substantial development cost while the incremental recovery and sweep efficiency were fairly modest. On the other hand, simulation studies showed that SWAG could improve the sweep efficiency and increase the ultimate oil recovery. The main objective of this pilot study was to test the possibility of conducting SWAG with the existing surface lines to lower the capital cost. Different scenarios to simultaneously inject water and gas have been investigated including mixing the water and gas at the drill site, at the well or at the central processing facilities. It was found that the most economically attractive option is to mix the gas upstream of the wellhead. Therefore, experimental studies were carried out followed by a pilot to test the feasibility and applicability of injecting simultaneous

water and gas. The final design consisted of a distribution network and a single surface line that can ship the two phase mixture to the injection well which can provide a steady state injection.

Ma et al. (1995) presented the results of a simultaneous water and gas injection pilot at the Kuparuk River Field, Alaska, U.S.A. After the field had been managed by IWAG, SWAG injection was studied to reduce capital and operational costs by eliminating the separate lines for water and gas and WAG conversion. Also, it was intended to improve sweep efficiency and hence increase oil recovery and manage gas production. Prior to the field pilot, a two-dimensional cross sectional reservoir simulation study was carried out using a compositional simulator to investigate the benefits of SWAG, IWAG, and miscible WAG. Different water/gas ratios sensitivities were also studied with the base case being primary recovery then waterflood followed by SWAG. Simulation results concluded that SWAG with 1:1 ratio resulted in the highest recovery of 5.0% OOIP, manageable produced GOR of 6.0 MSCF/STB, and lower water cuts due to the reduced water mobility. The SWAG pilot project started with three drill sites and modified injection lines, facilities, and instrumentation. The mixture of water and gas is shipped to multiple wells via a single surface line distribution network with inline static mixers. This process was granted a US patent #5,421,408. SWAG pilot project lasted only 17 days and it was terminated when injectivity losses were experienced. The injectivity loss was believed to be due to the lower bottom hole pressure (BHP) rather than relative permeability effects. The SWAG process was

considered a viable option overall based on the simulation results and the pilot even though the pilot did not last long enough to fully evaluate the process.

Robie et al. (1995) presented a field trial of simultaneous water and $CO_2$ injection in Rangely field, Colorado, USA. The water alternating gas and simultaneous water and gas injection projects in this field involved different stages handled by a multidisciplinary team to address both the reservoir management issues as well as the operational challenges. The main objective of this paper was to discuss the necessary mechanical modifications that would prevent carbonic acid backflow and cause corrosion, which occurs when water mixes with $CO_2$. The use of an automated surface control system that monitored and modified the flow rate of water and $CO_2$ mixture was highlighted as the main improvement in the field operational strategy. The trial was considered very successful since no backflow or corrosion was reported during the simultaneous injection field trial.

Quale et al. (2000) reported on the first SWAG injection in North Sea on the Siri field. The field is developed with five producers and two peripheral SWAG injectors (one horizontal and one deviated). The produced gas was mixed with water and injected at the wellhead as a two-phase mixture. The Siri reservoir is compartmentalized by several layers with good porosity and permeability. Therefore, the placement of SWAG injectors was intended to connect to the producers for better pressure support and delayed gas breakthrough. Some of the main challenges faced during SWAG injection were higher wellhead pressure requirement and hydrate formation. However, certain start-up and shut- in procedures were followed to meet those challenges. The preliminary

results of this field application were very motivating. It was reported that SWAG helped in achieving stable produced gas reinjection, full voidage replacement, meeting the local environmental regulations and eliminated the extra equipment requirements.

Christensen et al. (2001) presented an extensive review of water alternating gas (WAG) on 60 field cases. The study included non-hydrocarbon and hydrocarbon injection gases as wells as offshore and onshore fields. Most of the field applications were successful with only few reported unsuccessful cases which were very often attributed to operational problems. The increase in oil recovery due to WAG injection had been reported as about 5%; however, recoveries up to 20% had been reported in many fields such as Dollarhide, Rangely Weber, and Slaughter Estate. Most of the field applications were implemented in a tertiary mode and only newer applications in the North Sea were applied early in the field life. As for miscibility condition, 47 cases were reported as miscible, 10 as immiscible and 2 were not classified. WAG process was applied in all field rock types but the majority was in high permeability reservoirs. An example of low permeability field would be the Daqing field where the reservoir rock was tight chalk whereas Snorre was an example of high permeability sandstone. The distribution of WAG among carbonate and sandstone rocks was twenty-three and thirty-three respectively. Most of the fields were onshore and only six reported fields were offshore with hydrocarbon as the injection gas. The water/gas injection ratio was mostly 1:1 but higher ratios were also reported. Almost 50 % of the reviewed cases used $CO_2$ as the injected gas and have been reported to have higher oil recoveries (10 % vs. 8% for $N_2$). As regards of the injection patterns, it was found that regular patterns, especially

five-spot with close spacing, were the most dominant. The operational problems reported on all fields were fairly similar. These problems include injectivity loss, early breakthrough, corrosion, scale formation, different temperatures of injected phases and asphaltene and hydrate formation. However, some opposite findings were reported such as injectivity increase. For example, an injectivity increase was realized in Brage field and Kelly Snyder (carbonate reservoir) which was attributed to the rock dissolution.

Berge et al. (2002) reported on the behavior of SWAG injectivity in Siri field. A simulation model to study the field's injectivity was carried out using ECLIPSE reservoir simulator. It was found that the injectivity was strongly dependent on bottom hole pressure (BHP) and gas fraction. Also, the injectivity loss was due to the two phase relative permeability near the wellbore and high gas fraction. Therefore, it was concluded that hydraulic fracturing was inevitable because of the injectivity loss. The results of hydraulic fracturing varied between the two injectors; however, both resulted in an injectivity increase.

Quraini et al. (2007) presented a study on the recovery of heavy oil by $SWACO_2$ and $WACO_2$ injections in West Sak reservoir, Alaska, U.S.A. It also included an investigation of $CO_2$ storage in depleted heavy oil reservoirs. The study used ECLIPSE three-dimensional, three-phase black oil simulator that took into account the viscosity reduction and oil swelling caused by liquid $CO_2$ injection. The model was a scaled down one well model of the reservoir with dimensions of 500 ft by 500 ft and 30 ft thickness. The depth of the reservoir was 3500 ft, initial pressure of 1851 psig and reservoir temperature of 75° F. Five scenarios were considered in this study, namely,

waterflooding, continuous immiscible $CO_2$ injection, $WACO_2$, $SWACO_2$, and water and liquid $CO_2$ injections in depleted reservoir. These scenarios were compared to natural depletion in terms of oil recovery and $CO_2$ storage. It was concluded that higher heavy oil recoveries were obtained with $WACO_2$ and $SWACO_2$ injections than by water or $CO_2$ alone. The increase in oil recovery by $WACO_2$ and $SWACO_2$ reached up to 60% of OOIP compared to 30% OOIP by continuous water or gas injections. This was due to the significant improvement in sweep efficiency. Also, $CO_2$ storage in depleted heavy oil reservoirs was found to be an attractive option.

# CHAPTER III

# EXPERIMENTAL APPARATUS AND PROCEDURE

## 3.1 Miscibility (Slimtube) Apparatus

The slimtube apparatus is considered the industry standard and the most accurate method of determining MMP. Shown in **Fig. 3.1** is DB Robinson – Jefri slimtube miscibility apparatus used in this study. The slimtube apparatus has three main parts: the slimtube coil, upstream and downstream sections. The following is a detailed description of each part.

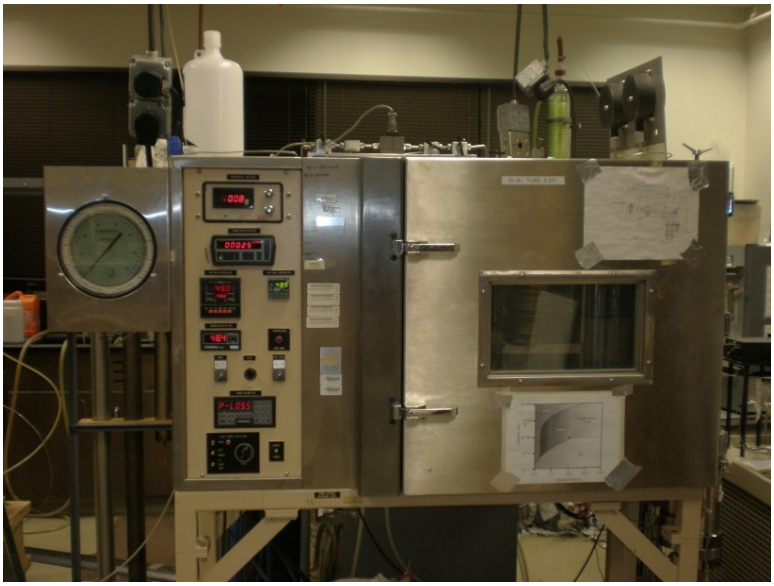

Fig. 3.1— DBR model Jefri slimtube miscibility apparatus

### 3.1.1 Slimtube Coil (Reservoir Medium)

The slimtube coil, reservoir medium shown in **Fig. 3.2**, has a stainless steel coiled tubing that is 40 ft. long and 0.25 inch outer diameter. It is packed with Ottawa sand with 35% porosity and a pre-calibrated pore volume of 82.27 $cm^3$. The coils are placed in an oven to maintain the required reservoir temperature. The slimtube coil has a small internal diameter and a very great length to create an environment where viscous fingering is extremely minimized by transverse dispersion.

Fig. 3.2— Slimtube coil shown inside the temperature bath (oven)

### 3.1.2 Upstream Section

The upstream section consists of four piston accumulators for oil, toluene, water, and solvent ($CO_2$). The solvent accumulator is placed inside the oven to maintain the same temperature as the coils while the other three accumulators are located outside the oven. The accumulators are connected to a Ruska pump that drives the fluids into the coils. Those main parts of the upstream section are shown in **Fig. 3.3**.

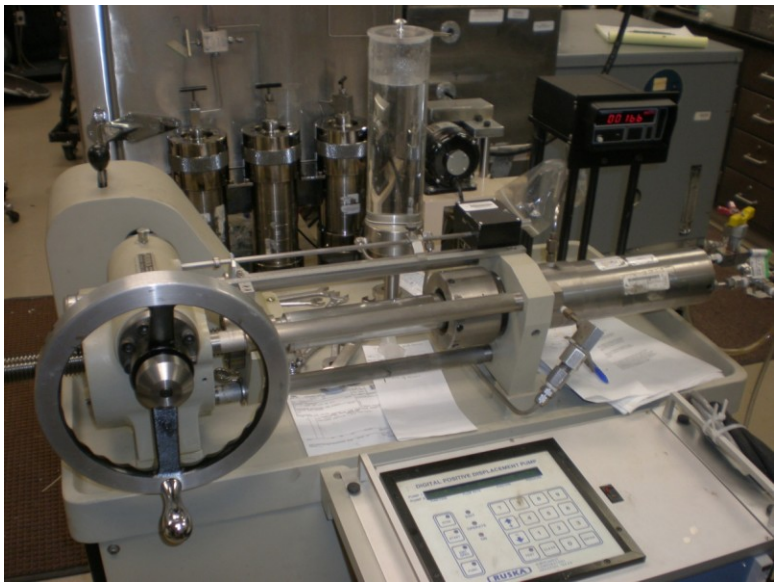

Fig. 3.3— Miscibility apparatus upstream section showing Ruska pump and accumulators

### 3.1.3 Downstream Section

The downstream section consists of a high pressure sight glass located immediately after the coils as shown in **Fig. 3.4**. The main objective of the sight glass is to enable visual inspection of the produced fluids. A back pressure regulator (BPR) is located downstream of the sight glass and is placed in an airbath. The BPR is used to maintain a test pressure inside the coils. Finally, the produced fluids are collected in a glass burette after the BPR at atmospheric pressure.

Fig. 3.4— Sight glass (downstream section)

The upstream and downstream pressures are measured using precision gauges as shown in **Fig. 3.5** while the pressure drop in the coils is measured using a pressure transducer. The temperatures inside the oven and the BPR airbath are set using electronic gauges and a chiller unit is used to maintain the required temperature.


Fig. 3.5— Pressure transducer and electronic gauges

### 3.2 Coreflood Apparatus

The coreflood apparatus is used for all fluid flow experiments which were designed to investigate certain parameters and meet the research objectives. It was assembled in-house to serve as high pressure/high temperature (HP/HT) medium where reservoir condition fluid flow displacements take place. It consists primarily of four main components:

- Injection system
- Coreflood cell
- Production system
- Data logging system

The universal System HD 350 X-ray computed tomography scanner (CT scanner) is used as a separate component to obtain cross-sectional scans of the coreflood cell and provide core characterizations.

### 3.2.1 Injection System

The injection system consists of two positive displacement pumps from ISCO Teledyne Company, shown in **Fig. 3.6**. These pumps supply distilled water to the bottom of floating piston accumulators filled with the desired fluid. Two accumulators are available for each experimental run: oil and $CO_2$. When water is used in an experiment, it is delivered to the core directly from the pump's piston.


Fig. 3.6— Injection pumps

### 3.2.2 Coreflood Cell

Shown in **Fig. 3.7** is the core flood cell. It is a TEMCO aluminum core-holder model RCHR-2. It can withstand a maximum confinement pressure of 2500 psi and temperature of 200 °F. It accommodates a core measuring 2-in in diameter and 6-in in length. The core is placed in a Nitrile sleeve with both ends secured to end plugs and a confinement pressure of 400 psi above the injection pressure. The confinement pressure is supplied by a Teledyne positive displacement pump which delivers HP/HT hydraulic oil to the core's annulus. The coreflood cell is placed inside an oven set to the desired temperature.

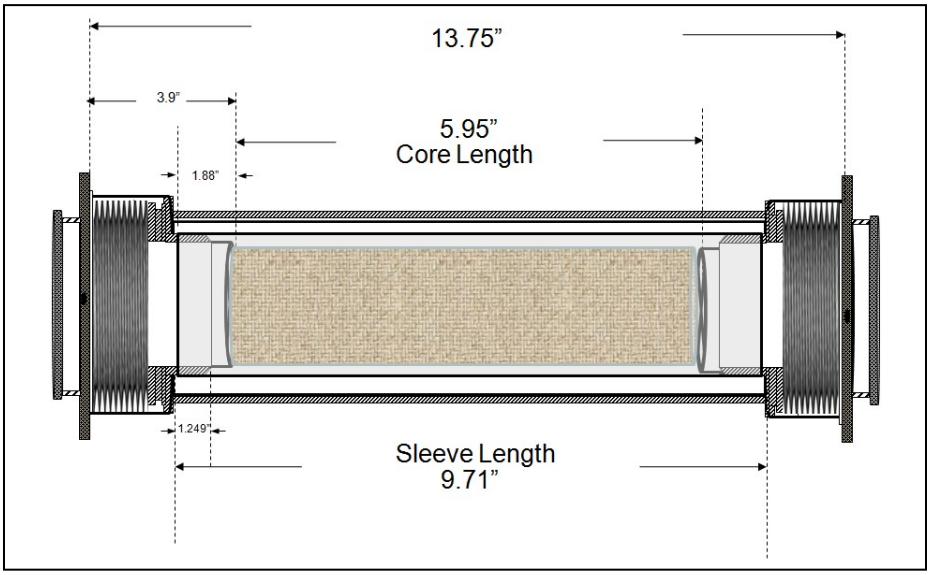


Fig. 3.7— Schematic of TEMCO coreflood cell

### 3.2.3 Production System

Produced fluids go through a dome type back pressure regulator (BPR) where the pressure is set to the desired value by applying nitrogen. Produced fluids are collected in a separator connected to a high pressure sight glass. The gas is vented from the top separator and is measured using a wet test meter that is connected to the data logger to automatically measure the produced gas every 30 seconds, **Fig. 3.8**. The liquid is collected from the bottom of the sight glass into a graduated cylinder.

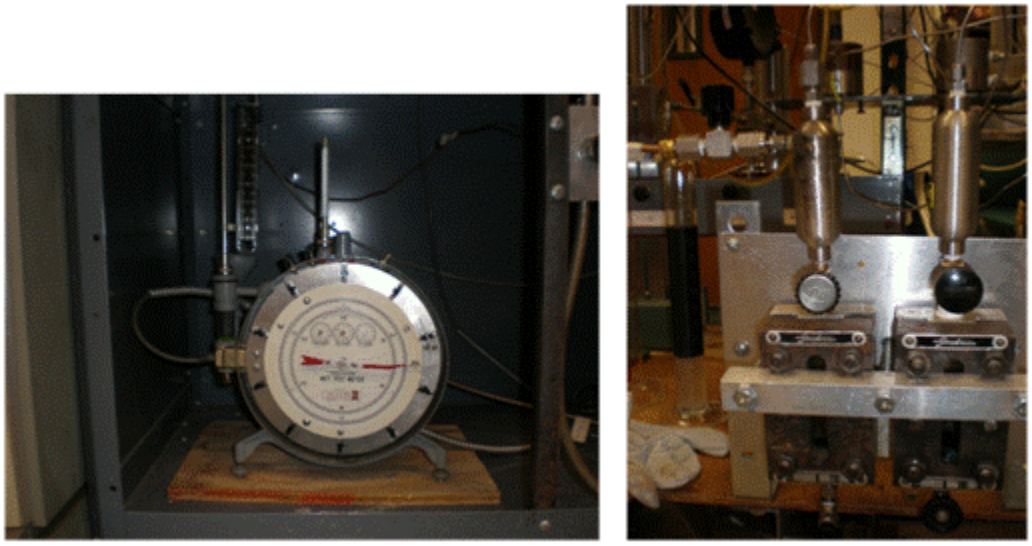

Fig. 3.8— Production section showing wet test meter (left) and separators (right)

### 3.2.4 Data Logging System

Two high pressure transducers and two thermocouples are connected at both ends of the core cell as shown in **Fig. 3.9**. These send a signal to a Hewlett Packard data logger to record the injection and production pressures and temperatures every 30 seconds and are displayed on a personal computer. The produced gas is measured using a wet test meter connected to a Hewlett Packard data logger that measures gas in 30-second intervals and displays it on another personal computer.

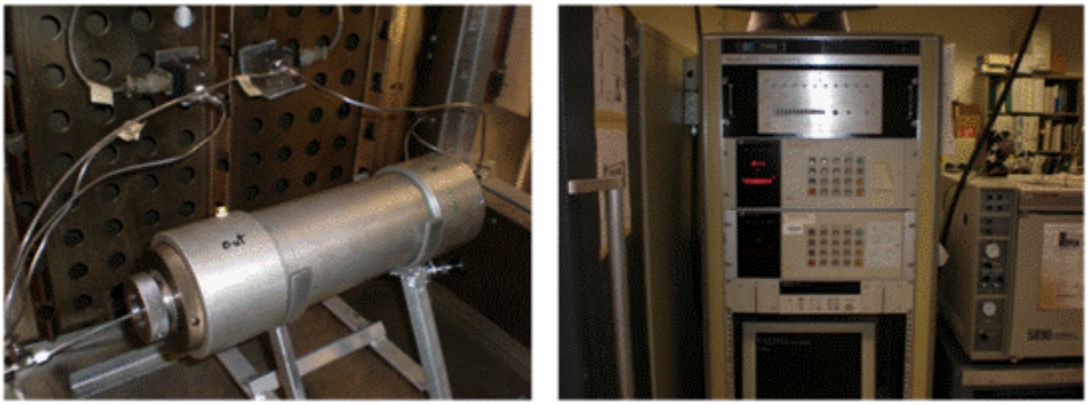

Fig. 3.9— Coreflood cell is shown on the left with pressure transducers at each end. Data logging system and personal computer are shown on the right

### 3.2.5 The Universal System HD 350 X-Ray CT Scanner

Shown in **Fig. 3.10** is the universal System HD 350 X-ray computed tomography scanner (CT scanner). It is used as a separate component to obtain cross-sectional scans of the coreflood cell. It is a nondestructive method to measure the cores' porosity, fluid saturations, and lithology distribution within the cores. It provides descriptive images of the core in cross-sectional slices.

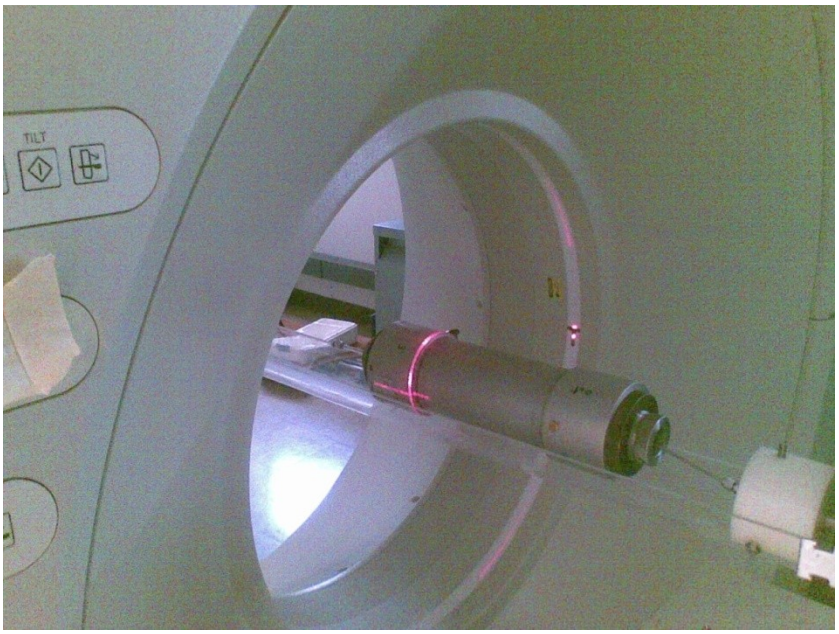


Fig. 3.10— Coreflood cell is shown inside the CT scanner

**Table 3.1** Shows a list of the equipment used in this study for both the slimtube and coreflood systems.

TABLE 3.1— EQUIPMENT USED IN EXPERIMENTS

| Equipment | Description |
|---|---|
| ISCO Pump | Model 500D, capacity 170-200 ml/min (depending on pressure) |
| ISCO Pump | Model 314, capacity 200 ml/hr |
| ISCO Pump | Model LC-5000, capacity 400 ml/hr |
| Ruska Pump | Model 2216-603A, max. pressure 10,000 psi, capacity 30 cc/min |
| Accumulator 1 | Ruska, model 31348, max. pressure 10,000 psi |
| Accumulator 2 | Phoenix, SN TAM-15C-2M-1, max. pressure 2000 psi, capacity 1500 cc |
| Accumulator 3 | Phoenix, SN TAM-15D-2M-2, max. pressure 2000 psi, capacity 1500 cc |
| BPR | Grove Valve and Regulator Co., model S-91-XW, range 100-3000 psi |
| Transducers | Omega, model DP 215-50, max pressure 3200 psi |
| Thermocouple | Omega J-type |
| Coreflood cell | TEMCO, model RCHR-2, SN: 2527, max. pressure 2500 psi, 200 °F |
| Wet test meter | GCA/Precision Scientific |
| Data logger | Hewlett-Packard data acquisition/switch unit, model 3497A |
| X-ray CT scanner | Universal systems, model HD-350 E |

## 3.3 Procedure

This section provides a detailed description of operation mechanism for each apparatus used during the experiments. It is divided into two sections: miscibility (slimtube) apparatus which describes the MMP determination procedure and the coreflood system which explains the fluid flow experiments.

### 3.3.1 Miscibility (Slimtube) Apparatus

The slimtube apparatus requires conducting at least five experiments at different pressures and measuring the cumulative recovery at 1.2 PV injected. To prepare and conduct each experiment, three main tasks are followed: slimtube cleaning, saturating with oil, and solvent injection.

#### 1. Slimtube Cleaning

Before and after each run the slimtube coils are flushed with two to three pore volumes (PV) of toluene. The cleaning is done at the test pressure and temperature. Ruska pump is set at an injection rate of 0.5 $cm^3$/min to push the toluene accumulator piston to drive the fluid into the coils. The BPR is connected to a nitrogen source and maintained at test pressure while the oven temperature is set to 120°F (test temperature). The cleaning continues until clear fluid is produced at the glass burette.

**2. Slimtube Saturation with Oil**

After cleaning the slimtube coils, oil is injected at 3 $cm^3$/hr (0.05 $cm^3$/min) for 48 hours until 2.2 PV are injected. It is important to keep the confinement pressure on the sight glass within 500 psi above the injection pressure. Once the slimtube coils are saturated, there must be 82.27 $cm^3$ of original oil in place (OOIP).

**3. Solvent Injection**

The solvent accumulator is filled with at least 2.5 PV of $CO_2$ prior to the test. Then, the $CO_2$ is pressurized to 50 psi above the test pressure before starting the injection. The experiment involves displacing oil by $CO_2$ at a certain pressure following the manual procedure (DB Robinson Design & Manufacturing Ltd. 2000). During the experiment, accurate recordings of the pressure drop, liquid production, and the phase distribution in the sight glass are essential to analyze the test. The experiment is considered complete when at least 1.2 PV of $CO_2$ has been injected or at least three identical liquid readings have been recorded in one-hour intervals. Steps from 1 to 3 are repeated at different pressures until 90% recovery or more is achieved. Then, pressure vs. 1.2 PV cumulative oil recovery is plotted and the pressure at which there is a change in slope is selected as the MMP value.

### 3.3.2 Coreflood System

The complete coreflood system is shown in **Fig. 3.11.** The reservoir temperature is selected to be 120$^{o}$F and the pressure is 100 psi above the MMP (determined by slimtube). It is equipped with an auto data logging system, Teledyne ISCO pumps, and an aluminum coreholder cell to allow for CT scans. The following are the main steps to conduct one test (one injection mode):

1. Place the core in the aluminum core holder and apply confinement pressure of 300 to 500 psi above the injection pressure.
2. Evacuate the core under temperature overnight. This is established by connecting the core holder outlet to a vacuum pump while the core holder is placed in the oven at the test temperature.
3. Weigh the dry core.
4. Scan the dry core using a fourth generation CT scanner to obtain vertical slices of 2 mm (0.08 in) spacing. The same parameters and the start and end positions of this scan should be followed for all subsequent scans.
5. Saturate the core with reservoir water. The saturation is accomplished by pulling the water into the core using the vacuum pump.

6. Inject 2 to 3 PVs of reservoir water to ensure steady state and hence complete saturation. The amount of water entering the core should be recorded. Use this step to apply Darcy's law and measure the permeability.
7. Weigh the 100% saturated core.
8. Scan the 100% water saturated core.
9. Calculate the core's porosity using CT scanner data. Confirm the results with the material balance calculations by using the weight of dry and saturated core and water density.
10. Saturate the core with west Texas light oil to reduce the water saturation to connate water ($S_{wc}$). This is accomplished by injecting 3 to 4 PVs of oil or until no further water is produced. For the fractured case, create artificial fractures using a saw and place it back in the core holder cell.
11. Flood the core with the injectant fluid at the desired mode.
12. Repeat Steps 1 to 11 for each injection mode to compare the results.

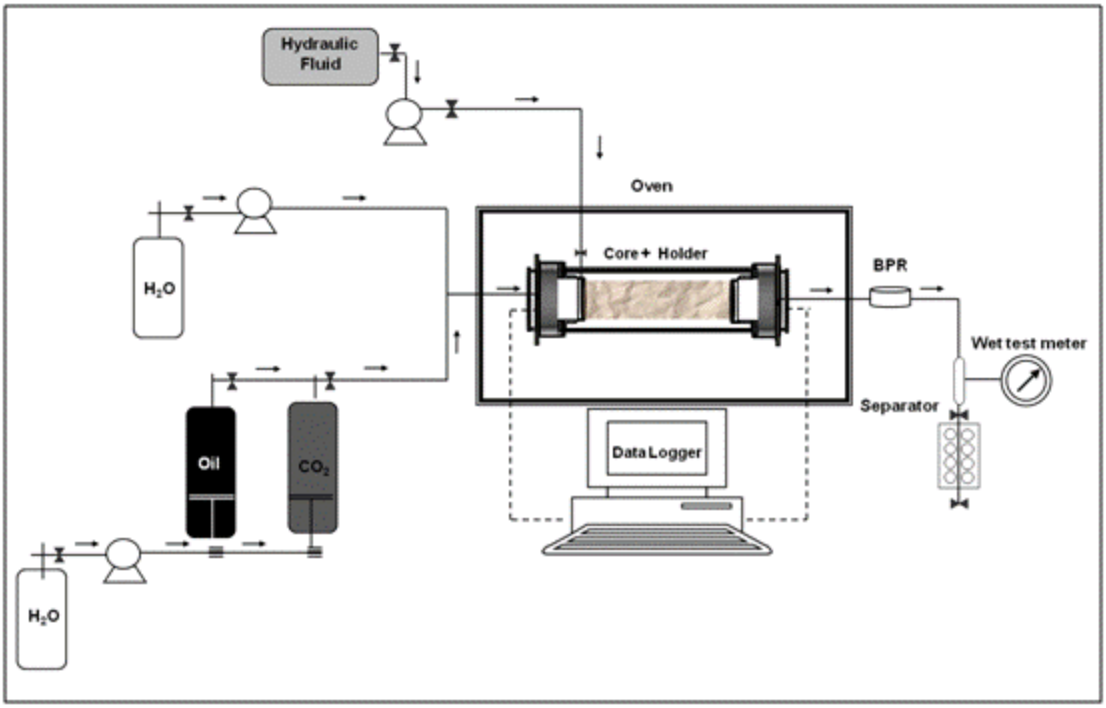


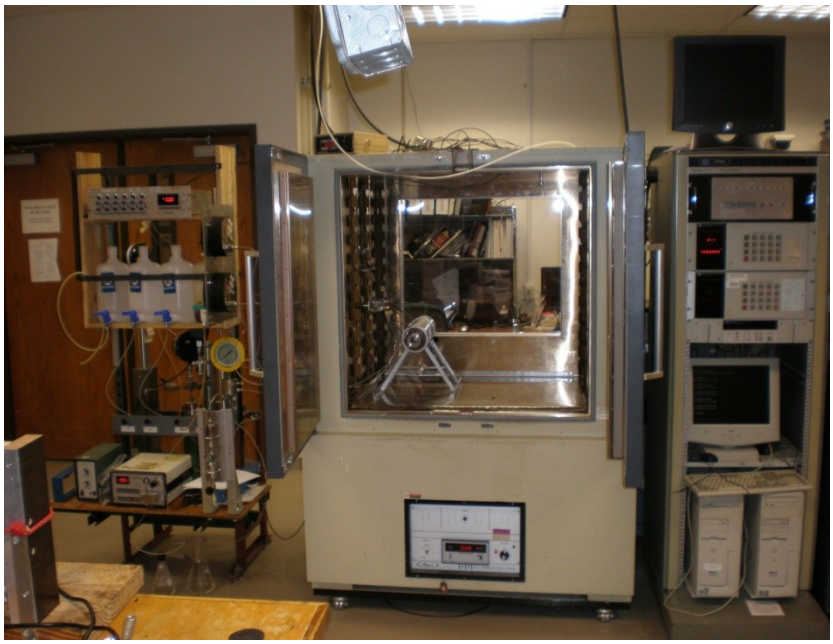

Fig. 3.11— Coreflood schematic (top) and an actual photo (bottom) of the complete coreflood system

### 3.3.3 Rock Properties

The carbonate cores used in this study are outcrop limestone drilled from Edwards Plateau in Texas (Kocurek Industries 2010). They have an intercrystelline and moldic porosity and classified as grainstone (grain-supported) rocks according to Dunham classification (Ahr 2008). **Fig. 3.12** is X-ray diffraction (XRD) results showing the elemental analysis of the core. The core is characterized by typical carbonate elements with calcite as the most abundant element. **Fig. 3.13a** is a scanning electron microscope (SEM) image showing the pore size at 50 um. **Fig. 3.13b** is the elemental analysis of the SEM image available in this area of the core. The figures show no evidence of clay content as the elemental analysis did not reveal any presence of Al or Si, which are the main chemical elements in any form of clay minerals. For example, Smectite and Kaolinite are the most common clay minerals found in reservoir cores. The chemical composition of Kaolinite is $Al_2Si_2O_5(OH)_4$ and it is characterized by layered silicate mineral. The SEM images showed the calcite grains with no evidence of layered clays while the elemental analysis showed no peaks for either Al or Si.

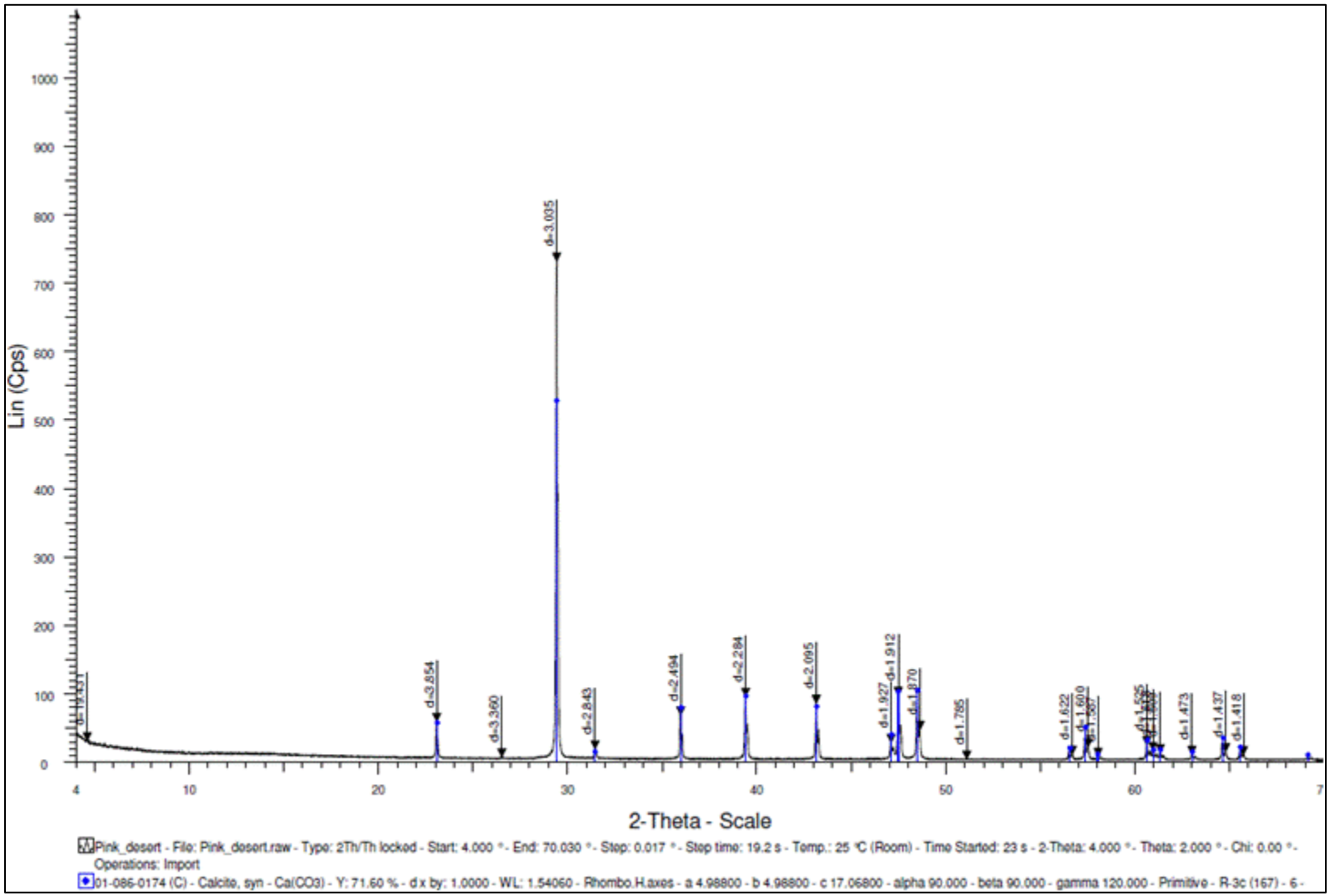


Fig. 3.12— XRD results showing the elemental analysis of the core

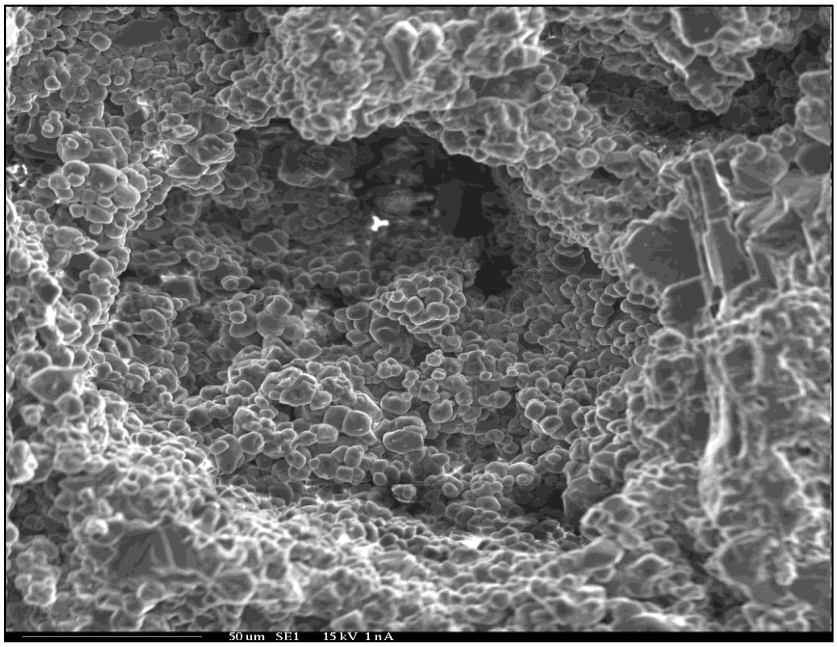


Fig. 3.13a— SEM image of the core showing the pore size at 50 µm

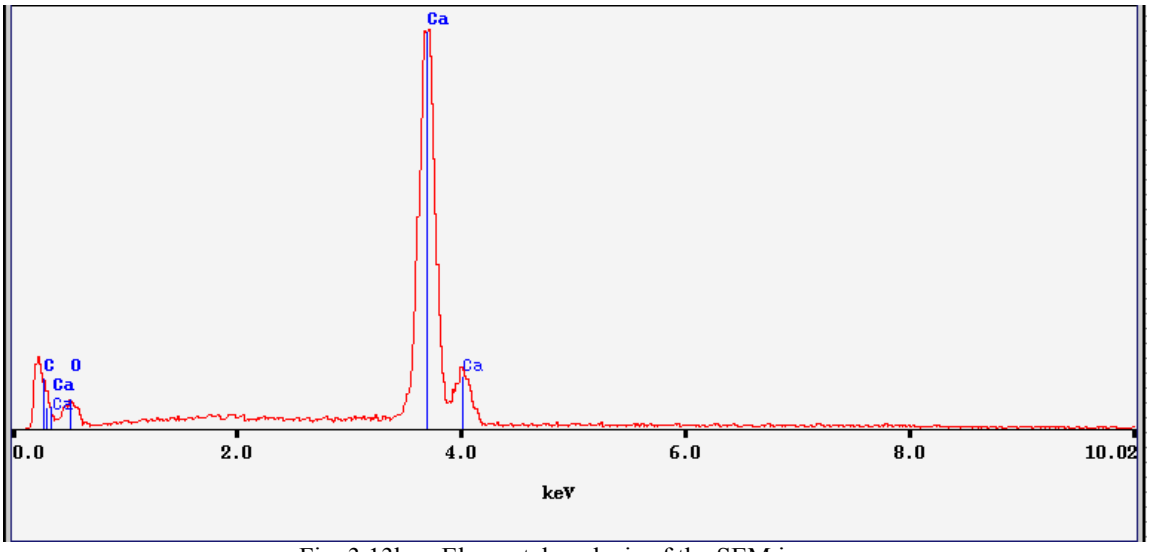


Fig. 3.13b— Elemental analysis of the SEM image

The average permeability of the cores is measured to be 90 md. The permeability was measured by applying Darcy's law when injecting water into a water-saturated core until a steady state flow is achieved. The porosity is measured by two methods: material balance (weight of dry and saturated core) and CT scanner method. **Fig. 3.14** shows CT slices of a dry core while **Fig. 3.15** shows CT slices of water saturated core. When the CT scanner method is used, the porosity of the core is calculated as follows:

$$\phi_{x,y} = \frac{CT_{x,y}^{100\%\ water} - CT_{x,y}^{dry}}{CT_{water} - CT_{air}} \quad \text{.....(3.1)}$$

where:

$CT_{x,y}^{100\%\ water}$ is the CT number for a fully saturated core

$CT_{x,y}^{dry}$ is the CT number for a dry core

$CT_{water}$ is the CT number for water defined as zero in Hounsfield units

$CT_{air}$ is the CT number for air defined as -1000 in Hounsfield units

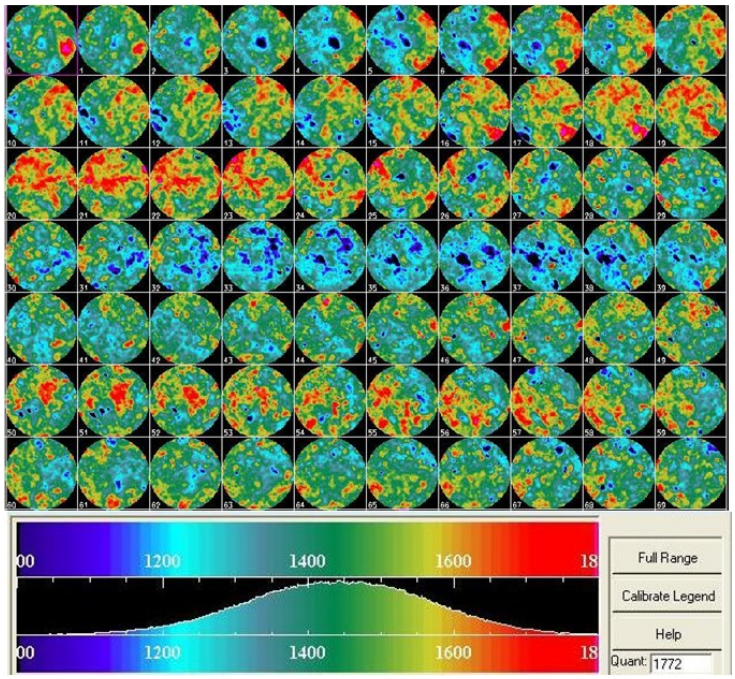


Fig. 3.14— CT images showing slices of dry core

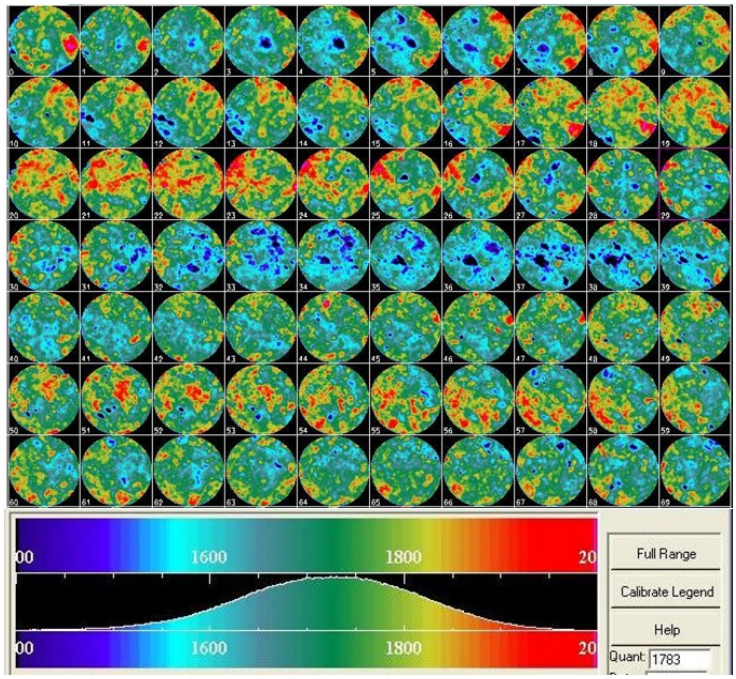


Fig. 3.15— CT images showing slices of fully water saturated core

# CHAPTER IV

# EXPERIMENTAL RESULTS

## 4.1 Minimum Miscibility Pressure (MMP)

The displacement of reservoir oil by injected $CO_2$ can occur by two main mechanisms: immiscible and multi-contact miscible (MCM). During the displacement, a mass transfer between oil and $CO_2$ occurs by vaporization, extraction, or condensation. When hydrocarbons transfer to the $CO_2$ phase, the process is called vaporization or extraction. The distinction is the $CO_2$ phase i.e. when $CO_2$ is gas, vaporization occurs and when $CO_2$ is the liquid-rich phase, it is called extraction. On the other hand, when $CO_2$ transfers to the hydrocarbon phase, the process is considered condensation (Glasø 1985; Yellig 1982). This process is very pressure dependent and many authors have shown that higher ultimate recoveries are obtained when the displacement is miscible. Theoretically, this is because of the absence of the interface between the oil and $CO_2$ which results in a capillary number ($N_c$) close to infinity. The capillary number controls the microscopic displacement efficiency and is defined by:

$$N_c = \frac{V\ \mu}{\sigma \cos\theta} \qquad \text{.....(4.1)}$$

For miscible displacements to occur, $CO_2$ has to be injected at a certain pressure (or higher) called the minimum miscibility pressure (MMP). The MMP is defined as the lowest pressure at which oil and $CO_2$ become one phase and miscible displacement is achieved. Every oil has a different MMP with $CO_2$ because each oil has a distinctive oil composition. Therefore, it is required to measure the MMP specifically for each oil.

For this study, the MMP was determined by three methods: slimtube (miscibility apparatus) experiments, a compositional simulator, and published correlations. For slimtube experiments, oil recovery at 1.2 PV of $CO_2$ injected is plotted versus pressure. The point of 90% (where the slope changed) was chosen to be the MMP. Then, a compositional simulator was fed with previously determined oil composition to match the experimental results (slimtube results). Finally, the published correlations are used to estimate the MMP for preliminary work and the starting pressure on the slimtube method. The following is a detailed description of each method

### 4.1.1 Slimtube (Experimental) Results

Five experimental runs at pressures of 1400, 1600, 1800, 1900, and 2000 psi were conducted. The oil recovery at 1.2 PV for each run is plotted versus pressure in **Fig 4.1**. The point, where the slope changed, occurred at 90% recovery when the test pressure was 1800 psi. Therefore, this pressure is considered the MMP for this west Texas oil and $CO_2$. The two tests conducted above this pressure, at 1900 and 2000 psi, also showed complete miscibility between oil and $CO_2$.

The chromatographic analysis of this west Texas oil showed high weight percent content of $C_5$ through $C_{30}$. The weight percent analysis showed 74 wt. % for $C_5$ through $C_{30}$. According to (Glasø 1985; Holm and Josendal 1982; Jarrell et al. 2002; Stalkup 1992), $CO_2$ forms multiple contact miscibility with oil by extracting $C_5$ through $C_{30}$ contents while the lighter ends ($C_2$ through $C_4$) have minimum effect. Since the majority of this oil's components lie between $C_5$ and $C_{30}$, the displacement process has been characterized as multi-contact miscible process with extraction drive type. These results have been verified by the compositional simulation method described later in this chapter.

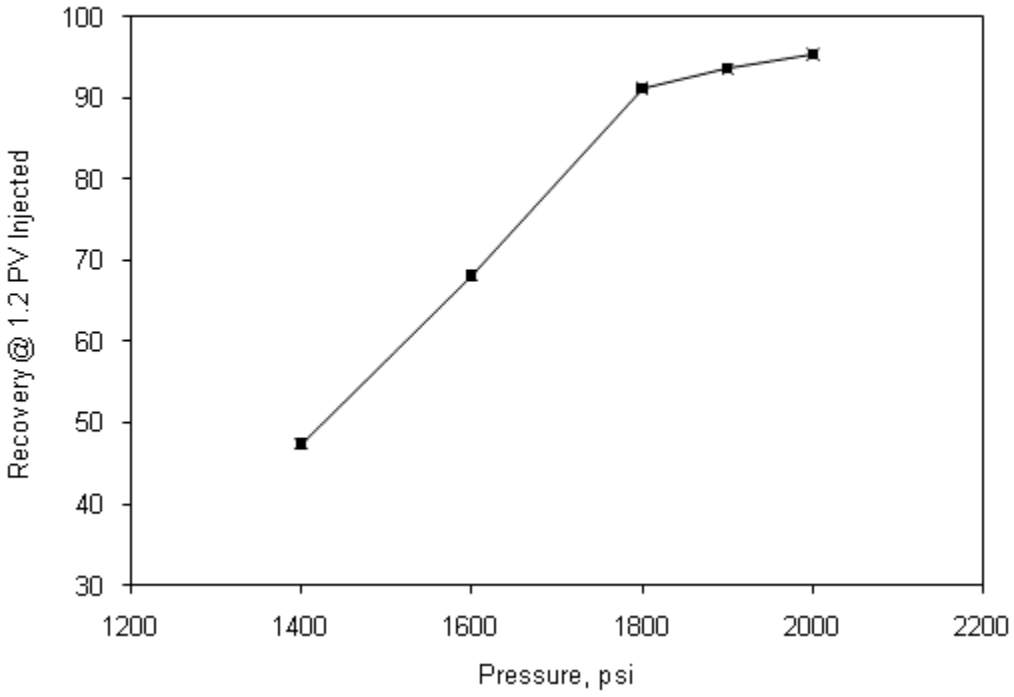


Fig. 4.1— Results of slimtube experiments showing MMP at 1800 psi

### 4.1.2 Compositional Simulation

The chromatographic analysis of west Texas oil provided five components and a $C_{7+}$ fraction for a total of six components as shown in **Table 4.1**. Then an ASTM simulation distillation provided weight percent analysis of 50 components ($C_1$ through $C_{60}$). These components were entered into a compositional simulator, Calsep PVTsim, to calculate the MMP. PVTsim has the options of both simulating slimtube experiments and calculating the MMP. The simulated slimtube experiments provided very well matched results with the actual slimtube experiments as shown in **Fig. 4.2**. It also determined that the MMP for this west Texas oil with $CO_2$ is at 1800 psi. The simulator indicated that this drive type is 100% vaporization with multi-contact miscible pressure at 1836 psi and first contact miscible pressure at 2273 psi.

TABLE 4.1—CHROMATOGRAPHIC ANALYSIS OF WEST TEXAS OIL

| Component | WT | LV | Mol % |
|---|---|---|---|
| iC4 | 0.01 | 0.02 | 0.04 |
| nC4 | 0.04 | 0.06 | 0.16 |
| iC5 | 0.17 | 0.24 | 0.54 |
| nC5 | 0.21 | 0.29 | 0.67 |
| C6 | 0.93 | 1.22 | 2.48 |
| C7+ | 98.64 | 98.18 | 96.11 |
| | 100 | 100.01 | 100 |

| | | |
|---|---|---|
| Mol WT of sample | 229.87 | gm/mol |
| Mol WT C7+ | 241.33 | gm/mol |
| Density of sample | 0.8714 | gm/cc |
| Density of C7+ | 0.8912 | gm/cc |

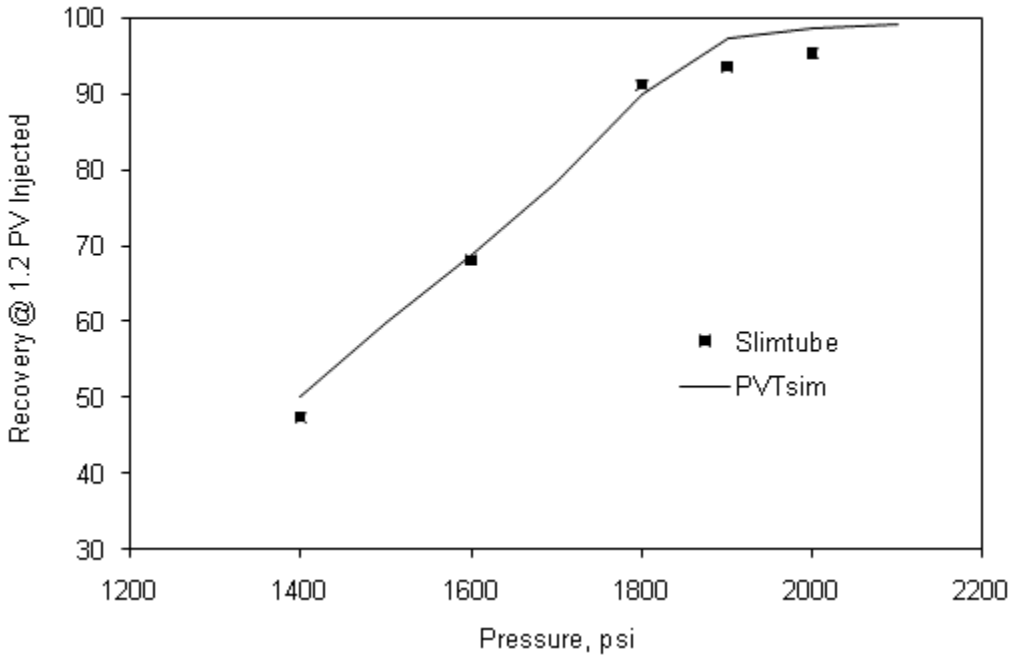


Fig. 4.2— Comparison between numerical simulation and experimental results to determine MMP

### 4.1.3 Published Correlations

This method is usually used for preliminary calculations only because its results are not reliable enough to conduct a project. Published correlations were used in this study to find the starting pressure on the slimtube experiments. A total of nine correlations were used to find a proper estimation of the MMP. Each correlation uses different parameters to estimate the MMP for different oils. The following is a brief description of each correlation method:

Benham et al. (1960) proposed a correlation for rich-gas miscible displacement. Then, Holm and Josendal (1982) found that $CO_2$ displacement is equivalent to 59 mole % methane and 41 mole % propane mixtures. Holm and Josendal correlation uses temperature, $C_{5+}$ molecular weight, $C_5$-$C_{30}$ content, and $CO_2$ density. They also concluded that $C_2$ through $C_4$ content has negligible effect on miscible displacement and methane content will not affect the MMP determination significantly.

Cronquist (1978) proposed a correlation that takes into an account three parameters: reservoir temperature, molecular weight of $C_{5+}$, and mole % of $C_1$. This correlation covers a wide range of API gravities and temperatures.

Yellig and Metcalfe (1980) suggested that MMP depends only on temperature. Oil composition has minor or no significant effect on the MMP between oil and $CO_2$. Therefore, their correlation uses temperature only as the input parameter. They also suggested that the $CO_2$ MMP should always be equal to or greater than the reservoir oil's bubble point pressure.

Johnson and Pollin (1981) correlation covers a wide range of API gravities, pure and diluted $CO_2$. This correlation takes into an account the following parameters: oil gravity, oil average molecular weight, temperature, and injected gas composition.

Alston et al. (1985) developed a correlation that accounts for $CO_2$ impurities. The main parameters of this correlation are: reservoir temperature, molecular weight for $C_{5+}$, volatile and intermediate oil fractions, and $CO_2$ composition.

GlasØ (1985) proposed a generalized MMP correlation for $N_2$, $CO_2$, and LPG. His correlation was based on Benham correlation but predicts any multiple contact miscible displacement. Similar to Holm and Josendal, he concluded that the $CO_2$ solubility in oil is equivalent to the solubility of a mixture containing 58 mole % methane and 42 mole % propane. The input parameters for this correlation are: mole percent of $C_2$-$C_6$ intermediate content, molecular weight of $C_{7+}$ and reservoir temperature.

Orr and Silva (1987) proposed an MMP correlation by calculating the minimum $CO_2$ density to establish miscibility, then back calculating the required pressure to achieve this density. The input parameters are the weight percent of $C_2$-$C_{37}$ and reservoir temperature.

Eakin and Mitch (1988) conducted 120 rising bubble experiments and came up with a generalized MMP correlation for $CO_2$, $N_2$, and LPG. The main input parameters are: molecular weight and pseudo-reduced temperature for $C_{7+}$ and solvent composition.

Yuan et al. (2005) developed a MMP correlation for pure and impure $CO_2$ displacements of multi-component oil using analytical gas flooding theory. This

correlation depends on reservoir temperature, molecular weight of $C_{7+}$, and the intermediate component ($C_2$-$C_6$) in the oil. For pure $CO_2$ MMP correlation, a data set consisting of seventy analytically calculated MMPs from nine oils was used. It was noted that this correlation is limited to oils that are similar to the nine oils used in their study since it was based on only nine Equation of State (EOS) characterizations.

The results of these calculated MMP values are summarized in **Table 4.2**. The table also shows a comparison between those calculated values and the measured MMP by calculating the resulted error. A summary of the proposed equations for each correlation is included in Appendix A for a quick reference.

TABLE 4.2—SUMMARY OF PUBLISHED CORRELATION RESULTS

| Method | Value, psi | Error,% |
|---|---|---|
| Slimtube | 1800 | |
| Holm and Josendal | 1900 | 5.6 |
| Cronquist | 1901 | 5.6 |
| GlasØ (no $C_2$-$C_6$) | 1826 | 1.4 |
| GlasØ (with $C_2$-$C_6$) | 3492 | 94.0 |
| Johnson and Pollin | 1548 | 14.0 |
| Alston | 2225 | 23.6 |
| Yellig and Metcalfe | 1497 | 16.8 |
| Orr and Silva | 1470 | 18.3 |
| Eakin and Mitch | 2232 | 24.0 |
| Yuan | 2978 | 65.4 |

### 4.1.4 Miscibility in the Core

The slimtube was only used to measure the MMP while all fluid flow experiments, which will test the different modes of $CO_2$ injection, are conducted on a coreflood set-up that uses a carbonate core. Therefore, confirming the miscibility conditions on the carbonate core was considered essential. The approach was to duplicate the slimtube miscible displacement experiment on the carbonate core.

Shown in **Fig. 4.3** is the miscibility test on the core cumulative oil production. The total produced oil at the end of the run (300 mins and 1.6 PV) is 53.25 $cm^3$, representing 75.37% of the original oil in place (OOIP). However, the total produced oil at 1.2 PV injected is 48.5 $cm^3$; representing 69.29 % of the original oil in place (OOIP).

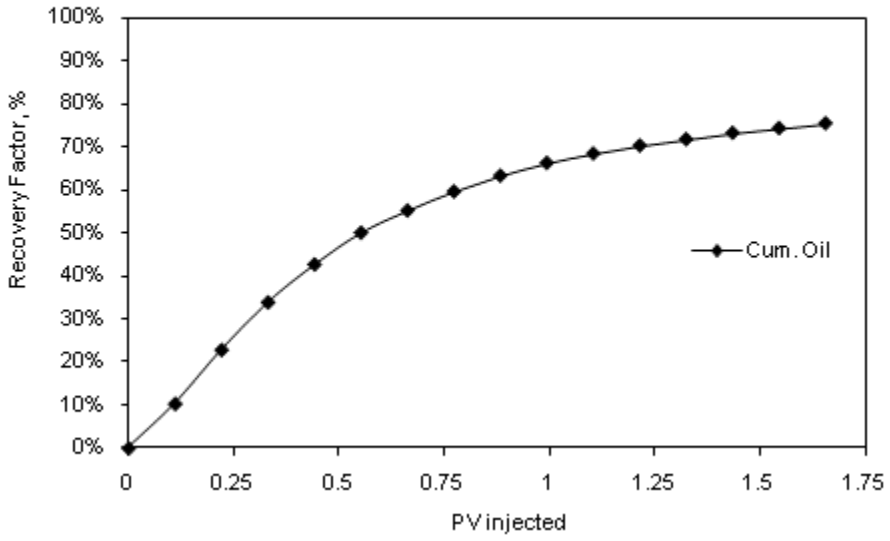


Fig. 4.3— Cumulative recovery from injecting continuous $CO_2$ into the core to test for miscibility

These results suggest that either multiple contact miscibility did not occur in the short core or the presence of heterogeneity and the wide particle size distribution lowered the overall recovery. Researchers have disagreed on the mechanisms that affect the multiple-contact miscible (MCM) displacement and control the ultimate oil recovery. Some argue that the displacement length is the most important factor in MCM displacement and maintain that 16 ft. is required for the MCM to occur (Hudgins et al. 1990; Jarrell et al. 2002; Negahban et al. 1990; Yellig 1982). Most notably, Yellig (1982) concluded that $CO_2$ injection rate has no effect on ultimate recovery whereas the length is detrimental in developing miscibility especially in linear coreflood systems.

To test for the length, the slimtube coil was placed ahead of the core holder, as shown in **Fig. 4.4**, to pre-equilibrate the oil with $CO_2$ prior to entering the core and provide sufficient length for miscibility. The slimtube and the core were then fully saturated with oil and flooded continuously with $CO_2$.

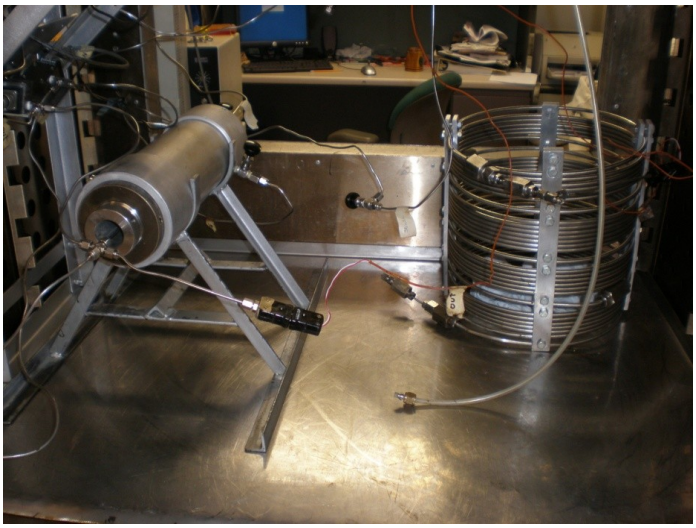

Fig. 4.4— Slimtube connected to the core to provide sufficient length

Shown in **Fig. 4.5** is the cumulative oil production from this arrangement (slimtube connected to the core). The total produced oil at the end of the run (400 mins and 1.14 combined PV) is 107.50 $cm^3$, representing 73% of the original oil in place (OOIP). The ultimate recovery from this combination is similar to the oil recovery from the carbonate core alone. Therefore, it was concluded that extra length does not promote higher recovery suggesting that the MCM displacement is practically independent of length. These results agree with previously published research which suggests that placing a slimtube ahead of the core will not support higher recovery (Shyeh-Yung 1991).

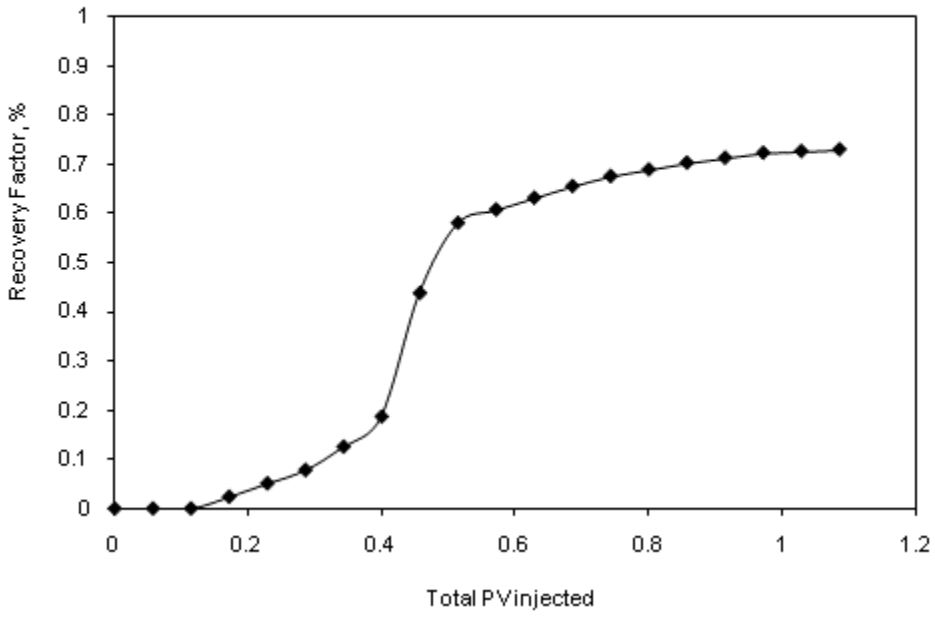


Fig. 4.5— Cumulative oil recovery from the combined slimtube and core

To further investigate the core's poor recovery, the core was CT scanned before and after the flood as shown in **Fig. 4.6.** The results of the scans showed that only large connected pores were swept by $CO_2$ while smaller pores had higher residual oil saturation. Therefore, it was concluded that heterogeneity (permeability variation) has caused small scale mixing which resulted in dispersive bypassing. This conclusion agrees with most researchers who attributed the decrease in recovery to dispersive bypassing as a result of rocks' heterogeneity rather than the length (Shelton and Schneider 1975; Stern 1991).

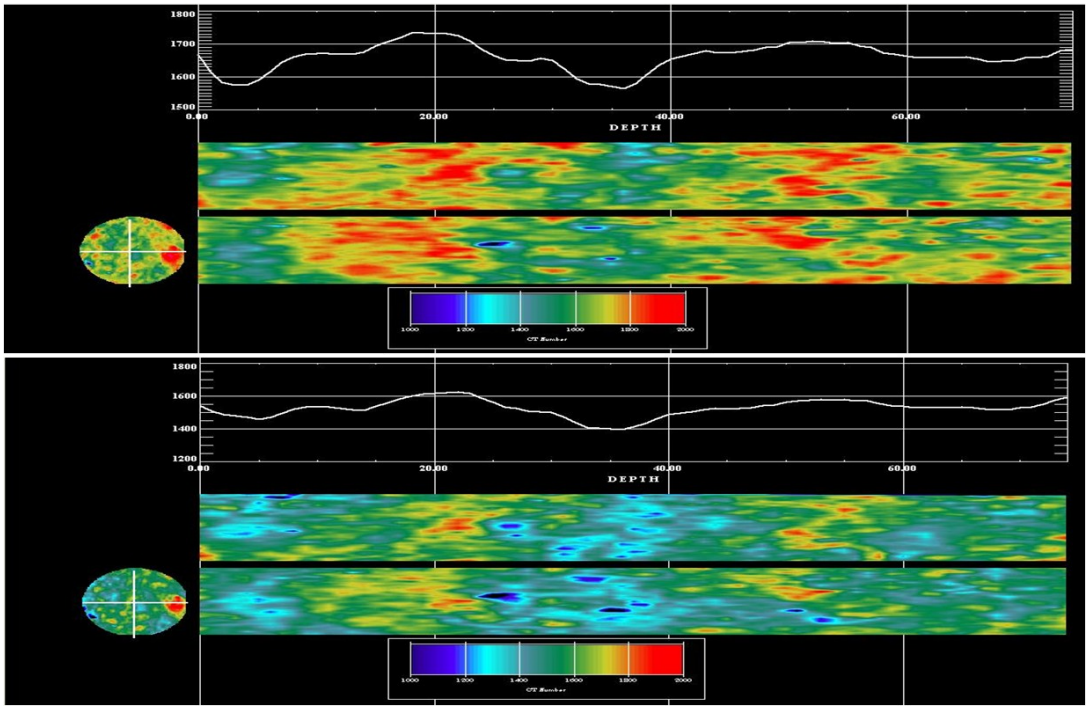


Fig. 4.6— CT scan images showing an orthoslab profile of the core before $CO_2$ (top) and after $CO_2$ (bottom)

The 1D longitudinal dispersivity equation is defined as follows:

$$K_l = D_e + \alpha_l v \quad \text{.....(4.2)}$$

where $K_l$ is the longitudinal dispersivity coefficient ($ft^2/D$); $D_e$ is the effective molecular diffusion; $\alpha_l$ is the longitudinal dispersivity (ft); and $\nu$ is the superficial velocity (ft/D). The longitudinal dispersivity is expressed as a dimensionless Peclet number in the following form:

$$N_{Pe} = \frac{L v}{K_l} \approx \frac{L}{\alpha_l} \quad \text{.....(4.3)}$$

where $N_{pe}$ is the dimensionless Peclet number and $L$ is the displacement length in ft. The longitudinal dispersivity varies with length as permeability variation increases and is greater in carbonate cores than the slimtube and most sandstone cores. The only case when the dispersivity is constant is when permeability variation is random (Jarrell et al. 2002).

According to equation (4.3), large longitudinal dispersivity results in small Peclet number while large displacement length results in large Peclet number. However, longitudinal dispersivity grows with length if permeability variation is high, which is the case in most carbonate reservoirs. Therefore, extra length will not increase the recovery and suggest higher miscibility.

## 4.2 Base Case Corefloods

The coreflood experiments are divided into three sets: base case, salinity effect, and fractured cores. Each set investigates a certain parameter on four main injection modes: continuous gas injection (CGI), waterflood (WF), water alternating gas (WAG), and simultaneous water and gas injection (SWAG). Other injection modes may be conducted directly after CGI or WF as necessary. For example, CGI is conducted after WF as a tertiary recovery mode and vice versa. Those injection modes are not primary but their results provide insightful conclusions and verify certain points. Initially, six coreflood runs have been conducted to establish a base case to which the rest of the runs can be accurately compared. The base case uses an unfractured carbonate core with fresh water for both saturation and injection. During the other sets, certain parameters have been changed to study their effect on each injection mode. However, several parameters have been kept constant to allow for accurate comparison.

The constant parameters include:

- Back pressure (injection pressure): 1900 psi
- Injection temperature: 120 °F
- Core dimensions: 2" diameter and 6" in length
- Injection rate: 0.5 $cm^3$/min (30 $cm^3$/hr)
- SWAG injection rate: changed to 0.25 $cm^3$/min (15 $cm^3$/hr) for both water and $CO_2$ to achieve 0.5 $cm^3$/min total injection
- Confinement (overburden) pressure: 300-500 psi above injection pressure

### 4.2.1 Continuous Gas Injection (CGI)

This run involves injecting $CO_2$ continuously into oil saturated core (secondary recovery mode) until ultimate recovery is reached. It was observed during this run that oil production starts very high and then drops rapidly as shown in **Fig. 4.7**. The pressure profile across the core is illustrated in **Fig. 4.8**. It shows that the differential pressure is almost constant throughout the run at about 5 psi with a peak at 7 psi.

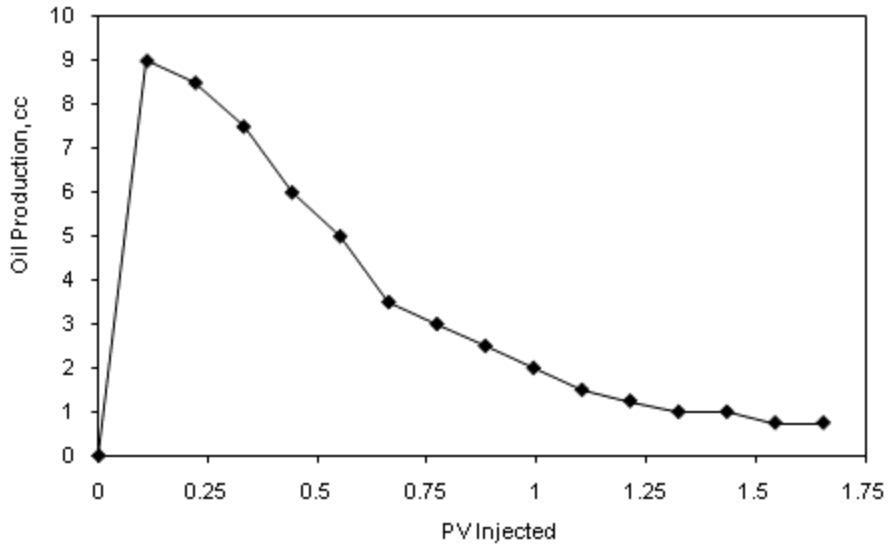


Fig. 4.7— CGI (base case): oil production rate

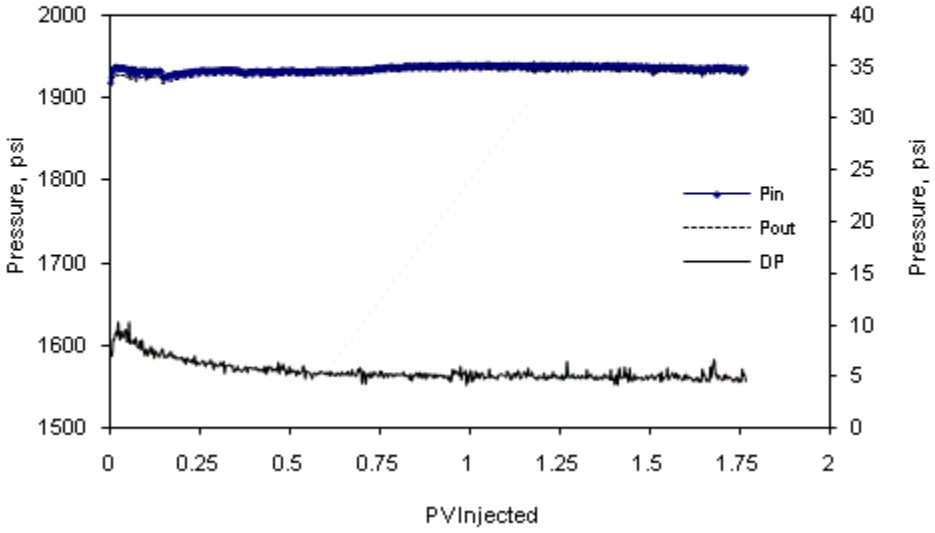


Fig. 4.8— CGI (base case): pressure profile

Shown in **Fig. 4.9** is the CGI cumulative fluid recovery. The total produced oil at the end of the run (300 mins and 1.66 PV) is 53.25 $cm^3$, representing 75.37 % of the original oil in place (OOIP). The cumulative produced $CO_2$ at standard conditions is 48 Liters at the end of the run with $CO_2$ breakthrough at 23.5 min (0.13 PV).

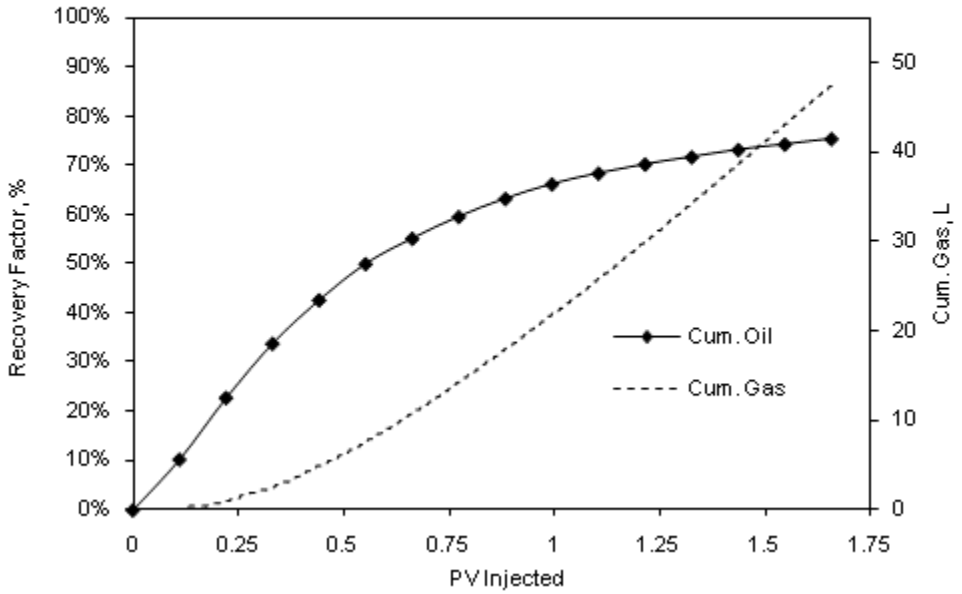


Fig. 4.9— CGI (base case): cumulative oil recovery and $CO_2$ production

### 4.2.2 Waterflood (WF) after CGI

Water is injected after the continuous gas injection (CGI) run as a tertiary recovery waterflood to evaluate how much extra oil can be produced. This is similar to WAG injection but with no regard to WAG ratio or slug size. The determining factor of injecting water is when CGI ultimate recovery is reached. The objective of this injection is to evaluate how much extra oil a wetting phase, water, can produce. Since gas $CO_2$ is considered a non-wetting phase, it was assumed that oil in smaller pores will be bypassed by $CO_2$. Water injection in this case does not aim to reduce $CO_2$ mobility, reduce gravity segregation or viscous fingering as in the case of WAG injection.

Shown in **Fig. 4.10** is the WF after CGI cumulative fluid production. The total produced oil at the end of the run (120 mins and 0.66 PV) is 2.0 $cm^3$; representing only 2.86 % of the original oil in place (OOIP) and 11.94% from the oil in place (OIP) left after CGI. It was noticed that there was a significant delay in oil production until almost water breakthrough. It also produced a total of 16.8 Liters of $CO_2$ at standard conditions. The production of $CO_2$ was increasing at a constant rate until water breakthrough (90 mins) during which $CO_2$ production stopped. The pressure profile of this run is shown in **Fig. 4.11.** An increase in the differential pressure across the core was observed until water breakthrough where the pressure started to stabilize.

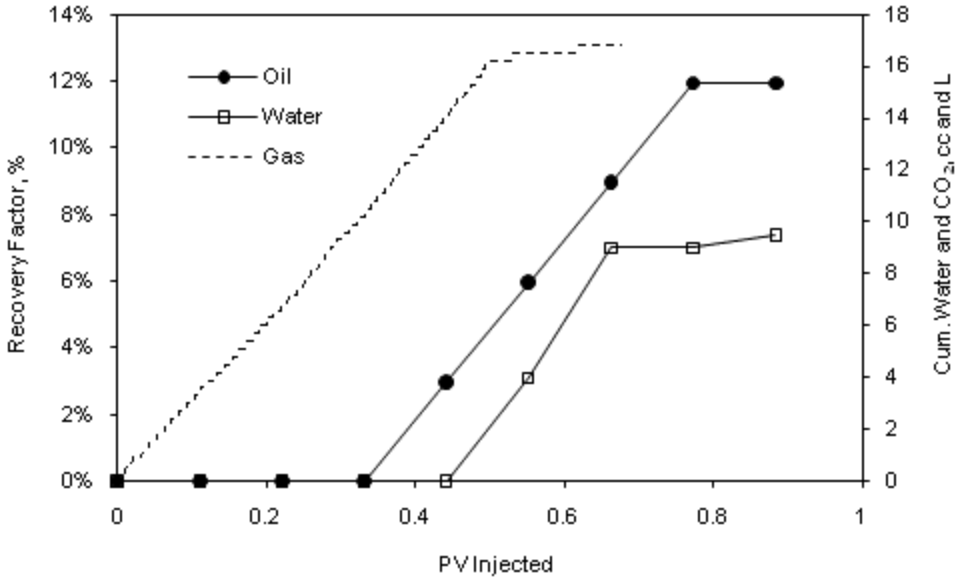


Fig. 4.10— WF after CGI (base case): cumulative oil, water, and $CO_2$ recovery

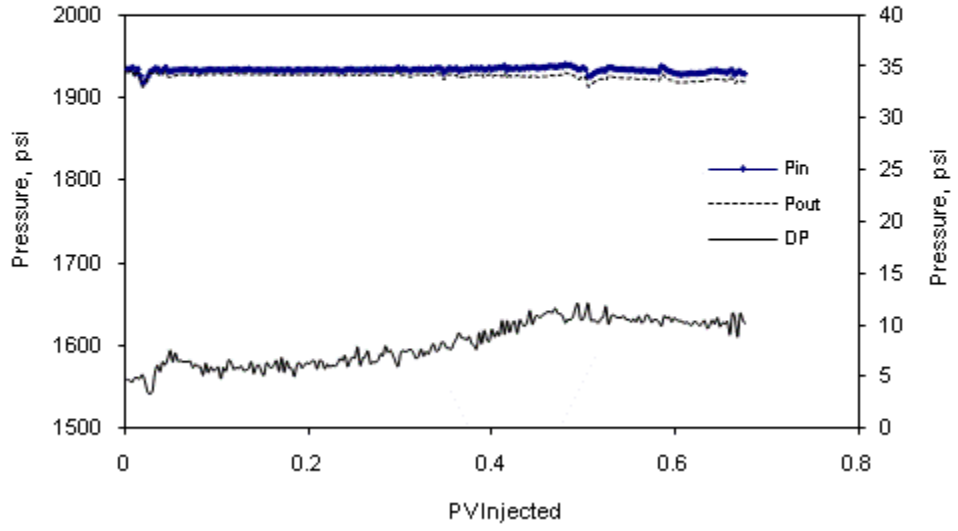


Fig. 4.11— WF after CGI (base case): pressure profile

### 4.2.3 Water Alternating Gas (WAG) Injection

This run involves injecting $CO_2$ in alternating cycles with water into oil saturated core (secondary recovery mode) until ultimate recovery is reached. Each fluid cycle lasts about 0.33 pore volume (PV) or 60 minutes. The drop in oil production rates is less severe than CGI as shown in **Fig. 4.12**, which indicates that water reduced the $CO_2$ unfavorable high mobility and improved the flood profile. The pressure profile across the core is illustrated in **Fig. 4.13**. The differential pressure was observed to change during each fluid cycle. An increase in injection pressure at each water cycle was evident suggesting a reduced rock relative permeability to water which may cause injectivity abnormality in field applications during WAG injection. The highest differential pressure was recorded to be 16 psi.

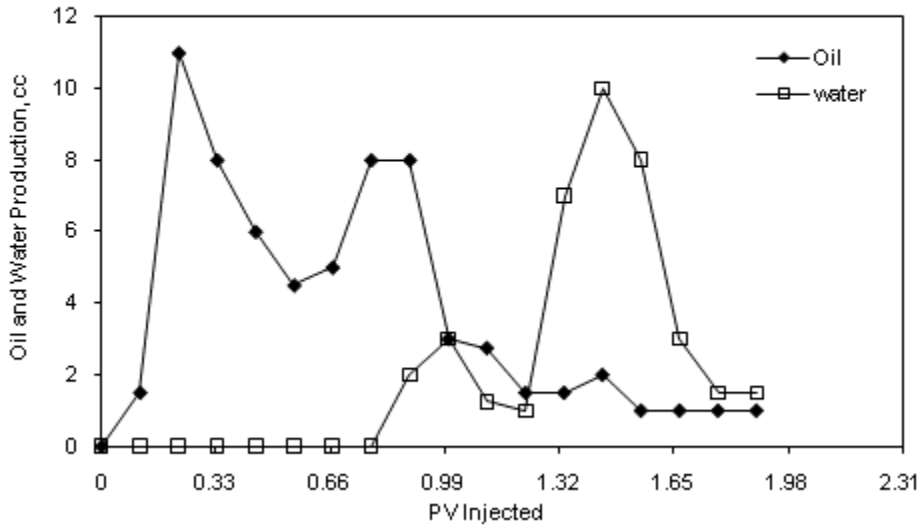


Fig. 4.12— WAG (base case): oil and water production rates

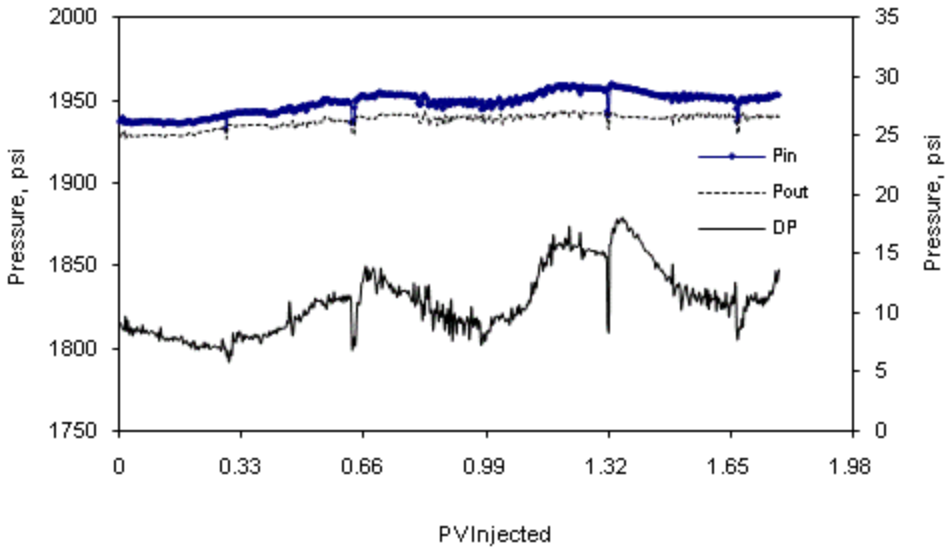


Fig. 4.13— WAG (base case): pressure profile

Shown in **Fig. 4.14** is the WAG cumulative oil and gas production. The total produced oil at the end of the run (340 mins and 1.89 PV) is 67 $cm^3$, representing 92.7 % of the original oil in place (OOIP). The cumulative produced $CO_2$ at standard conditions is 28.2 Liters at the end of the run with $CO_2$ breakthrough at 34.5 min (0.192 PV).

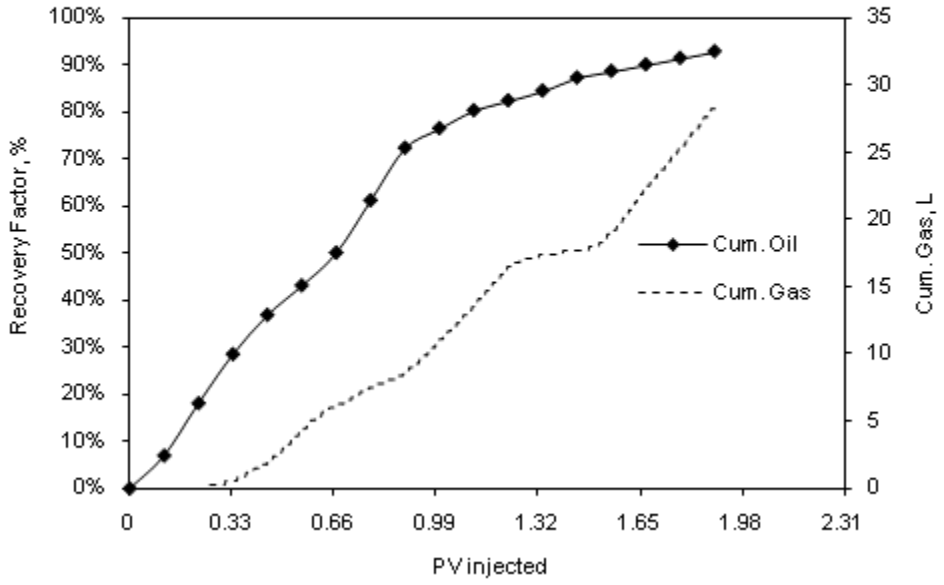


Fig. 4.14— WAG (base case): cumulative oil recovery and $CO_2$ production

### 4.2.4 Simultaneous Water and Gas (SWAG) Injection

This run involves injecting $CO_2$ and water simultaneously into oil saturated core (secondary recovery mode) until ultimate recovery is reached. The total fluid injection rate is 0.5 $cm^3$/min (30 $cm^3$/hr). This total injection rate is divided between the two fluids: water and $CO_2$. Each fluid is injected at a rate of 0.25 $cm^3$/min (15 $cm^3$/hr) in order to achieve a 1:1 SWAG volume ratio. This premium injection mode is meant to improve the displacement profile and reduce the $CO_2$ requirements.

Oil and water rates are more uniform than the previous two injection modes (CGI and WAG) as shown in **Fig. 4.15**. The differential pressure across the core is shown in **Fig. 4.16.** It shows slight oscillations at the beginning until water breakthrough, and then becomes constant throughout the run at about 8 psi. These factors indicate that $CO_2$ and water were moving more uniformly inside the core than CGI and WAG.

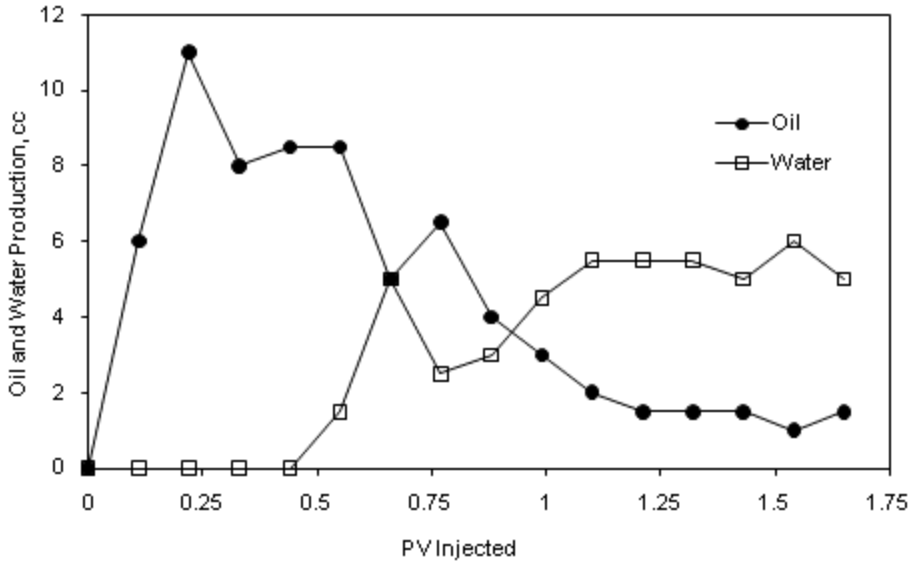


Fig. 4.15— SWAG (base case): oil and water production rates

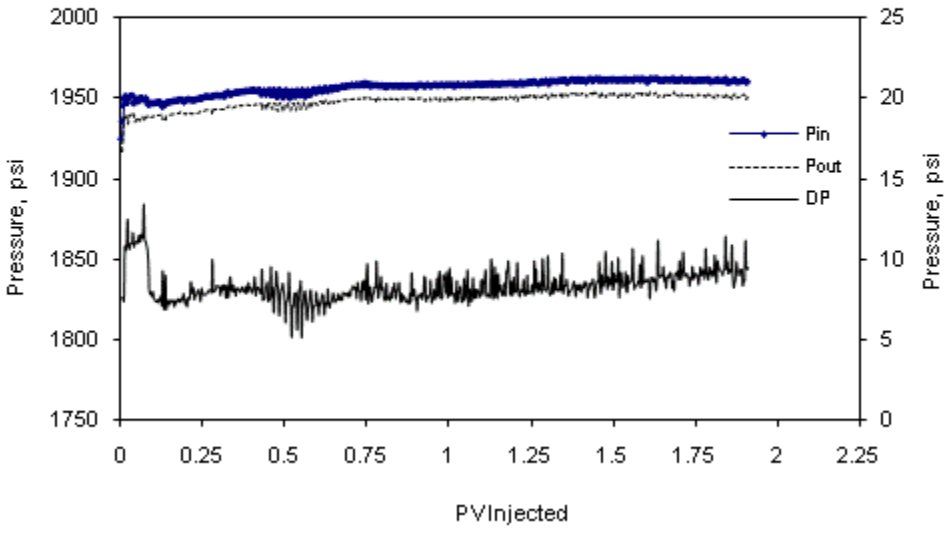


Fig. 4.16— SWAG (base case): pressure profile

Shown in **Fig. 4.17** is SWAG cumulative oil and gas production. The total produced oil at the end of the run (300 mins and 1.65 PV) is 69.5 $cm^3$, representing 98.6% of the original oil in place (OOIP). The cumulative produced $CO_2$ at standard conditions is 17.7 Liters at the end of the run with $CO_2$ breakthrough at 28 min (0.156 PV).

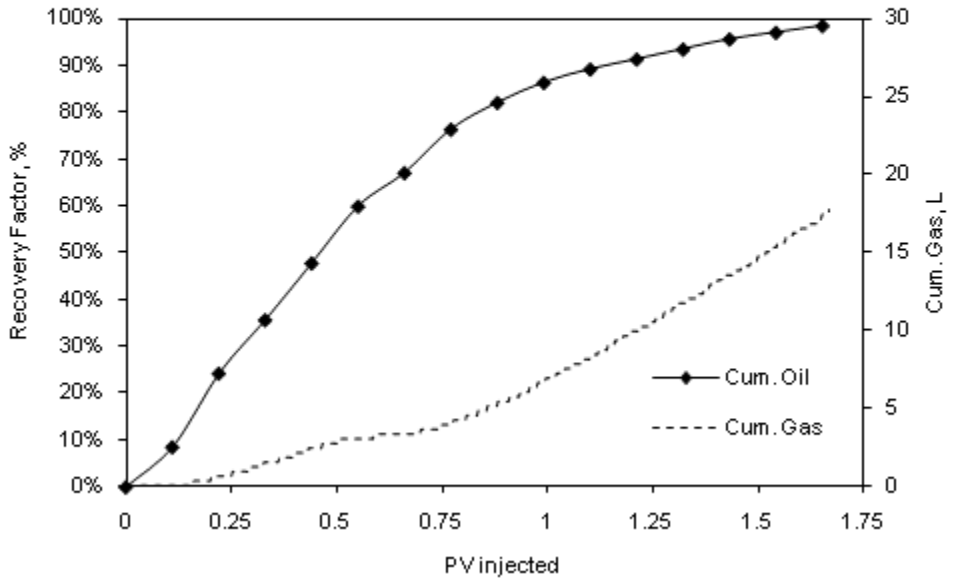


Fig. 4.17— SWAG (base case): cumulative oil recovery and $CO_2$ production

### 4.2.5 Waterflood (WF)

This run involves injecting water only into oil saturated core (secondary recovery mode) until ultimate recovery is reached. Production rates and the differential pressure across the core are illustrated in **Figs. 4.18** and **4.19**, respectively. It shows that oil production is high before water breakthrough, and then it slows down significantly. The differential pressure is almost constant throughout the run at about 10 psi. Shown in **Fig. 4.20** is waterflood cumulative oil production. The total produced oil at the end of the run (280 mins and 1.5 PV) is 42 $cm^3$, representing 54.7 % of the original oil in place (OOIP).

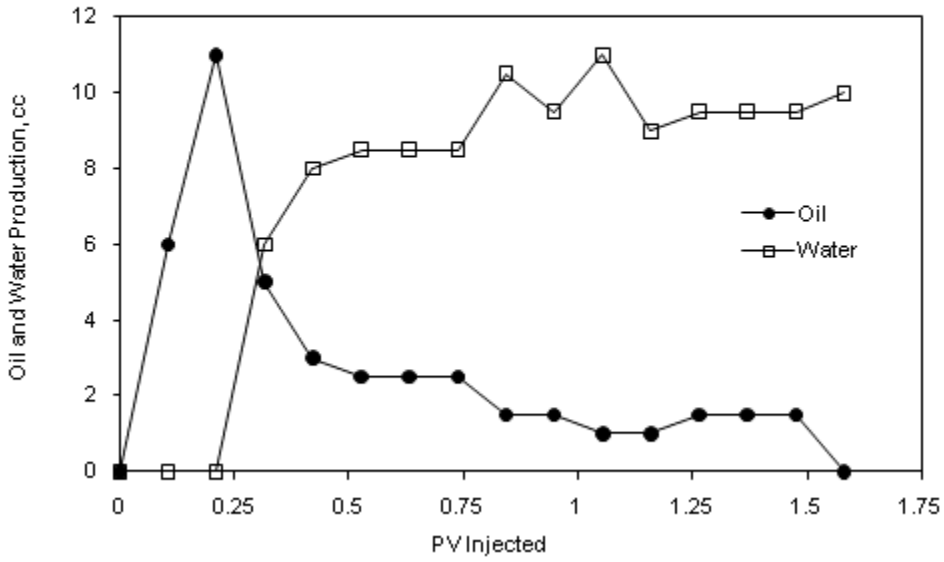


Fig. 4.18— WF (base case): oil and water production rates

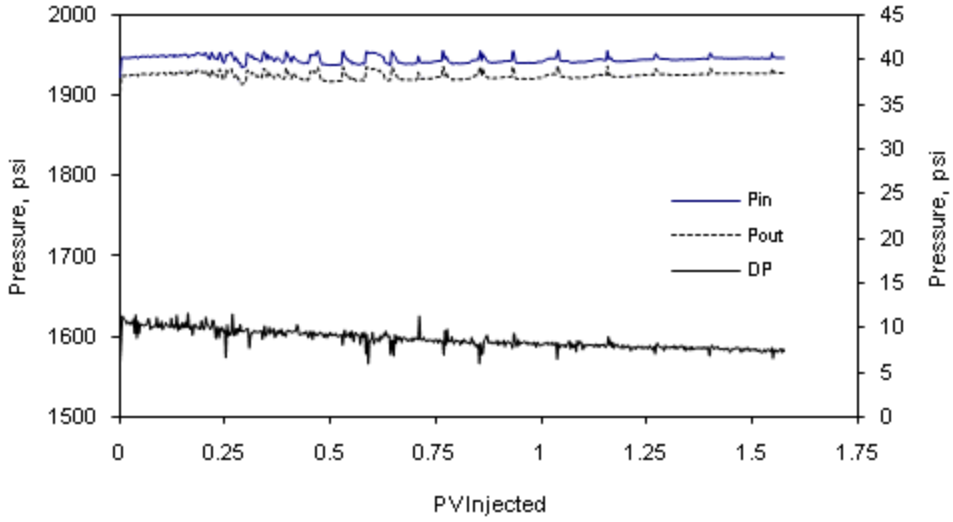


Fig. 4.19— WF (base case): pressure profile

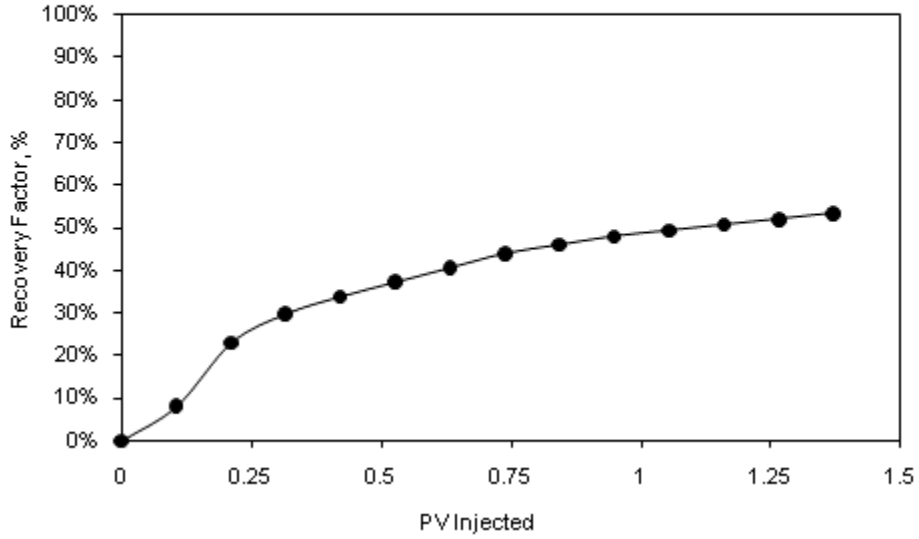


Fig. 4.20— WF (base case): cumulative oil recovery

### 4.2.6 Continuous Gas Injection (CGI) after WF (CGI in Tertiary Mode)

This run followed directly the fresh waterflood. It involves injecting $CO_2$ continuously into the waterflooded core (tertiary recovery mode) until ultimate recovery is reached. It was observed during this run that oil production is significantly delayed as shown in **Fig. 4.21**. Initially, only water is produced until $CO_2$ breakthrough, then oil production commences. This behavior is totally different from secondary recovery CGI because of the presence of water which has to be displaced by $CO_2$ to reach the oil. The differential pressure across the core is illustrated in **Fig. 4.22**. It shows that pressure starts high at around 12 psi until $CO_2$ breakthrough then drops down to 8 psi. This is because the rock relative permeability to $CO_2$ is low whereas the relative permeability to water is high. Therefore, the pressure stays high until the water is displaced and oil is mobilized. Moreover, the presence of water delayed the $CO_2$ breakthrough to 93.5 minutes compared to 23.5 minutes during the secondary injection.

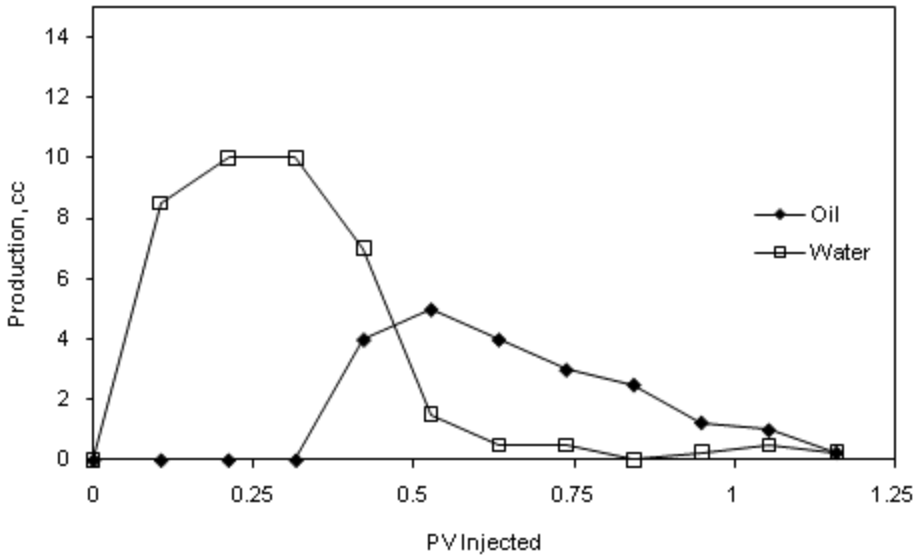


Fig. 4.21— Tertiary CGI (base case): oil and water production rates

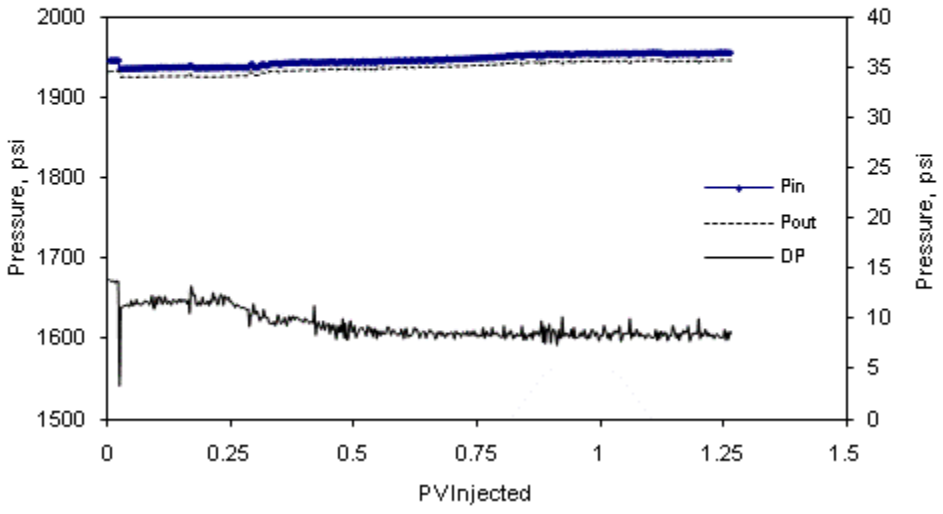


Fig. 4.22— Tertiary CGI (base case): pressure profile

Shown in **Fig. 4.23** is the CGI cumulative oil production. The total produced oil at the end of the run (240 mins and 1.3 PV) is 21 $cm^3$, representing 28.4 % of the original oil in place (OOIP) and 65.63% of remaining oil in place (OIP) after waterflood. The cumulative produced $CO_2$ at standard conditions is 24.9 Liters at the end of the run with a $CO_2$ breakthrough at 93.5 min (0.493 PV).

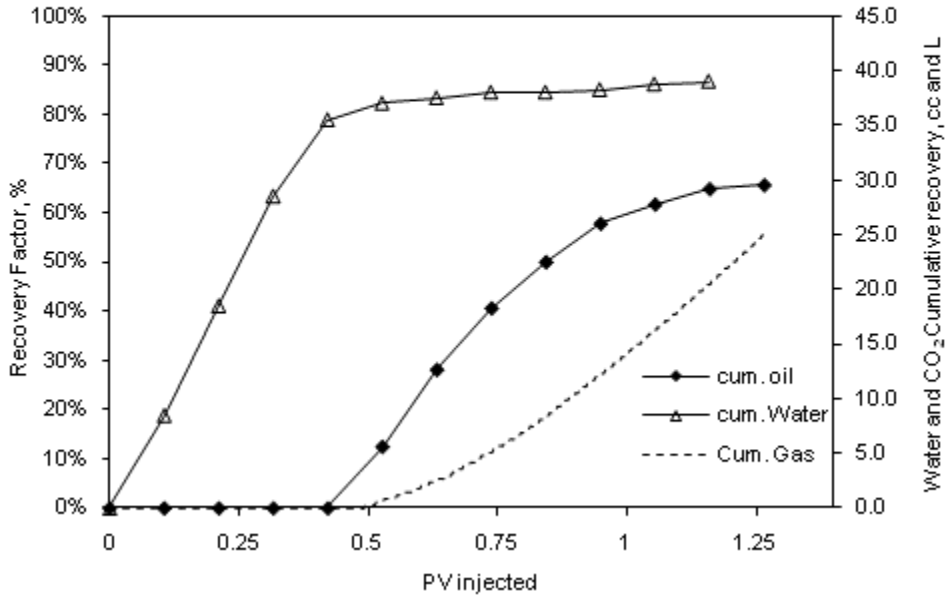


Fig. 4.23— Tertiary CGI (base case): cumulative oil, water and $CO_2$ recovery

### 4.3 Salinity Effect ($CO_2$ Solubility in Water)

The salinity effect was investigated by studying three different brines: 6% NaI doped water, 20 wt.% NaCl doped water and 0 wt.% (fresh) water. The fresh water case is the base case that has been discussed in the previous section. The 6 wt. % and 20 wt. % represent waters with 60,000 and 20,000 ppm, respectively. This section will discuss the effect of changing water salinity on WF, WAG, and SWAG. This study was specially designed to study the effect of water salinity on SWAG and WAG where large amounts of water are used during the injection. For all salinity levels, the injection and saturation waters have the same salinity for all injection modes. When the salinity of used water changes during $CO_2$ injection, it affects $CO_2$ solubility in water. It was found that a decrease in water salinity increases $CO_2$ solubility in water at the same pressure and temperature (Jarrell et al. 2002). $CO_2$ dissolved in water has long been considered unavailable to contact oil and when $CO_2$ solubility increases in water by decreasing the salinity, a decrease in oil recovery was assumed (Jarrell et al. 2002; Kulkarni and Rao 2005; Stalkup 1992). There is very limited experimental data to support this mechanism especially for rocks with high heterogeneity where bypassing is expected. The displacement by $CO_2$ alone is more superior to water with dissolved $CO_2$. However, the latter has far better displacement efficiency than WF alone (Holm 1963). **Fig. 4.24** shows $CO_2$ solubility in fresh water while **Fig. 4.25** shows the $CO_2$ solubility correction factor for different salinities.

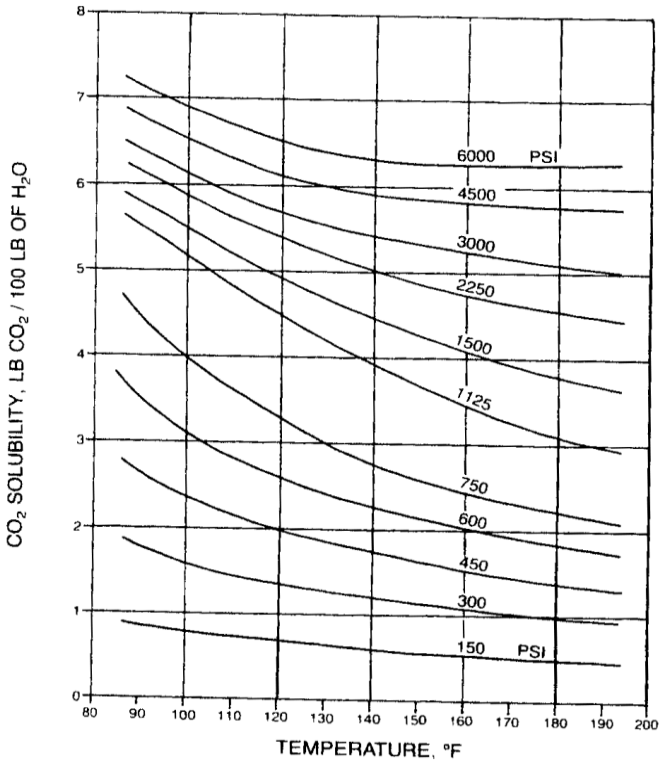


Fig. 4.24— $CO_2$ solubility in water as a function of pressure and temperature (Stalkup 1992)

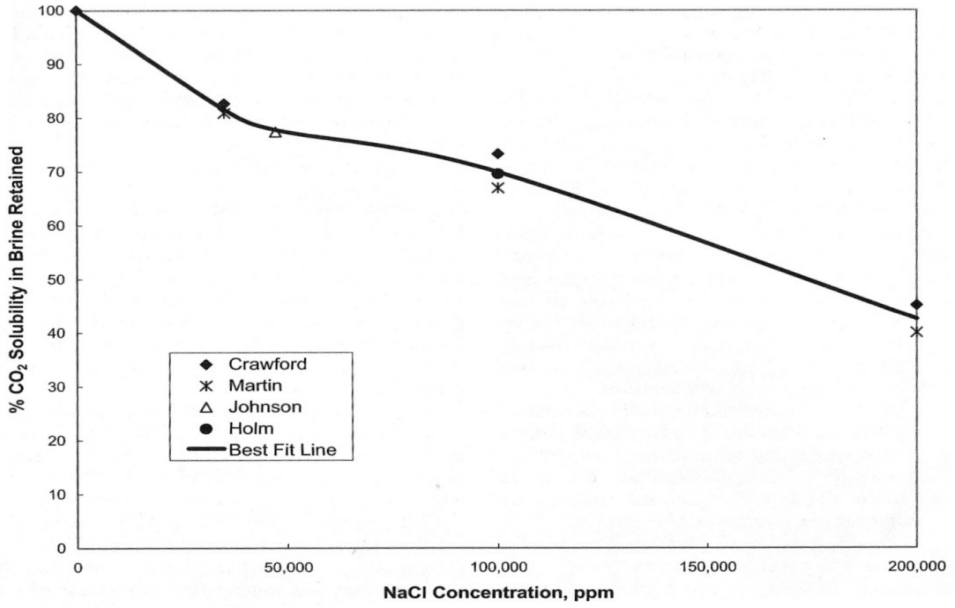


Fig. 4.25— Salinity correction for $CO_2$ solubility in water, independent of pressure and temperature (Jarrell et al. 2002)

### 4.3.1 Saline Waterflood (WF)

This run involves injecting water doped with 6 wt. % NaI into oil saturated core (secondary recovery mode) until ultimate recovery is reached. The objective of this run is to investigate if there is a change in cumulative oil recovery due to the salinity change before adding $CO_2$.

Shown in **Fig. 4.26** is waterflood cumulative oil recovery. The total produced oil at the end of the run (280 min and 1.5 PV) is 40.5 $cm^3$, representing 53.4 % of the original oil in place (OOIP). This indicates that the recovery for this salinity level is identical to the recovery of the fresh water case discussed in Section 4.2.5. Therefore, it was concluded that if any changes occur during WAG and SWAG injections, it will be attributed solely to the $CO_2$ solubility in water.

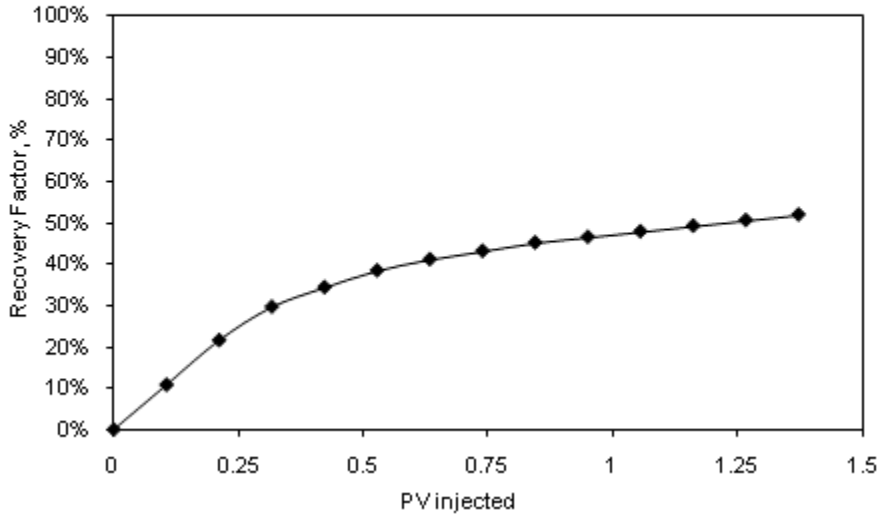


Fig. 4.26— WF (6 wt. % NaI): cumulative oil recovery

### 4.3.2 Saline Water Alternating Gas (WAG) Injection

The same procedure during WAG base case was followed in this run with the only change is in the salinity of the water. Two salinities were studied for WAG: 6 wt. % (60,000 ppm) and 20 wt. % (200,000 ppm).

Shown in **Fig. 4.27** is WAG cumulative oil and gas production when using 6 wt. % NaI doped water. The total produced oil at the end of the run (340 mins and 1.86 PV) is 62 $cm^3$, representing 86.5 % of the original oil in place (OOIP). This indicates a 6% decrease in oil recovery compared to the base case which used fresh water. The cumulative produced $CO_2$ at standard conditions is 30.6 Liters at the end of the run with $CO_2$ breakthrough at 37 min (0.202 PV).

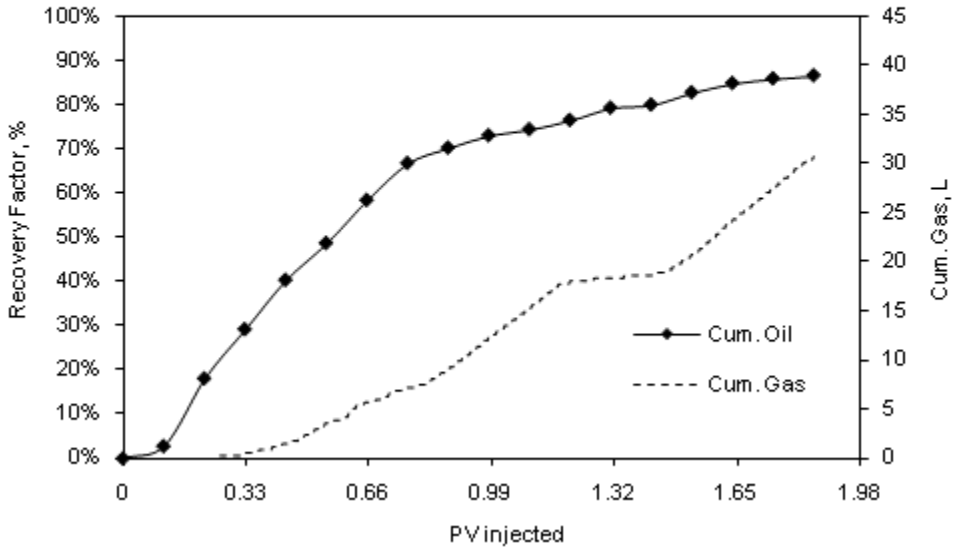


Fig. 4.27— WAG (6 wt. % NaI): cumulative oil and $CO_2$ recovery

Shown in **Fig. 4.28** is WAG cumulative oil and gas production when using 20 wt.% NaCl doped water. The total produced oil at the end of the run (340 mins and 1.88 PV) is 53 $cm^3$, representing 75 % of the original oil in place (OOIP). This indicates a 17.7% decrease in oil recovery compared to the base case which used fresh water. The cumulative produced $CO_2$ at standard conditions is 35.1 Liters at the end of the run with a $CO_2$ breakthrough at 22 min (0.121 PV).

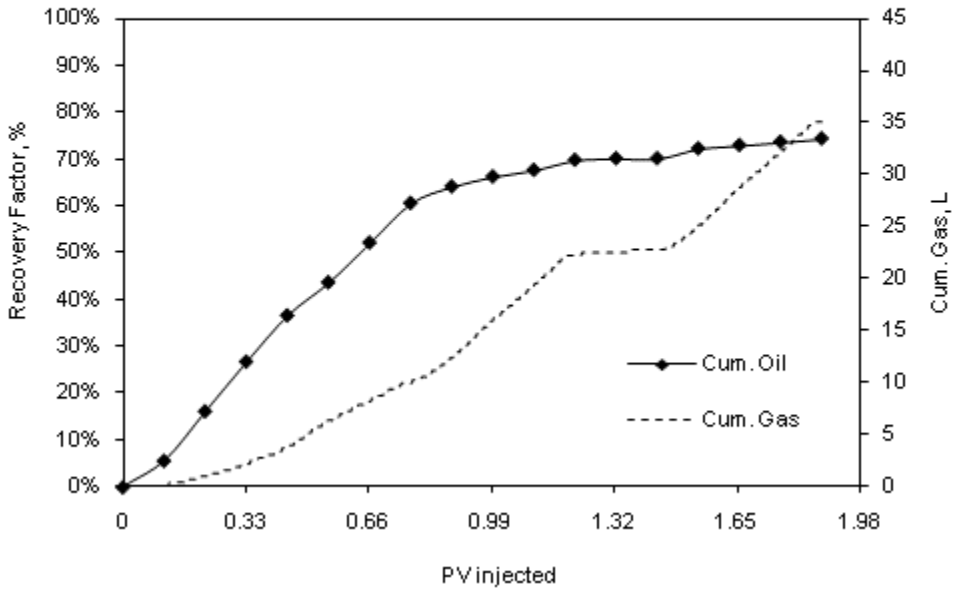


Fig. 4.28— WAG (20 wt. % NaCl): cumulative oil and $CO_2$ recovery

### 4.3.3 Saline Simultaneous Water and Gas (SWAG) Injection

The same procedure as SWAG base case was followed in this case with the only change is in the salinity of the water. Similar to WAG, two salinities were studied for SWAG: 6 wt. % (60,000 ppm) and 20 wt. % (200,000 ppm).

Shown in **Fig. 4.29** is SWAG cumulative oil and gas production when using 6 wt. % NaI doped water. The total produced oil at the end of the run (300 mins and 1.66 PV) is 65.5 $cm^3$, representing 90.7 % of the original oil in place (OOIP). This indicates an 8% decrease in oil recovery compared to the base case which used fresh water. The cumulative produced $CO_2$ at standard conditions is 18 Liters at the end of the run with $CO_2$ breakthrough at 29.5 min (0.163 PV).

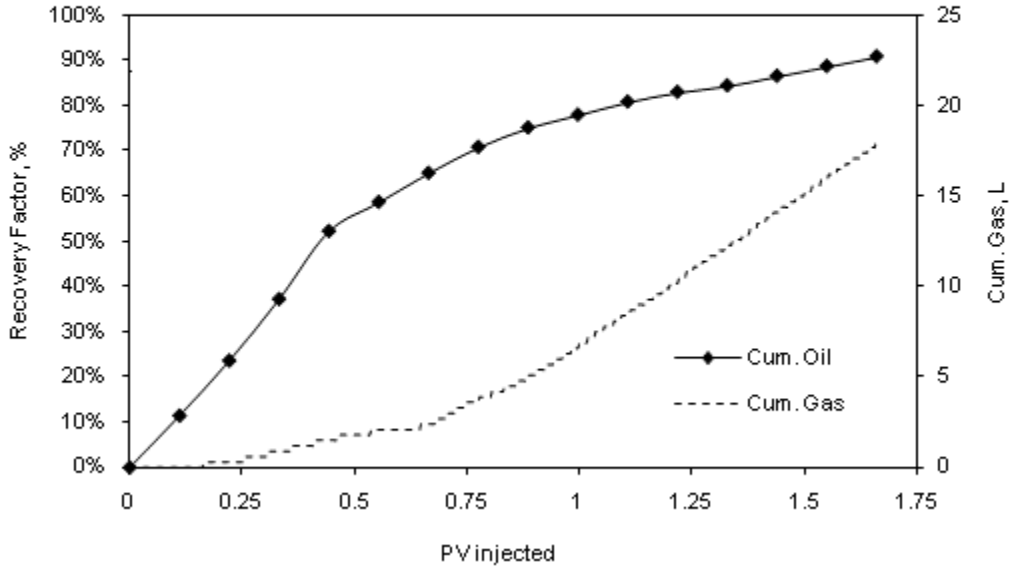


Fig. 4.29— SWAG (6 wt. % NaI): cumulative oil and $CO_2$ recovery

Shown in **Fig. 4.30** is SWAG cumulative oil and gas production when using 20 wt. % NaCl doped water. The total produced oil at the end of the run (300 mins and 1.64 PV) is 59 $cm^3$, representing 81.5 % of the original oil in place (OOIP). This indicates a 17% decrease in oil recovery compared to the base case which used fresh water. The cumulative produced $CO_2$ at standard conditions is 20.7 Liters at the end of the run with $CO_2$ breakthrough at 23 min (0.126 PV).

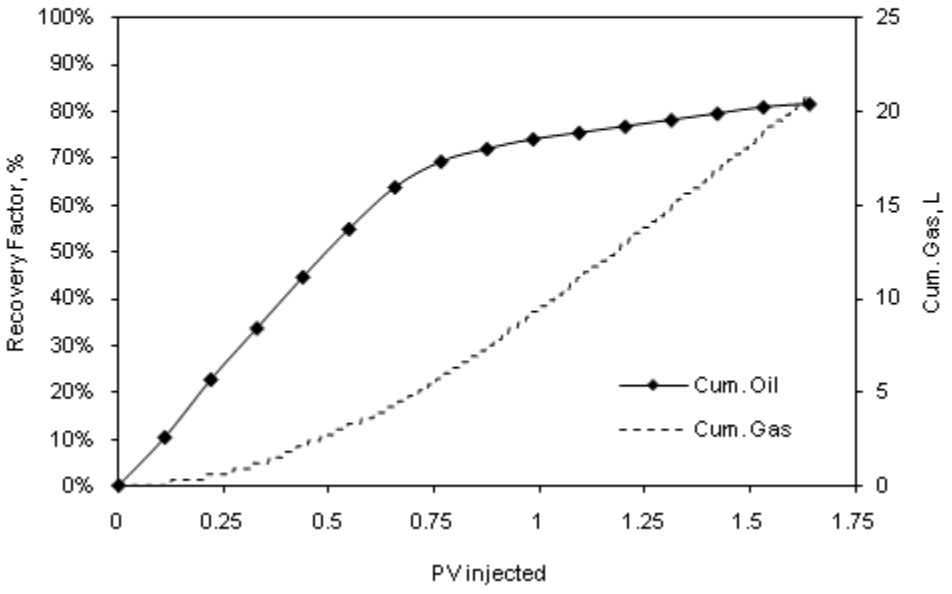


Fig. 4.30— SWAG (20 wt. % NaCl): cumulative oil and $CO_2$ recovery

## 4.4 Fractured Cores

During this set of experiments fresh water (0 wt. %) was used in an artificially fractured carbonate cores. The fresh water was chosen to provide direct comparison to the base case when fractures are present. The fractures were created after the oil saturation by sawing the core in the desired direction. This procedure ensures that the core has reached the same connate water level as the base case. After creating the fractures, the fractured core is placed in the core holder cell and re-saturated with 1-2 PVs of oil to ensure the fracture is free of air and full of oil. Two sets of fractures were created: one horizontal fracture along the length of the core connecting the core's inlet and outlet and creating an elongated slab model, and two fractures one horizontal and one vertical creating a sugar cube model. CGI, WAG, SWAG and WF injections were conducted on each set and the results were compared to the base case (unfractured core). Each type of fracture set will be presented in a separate section and each injection mode will be presented as a subsection. **Fig. 4.31** shows a schematic side view of the one fracture case (elongated slab). **Fig. 4.32** shows a schematic side view of the two fractures case (sugar cube model).

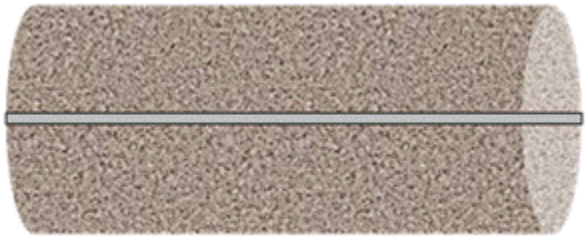

Fig. 4.31— One horizontal fracture (elongated slab)

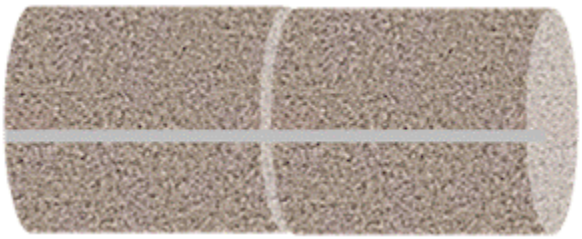

Fig. 4.32— Two fractures, one horizontal and one vertical (sugar cube model)

### 4.4.1 Horizontal Fracture (One Fracture)

During this set of experiments, one horizontal fracture is created along the length of the core connecting the inlet and outlet as shown in **Fig. 4.31**. This case creates an elongated slab shape factor with two matrix slabs and one fracture plane. The water used in these experiments is fresh water to enable precise comparison to the base case. Six injection modes were evaluated on this shape factor: CGI, WAG after CGI (tertiary recovery mode), WF, CGI in tertiary mode, WAG, and SWAG. Each injection mode is presented as a subsection in this chapter.

#### 4.4.1.1 CGI in a One-fracture Core

This run involves injecting $CO_2$ continuously into oil saturated core with one horizontal fracture (secondary recovery mode) until ultimate recovery is reached. It was observed during this run that oil production starts very high and then drops dramatically as shown in **Fig. 4.33**. This indicates that CGI produced very little from the matrix and then cycled quickly through the fracture. The pressure profile across the core is illustrated in **Fig. 4.34** It shows that the differential pressure is almost constant throughout the run at about 3 psi.

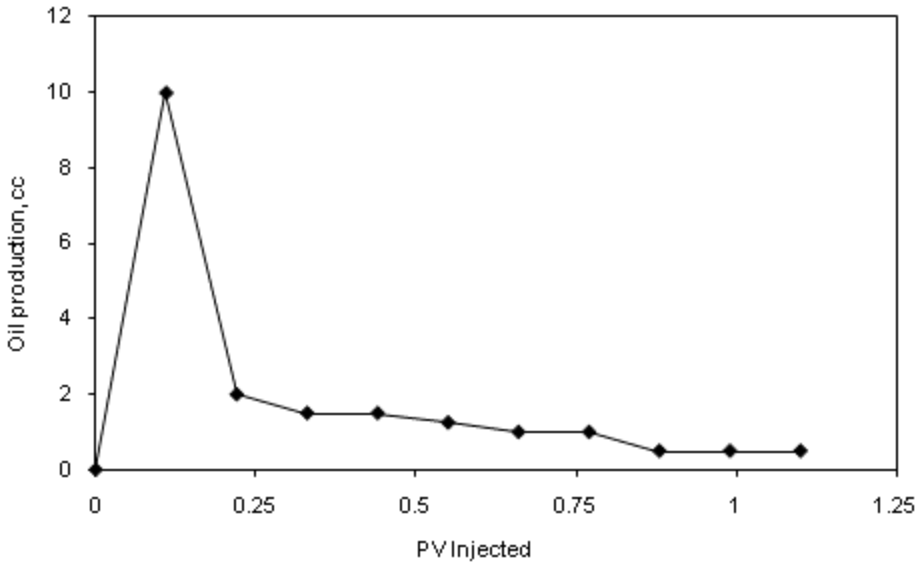


Fig. 4.33— CGI (one-fracture): oil production rate

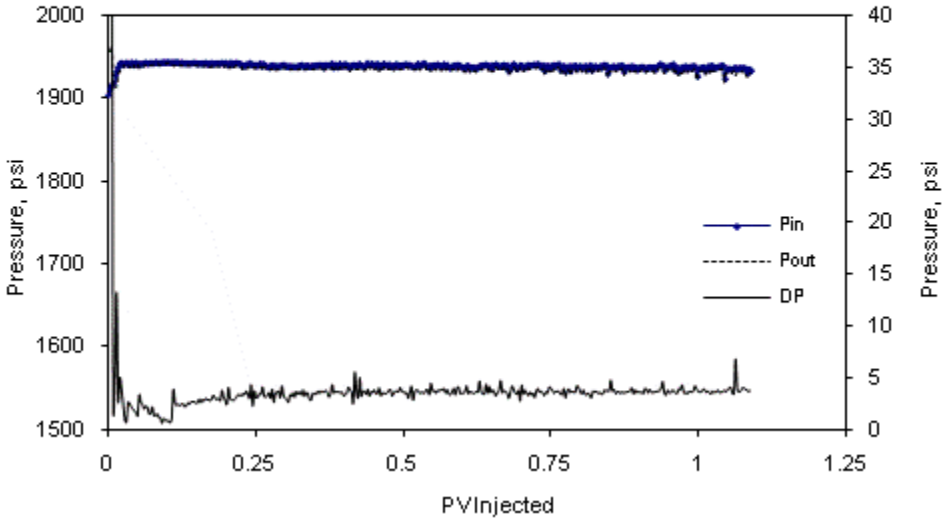


Fig. 4.34— CGI (one-fracture): pressure profile

Shown in **Fig. 4.35** is the fractured core CGI cumulative fluid recovery. The total produced oil at the end of the run (200 mins and 1.1 PV) is 19.75 $cm^3$, representing 27.43 % of the original oil in place (OOIP). The cumulative produced $CO_2$ at standard conditions is 39.9 Liters at the end of the run with $CO_2$ breakthrough at 9 min (0.05 PV).

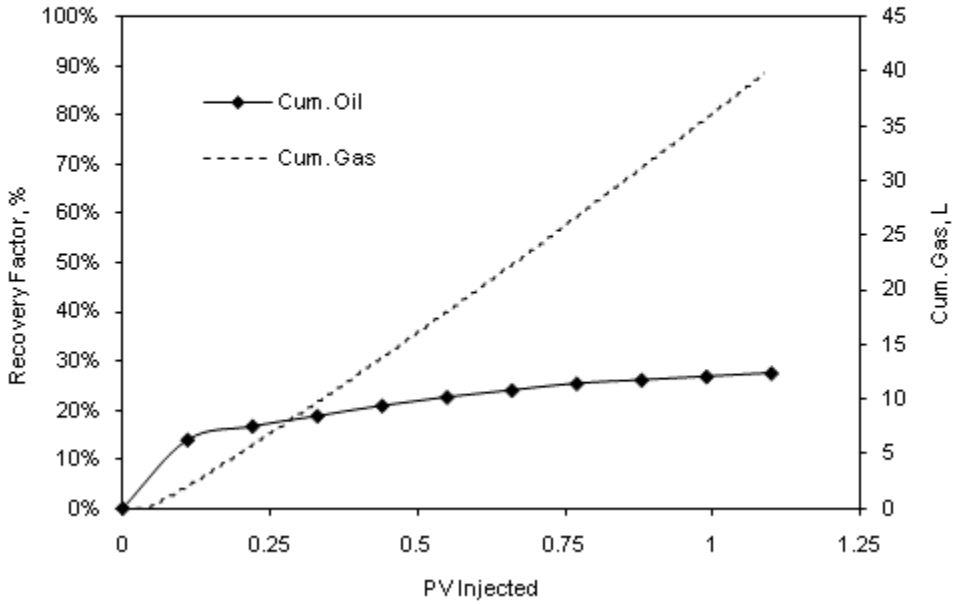


Fig. 4.35— CGI (one-fracture): cumulative oil and $CO_2$ recovery

#### 4.4.1.2 WAG Injection after CGI (Tertiary Mode) in a One-fracture Core

WAG injection commenced after the continuous gas injection (CGI) run as a tertiary recovery method to evaluate how much extra oil can be produced prior to terminating the experiment. The objective of this injection is to evaluate how much water can reduce the $CO_2$ high mobility and improve recovery. The slug size and WAG ratio are 0.33 PV and 1:1, respectively. This is similar to the previously discussed WAG injection experiments. However, the difference is that the first slug in this case is water since it directly followed the CGI.

Shown in **Fig. 4.36** is the WAG after CGI cumulative fluid recovery. The total produced oil at the end of the run (200 mins and 1.1 PV) is 14.0 $cm^3$; representing 19.44 % of the original oil in place (OOIP) and 26.8% from the remaining oil in place (OIP) left after CGI. This brings the total recovery from both injection modes (CGI and WAG) to 46.88% of the OOIP. This means that WAG injection almost doubled the recovery from this core indicating the benefits of water to hinder the $CO_2$ high mobility. WAG also produced a total of 18.3 Liters of $CO_2$ at standard conditions with instantaneous $CO_2$ production. **Fig. 4.37** shows the pressure profile of the WAG injection experiment. One striking fact is the absence of differential pressure spikes during water cycles that were observed in previous WAG injection experiments.

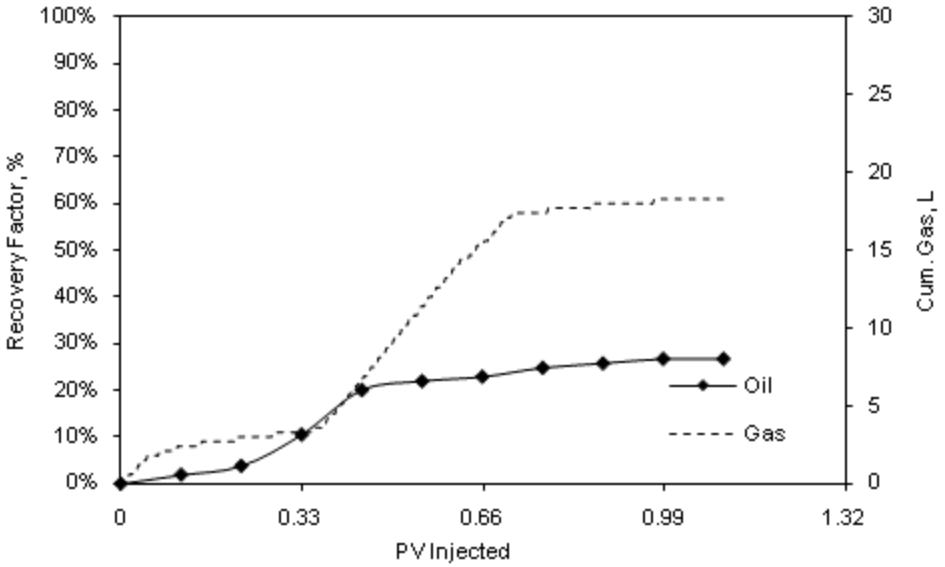


Fig. 4.36— WAG after CGI (one-fracture): cumulative oil and $CO_2$ recovery

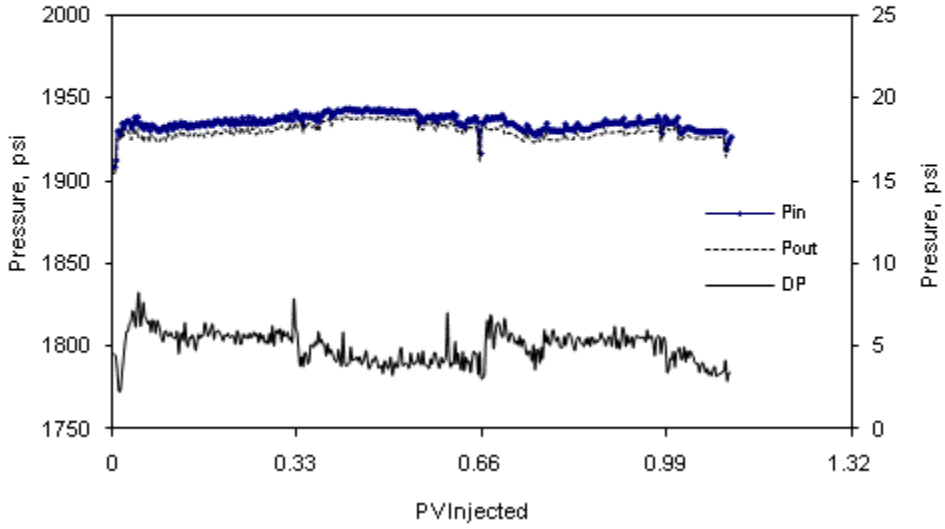


Fig. 4.37— WAG after CGI (one-fracture): pressure profile

#### 4.4.1.3 Waterflood (WF) in a One-fracture Core

This run involves injecting fresh water only into oil saturated core with one horizontal fracture (secondary recovery mode) until ultimate recovery is reached. Oil and water production rates are illustrated in **Fig. 4.38**. It was noticed that there was no remarkable difference in oil recovery between the fractured and unfractured cores. However, the oil production rate is slightly lower in the fractured core and water breakthrough was earlier. This is because, unlike $CO_2$, water is a wetting phase which allowed for better imbibition in the core's matrix and better contact with the core's oil than $CO_2$. The pressure profile for this experiment is illustrated in **Fig. 4.39**. The differential pressure showed some oscillations early in the experiment until about 0.5 PV injected, and then it was almost constant throughout the run at about 6 psi. This is because of the two phase movement in the fracture and matrix, until mostly water was being produced resulting in higher relative permeability to water.

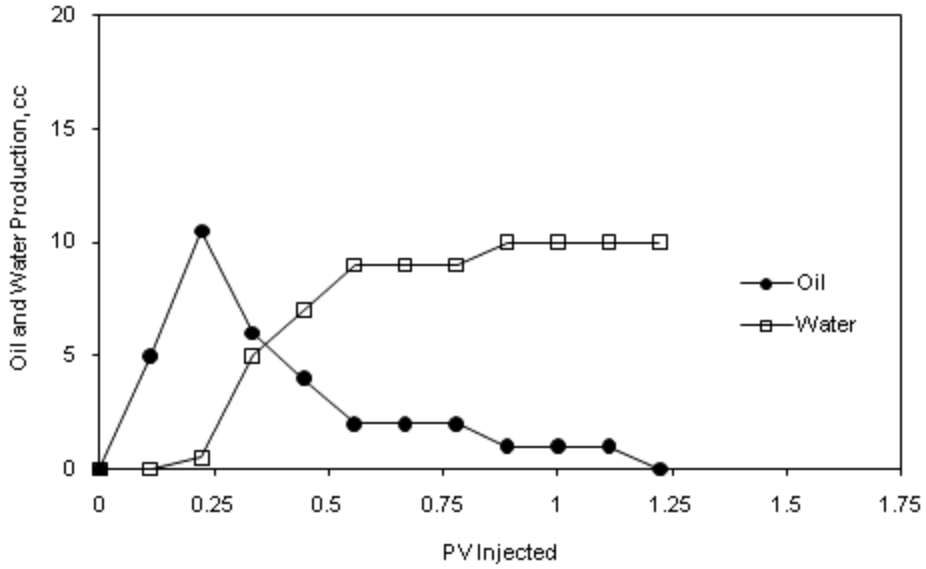


Fig. 4.38— WF (one-fracture): oil and water production rates

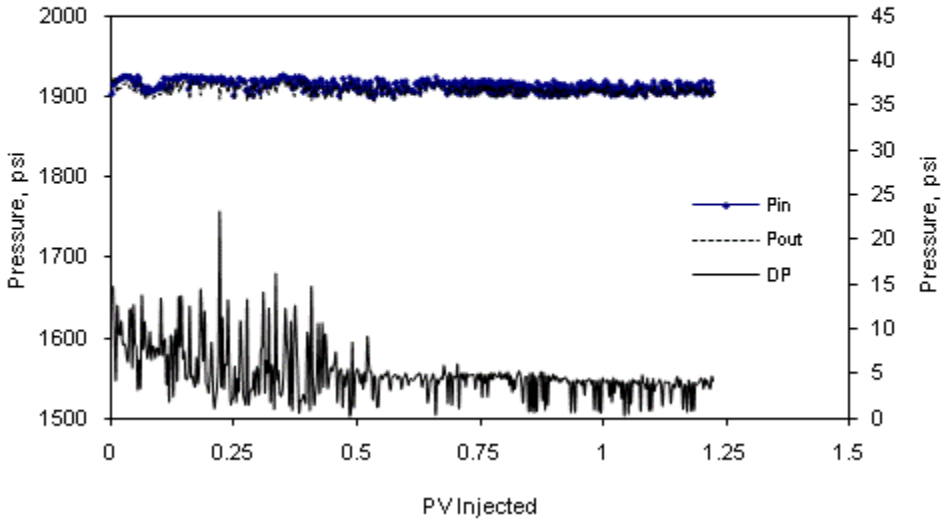


Fig. 4.39— WF (one-fracture): pressure profile

Shown in **Fig. 4.40** is waterflood cumulative oil production. The total produced oil at the end of the run (220 mins and 1.2 PV) is 34.5 $cm^3$, representing 47.26 % of the original oil in place (OOIP). This is only 7% decrease from the unfractured case indicating good imbibition of the water in the matrix compared to the $CO_2$.

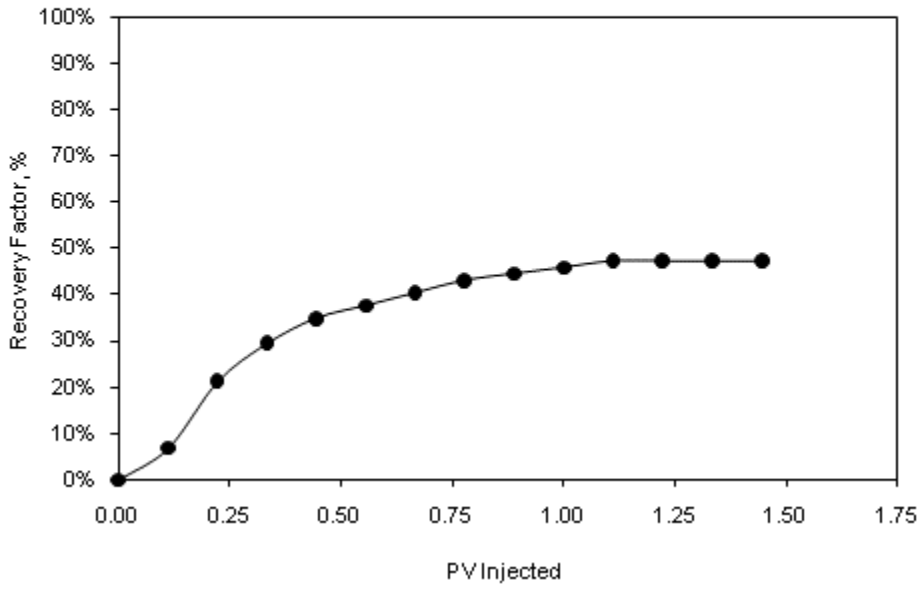


Fig. 4.40— WF (one-fracture): cumulative oil recovery

#### 4.4.1.4 CGI after WF (Tertiary Mode) in a One-fracture Core

This run followed directly the fresh waterflood in the fractured core. It involves injecting $CO_2$ continuously into the waterflooded core with one fracture (tertiary recovery mode) until ultimate recovery is reached. It was observed during this run that oil production is delayed as shown in **Fig. 4.41**. However, the oil production started earlier than the unfractured core. Initially, only water was produced until $CO_2$ breakthrough, then oil production commenced. Moreover, the presence of water delayed the $CO_2$ breakthrough to 57 minutes compared to secondary mode injection in fractured core; however it is still 36.5 min. earlier than the unfractured core. The differential pressure across the core is illustrated in **Fig. 4.42**. It shows that pressure starts very high at around 12 psi until $CO_2$ breakthrough then drops down to 5 psi.

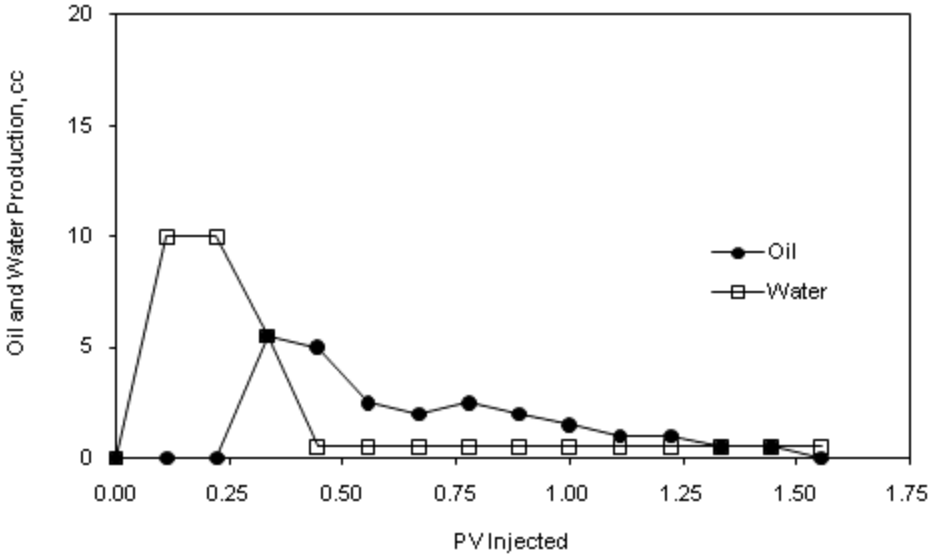


Fig. 4.41— Tertiary CGI (one-fracture): oil and water production rates

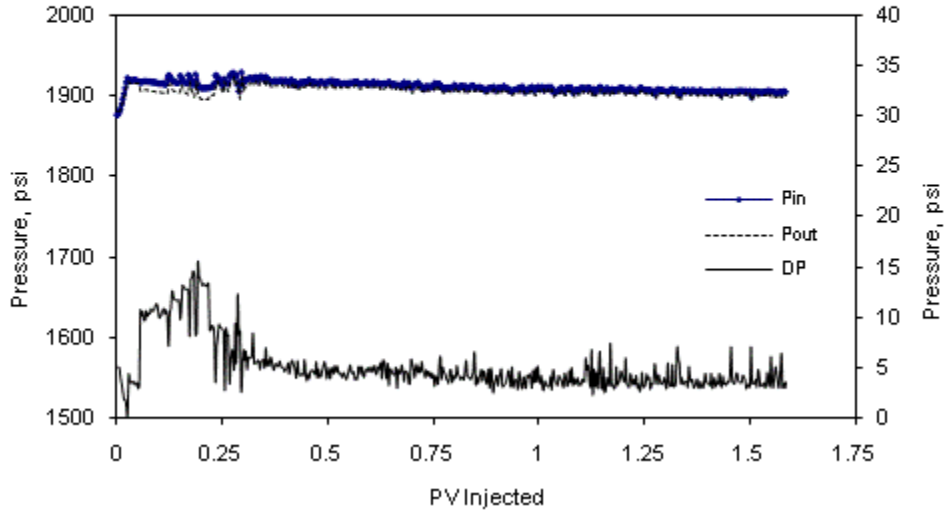


Fig. 4.42— Tertiary CGI (one-fracture): pressure profile

Shown in **Fig. 4.43** is the CGI cumulative fluid recovery. The total produced oil at the end of the run (260 mins and 1.44 PV) is 24 $cm^3$, representing 32.9% of the original oil in place (OOIP) and 62.34% of remaining oil in place (OIP) after waterflood. The cumulative produced $CO_2$ at standard conditions is 36.6 Liters at the end of the run with $CO_2$ breakthrough at 57 min (0.32 PV).

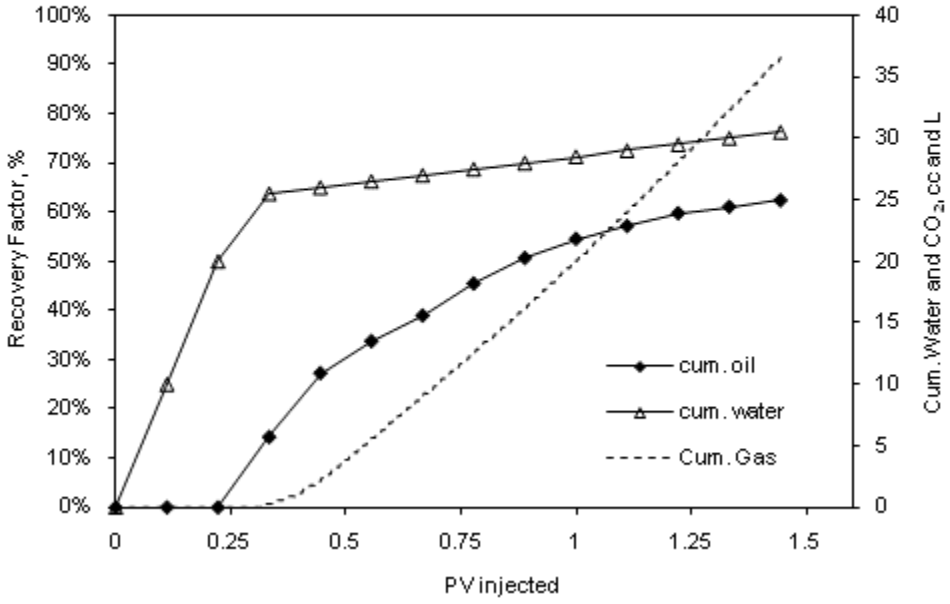


Fig. 4.43— Tertiary CGI (one-fracture): cumulative oil, water and $CO_2$ recovery

#### 4.4.1.5 WAG Injection in a One-fracture Core

This run involves injecting $CO_2$ in alternating cycles with fresh water into a core with one fracture (secondary recovery mode) until ultimate recovery is reached. The production rates and pressure profile are shown in **Figs. 4.44** and **4.45**, respectively. Sever pressure increase during the water cycle was not observed during this run because of the fracture. Shown in **Fig. 4.46** is the WAG cumulative oil and gas production. The total produced oil at the end of the run (340 mins and 1.87 PV) is 53 $cm^3$, representing 70 % of the original oil in place (OOIP). The cumulative produced $CO_2$ at standard conditions is 30 Liters at the end of the run with $CO_2$ breakthrough at 15 min (0.082 PV).

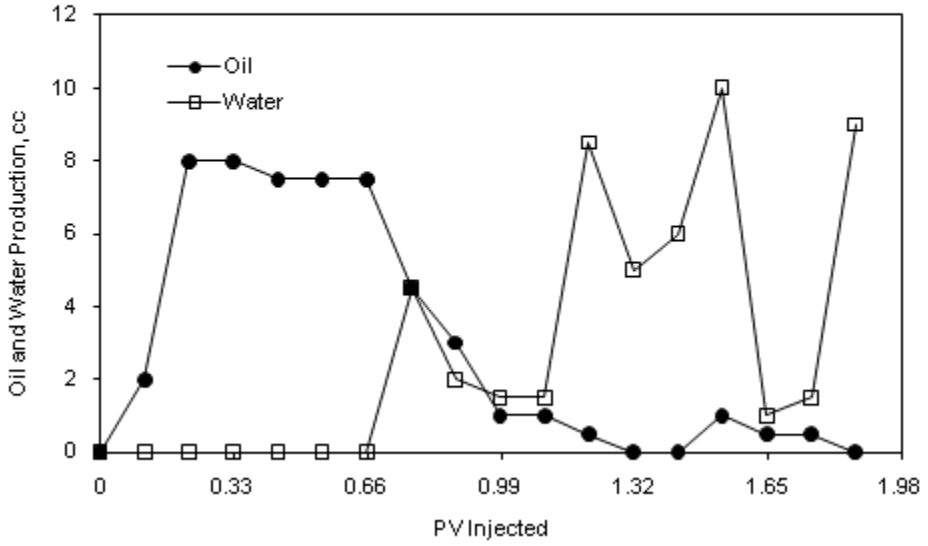


Fig. 4.44— WAG (one-fracture): oil and water production rates

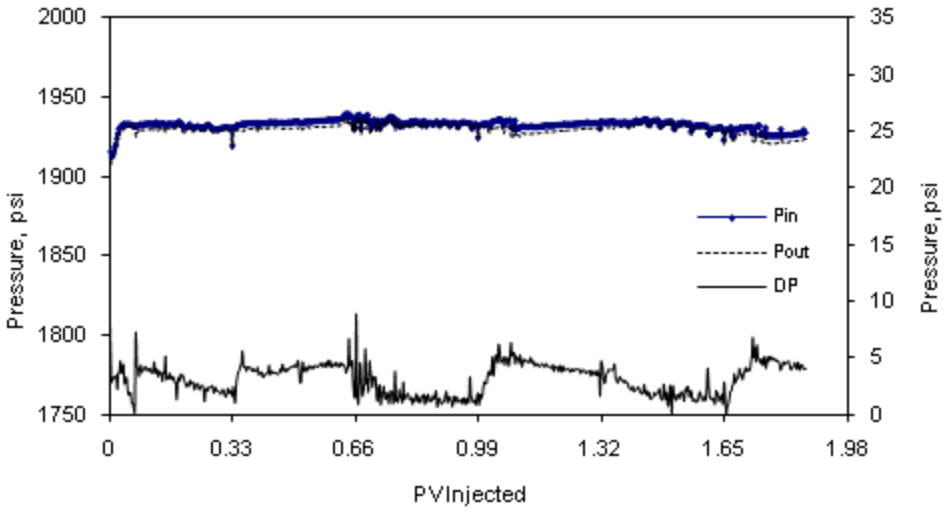


Fig. 4.45— WAG (one-fracture): pressure profile

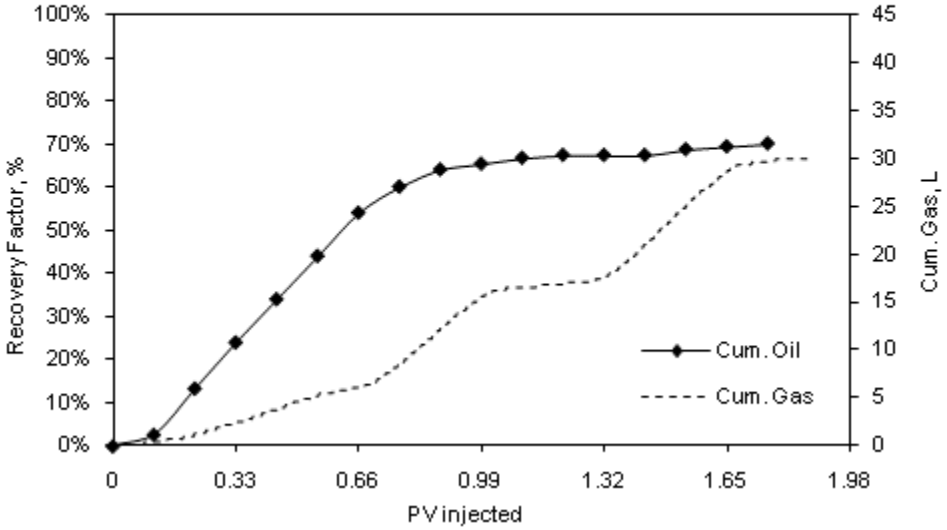


Fig. 4.46— WAG (one-fracture): cumulative oil and $CO_2$ recovery

#### 4.4.1.6 SWAG Injection in a One-fracture Core

This run involves injecting $CO_2$ and fresh water simultaneously into a core with one fracture until ultimate recovery is reached. Production rates and pressure profile are shown in **Figs. 4.47** and **4.48**, respectively. The water breakthrough occurred earlier than the unfractured core while the pressure profile shows higher differential pressure at the beginning of the experiment until water breakthrough, and then becomes constant at about 5 psi. Shown in **Fig. 4.49** is SWAG cumulative oil and gas production. The total produced oil at the end of the run (300 mins and 1.66 PV) is 53 $cm^3$, representing 71.6 % of the original oil in place (OOIP). The cumulative produced $CO_2$ at standard conditions is 23.1 Liters at the end of the run with $CO_2$ breakthrough at 14.5 min (0.08 PV).

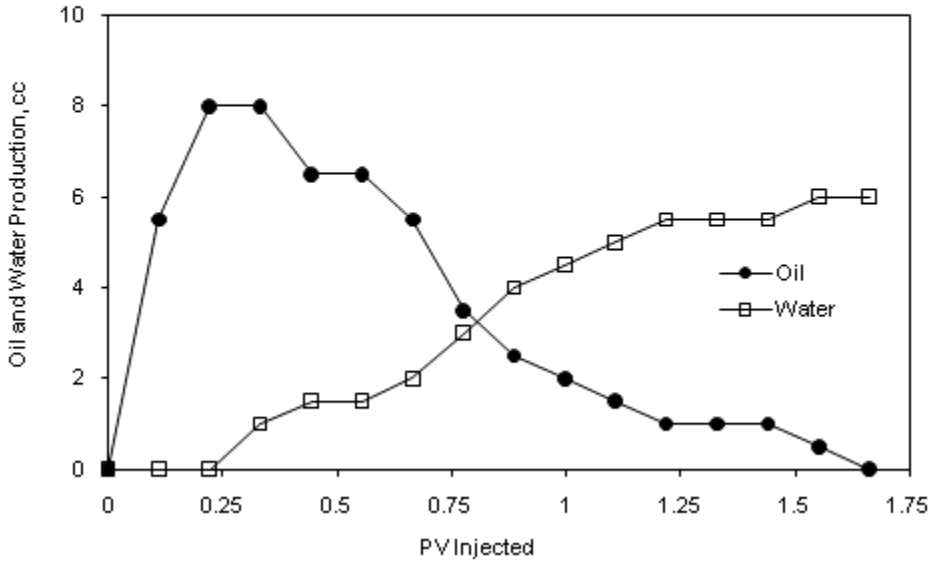


Fig. 4.47— SWAG (one-fracture): oil and water production rates

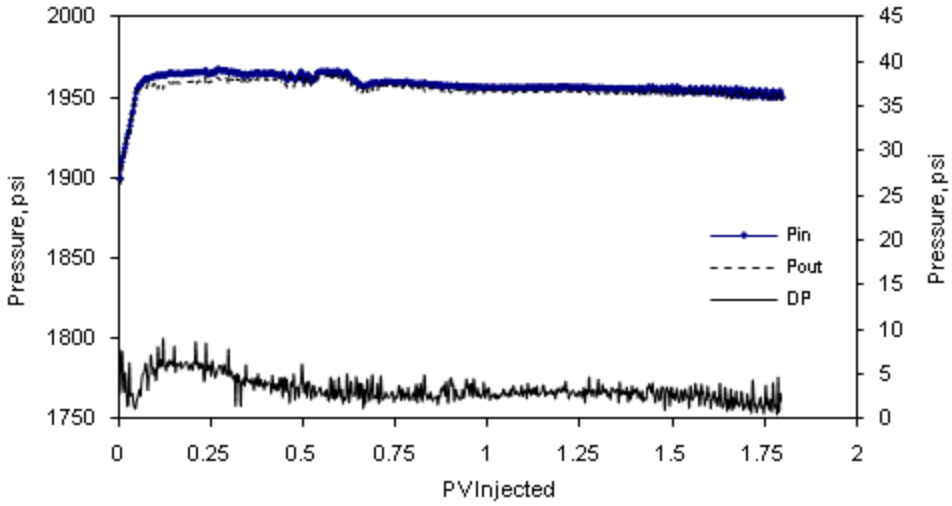


Fig. 4.48— SWAG (one-fracture): pressure profile

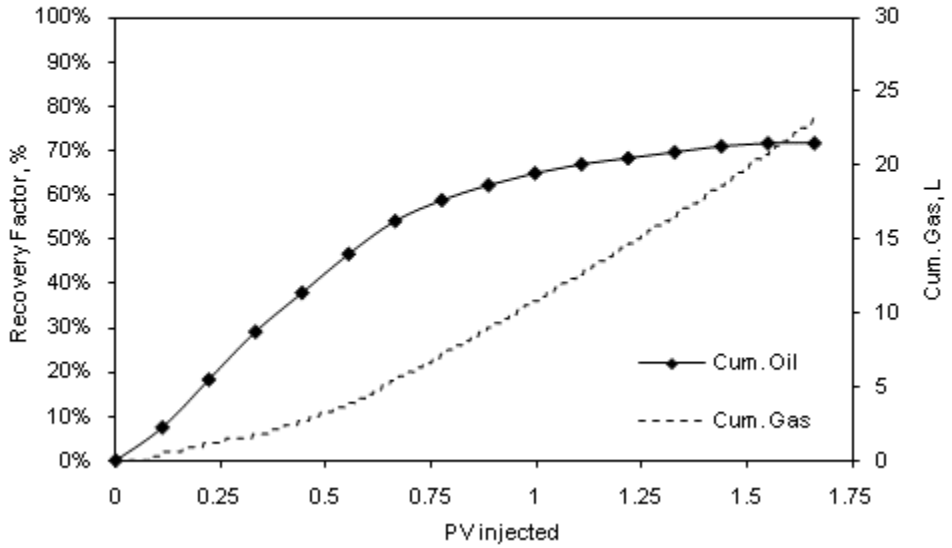


Fig. 4.49— SWAG (one-fracture): cumulative oil and $CO_2$ recovery

### 4.4.2 Horizontal and Vertical Fractures (Two Fractures)

During this set of experiments, two fractures were artificially created on the core. One horizontal fracture is created along the length of the core connecting the inlet and outlet. Then, another fracture (vertical) was created perpendicular to the previous fracture. This case creates a sugar cube model with four matrix blocks and two fracture planes. The water used in these experiments is fresh water to enable precise comparison to the base case. The core is fully saturated with oil at the beginning of each run which means the corefloods are conducted at a secondary recovery mode. Four injection modes were evaluated on this shape factor: CGI, WF after CGI (tertiary recovery mode), WAG, and SWAG. Each injection mode is presented as a subsection in this chapter.

#### 4.4.2.1 CGI in a Two-fracture Core

This run involves injecting $CO_2$ continuously into oil saturated core with two fractures until ultimate recovery is reached. The oil production is shown in **Fig. 4.50** and it follows the same trend as the previous cases of CGI. The difference is that the drop in oil production is less severe than the one-fracture case. This indicates that more matrix oil was produced than the one fracture case because of the vertical fracture in the middle. The pressure profile of this experiment is illustrated in **Fig. 4.51.** It shows that differential pressure is almost constant throughout the run at about 5 psi.

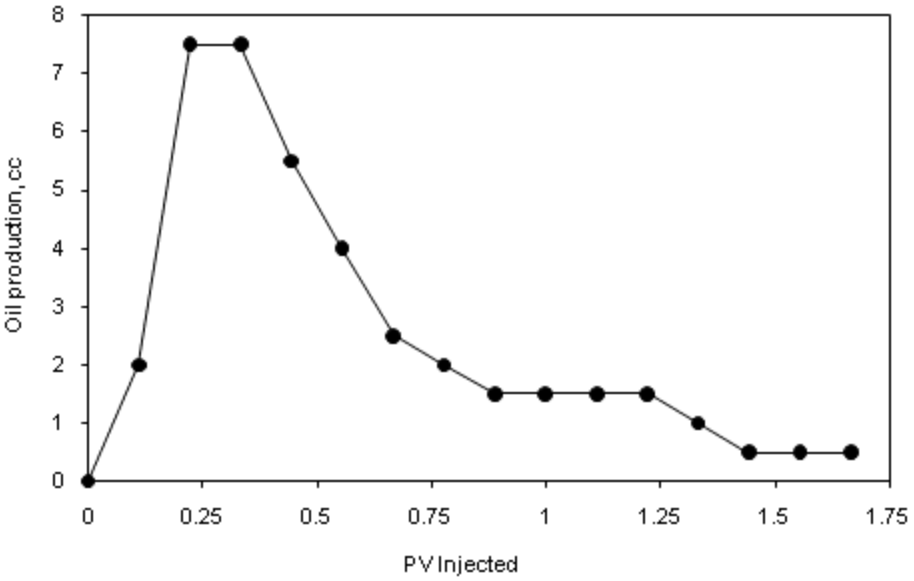


Fig. 4.50— CGI (two-fracture): oil production rate

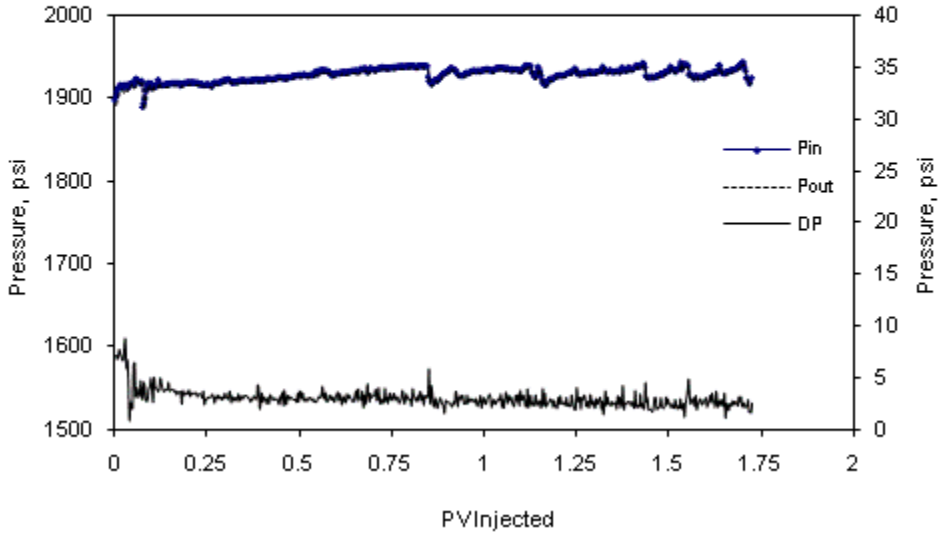


Fig. 4.51— CGI (two-fracture): pressure profile

Shown in **Fig. 4.52** is the CGI cumulative fluid recovery for the core with two fractures. The total produced oil at the end of the run (300 mins and 1.66 PV) is 39.5 $cm^3$, representing 54.86 % of the original oil in place (OOIP). The cumulative produced $CO_2$ at standard conditions is 50.1 Liters at the end of the run with $CO_2$ breakthrough at 14 min (0.078 PV).

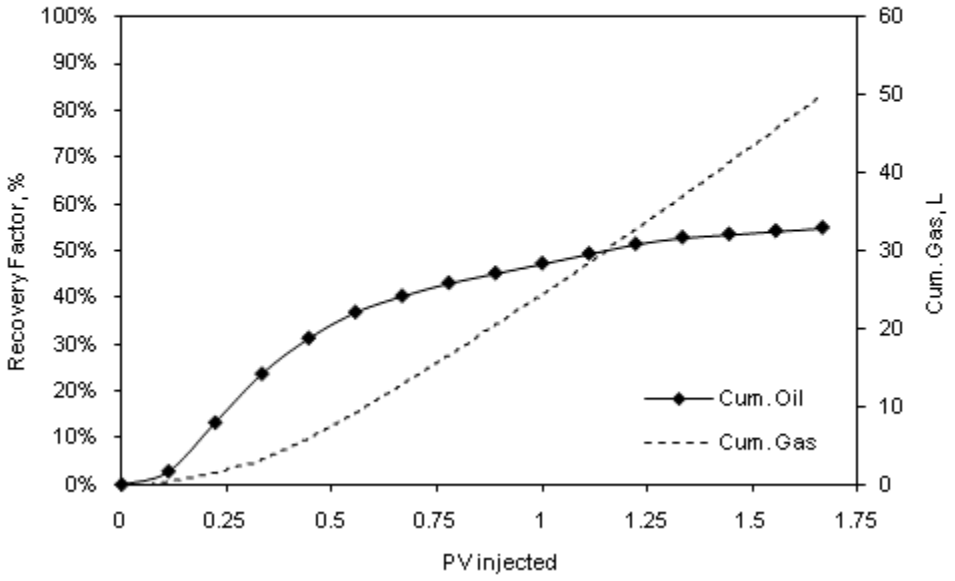


Fig. 4.52— CGI (two-fracture): cumulative oil and $CO_2$ recovery

#### 4.4.2.2 WF after CGI in a Two-fracture Core

Water is injected immediately after the continuous gas injection (CGI) run (tertiary recovery WF). The objective of this injection is to evaluate how much bypassed oil can be produced when injecting a wetting phase in the presence of the fractures.

Shown in **Fig. 4.53** is the WF after CGI cumulative fluid recovery. The total produced oil at the end of the run (180 mins and 1.0 PV) is 15 $cm^3$; representing 21.13 % of the original oil in place (OOIP) and 47.62 % of the remaining oil in place (OIP) left after CGI. This brings the total recovery from both injection modes (CGI and WF) to 76.76 % of the OOIP. The total produced $CO_2$ at standard conditions is 11.1 Liters. The production of $CO_2$ was increasing at a constant rate until the start of oil production. This may have caused the delay in oil production until about 0.25 PV. This was evident from the increase in the differential pressure across the core until 0.25 PV injected and then it becomes constant as shown in **Fig. 4.54.** This indicates that the rock's relative permeability to water is low after the $CO_2$ injection until the oil is mobilized.

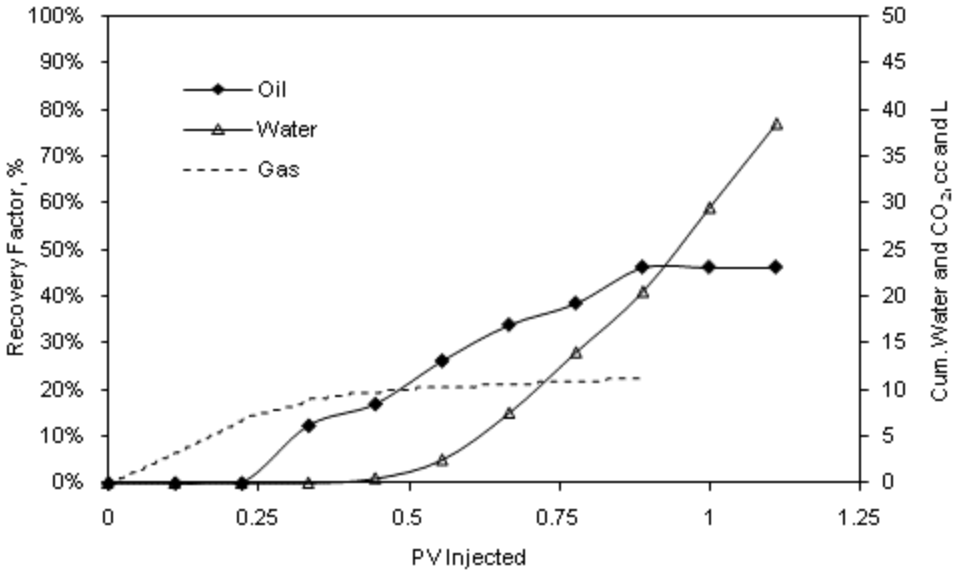


Fig. 4.53— WF after CGI (two-fracture): cumulative oil, water and $CO_2$ recovery

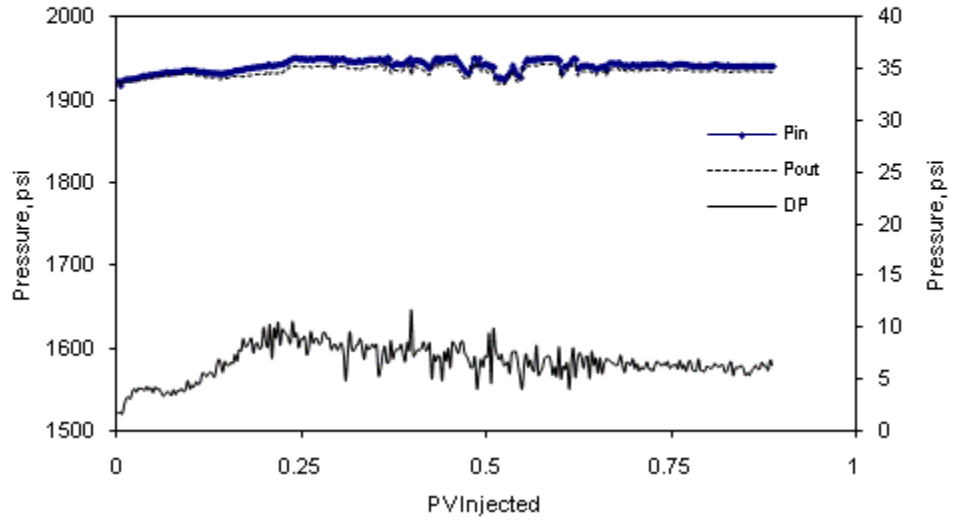


Fig. 4.54— WF after CGI (two-fracture): pressure profile

### 4.4.2.3 WAG Injection in a Two-fracture Core

This run involves injecting $CO_2$ in alternating cycles with fresh water into oil saturated core with two fractures until ultimate recovery is reached. The production rates and pressure profile are shown in **Figs. 4.55** and **4.56**, respectively. Pressure increase during the water cycle was less severe than the unfractured core. However, pressure oscillations were noticed during water breakthrough. Shown in **Fig. 4.57** is the WAG cumulative oil and gas production. The total produced oil at the end of the run (340 mins and 1.86 PV) is 58 $cm^3$, representing 79.86 % of the original oil in place (OOIP). The cumulative produced $CO_2$ at standard conditions is 30.6 Liters at the end of the run with $CO_2$ breakthrough at 35 min (0.19 PV).

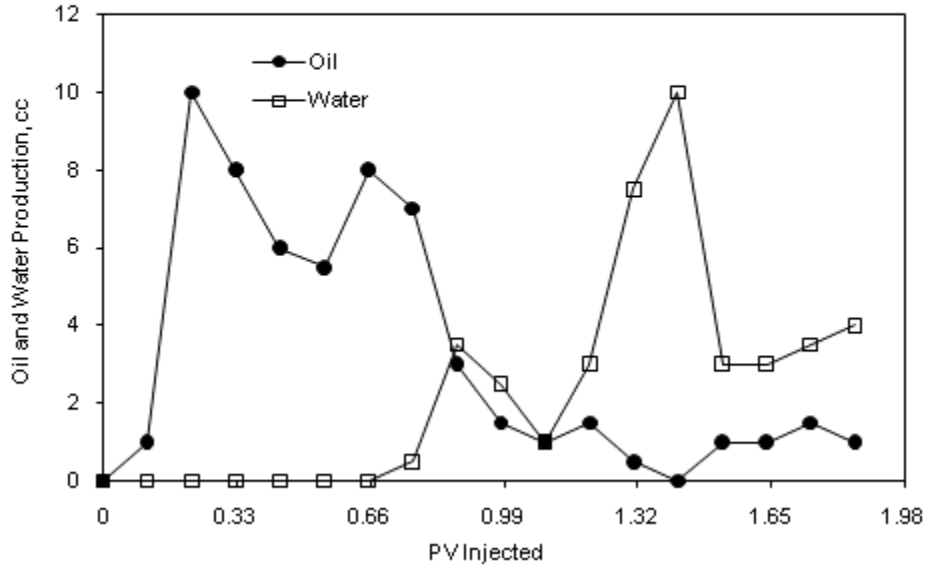


Fig. 4.55— WAG (two-fracture): oil and water production rates

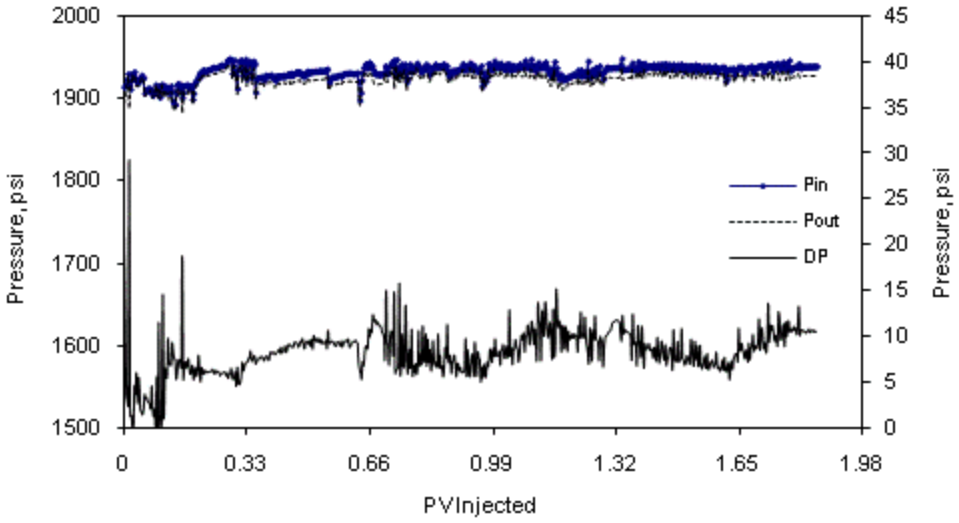


Fig. 4.56— WAG (two-fracture): pressure profile

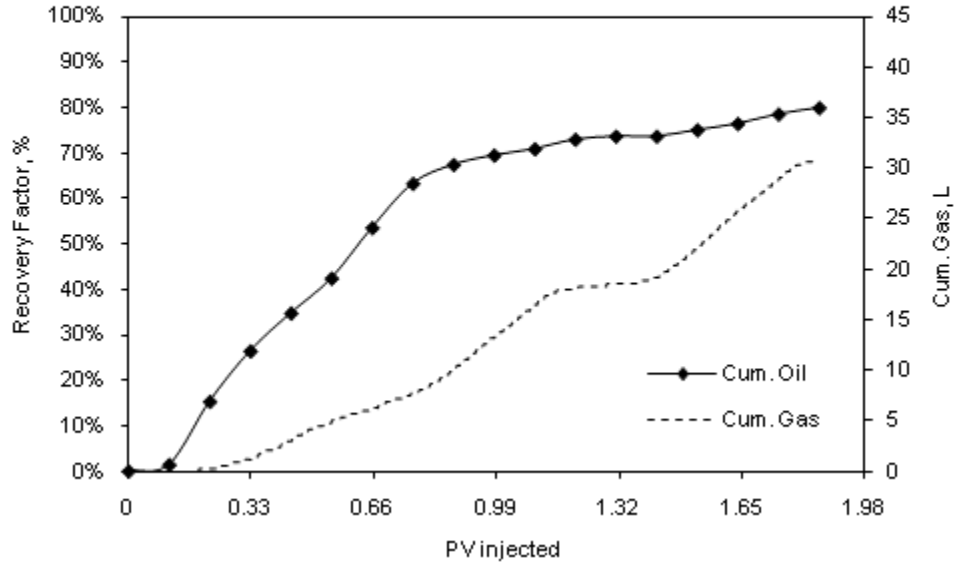


Fig. 4.57— WAG (two-fracture): cumulative oil and $CO_2$ recovery

#### 4.4.2.4 SWAG Injection in a Two-fracture Core

This run involves injecting $CO_2$ and fresh water simultaneously into oil saturated core with two fractures until ultimate recovery is reached. Production rates and pressure profile are shown in **Figs. 4.58** and **4.59**, respectively. The differential pressure shows slight pressure oscillation at water breakthrough, and then becomes constant at about 4 psi. Shown in **Fig. 4.60** is SWAG cumulative oil and gas production. The total produced oil at the end of the run (300 mins and 1.68 PV) is 57 $cm^3$, representing 79.16 % of the original oil in place (OOIP). The cumulative produced $CO_2$ at standard conditions is 24.3 Liters at the end of the run with $CO_2$ breakthrough at 24.5 min (0.137 PV).

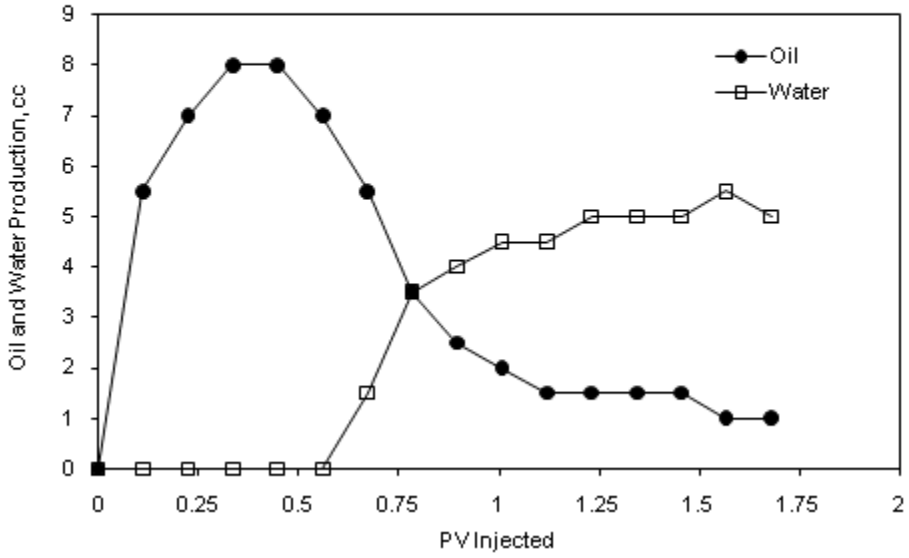


Fig. 4.58— SWAG (two-fracture): oil and water production rates

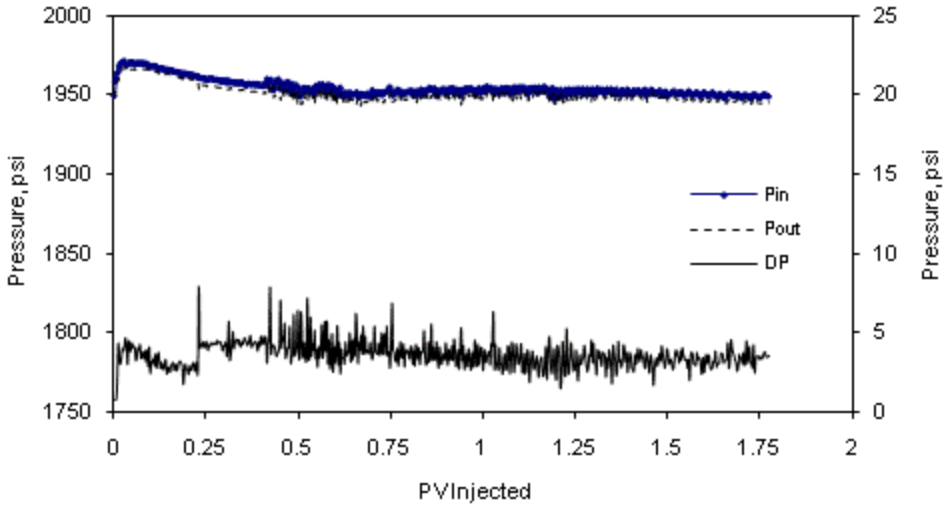


Fig. 4.59— SWAG (two-fracture): pressure profile

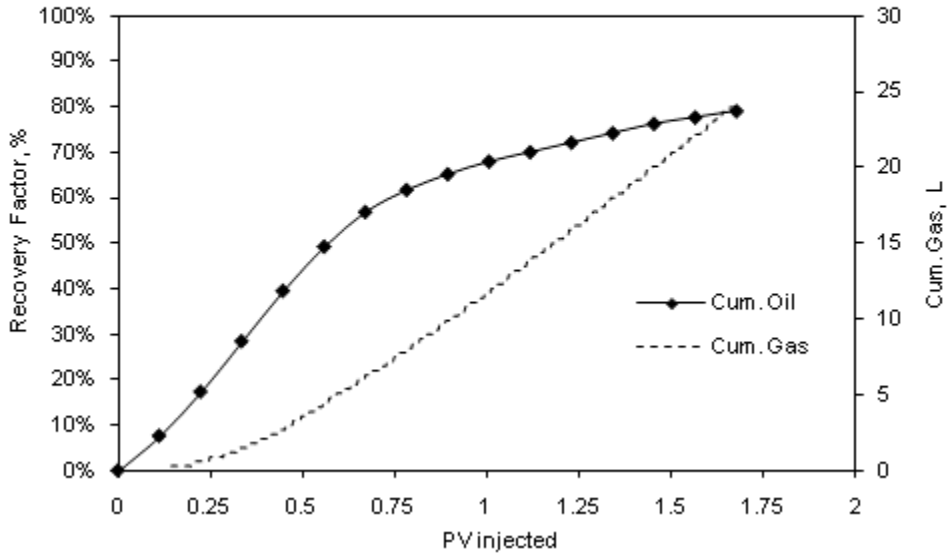


Fig. 4.60— SWAG (two-fracture): cumulative oil and $CO_2$ recovery

## 4.5 Comparison and Discussion of the Experimental Results

This section will compare the results obtained from the coreflood experiments. The first comparison is between the different injection modes during the base case. The objective of this comparison is to provide general characteristics of each injection mode, quantify cumulative fluid recoveries, and compare the amounts of used $CO_2$. The base case will serve as a base line for each injection mode for precise comparison.

The objective of the second comparison is to investigate the effect of altering the water salinity on each injection mode and it will be compared to the base case. The third comparison will evaluate the effect of fractures (extreme heterogeneity) on each injection mode and will be compared to the base case. Finally, all injection modes will be compared to each other during the presence of fractures to quantify the effect of fractures on ultimate oil recovery during each injection mode.

### 4.5.1 Base Case (Evaluation of Different Injection Modes)

The results of the base case are discussed in Section 4.2 in this chapter. It has been shown that injection modes in decreasing order of oil recovery are as follows: SWAG, WAG, CGI and WF. Cumulative oil and water recoveries for all $CO_2$ injection modes are shown in **Fig. 4.61** and cumulative $CO_2$ production is shown **Fig. 4.62**. The displacement efficiency of all $CO_2$ injection modes has shown better results than WF because of the low IFT between the injected $CO_2$ and the core's oil during miscible injection. The WF has resulted in very poor recovery (54 % of OOIP). On the other hand, SWAG and WAG injections have shown excellent ultimate oil recoveries (>90%) with significant reduction in the amount of injected $CO_2$ compared to CGI. The decrease in the amount of injected $CO_2$ is quantified to be 40% and 60% during WAG and SWAG, respectively. This will have significant impact on the economics during field applications. When comparing the two premium injection modes, WAG and SWAG, the latter has shown higher oil recoveries, less $CO_2$ requirements and better pressure profile which indicates better injectivity.

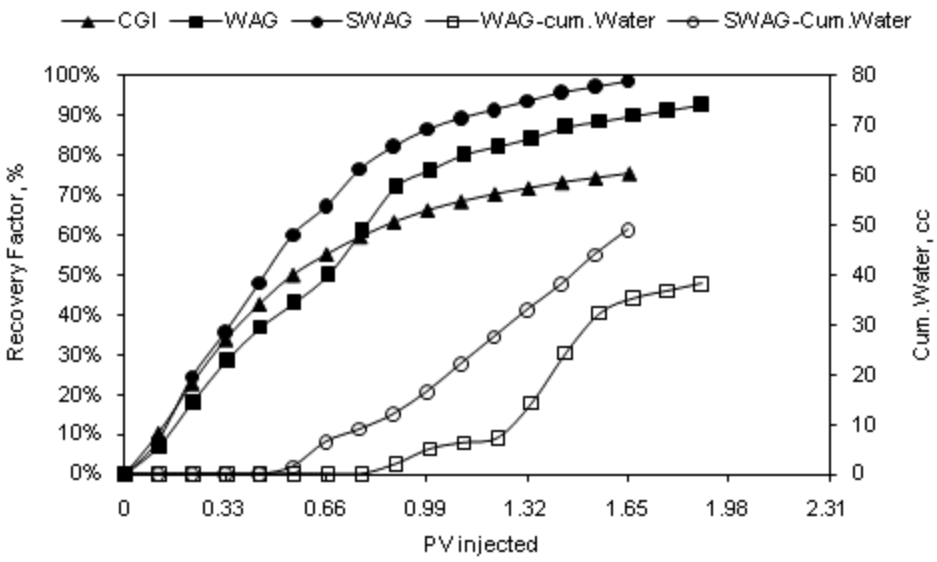


Fig. 4.61— Base Case: cumulative oil recovery and water production comparison between all injection modes

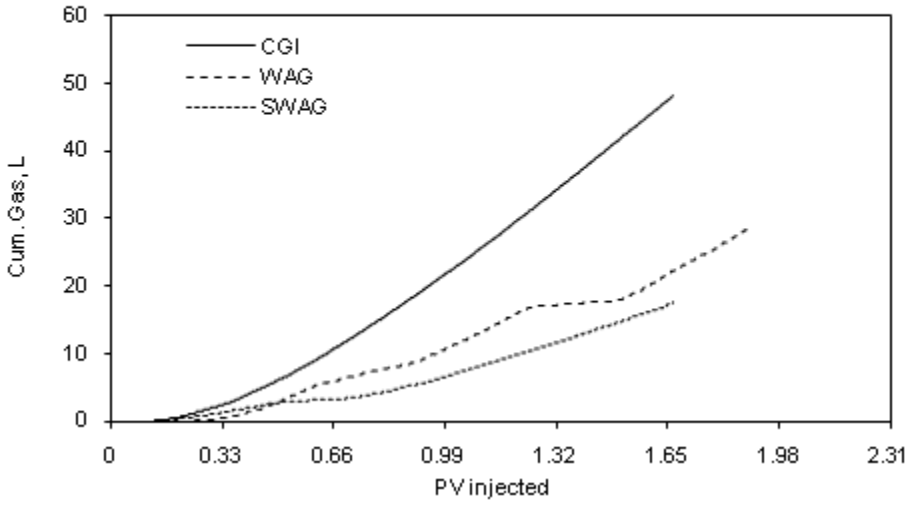


Fig. 4.62— Base Case: $CO_2$ cumulative production comparison between all injection modes

Continuous $CO_2$ injection (CGI) was conducted at both secondary and tertiary modes and the results are compared in **Fig. 4.63**. Secondary injection clearly resulted in higher recovery (10%) when comparing the results of $CO_2$ injection alone.

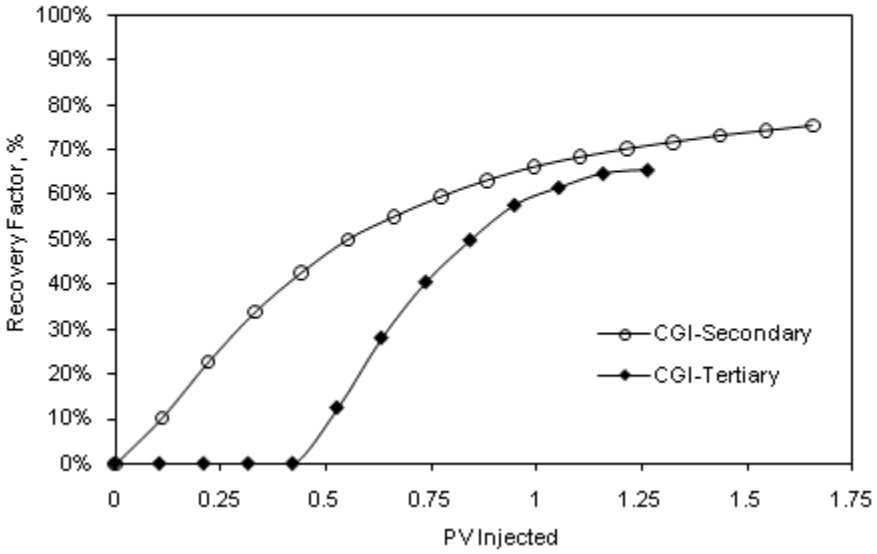


Fig. 4.63— Comparison between CGI in secondary and tertiary modes

However, when combining the total recovery of both WF followed by $CO_2$, the ultimate recovery in this case (tertiary recovery) is 8% higher than CGI in secondary mode as shown in **Fig. 4.64**. One point to consider in the latter case though is the delay in the timing of the increase in recovery. Therefore, operators should consider both the time of first oil production and the ultimate recovery when designing $CO_2$ injection projects.

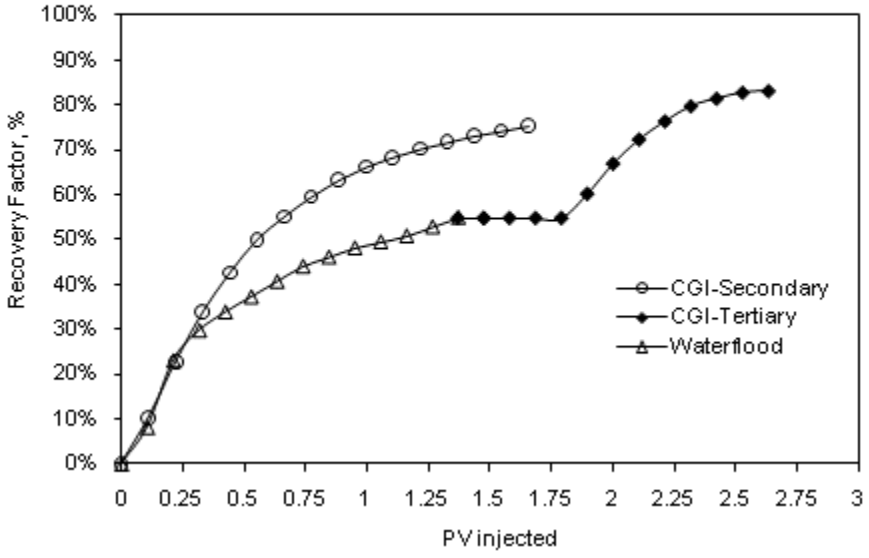


Fig. 4.64— Comparison between CGI in secondary and tertiary modes considering both WF and CGI tertiary recovery

### 4.5.2 Salinity Effect ($CO_2$ Solubility in Water)

This section compares the results of the experimental runs discussed in Section 4.3 in this chapter to the base case results. WF, WAG, and SWAG have used different water salinity levels. Therefore, their results were compared to the base case which uses fresh water (0 wt. %).

The increase of $CO_2$ solubility in water has been considered a loss in $CO_2$ where it cannot be available to contact oil. However, the results of this experimental study indicate otherwise. For this carbonate rock, CGI has resulted in bypassed oil. Also, when WAG and SWAG injections were implemented at all salinity levels, an increase in recovery was realized with significant reduction in $CO_2$ requirement. This indicates that the $CO_2$-water mixture that follows the $CO_2$ slug at the displacement front was successful in contacting the bypassed oil after the $CO_2$. Therefore, an increase in $CO_2$ dissolved in water made this mixture more effective in increasing oil recovery.

The first salinity change was conducted on WF alone. The objective of this step is to verify that the change in salinity during WF alone has no effect on oil recovery. This will consequently indicate that any change on oil recovery during WAG and SWAG injections can be attributed to the $CO_2$ solubility in water. **Fig. 4.65** shows the cumulative oil recovery comparison between 0 wt. % (fresh water) and 6 wt. % (saline water). **Fig. 4.66** shows water cut comparison between the two salinities.

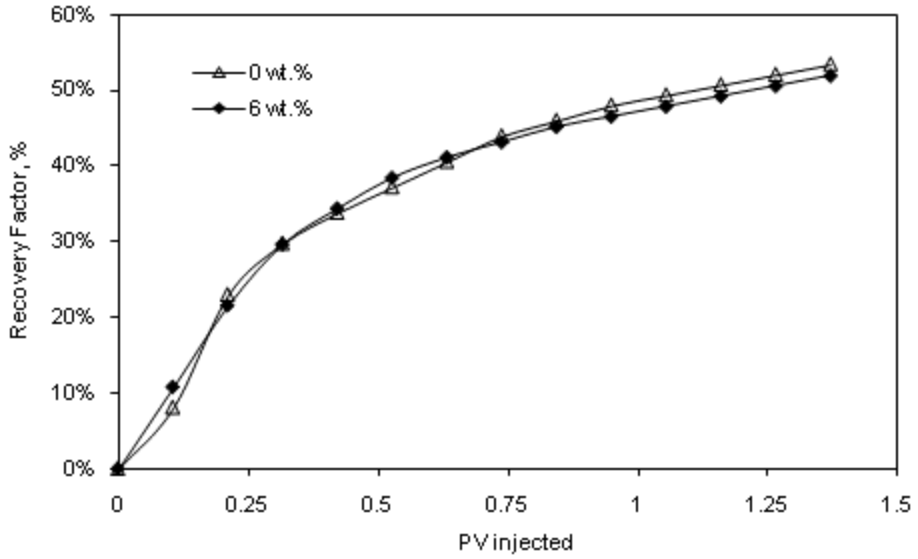


Fig. 4.65— WF cumulative oil recovery comparison between two salinity levels

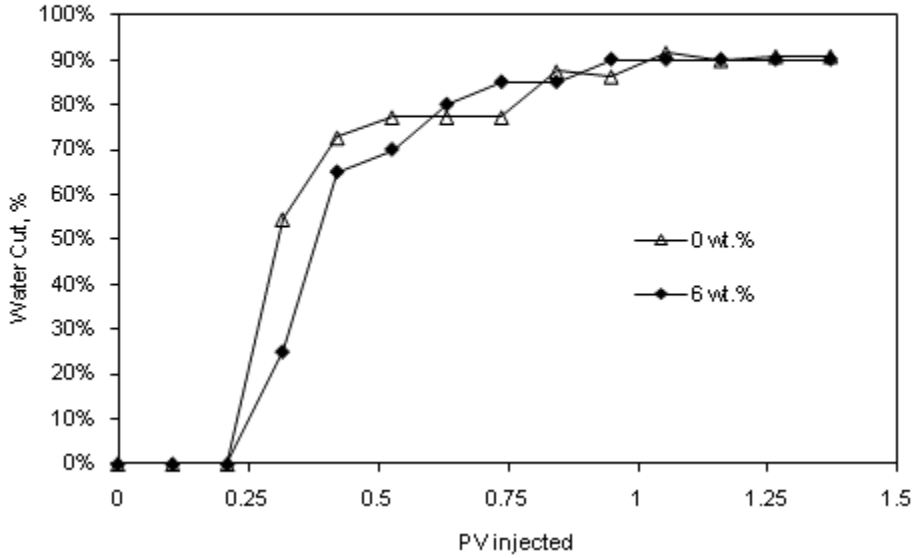


Fig. 4.66— WF water cut comparison between two salinity levels

Clearly, the two experimental runs were identical and the salinity change has no effect on oil recovery on those carbonate rocks. Many publications (Pu et al. 2008; Sharma and Filoco 2000) have shown that altering water salinity has no effect on waterflood oil recovery. On the other hand, some researchers have indicated that altering water salinity can have a major impact on oil recovery only in the presence of clays (Skrettingland et al. 2010; Yildiz et al. 1999). Other researchers (Fathi et al. 2010) have emphasized on the importance of active ions such $Ca^{2+}$, $Mg^{2+}$, and $SO_4^{2-}$ in the injected water to create an effect on oil recovery. They also indicated that test temperature above 90° C is essential for the effect to be significant. None of these factors are applicable in this study. Specifically, the salt used here is monovalent cation ($Na^{+}$) and the rock is a limestone core consisting of pure calcite and contains no evidence of clays (Chapter III, Section 3.3.3). Therefore, no change was expected from the WF alone and any change in oil recovery during the subsequent salinity alterations will be solely attributed to the $CO_2$ solubility in water.

WAG and SWAG oil recoveries on the other hand, have shown a significant dependence on water salinity. Two salinity levels were considered for those injection modes: 6 wt. % and 20 wt. % and their results were compared to the base case (0 wt. %). **Fig. 4.67** shows a comparison of cumulative oil recovery and water production for all salinity levels during WAG injection. The results of these different salinity levels indicate that oil recovery increased with decreasing salinity. This mechanism was attributed to the increase of $CO_2$ solubility in water with decreasing salinity (**Fig. 4.25**). The oil recovery at 0 wt. % salt content was measured to be 92.7% OOIP. When water salinity increased to 6 wt. % salt content, the oil recovery was measured to be 86.5% OOIP which is a 6% decrease. At 20 wt. % salt content, the oil recovery was measured to be 74.3% OOIP which is 18% decrease compared to the base case.

**Fig. 4.68** shows the cumulative $CO_2$ production at standard condition for all salinity levels. It is clear that with the increase in salinity (decrease in $CO_2$ solubility in water), an increase in $CO_2$ production is realized at the outlet.

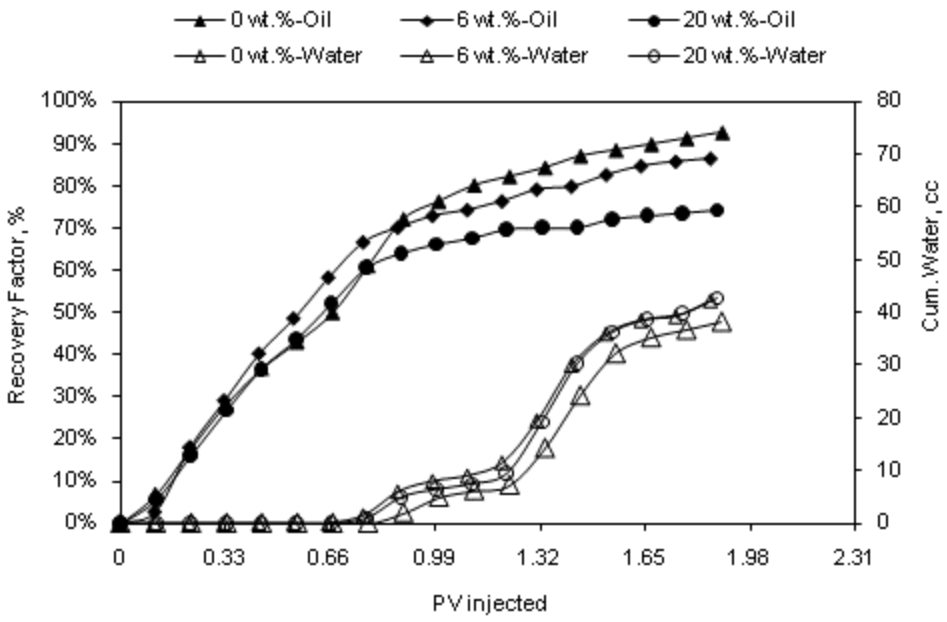


Fig. 4.67— WAG cumulative oil recovery and water production comparison between three salinity levels

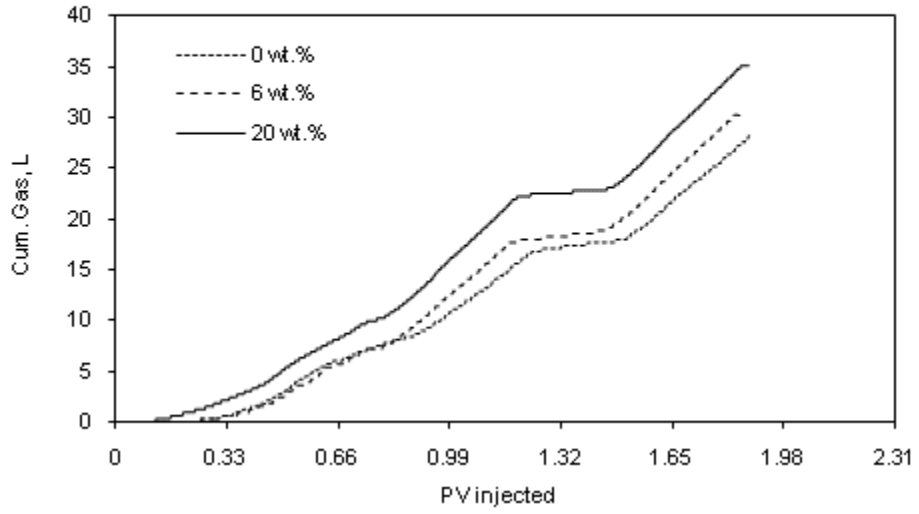


Fig. 4.68— WAG cumulative $CO_2$ production comparison between three salinity levels

SWAG oil recovery has also shown a significant dependence on water salinity. Similar to WAG, two salinity levels were considered for this injection mode: 6 wt. % and 20 wt. % and their results were compared to the base case (0 wt. %). **Fig. 4.69** shows a comparison of cumulative oil recovery and water production for all salinity levels. The results of these different salinity levels showed the same trend seen on WAG oil recovery; the oil recovery increased with decreasing salinity.

During this injection mode, the oil recovery at 0 wt. % salinity level was measured to be 98.6% OOIP. When the water salinity increased to 6 wt. % and 20 wt. %, the oil recoveries decreased to 90.7% and 81.5%, respectively. This corresponds to a decrease of 8% and 17% respectively with increasing water salinity.

**Fig. 4.70** shows the cumulative $CO_2$ production at standard condition for all salinity levels. Higher salinities resulted in higher cumulative produced $CO_2$. One striking fact seen on this figure is that the case of 20 wt. % shows a steeply rising cumulative $CO_2$ production with no flat regions. On the other hand, both cases of 0 and 6 wt. % cumulative $CO_2$ production have shown a flat region at around 0.5 PV (water breakthrough). The flat region in $CO_2$ cumulative production indicates that $CO_2$ is being dissolved in water at those salinity levels, whereas during higher salinity (20 wt. %), this mechanism vanishes.

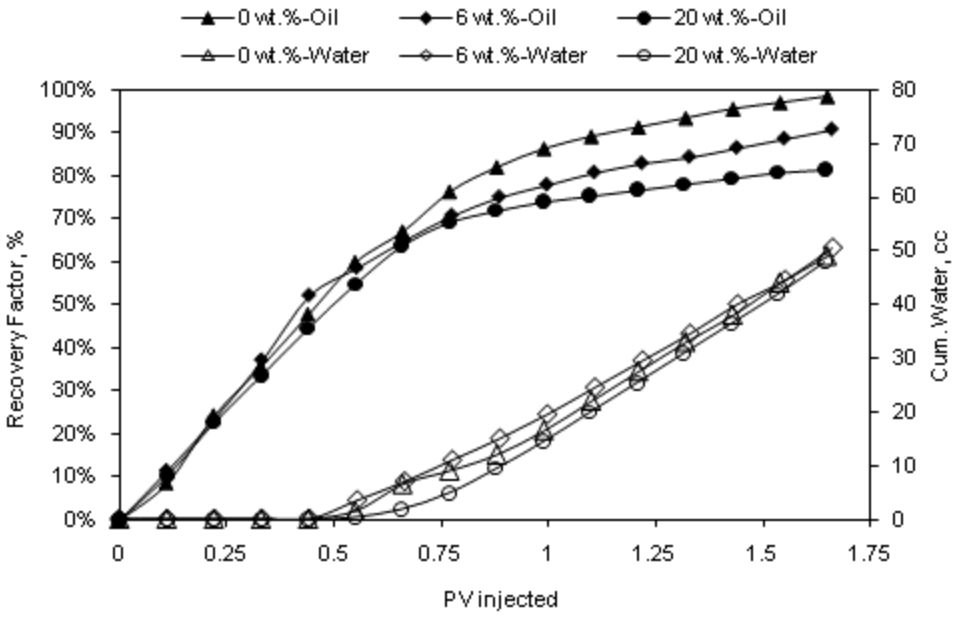


Fig. 4.69— SWAG cumulative oil recovery and water production comparison between three salinity levels

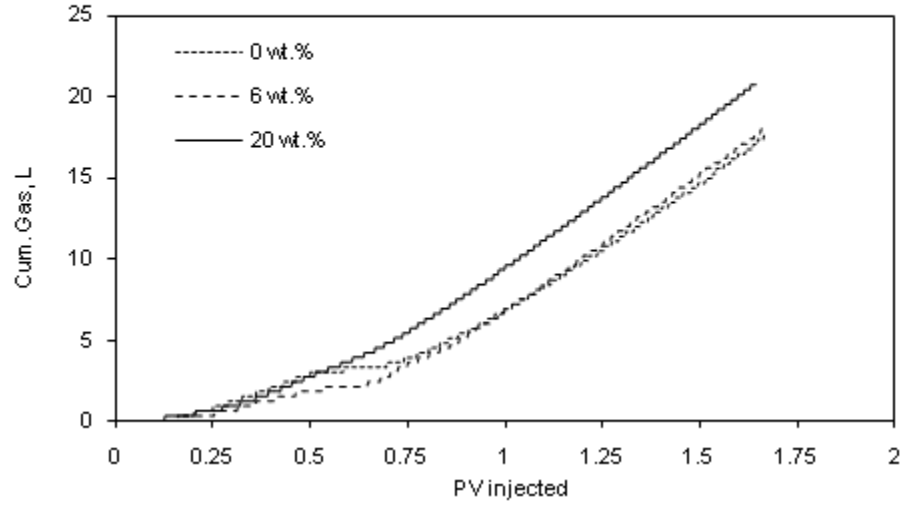


Fig. 4.70— SWAG cumulative $CO_2$ production comparison between three salinity levels

### 4.5.3 Fractured Cores

This section compares the results of the fractured core cases for each injection mode to the base case. For example, it will compare CGI in an unfractured core to the CGI in a core with one and two fractures. Then, it will compare the four injection modes: CGI, WAG, SWAG, and WF with and without fractures. This comparison will show how the fractures deteriorate the oil recovery during CGI, and then it will show how the oil recovery can be improved in fractured cases during WAG and SWAG.

Shown in **Fig. 4.71** is the CGI cumulative oil recovery comparison between the base case and the fractured cases. The base case CGI resulted in 75.37 % of the OOIP while the one-fracture and two-fracture cases resulted in 27.43% and 54.86% of OOIP, respectively. It is clear that CGI mode is greatly affected by the presence of fractures where $CO_2$ keeps cycling through the fracture with very low matrix invasion.

Shown in **Fig. 4.72** is the CGI cumulative $CO_2$ production for unfractured and fractured cases. The fractured cases have shown higher $CO_2$ production, earlier breakthrough, and more steeply rising $CO_2$ production profile (higher slope). The high slope indicates higher $CO_2$ production rate.

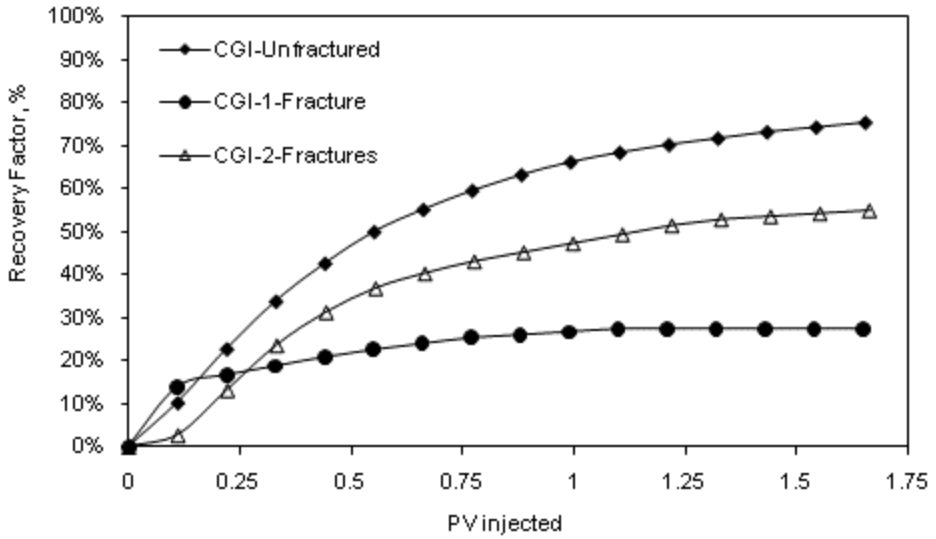


Fig. 4.71— CGI cumulative oil recovery comparison between unfractured and fractured cores

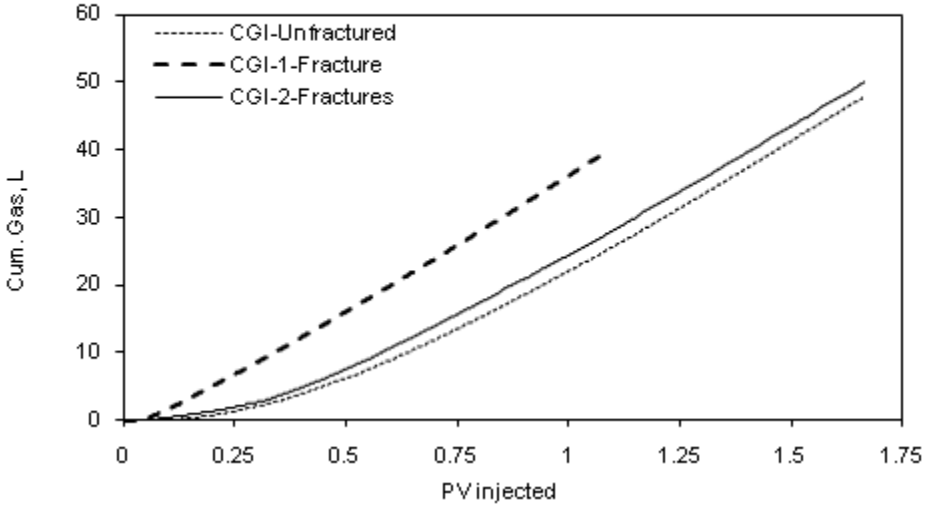


Fig. 4.72— CGI cumulative $CO_2$ production comparison between unfractured and fractured cores

Unlike $CO_2$, water has shown better matrix invasion and less decrease in oil recovery during the fractured case. This is because water is a wetting phase and it is expected to imbibe better in the matrix than $CO_2$. Shown in **Fig. 4.73** is the WF cumulative oil recovery comparison between the unfractured and fractured cases. The unfractured case resulted in 54.7 % while the fractured case resulted in 47.26 % of OOIP. This represents a decrease in recovery of 7.5% which is less severe than the decrease in recovery during the $CO_2$ injection.

**Fig. 4.74** shows the water cut comparison between unfractured and fractured cases. The fractured case resulted in an earlier water breakthrough and higher water production. The earlier breakthrough indicates that viscous forces dominate in the fractured case and there is less imbibition than the unfractured case (Guzman and Aziz 1992). This is caused by the high flow of water in the fracture than in the matrix.

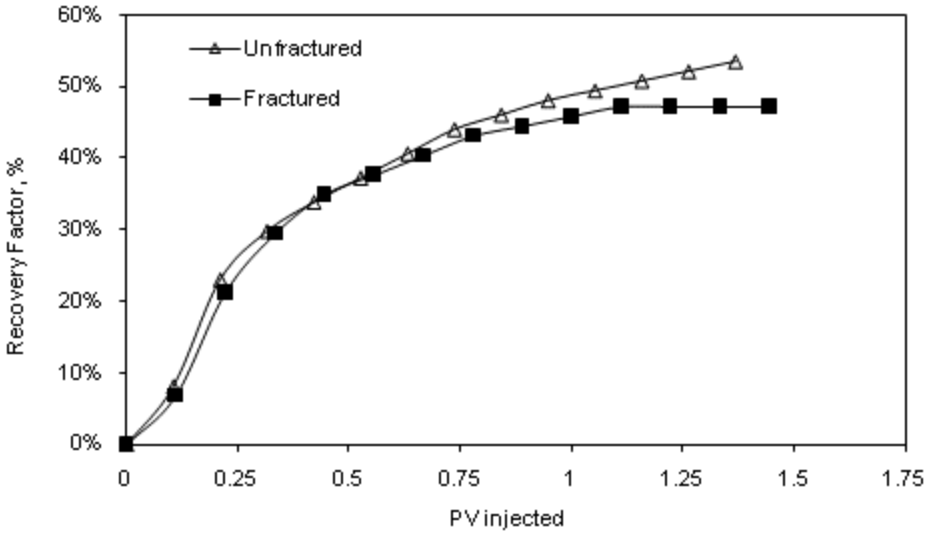


Fig. 4.73— WF cumulative oil recovery comparison between unfractured and fractured cores

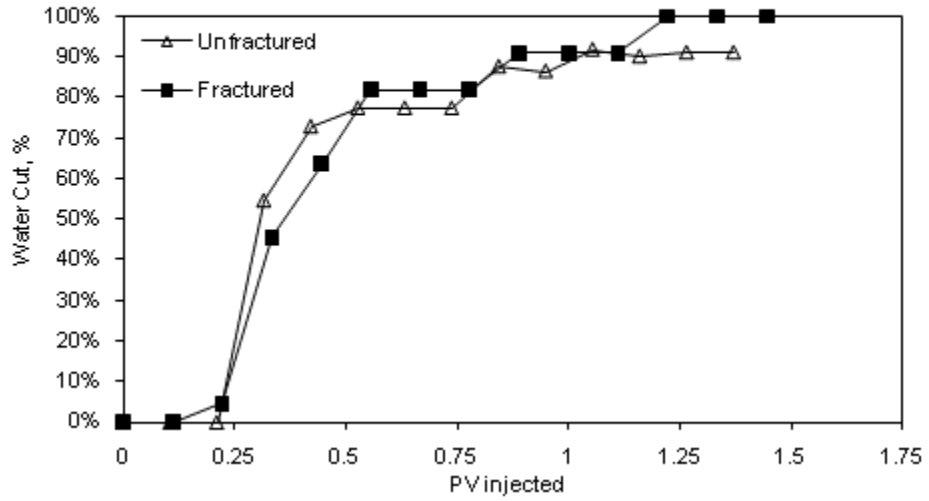


Fig. 4.74— WF water cut comparison between unfractured and fractured cores

Since CGI has resulted in very poor recovery during the fractured cases, other ways to improve it were undertaken. The first measure was conducting CGI in a tertiary recovery mode to take advantage of the presence of water that could lower $CO_2$ mobility. In unfractured case, CGI in tertiary mode has shown significant delays in gas breakthrough because of the presence of water that acted to lower its mobility. This mechanism helped in lowering the high $CO_2$ flow through the fracture in the fractured core.

Shown in **Fig. 4.75** is the tertiary recovery CGI comparison between unfractured and fractured cases. Tertiary CGI in unfractured core resulted in 65.63 % while the fractured case resulted in 62.34% of residual oil after waterflood. The decrease in oil recovery is only 3.5 % which is marginal compared to the decrease in oil recovery during the secondary recovery mode. **Fig. 4.76** shows the cumulative produced $CO_2$ at standard conditions for the unfractured and fractured cases. The unfractured case produced 24.9 Liters of $CO_2$ at the end of the run with a breakthrough at 94 min. On the other hand, the fractured case produced 36.6 Liters of $CO_2$ at the end of the run with a breakthrough at 57 min. the fractured case resulted in higher $CO_2$ production and earlier breakthrough. However, the early $CO_2$ breakthrough in this case was actually advantageous because in tertiary injection mode, oil recovery starts with the $CO_2$ breakthrough as seen in both cases.

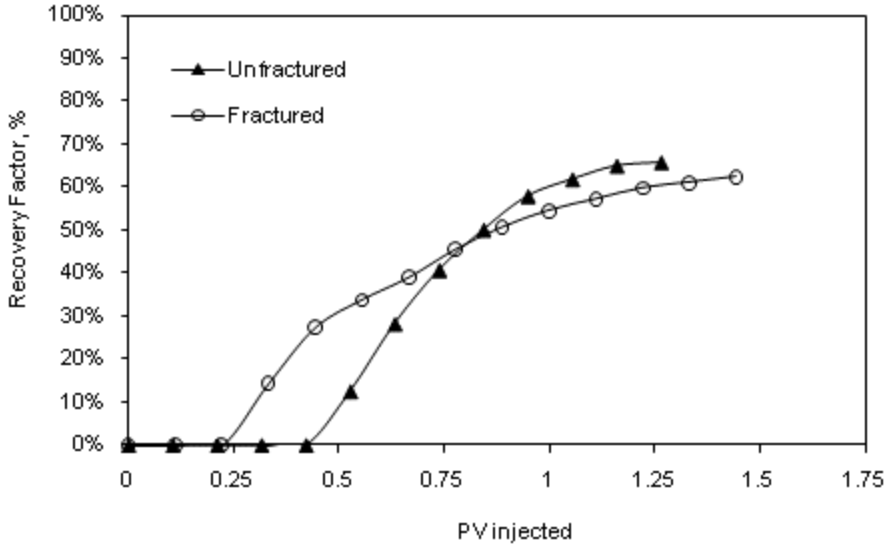


Fig. 4.75— Tertiary CGI cumulative oil recovery comparison between unfractured and fractured cores

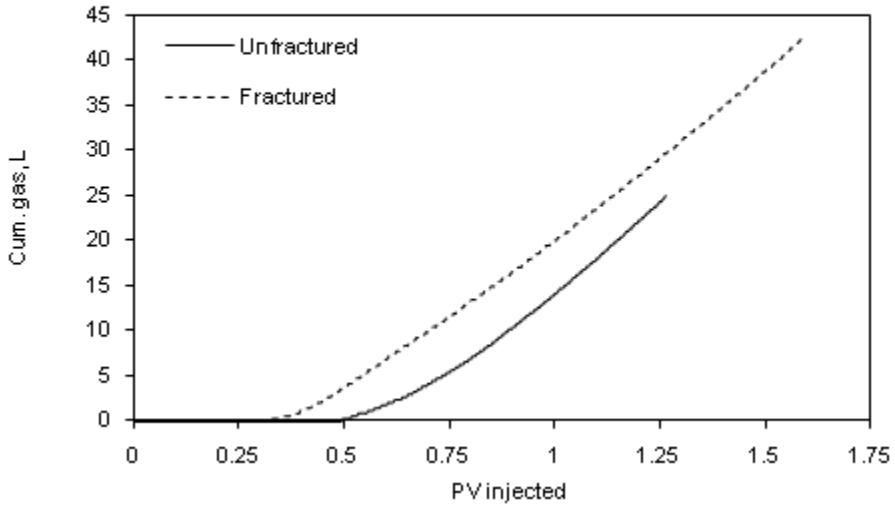


Fig. 4.76— Tertiary CGI cumulative $CO_2$ production comparison between unfractured and fractured cores

Another measure to improve the $CO_2$ oil recovery in fractured cores is to inject it along with water simultaneously (SWAG) or in alternating cycles (WAG). This aims to reduce the $CO_2$ high mobility by water which has higher viscosity. Shown in **Fig. 4.77** is WAG cumulative oil recovery and water production comparison between unfractured and fractured cores. The cumulative oil recovery on the unfractured core is 92.7% while the one-fracture and two-fracture cases resulted in 70 % and 79.86% of OOIP, respectively. Although the decrease in oil recovery is significant, it is less severe than CGI. Moreover, the amount of used $CO_2$ in WAG injection is 40% less than the CGI.

Shown in **Fig. 4.78** is WAG cumulative $CO_2$ production comparison between unfractured and fractured cores. Fractured cores have resulted in higher $CO_2$ production than unfractured cores; however, the difference is not significant. One distinct feature in this figure is that during water cycles, the $CO_2$ production is really suppressed. But, during $CO_2$ cycles, a significant increase in the $CO_2$ production is seen in the fractured cases.

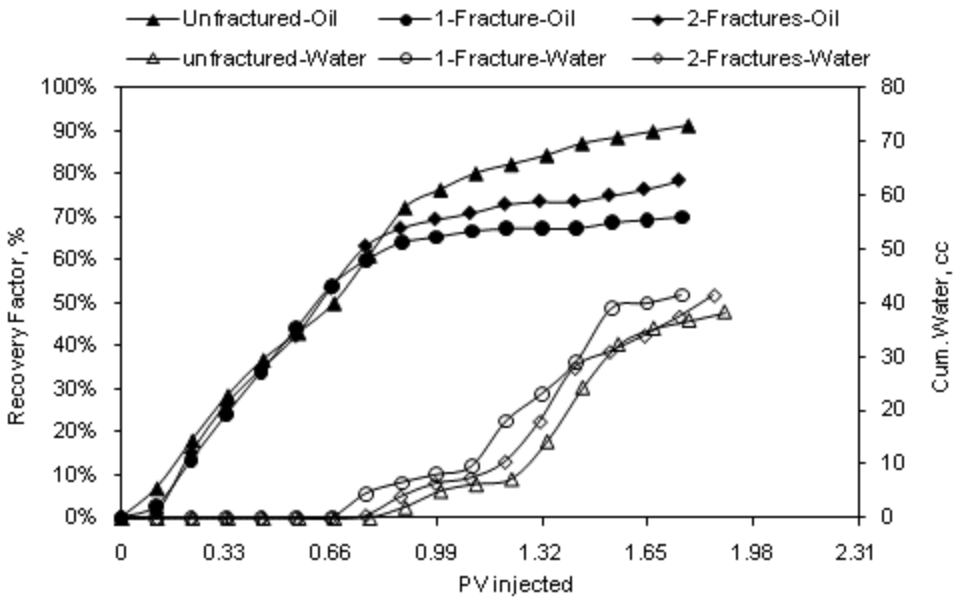


Fig. 4.77— WAG cumulative oil recovery and water production comparison between unfractured and fractured cores

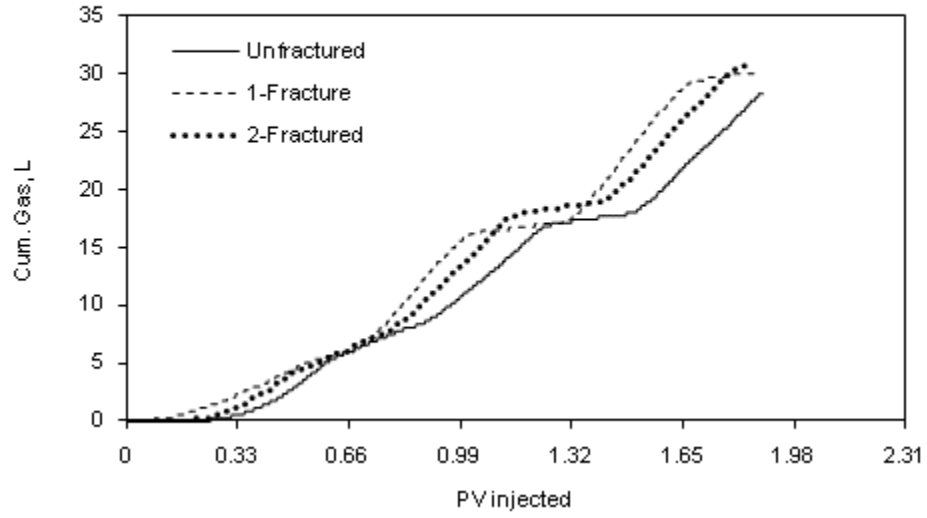


Fig. 4.78— WAG cumulative $CO_2$ production comparison between unfractured and fractured cores

Shown in **Fig. 4.79** is SWAG cumulative oil recovery and water production comparison between unfractured and fractured cores. The cumulative oil recovery on the unfractured core is 98.5% while the one-fracture and two-fracture cases resulted in 71.6 % and 79.16 % of OOIP, respectively. Similar to WAG, the decrease in oil recovery is less significant than CGI. Moreover, the amount of used $CO_2$ in SWAG injection is less than both CGI and WAG.

Shown in **Fig. 4.80** is SWAG cumulative $CO_2$ production comparison between unfractured and fractured cores. Fractured cores yielded higher $CO_2$ production than unfractured cores. Unlike WAG, the difference is significant because in this injection mode, $CO_2$ is never shut-in. However, it is less severe than CGI because of the presence of water and the lower rate of injection. One distinct feature in this figure is the absence of a flat region in $CO_2$ production around water breakthrough at 0.5 PV (seen in unfractured case). This is attributed to the higher flow of $CO_2$ in fractures which increased its velocity and lowered the amounts that can be dissolved in water. This feature was only observed previously during the high salinity case (20 wt. %) where the amount of dissolved $CO_2$ in water was very low.

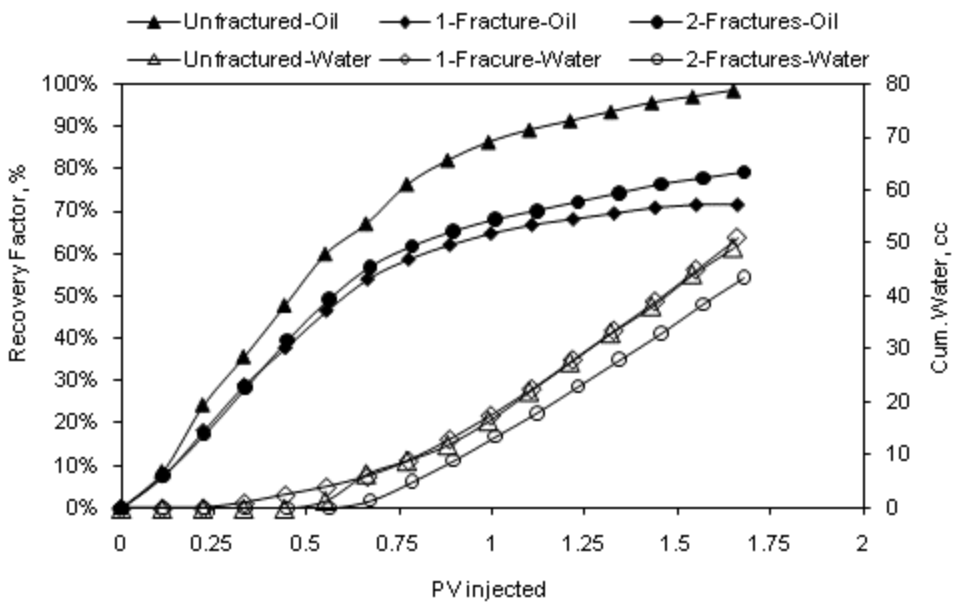


Fig. 4.79— SWAG cumulative oil recovery and water production comparison between unfractured and fractured cores

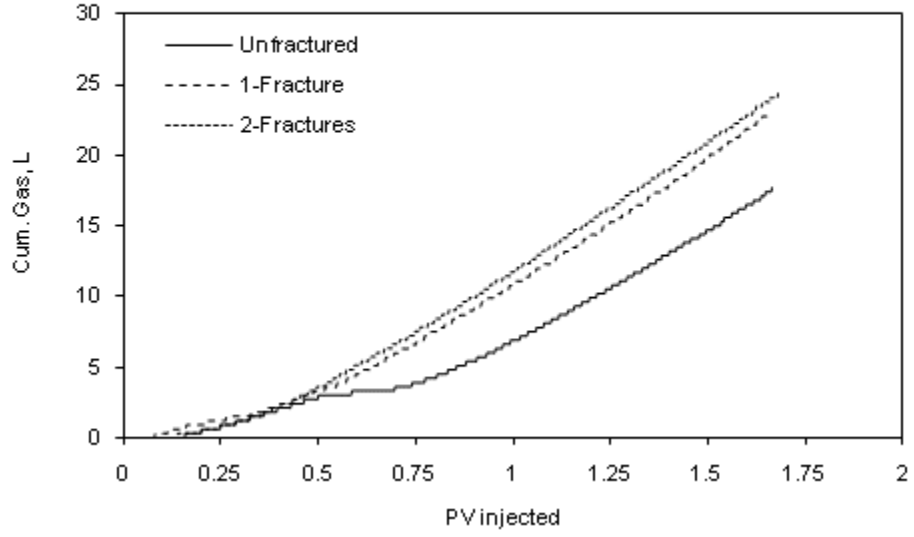


Fig. 4.80— SWAG cumulative $CO_2$ production comparison between unfractured and fractured cores

The final comparison will be between the three $CO_2$ injection modes in unfractured and fractured cases. The objective of this comparison is to show the improvement in oil recovery when implementing WAG and SWAG over CGI. As shown earlier, CGI has resulted in the poorest recovery in fractured cases whereas WAG and SWAG has shown less severe oil recovery deterioration in fractured cases. This is because WAG and SWAG use a wetting phase, water, which helps to increase matrix imbibiton by lowering the $CO_2$ high mobility. Shown in **Fig. 4.81** is the cumulative oil recovery and water production for the three injection modes comparing the base case to the one-fracture case. **Fig. 4.82** shows $CO_2$ cumulative production during the three injection modes comparing the base case to the one-fracture case. **Figs. 4.83** and **4.84** show a comparison between the base case and the two-fracture case in the same manner. The benefits of WAG and SWAG have been already been shown during the base case. However, during the fractured cases, the benefits have become more pronounced. This concludes that as the heterogeneity in a reservoir increases (i.e. vugs, permeability variation, or fractures); the need for WAG and SWAG implementation becomes more essential.

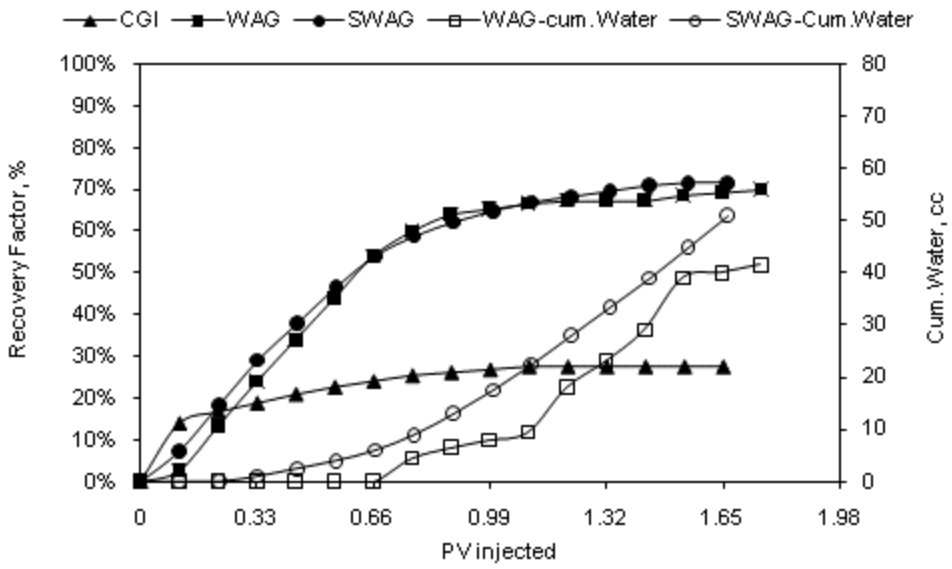


Fig. 4.81— Cumulative oil recovery and water production for all injection modes comparison between unfractured and one-fracture cases

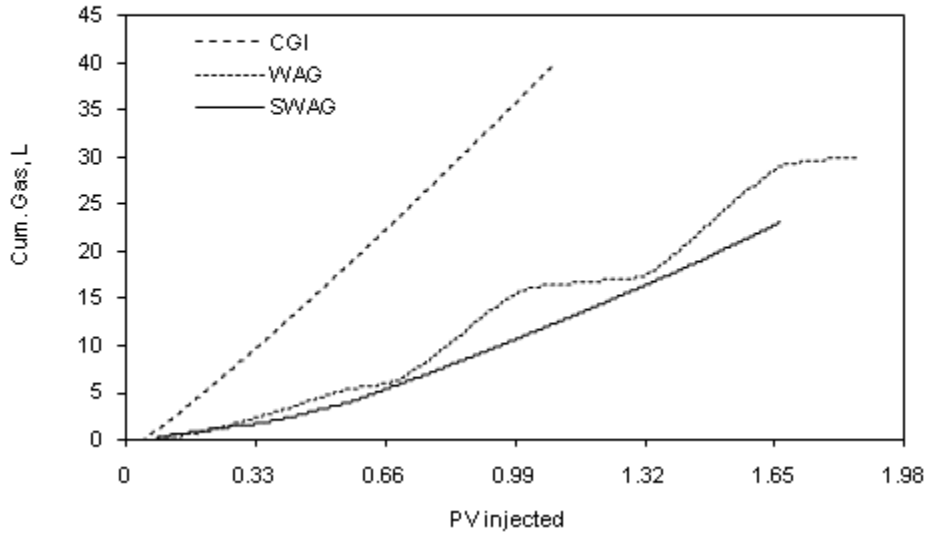


Fig. 4.82—Cumulative $CO_2$ production for all injection modes comparison between unfractured and one-fracture cases

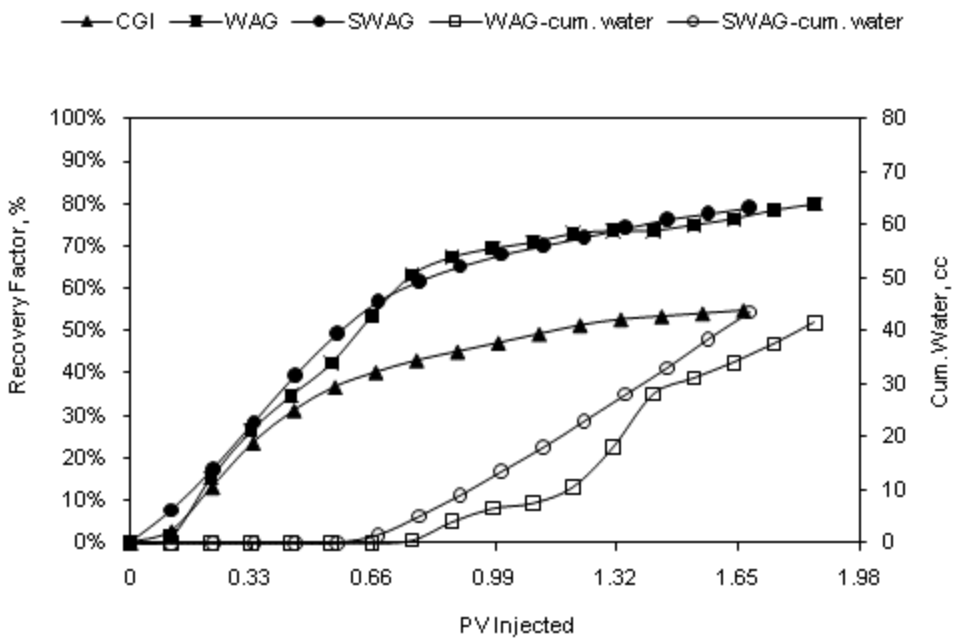


Fig. 4.83— Cumulative oil recovery and water production for all injection modes comparison between unfractured and two-fracture cases

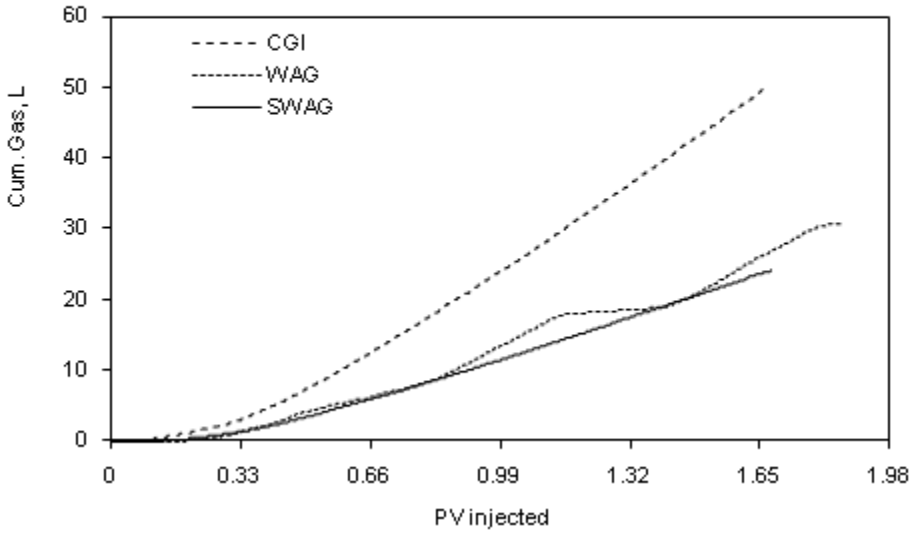


Fig. 4.84—Cumulative $CO_2$ production for all injection modes comparison between unfractured and two-fracture cases

# CHAPTER V

# SIMULATION STUDY

## 5.1 Simulation Model

Based on the experimental coreflood results, a numerical simulation model was constructed to model the experiments. The results were simulated with the Computer Modeling Group's (CMG) commercial reservoir simulator IMEX. It is a black oil simulator with a pseudo-miscible with no chase gas option. It contains three phases: oil, water, and solvent ($CO_2$). To simulate the experiments, a 2-D model was built with Cartesian grids 100 × 1 × 10 resulting in 1000 cells as shown in **Fig. 5.1**.

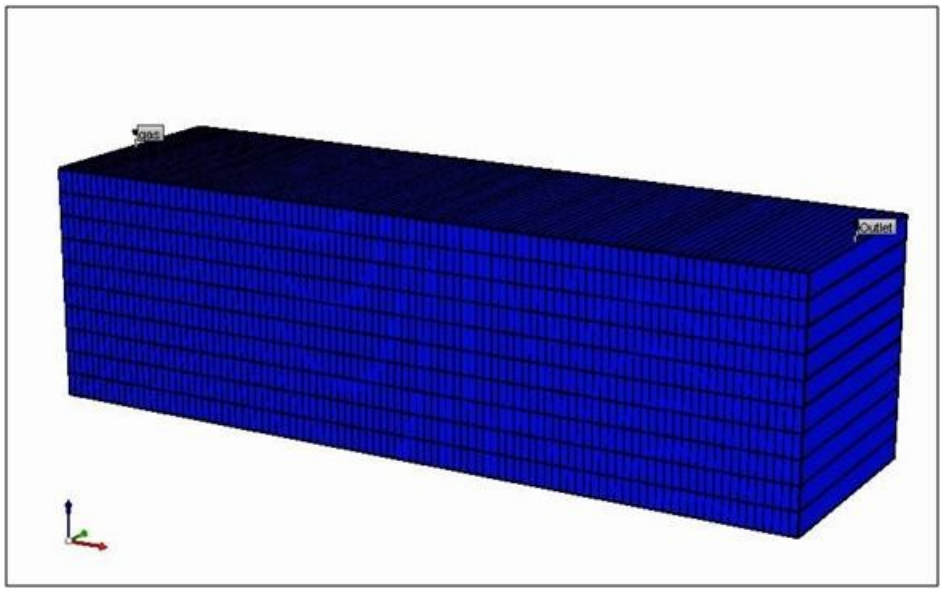


Fig. 5.1—Simulation model Cartesian grids representing the carbonate core

## 5.2 History Matching Experimental Results

Initially, the total volume was matched by converting the laboratory core cylindrical volume into a rectangular shape. Then, core porosity, permeability and end-point relative permeability points, which were measured experimentally, were used to match the pore volume and the pressure in the core. Finally, relative permeability curves and omegas-os (oil and $CO_2$ mixing parameter) were used to tune the simulation model to match gas and water breakthroughs and cumulative oil recovery.

### 5.2.1 Unfractured Core Simulation Match

**Figs. 5.2** through **5.5** show the unfractured core cumulative oil recovery match between the experimental results and the simulation model for CGI, WF, WAG and SWAG, respectively.

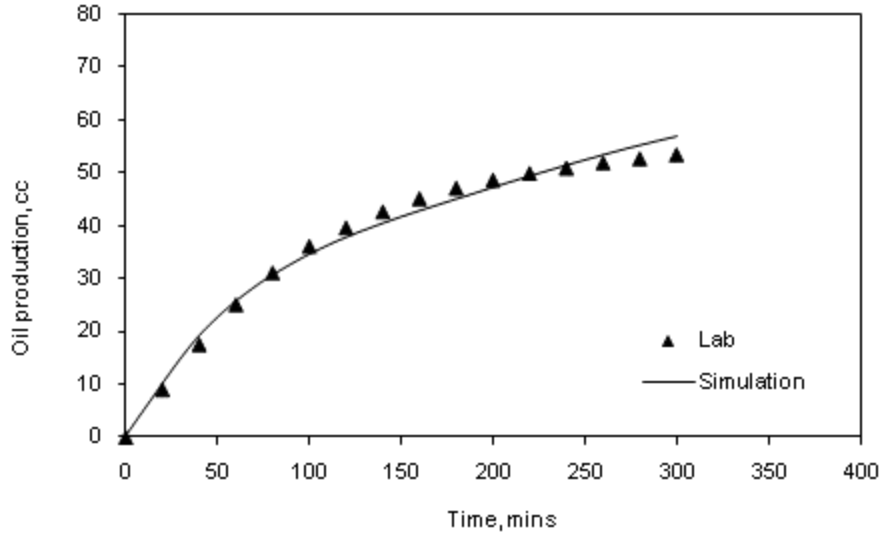


Fig. 5.2—CGI: cumulative oil recovery match between experimental results and simulation

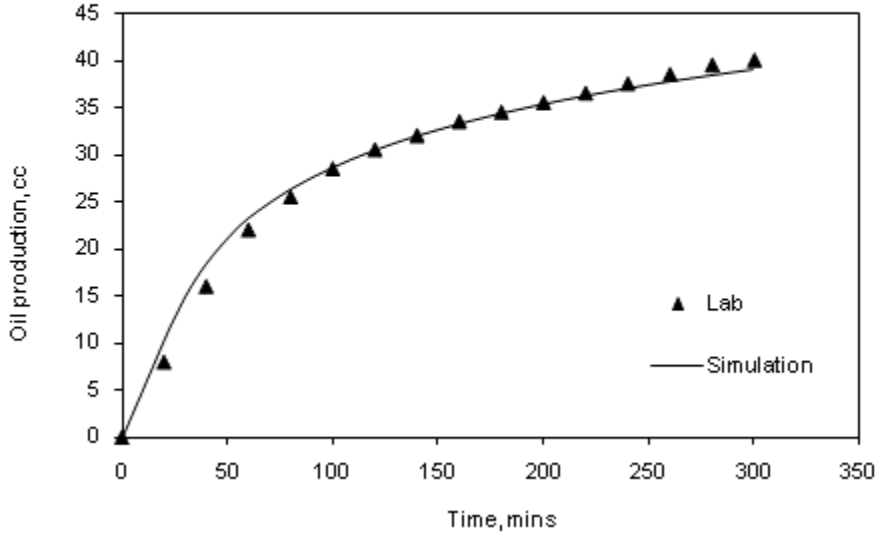


Fig. 5.3—WF: cumulative oil recovery match between experimental results and simulation

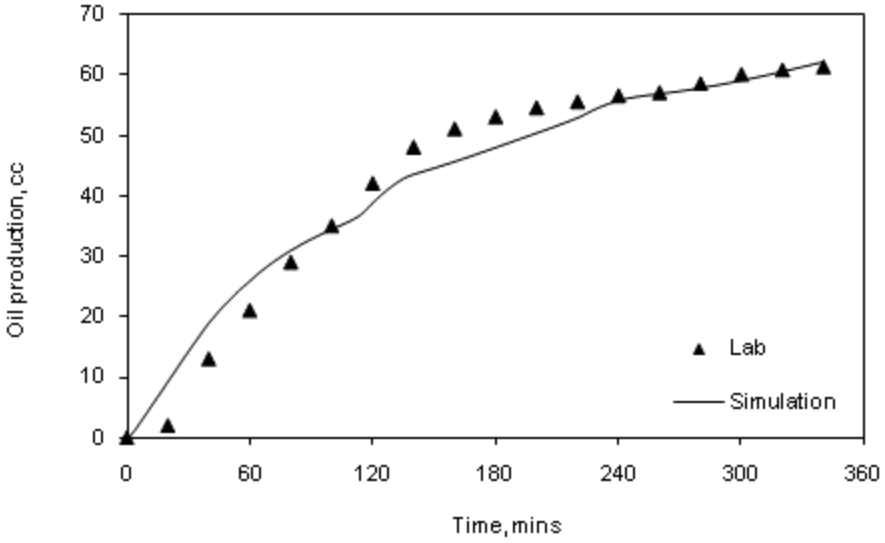


Fig. 5.4—WAG: cumulative oil recovery match between experimental results and simulation

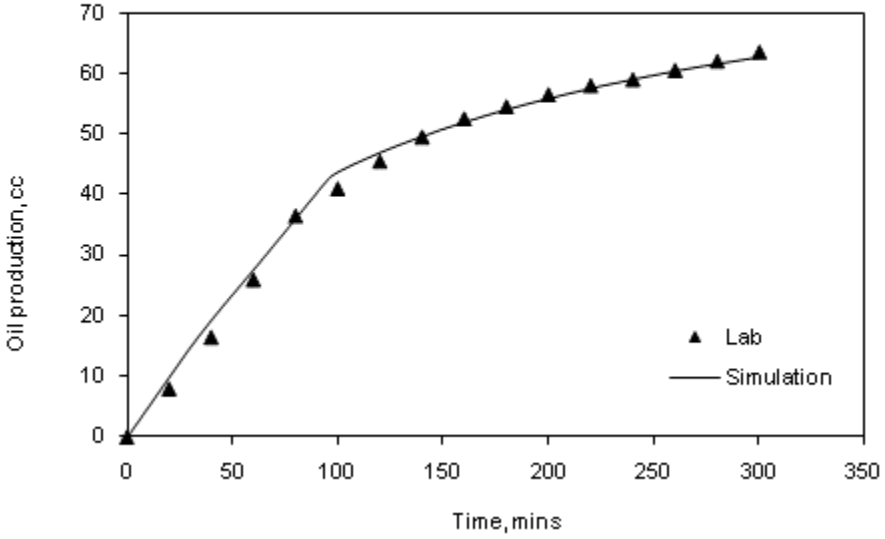


Fig. 5.5—SWAG: cumulative oil recovery match between experimental results and simulation

When a satisfactory history match was obtained, the experiments were modeled to study the fluid flow in the core. Shown in **Figs. 5.6** through **5.9** is the oil saturation comparison between CGI, WF, WAG, and SWAG, respectively, at 0.5 PV injected (90 min) in the I-K direction. The simulation shows that the $CO_2$ has a superior displacement to WF for the oil it contacts. This is evident when comparing CGI to WF especially near the core inlet. However, $CO_2$ does not move as uniformly in the core which reduces the recovery from the middle and the bottom of the core; whereas WF has a better conformance at the displacement front. Combining the two adds up the advantages of both and results in excellent displacement efficiency as seen in WAG and SWAG injections. During WAG and SWAG injections, the improvement in oil recoveries is a result of a better conformance provided by the injected water which hindered the $CO_2$ high mobility. This is seen by the improved displacement front during WAG and SWAG.

Shown in **Figs. 5.10** through **5.13** is the oil saturation comparison between CGI, WF, WAG, and SWAG, respectively, at the end of each run. It is clear that during CGI, $CO_2$ segregates to the top sweeping the top portion of the core and leaving the bottom part. On the other hand, this phenomenon is suppressed during the SWAG injection. SWAG injection has resulted in the best displacement profile and hence the best cumulative oil recovery among all injection modes.

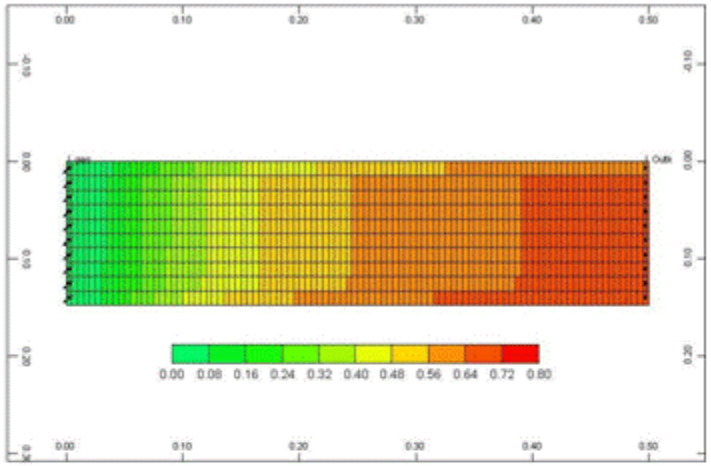


Fig. 5.6—CGI oil saturation at 0.5 PV injected

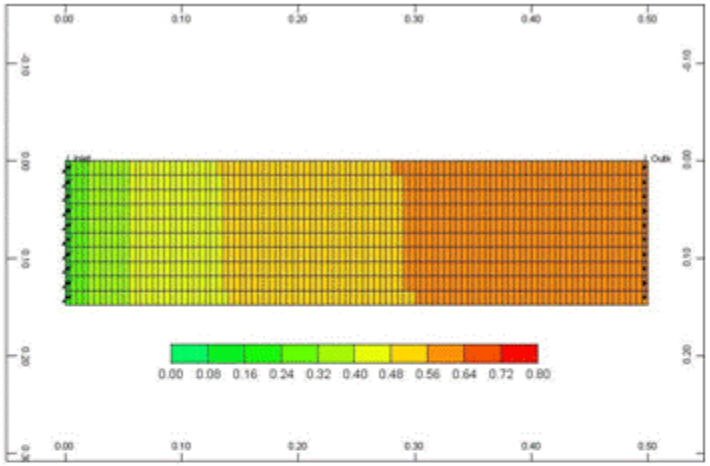


Fig. 5.7—WF oil saturation at 0.5 PV injected

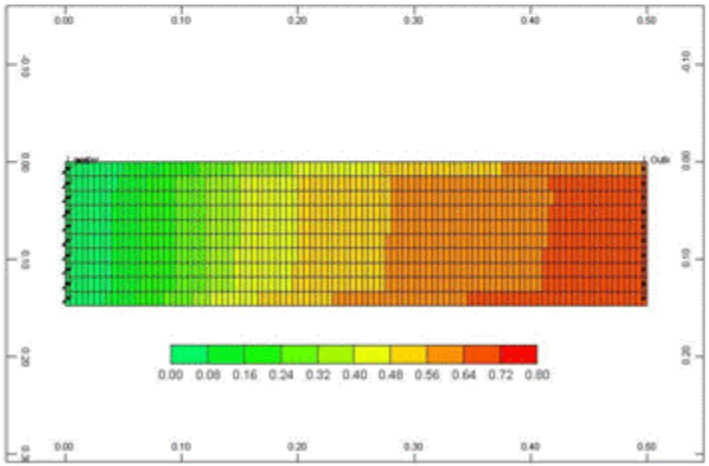


Fig. 5.8—WAG oil saturation at 0.5 PV injected

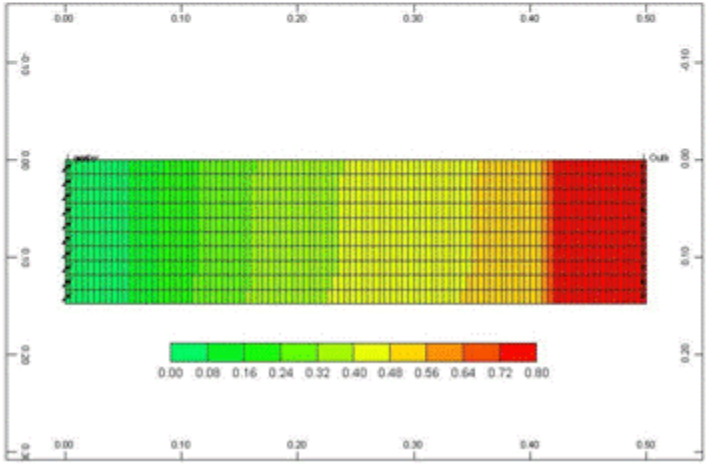


Fig. 5.9—SWAG oil saturation at 0.5 PV injected

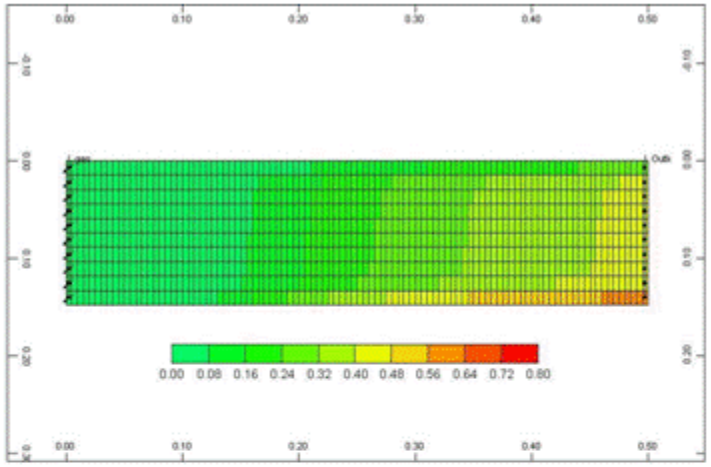


Fig. 5.10—CGI oil saturation at the end of the run

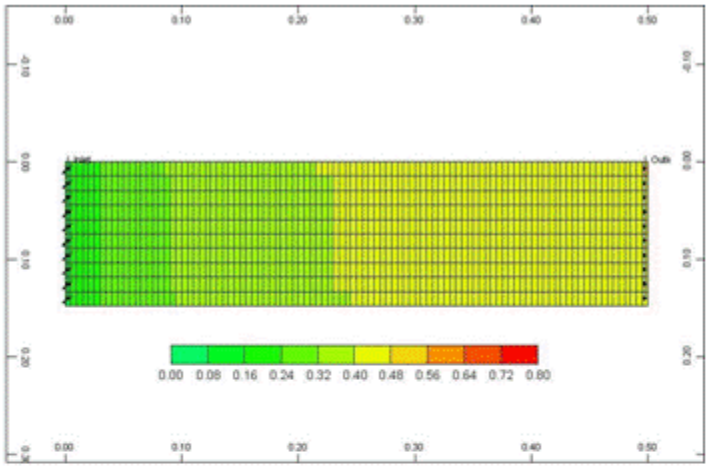


Fig. 5.11—WF oil saturation at the end of the run

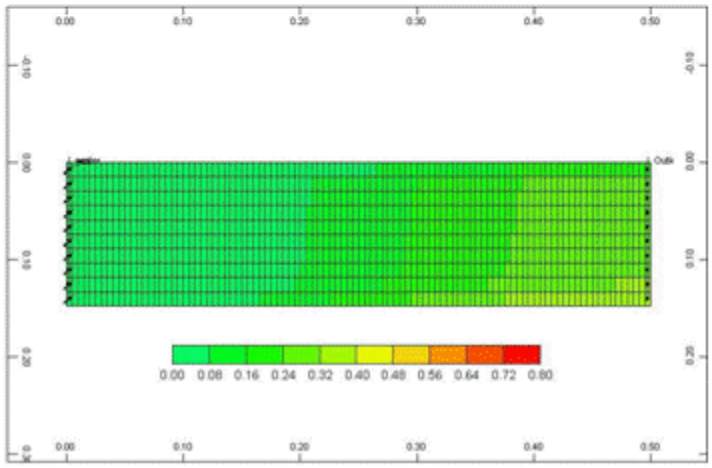


Fig. 5.12—WAG oil saturation at the end of the run

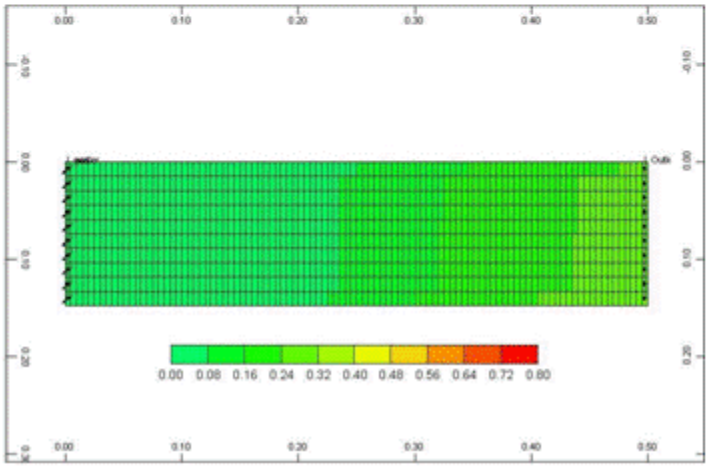


Fig. 5.13—SWAG oil saturation at the end of the run

### 5.2.2 Fractured Core Simulation Match

The fractured cases were matched in a similar manner to the unfractured case, except for the fractures in the core. The fractures were represented by high permeability grids in the same location as in the core. The fracture width, which was experimentally measured to be 0.003 in., was represented by the thickness of those high permeability grids. The grids were minimized to 31 × 1 × 11 to minimize the simulation time and better visualize the fractures. The reduction in grids resulted in no change in the cumulative oil recovery which justifies the approach. The grids were then refined around the fractures to eliminate any numerical dispersion during $CO_2$ injection. The fractures were also represented by unit porosity because it was artificially made with a saw (Guzman and Aziz 1992; Muralidharan et al. 2004). **Figs. 5.14** and **5.15** show the girds of the fractures in the core during the one-fracture and two-fracture cases, respectively.

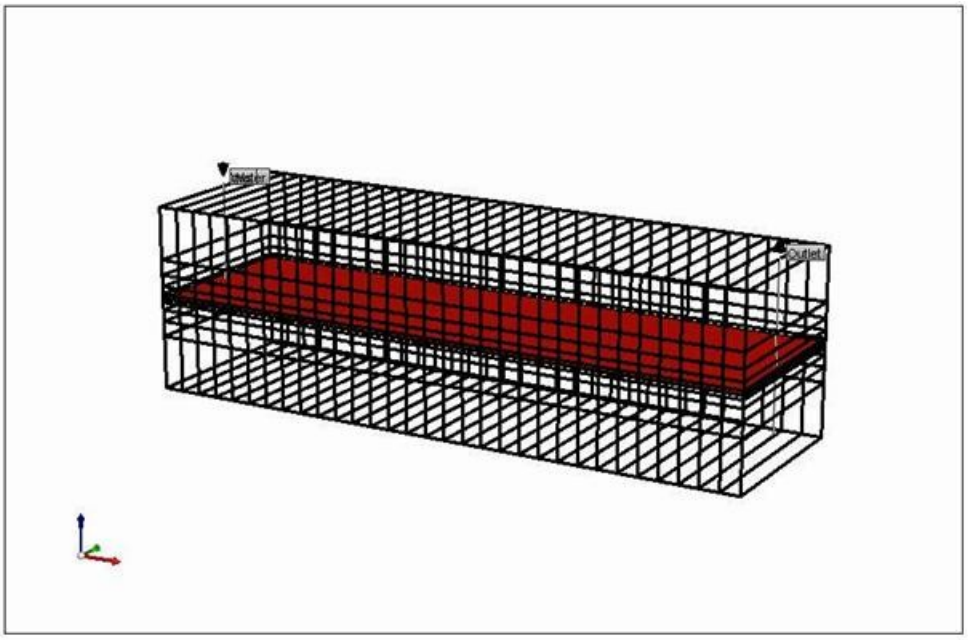


Fig. 5.14— (One-fracture case) horizontal fracture in the core

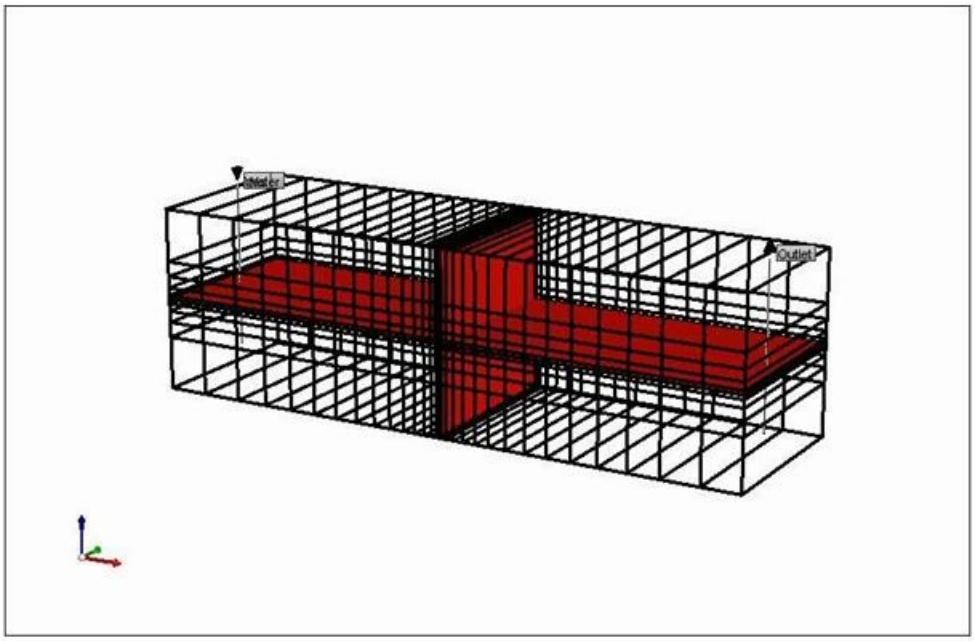


Fig. 5.15— (Two-fracture case) horizontal and vertical fractures in the core

**Figs. 5.16** through **5.19** show the one-fracture case cumulative oil recovery match between the experimental results and the simulation model for CGI, WF, WAG and SWAG, respectively.

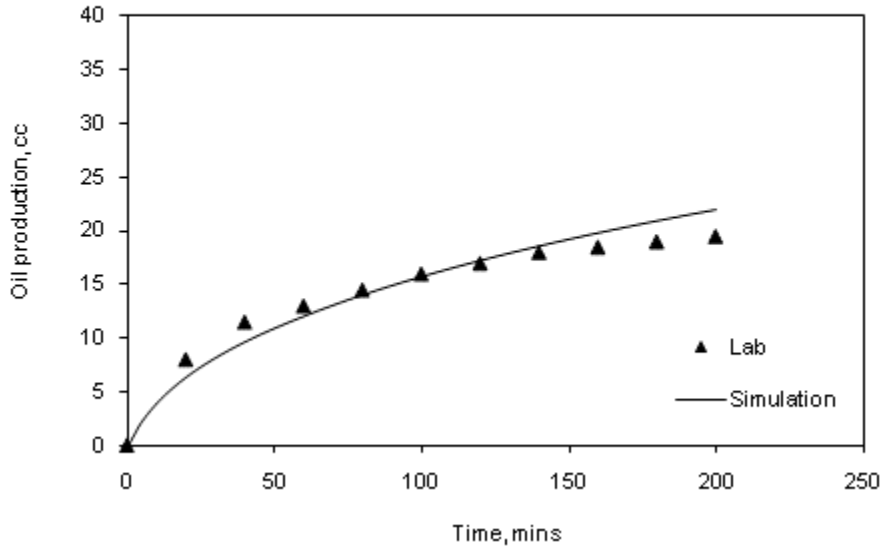


Fig. 5.16—CGI (one-fracture): cumulative oil recovery match between experimental results and simulation

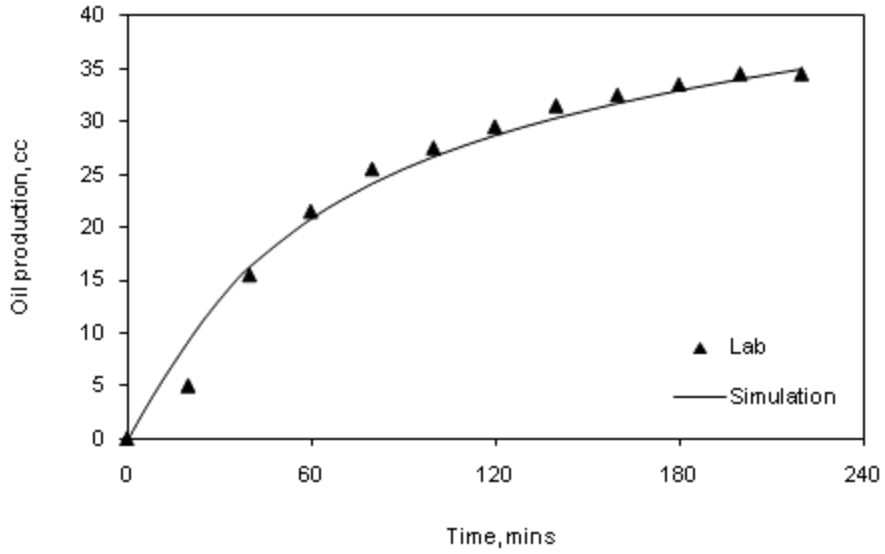


Fig. 5.17—WF (one-fracture): cumulative oil recovery match between experimental results and simulation

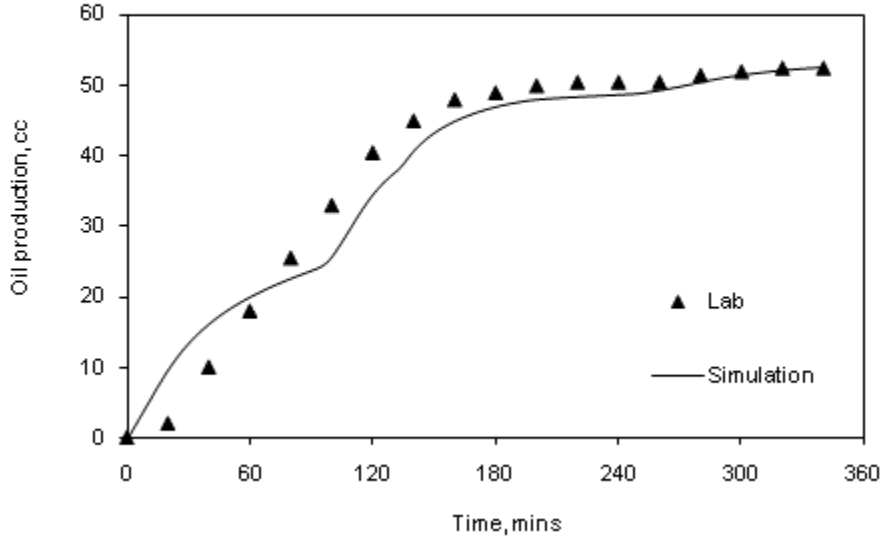


Fig. 5.18—WAG (one-fracture): cumulative oil recovery match between experimental results and simulation

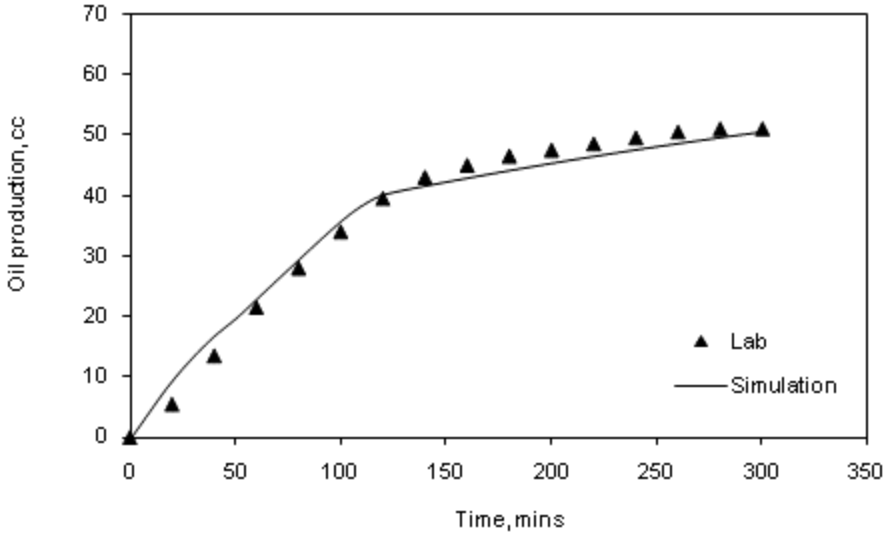


Fig. 5.19—SWAG (one-fracture): cumulative oil recovery match between experimental results and simulation

**Figs. 5.20** through **5.23** show oil saturation for the one-fracture case (in I-K direction) at the beginning of the runs for CGI, WF, WAG, and SWAG, respectively. The simulation shows that WF has the best imbibition at the beginning of the experiment even though water started to channel through the fracture. Since SWAG involves water injection from the beginning of the experiment, it showed better displacement than CGI and WAG around the inlet before channeling through the fracture.

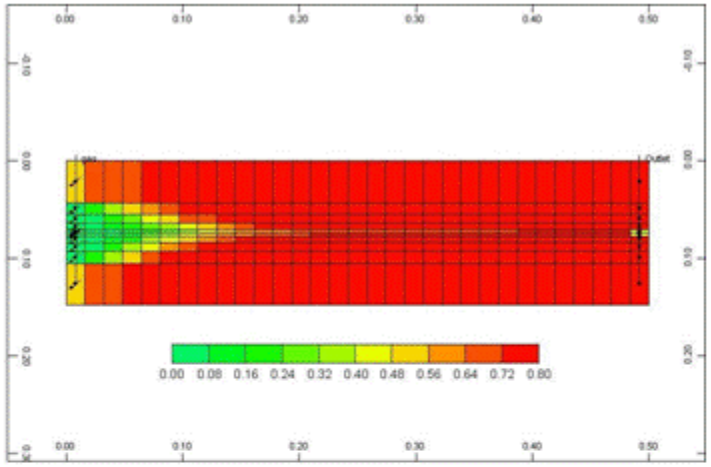


Fig. 5.20—CGI (one-fracture) oil saturation at the beginning of the run

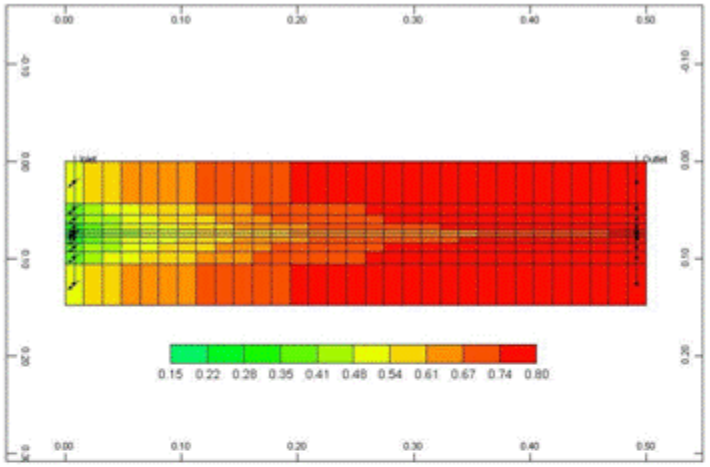


Fig. 5.21—WF (one-fracture) oil saturation at the beginning of the run

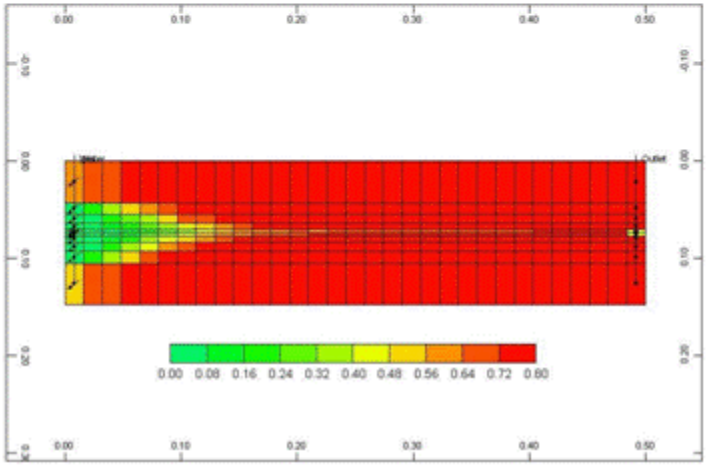


Fig. 5.22—WAG (one-fracture) oil saturation at the beginning of the run

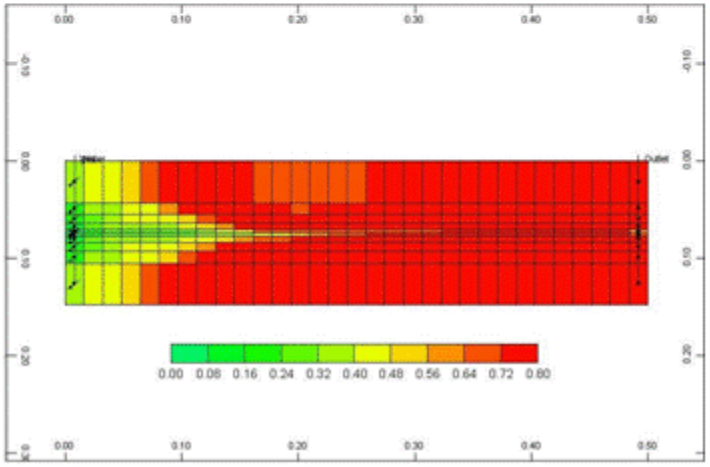


Fig. 5.23—SWAG (one-fracture) oil saturation at the beginning of the run

**Figs. 5.24** through **5.27** show the oil saturation at the end of the runs (in I-K direction) for all injection modes during the one-fracture case. At the end of the experiments, WF showed fairly good displacement profile but the residual oil after the flood was high. On the other hand, SWAG showed both good displacement profile and low residual oil. WAG resulted in the same residual oil as SWAG but displacement profile was less uniform. Finally, CGI has resulted in the poorest displacement and the highest residual oil saturation especially away from the inlet and at the bottom of the core.

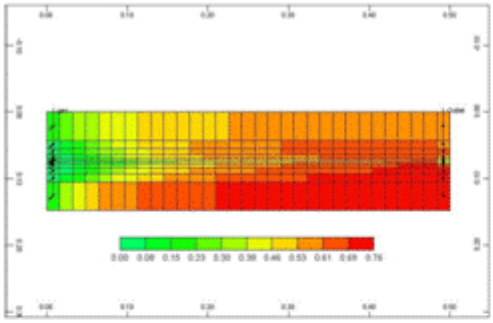

Fig. 5.24—CGI (one-fracture) oil saturation at the end of the run

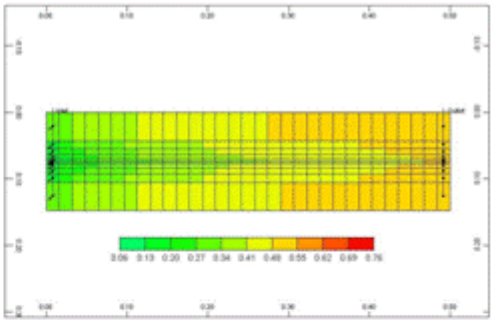

Fig. 5.25—WF (one-fracture) oil saturation at the end of the run

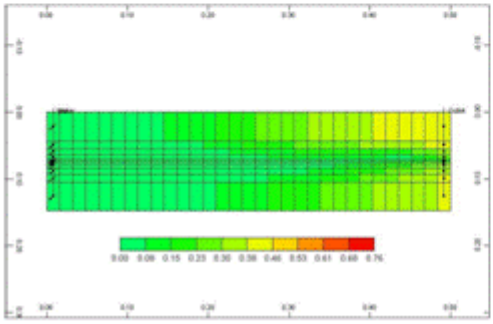

Fig. 5.26—WAG (one-fracture) oil saturation at the end of the run

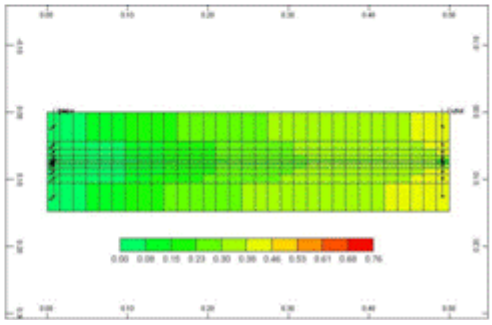

Fig. 5.27—SWAG (one-fracture) oil saturation at the end of the run

**Figs. 5.28** through **5.30** show the two-fracture case cumulative oil recovery match between the experimental results and the simulation model for CGI, WAG and SWAG, respectively.

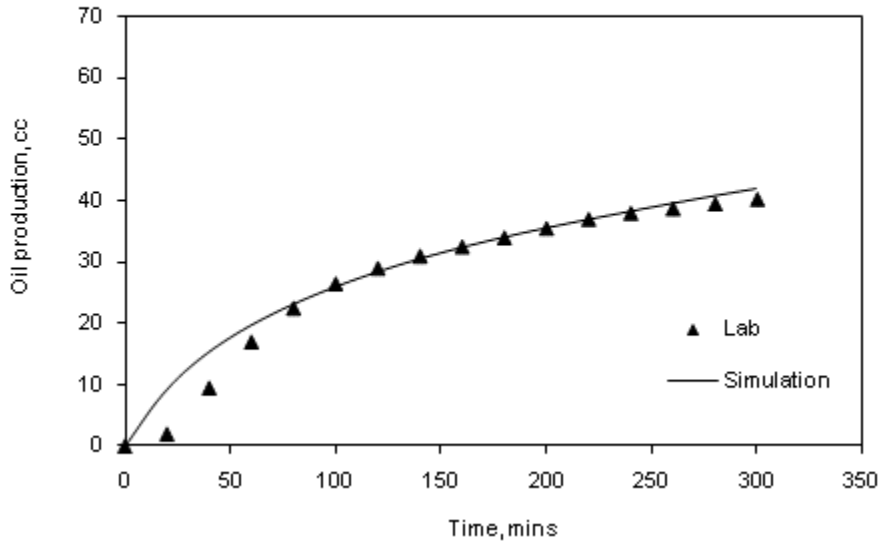


Fig. 5.28—CGI (two-fracture): cumulative oil recovery match between experimental results and simulation

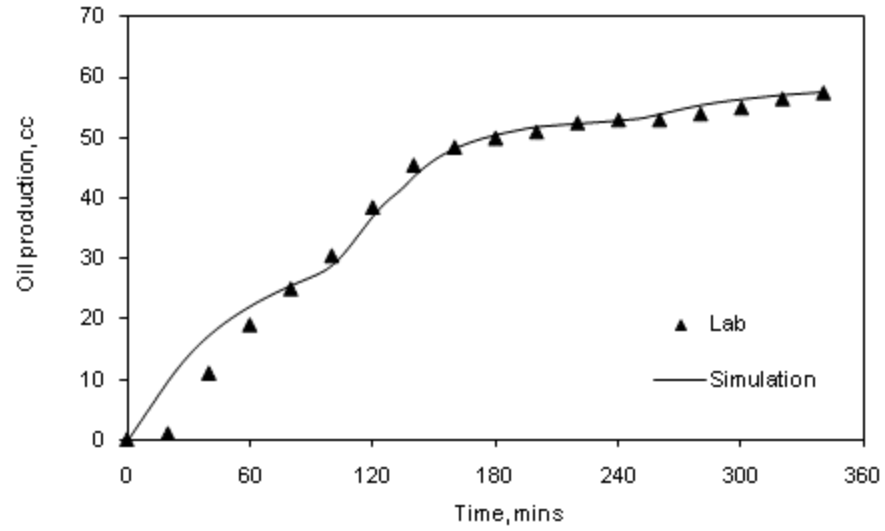


Fig. 5.29—WAG (two-fracture): cumulative oil recovery match between experimental results and simulation

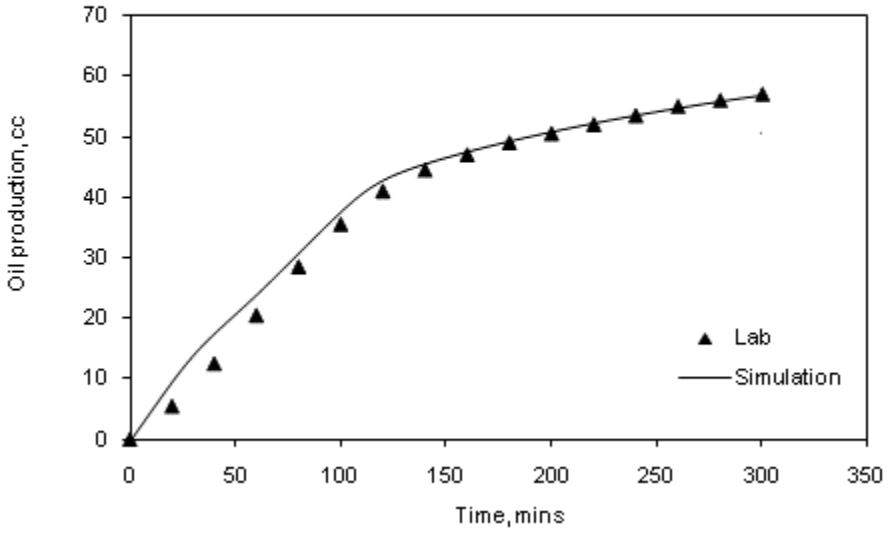


Fig. 5.30—SWAG (two-fracture): cumulative oil recovery match between experimental results and simulation

**Figs. 5.31** through **5.33** show the two-fracture case oil saturation (in I-K direction) at 0.5 PV injected for CGI, WF, WAG, and SWAG, respectively. The beginning of the two-fracture case is very similar to the one-fracture case until 0.5 PV is injected. As shown in the figures, the presence of the middle vertical fracture caused the fluids to diffuse upward and contact more oil. The simulation shows that extra oil (compared to one-fracture case) has been contacted because of the vertical fracture.

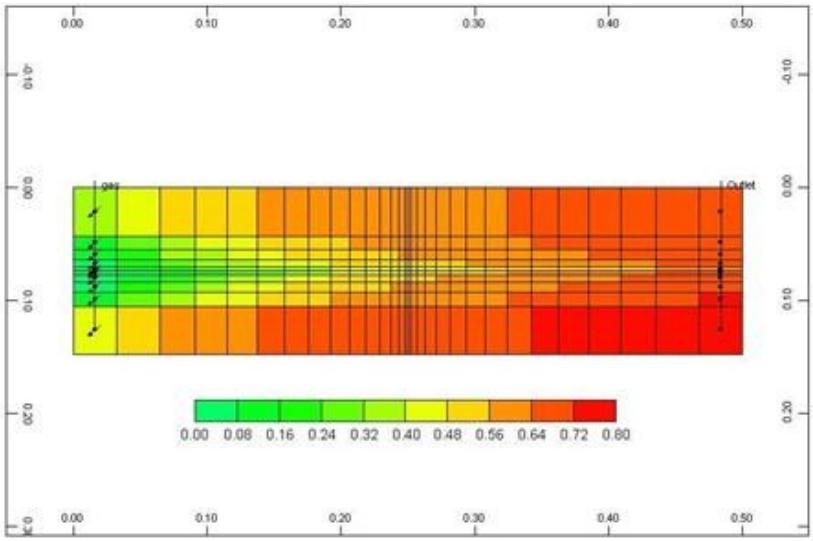


Fig. 5.31—CGI oil (two-fracture) saturation at 0.5 PV injected

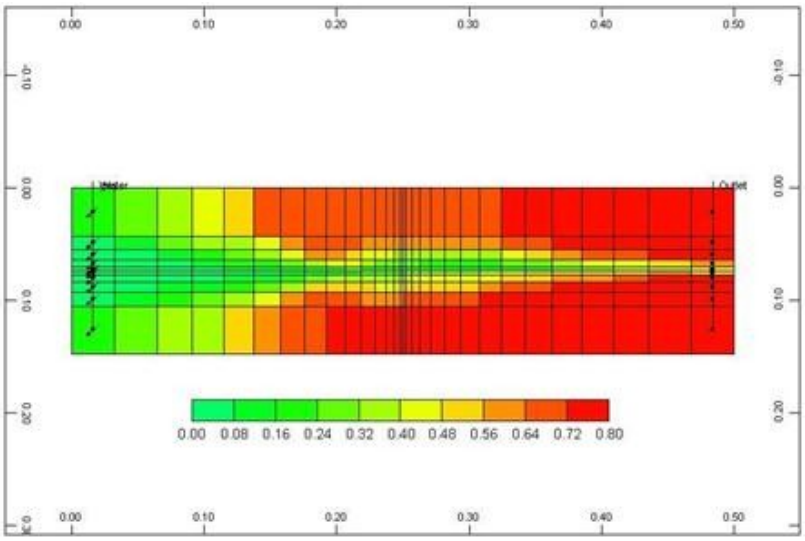


Fig. 5.32—WAG (two-fracture) oil saturation at 0.5 PV injected

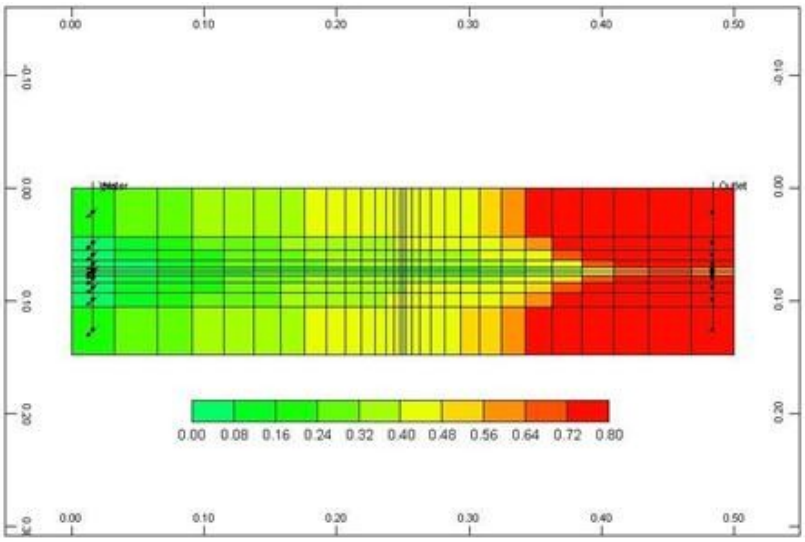


Fig. 5.33—SWAG (two-fracture) oil saturation at 0.5 PV injected

**Figs. 5.34** through **5.36** show the oil saturation at the end of the runs (in I-K direction) for all injection modes during the two-fracture case. In this case, SWAG still has the best displacement profile and lowest residual oil.

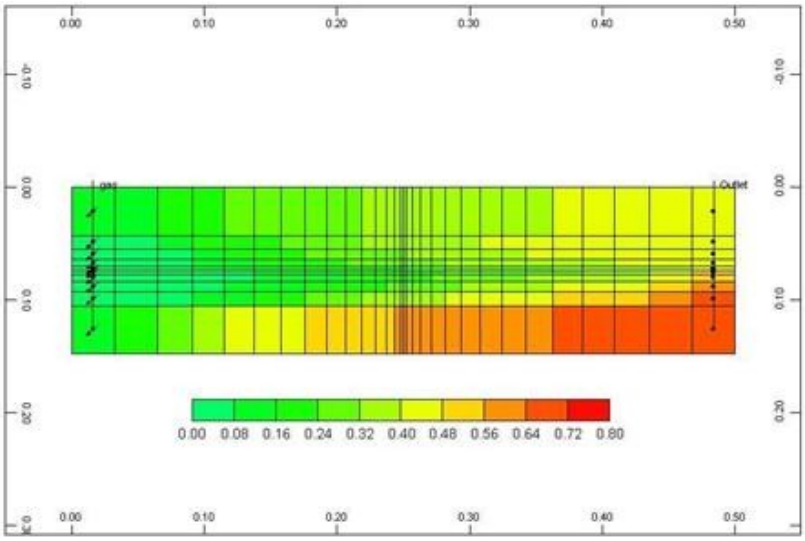


Fig. 5.34—CGI (two-fracture) oil saturation at the end of the run

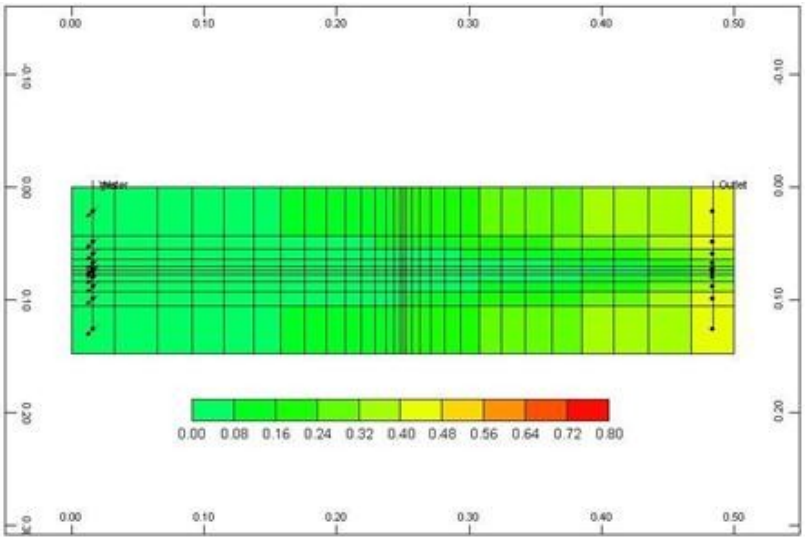


Fig. 5.35—WAG (two-fracture) oil saturation at the end of the run

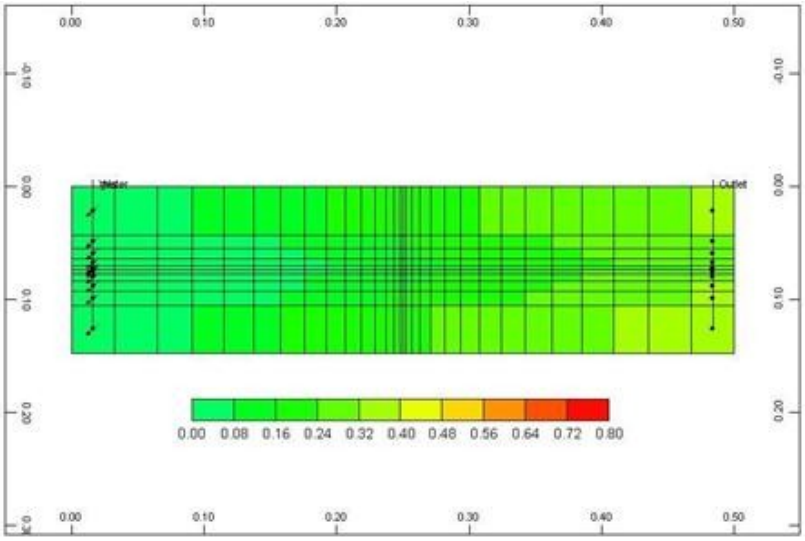


Fig. 5.36—SWAG (two-fracture) oil saturation at the end of the run

## 5.3 Sensitivity Study

The tuned simulation model, which was used to match different experimental cases, was extended to conducted sensitivity studies on some important parameters. The main advantage of having this tuned model is to minimize the time used for experimental work and allow for a wider range of parameters that can be investigated. The extended model was used to study the following parameters: permeability variation in the core, WAG ratio and slug size, and SWAG volume ratio.

### 5.3.1 Permeability Variation

In this study, extreme heterogeneity (other than fractures) was created in the core in the form of different permeabilites. Two types of variations were considered: permeability variation in the vertical direction (k-direction) creating layered reservoirs and permeability variation in the horizontal direction (i-direction) creating sequenced reservoirs. Three permeability values were considered, 0.1, 100, and 1000 mD. These values denote low (L), medium (M), and high (H) permeabilites, respectively. Then, all six permutations of these values were considered (in both direction) and the results were compared to the homogenous case and to each other for each injection mode. **Fig. 5.37** shows an example of one of the permutations (HML) in the k-direction while **Fig. 5.38** shows an example of the same arrangement (HML) in the i-direction.

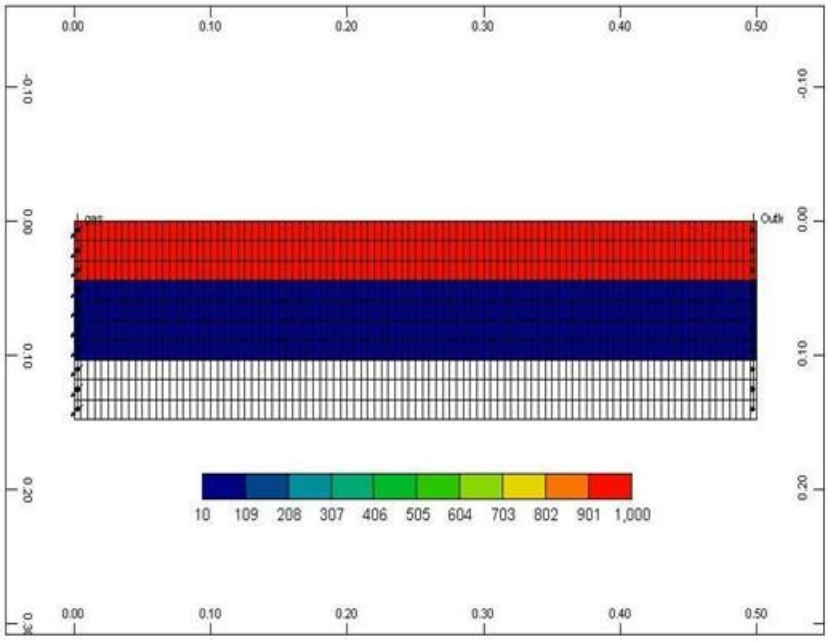


Fig. 5.37—Permeability variation in the k-direction (HML)

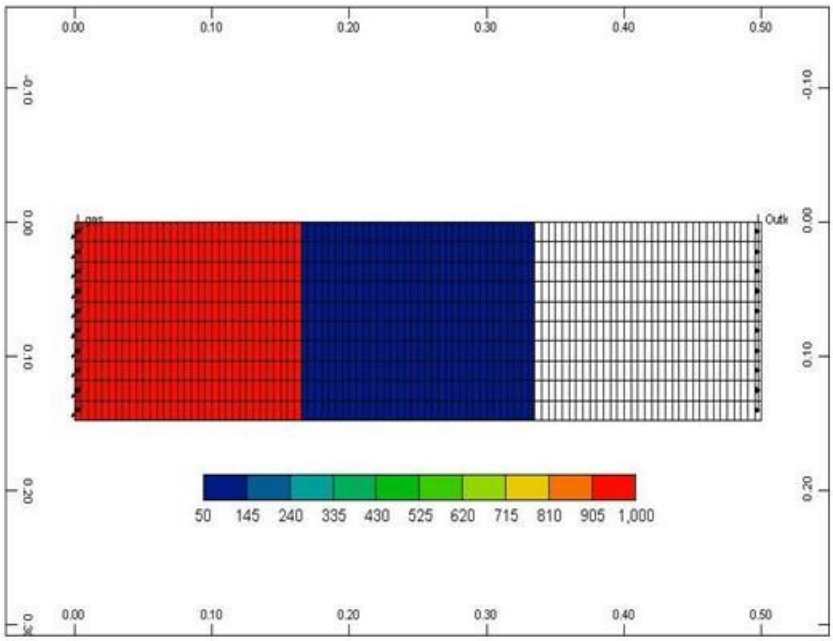


Fig. 5.38—Permeability variation in the i-direction (HML)

The simulation showed that oil recovery is more sensitive to layered reservoirs than sequenced reservoirs. During the layered reservoirs, the oil recovery was reduced significantly compared to the homogenous case. On the other hand, during sequenced reservoirs, the change in oil recovery is less pronounced and the homogenous case is not always the best scenario. This is because for the layered reservoirs, the injected fluid can follow an easier path through higher permeability layers and the oil in low permeability layers is left behind. However, for the sequenced reservoirs, the injected fluid has to go through the low permeability layer and produce its oil which is reflected in the higher differential pressure in the core.

In practice, layered reservoirs may commonly exist as a result of the depositional environments. Therefore, the results of these simulation runs would provide valuable data to the reservoir management of a layered field during $CO_2$ injection. On the other hand, sequenced permeabilities are less common; however, manmade applications can create (or aggravate) similar circumstances. For example, gel placements are common practices in reservoirs where high permeability streaks can negatively affect oil recovery. Another example is carbonate reservoirs acidizing where a zone's permeability is increased by a factor or two. The decreased permeability by gel can be represented by the low permeability value whereas the acidized zones can be represented by the high permeability value. Therefore, the results of these simulations will provide valuable information on the behavior of the injected $CO_2$ during those artificial cases. Hence, the results can be used as guidelines for the engineers to design their treatment programs.

### 5.3.1.1 Layered Reservoirs

During all $CO_2$ injection modes, the cumulative oil recovery factor from the layered reservoirs has shown the same preference to the permeability arrangement even though the decrease in oil recovery is different from each injection mode. For CGI, WAG and SWAG, the oil recovery factor resulted in paired values depending on the location of the low permeability.

**Fig. 5.39** shows CGI cumulative oil recovery comparison for the layered reservoirs (variation in k-direction).

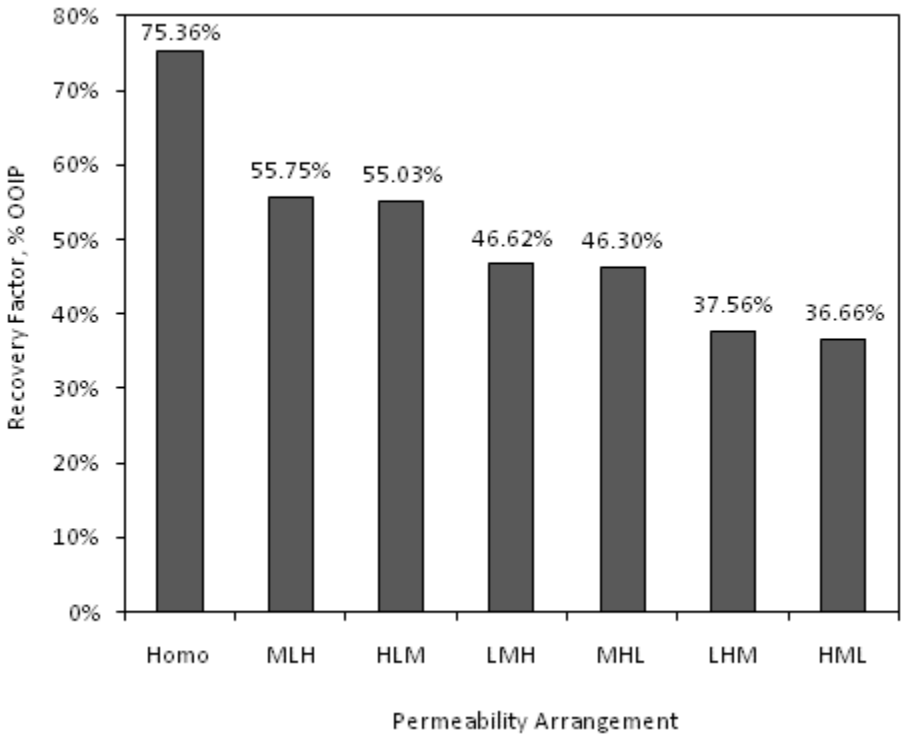


Fig. 5.39—CGI: cumulative oil recovery comparison between layered reservoirs

The simulation shows higher oil recovery is obtained when the low permeability value is in the middle especially if the medium permeability value is on the top. When the low permeability is at the edges, higher oil recovery is obtained when the low permeability is on the top part and the medium permeability is on the top of the high permeability.

**Figs. 5.40** through **5.45** show CGI oil saturation profile (in I-K direction) during the layered reservoirs at the end of each run in the order of highest recovery. The oil recovery performance was distributed in pairs depending on the location of the low permeability layer. The highest recovery is seen when the low permeability (flow barrier) is in the middle. As seen on the figures, this case resulted in uniform oil displacement from the medium and high permeabilities because of the barrier in the middle. The other two pairs in terms of recovery are when the low permeability is at the edges. Between the two cases in those pairs, the medium permeability on top of the high permeability resulted in higher recovery because of the controlled gravity segregation. When the high permeability is at the top, the worst recovery is obtained because it combines the high fluid flow through this layer with $CO_2$ tendency to segregate to the top.

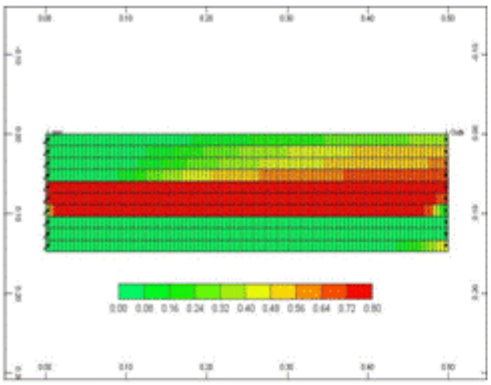

Fig. 5.40—CGI-MLH oil saturation

at the end of the run

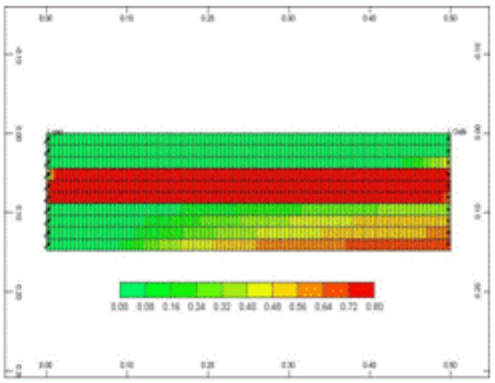

Fig. 5.41—CGI-HLM oil saturation

at the end of the run

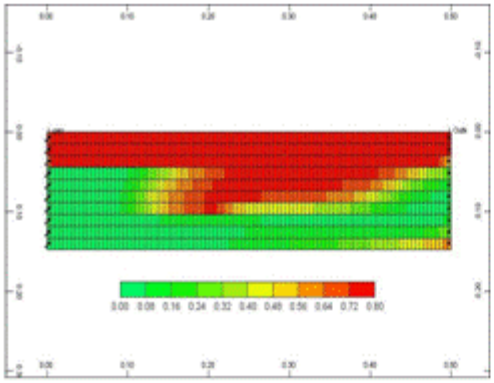

Fig. 5.42—CGI-LMH oil saturation

at the end of the run

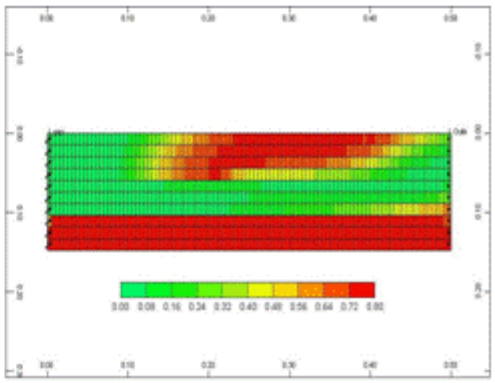

Fig. 5.43—CGI-MHL oil saturation

at the end of the run

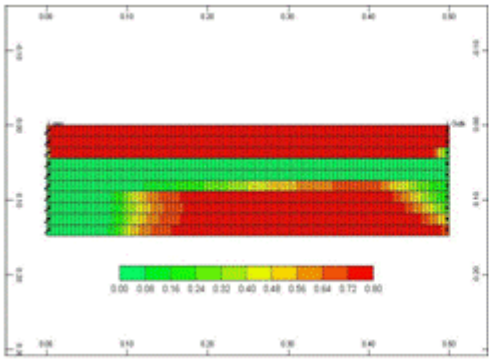

Fig. 5.44—CGI-LHM oil saturation

at the end of the run

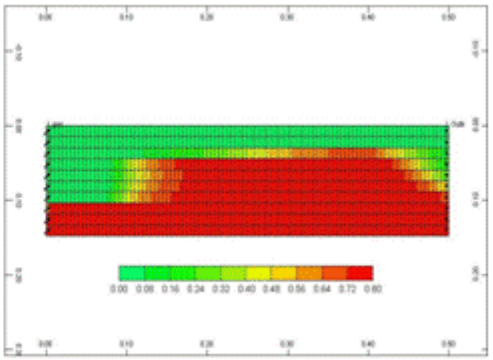

Fig. 5.45—CGI-HML oil saturation

at the end of the run

**Fig. 5.46** shows WF cumulative oil recovery comparison for the layered reservoirs (variation in k-direction). WF has shown opposite results in oil recovery from the CGI in layered reservoirs. This is because of the density difference between water and $CO_2$ where water has the tendency to segregate to the bottom.

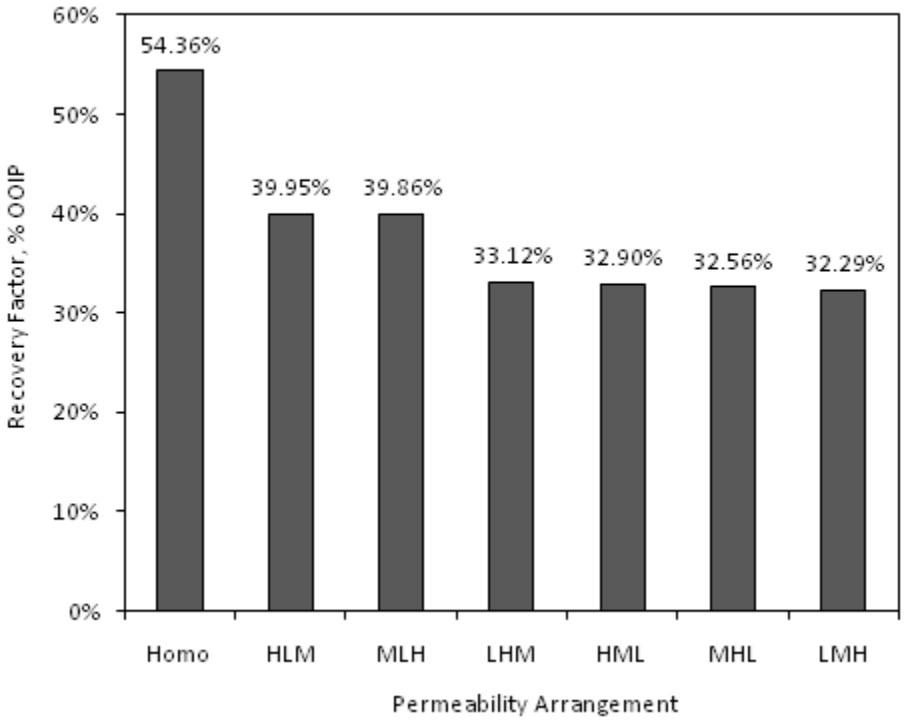


Fig. 5.46—WF: cumulative oil recovery comparison between layered reservoirs

During WF, higher permeability on the top of the reservoir resulted in higher oil recovery. However, similar to CGI, higher oil recoveries were obtained when the low permeability value is in the middle. **Figs. 5.47** through **5.52** show WF oil saturation profile (in I-K direction) during the layered reservoirs at the end of each run in the order of highest recovery. The oil recovery performance was distributed in pairs depending on the location of the low permeability layer. The highest recovery is seen when the low permeability (flow barrier) is at the middle. As seen in the figures, this case resulted in uniform recovery from the medium and high permeabilities because of the barrier in the middle. The second pair in terms of recovery is when the low permeability is at the edges. Between the two cases in this pair, the high permeability on top of the medium resulted in higher recovery because of the water tendency to segregate to the bottom. When the high permeability is at the bottom, the worst recovery is obtained because it combines the high fluid flow through this layer with the water tendency to segregate to the bottom.

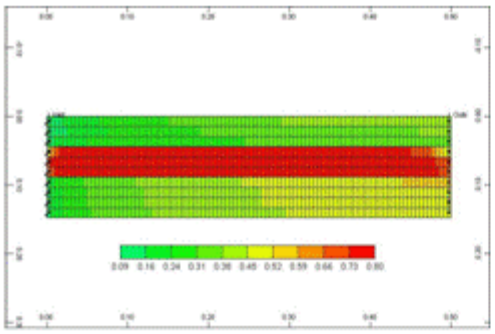

Fig. 5.47—WF-HLM oil saturation at the end of the run

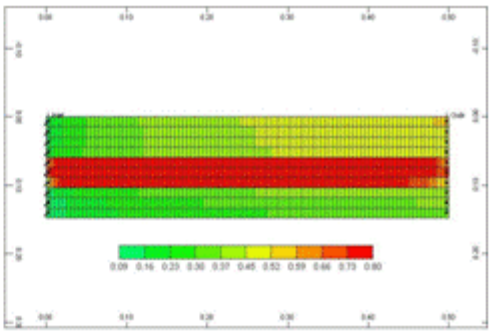

Fig. 5.48—WF-MLH oil saturation at the end of run

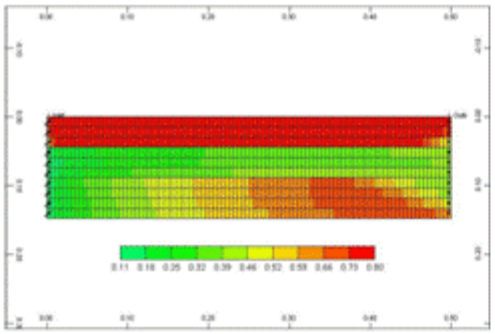

Fig. 5.49—WF-LHM oil saturation at the end of the run

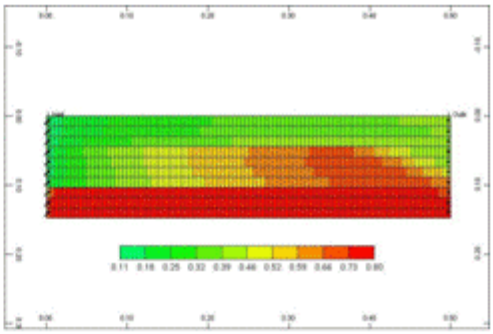

Fig. 5.50—WF-HML oil saturation at the end of the run

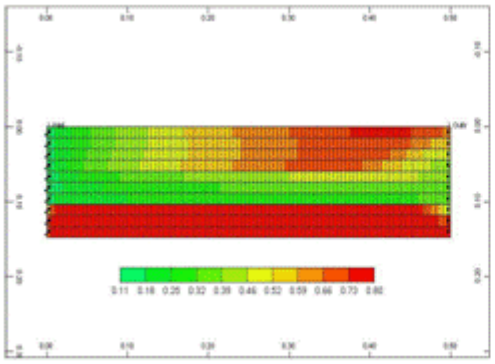

Fig. 5.51—WF-MHL oil saturation at the end of the run

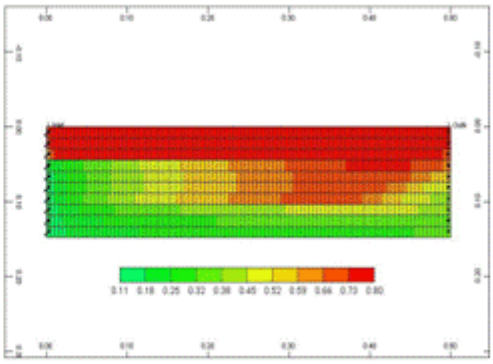

Fig. 5.52—WF-LMH oil saturation at the end of the run

**Fig. 5.53** shows WAG cumulative oil recovery comparison for the layered reservoirs (variation in k-direction). WAG has shown the same results as the CGI in terms of the permeability arrangement for the oil recovery.

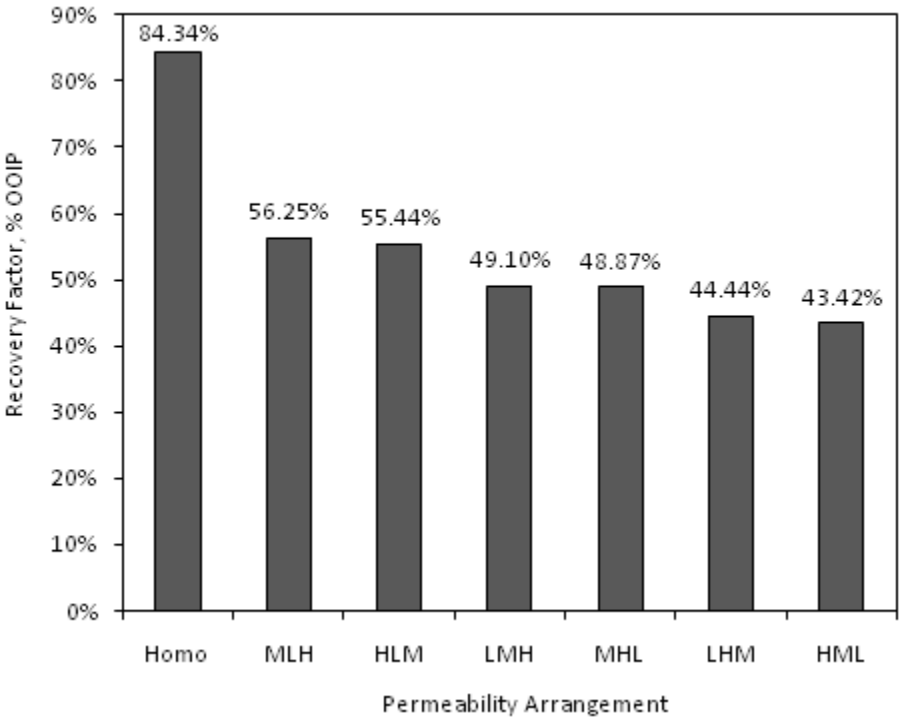


Fig. 5.53—WAG: cumulative oil recovery comparison between layered reservoirs

**Figs. 5.54** through **5.59** show WAG oil saturation profile (in I-K direction) during the layered reservoirs at the end of each run in the order of highest recovery.

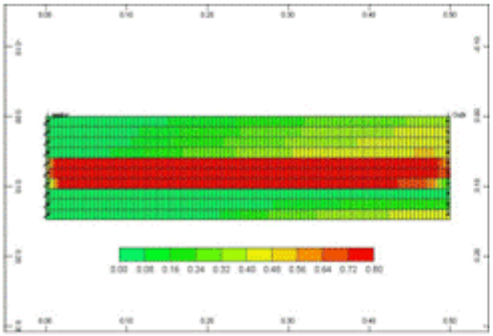

Fig. 5.54—WAG-MLH oil saturation at the end of the run

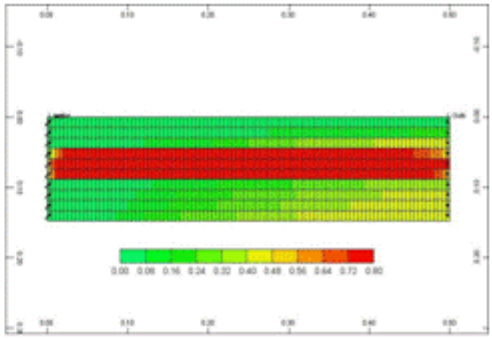

Fig. 5.55—WAG-HLM oil saturation at the end of the run

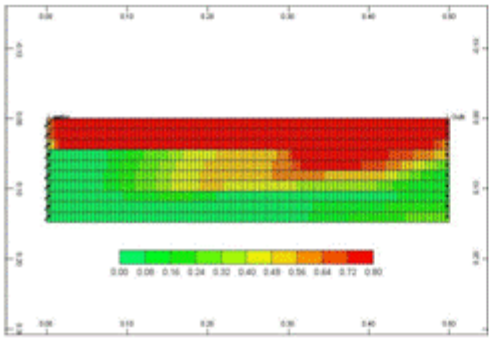

Fig. 5.56—WAG-LMH oil saturation at the end of the run

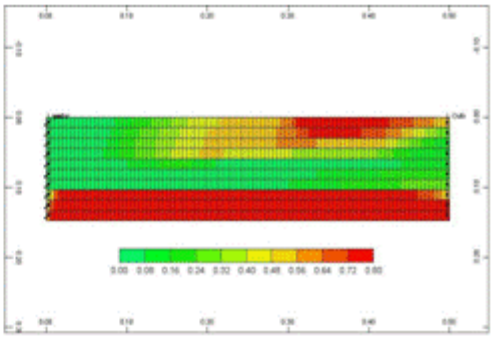

Fig. 5.57—WAG-MHL oil saturation at the end of the run

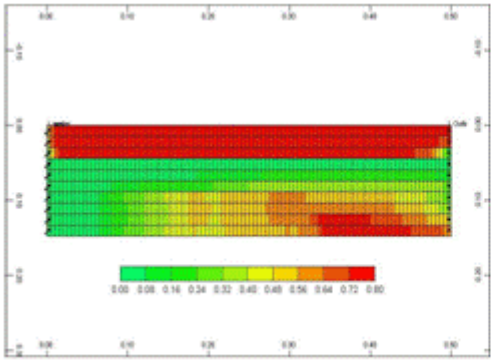

Fig. 5.58—WAG-LHM oil saturation at the end of the run

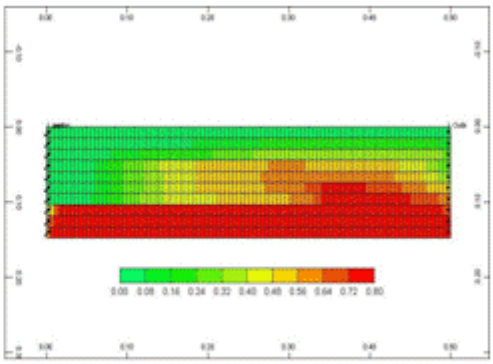

Fig. 5.59—WAG-HML oil saturation at the end of the run

**Fig. 5.60** shows SWAG cumulative oil recovery comparison for the layered reservoirs (variation in k-direction). Again, SWAG has resulted in similar permeability arrangement as CGI and WAG for the oil recovery.

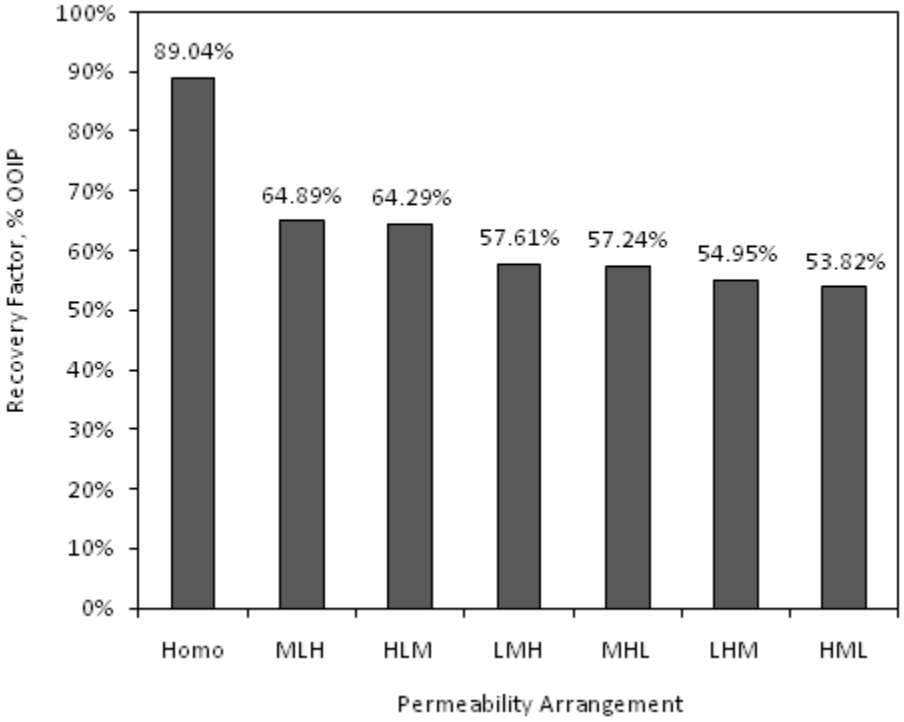


Fig. 5.60—SWAG: cumulative oil recovery comparison between layered reservoirs

**Figs. 5.61** through **5.66** show SWAG oil saturation profile (in I-K direction) for the layered reservoirs at the end of each run in the order of highest recovery. One striking fact about SWAG injection in layered reservoirs is that it is the only injection mode that produced noticeable amounts of oil from the low permeability layer especially when the low permeability layer is at the middle of the reservoir.

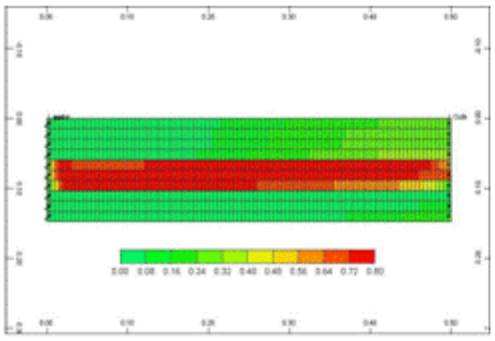

Fig. 5.61—SWAG-MLH oil saturation at the end of the run

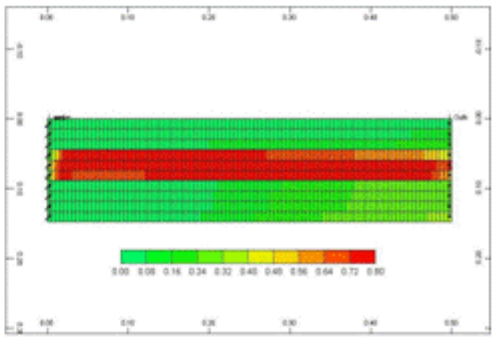

Fig. 5.62—SWAG-HLM oil saturation at the end of the run

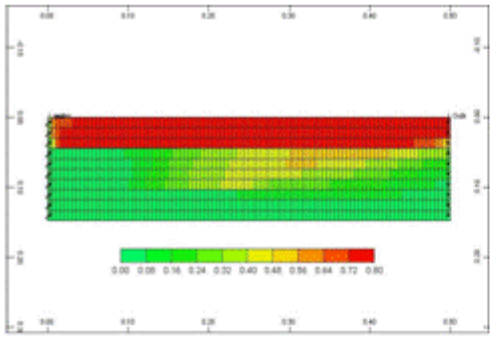

Fig. 5.63—SWAG-LMH oil saturation at the end of the run

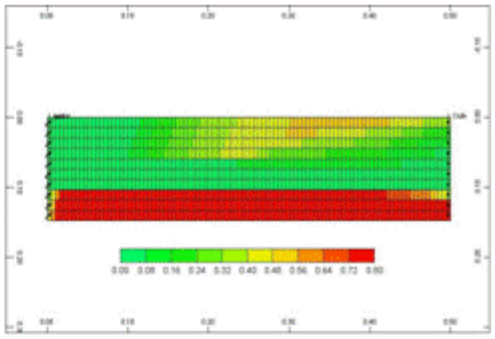

Fig. 5.64—SWAG-MHL oil saturation at the end of the run

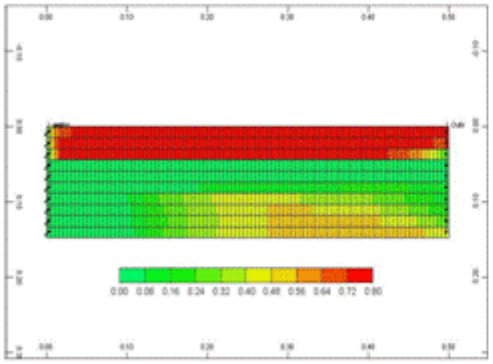

Fig. 5.65—SWAG-LHM oil saturation at the end of the run

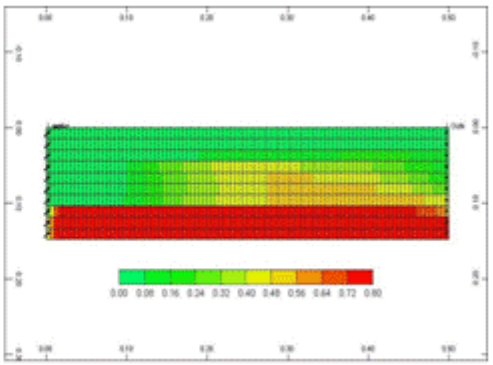

Fig. 5.66—SWAG-HML oil saturation at the end of the run

### 5.3.1.2 Sequenced Reservoirs

**Fig. 5.67** shows CGI cumulative oil recovery comparison for the sequenced reservoirs (variation in i-direction). The simulation shows that for sequenced reservoirs, CGI oil recovery is strongly dependent on the location of the low permeability value and its location in reference to the core's outlet. Higher oil recovery is obtained when the low permeability value is near the outlet followed by the low permeability in the middle and finally, when the low permeability is near the inlet.

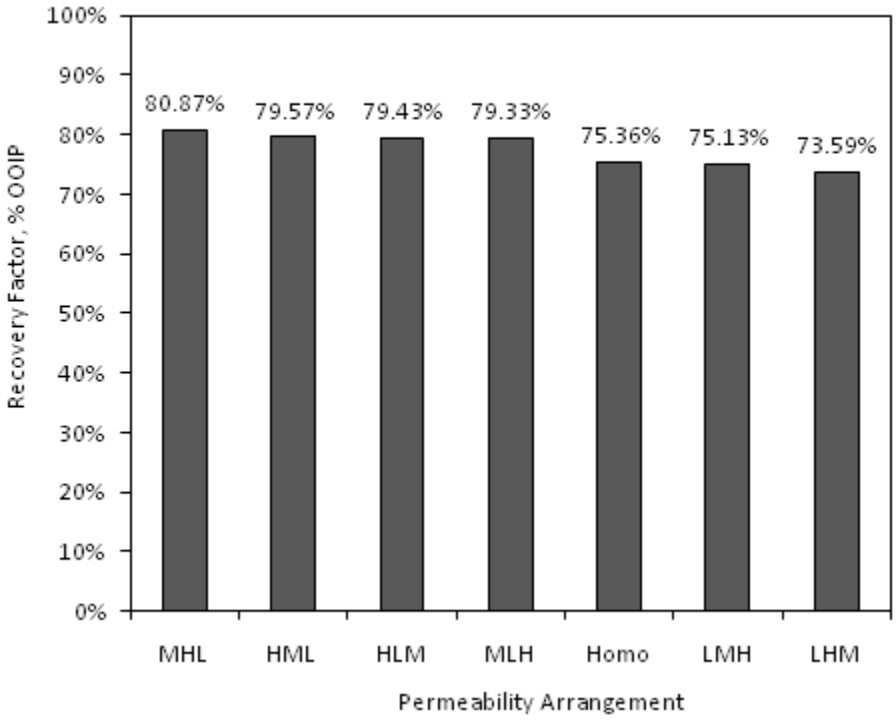


Fig. 5.67—CGI: cumulative oil recovery comparison between sequenced reservoirs

**Figs. 5.68** through **5.71** show the oil saturation and pressure profiles (in I-K direction) comparison between the best and worst case scenarios at the end of the runs. When the low permeability value is near the outlet (e.g. MHL), it allowed for more controlled displacement. On the other hand, when the low permeability is near the inlet, it increases the injection pressure, delays the oil production, and does not help in reducing the high $CO_2$ mobility as evident by the oil recovery profile.

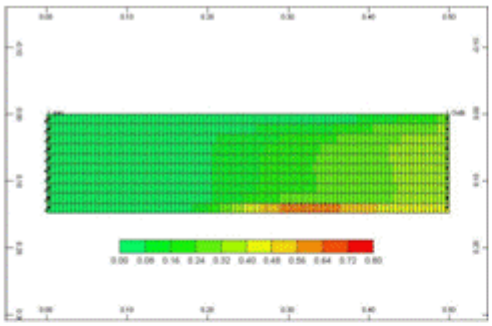

Fig. 5.68—CGI-MHL oil saturation at the end of the run

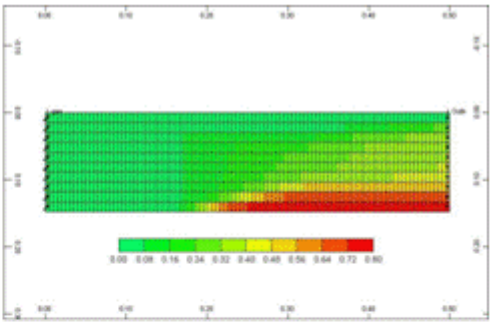

Fig. 5.70—CGI-LHM oil saturation at the end of the run

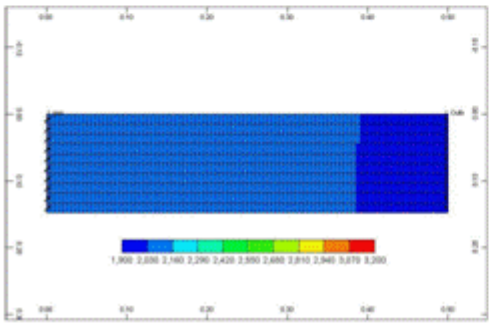

Fig. 5.69—CGI-MHL pressure at the end of the run

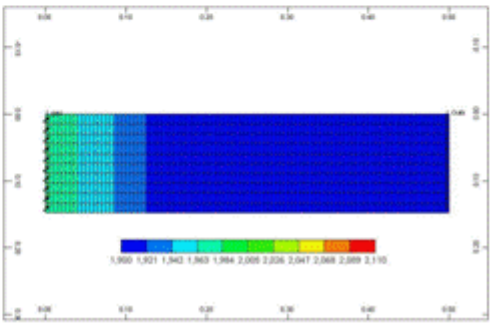

Fig. 5.71—CGI-LHM pressure at the end of the run

**Fig. 5.72** shows WF cumulative oil recovery comparison for the sequenced reservoirs (variation in i-direction). WF has shown absolute opposite results from those obtained during CGI. During WF, higher recoveries are obtained when the low permeability is near the inlet and other permeability values have no effect on oil recovery. This is evident in the oil recovery where a change is only seen when the low permeability location is changed while the change in the location of other permeability values has no effect on oil recovery. One more contrast between the two injection modes is that the change in oil recovery because of the permeability change is very small compared to the change in oil recovery during CGI.

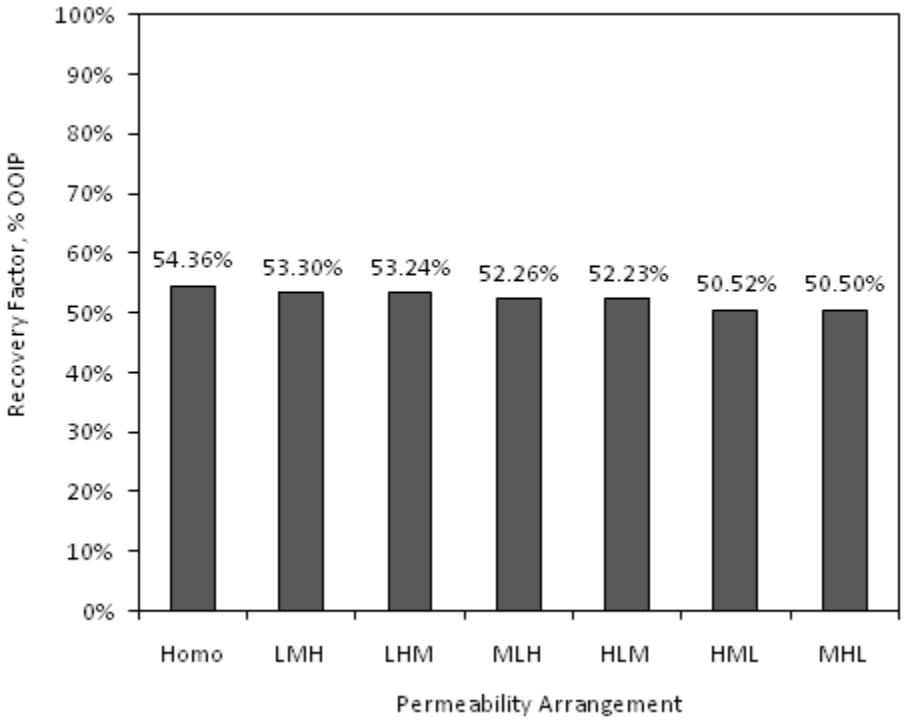


Fig. 5.72—WF: cumulative oil recovery comparison between sequenced reservoirs

**Figs. 5.73** through **5.76** show the oil saturation and pressure profiles (in I-K direction) comparison between the best and worst case scenarios at the end of the runs. The best case (LMH) showed the best displacement front because of the gradual decrease in pressure inside the core. On the other hand, the worst case (MHL) resulted in high pressure value in most of the length of the core.

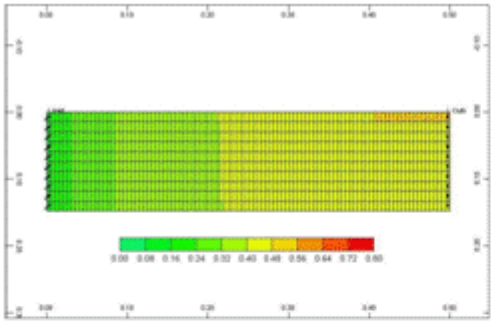

Fig. 5.73—WF-LMH oil saturation at the end of the run

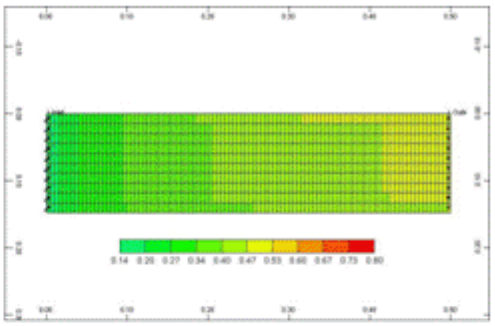

Fig. 5.75—WF-MHL oil saturation at the end of the run

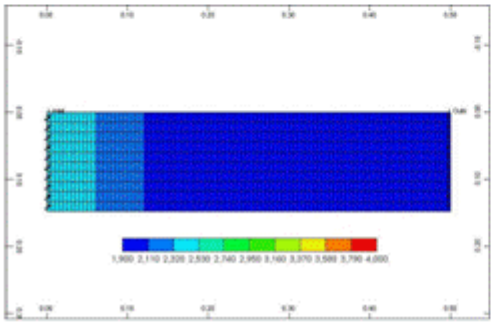

Fig. 5.74—WF-LMH pressure at the end of the run

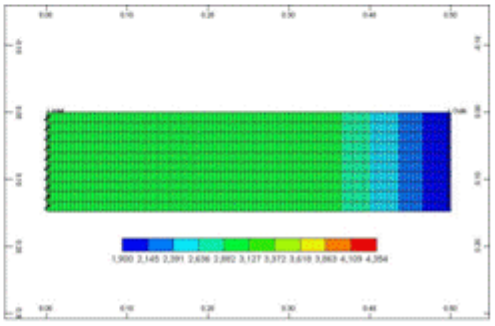

Fig. 5.76—WF-MHL pressure at the end of the run

**Fig. 5.77** shows WAG cumulative oil recovery comparison for the sequenced reservoirs (variation in i-direction). WAG oil recovery during the sequenced reservoirs has shown sensitivity to the permeability value near the inlet. This is because in this injection mode, $CO_2$ is injected alternately with water which reduces the rock's relative permeability to water after the $CO_2$ cycle (increases differential pressure).

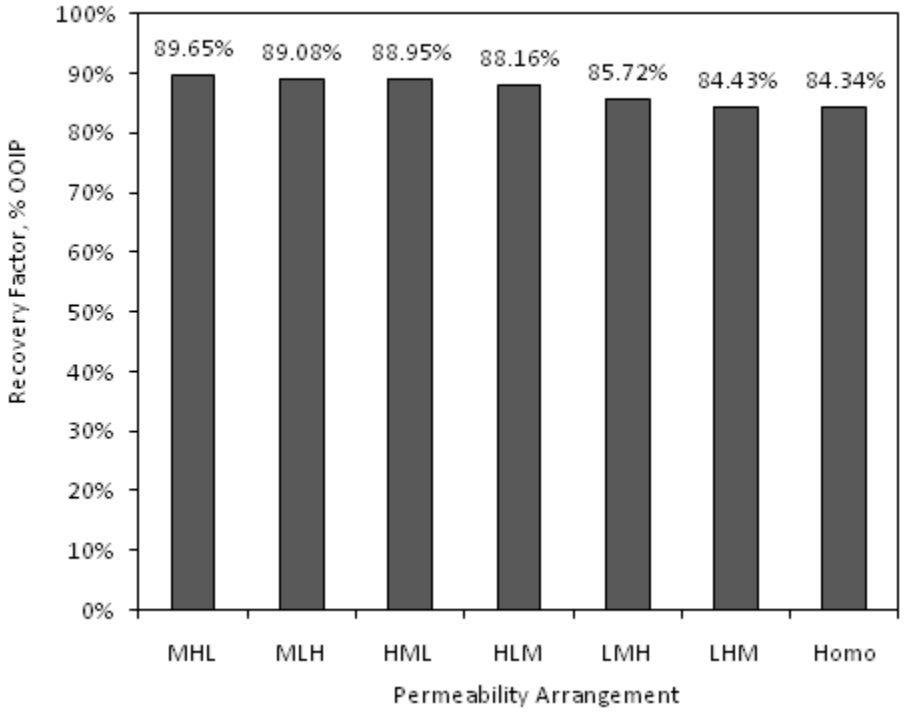


Fig. 5.77—WAG: cumulative oil recovery comparison between sequenced reservoirs

**Figs. 5.78** through **5.81** show the oil saturation and pressure profiles (in I-K direction) comparison between the best and worst case scenarios at the end of the runs. Similar to CGI, the MHL has resulted in a very uniform displacement front because of the low permeability near the outlet.

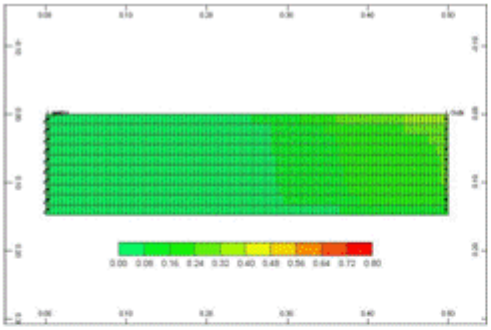

Fig. 5.78—WAG-MHL oil saturation at the end of the run

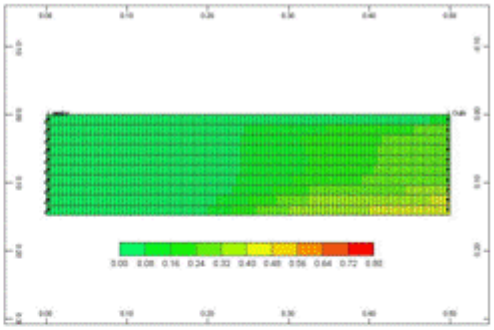

Fig. 5.80—WAG-LHM oil saturation at the end of the run

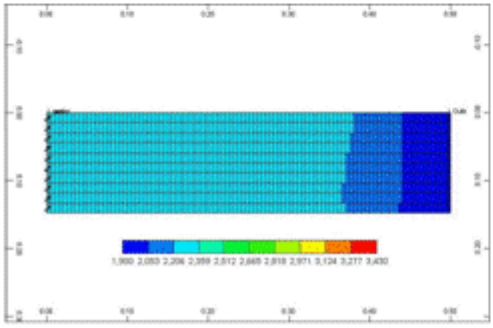

Fig. 5.79—WAG-MHL pressure at the end of the run

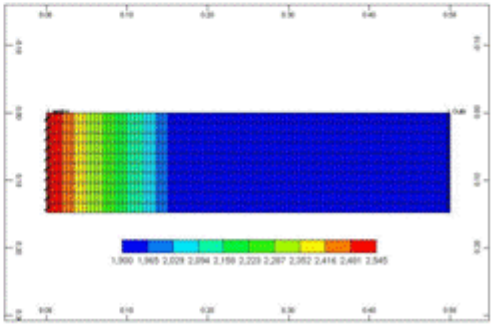

Fig. 5.81—WAG-LHM pressure at the end of the run

**Fig. 5.82** shows SWAG cumulative oil recovery comparison for the sequenced reservoirs (variation in i-direction). The simulation shows that SWAG oil recovery depends on the permeability value near the outlet. The highest oil recovery was obtained when the high permeability (H) was near the outlet. Then, the oil recovery decreases as this value decreases. The best oil recovery was obtained with LMH arrangement because it resulted in a uniform pressure gradient in the core (gradual decrease).

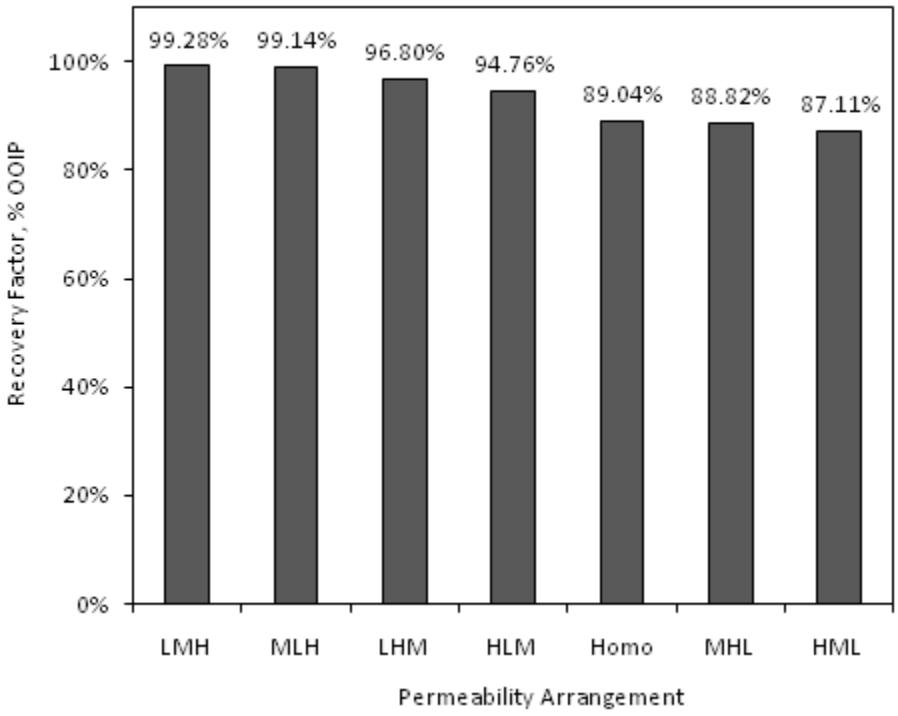


Fig. 5.82—SWAG: cumulative oil recovery comparison between sequenced reservoirs

**Figs. 5.83** through **5.86** show the oil saturation and pressure profiles (in I-K direction) comparison between the best and worst case scenarios at the end of the runs.

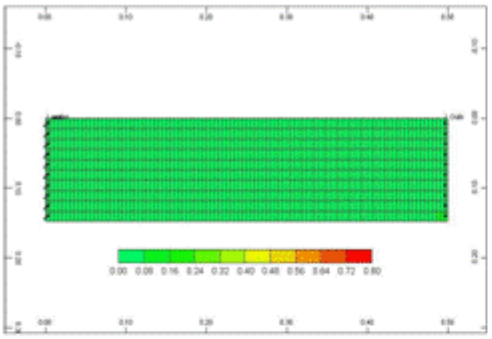

Fig. 5.83—SWAG-LMH oil saturation at the end of the run

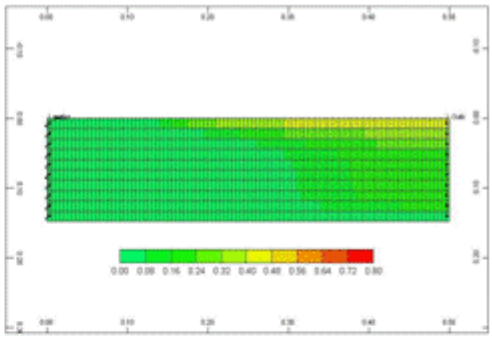

Fig. 5.85—SWAG-HML oil saturation at the end of the run

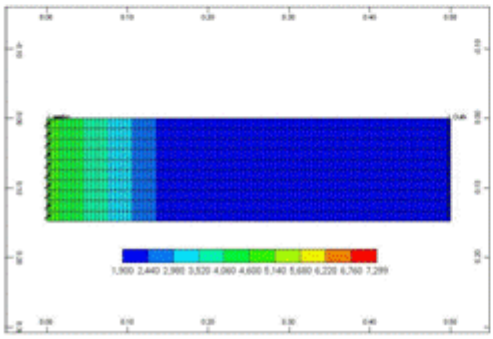

Fig. 5.84—SWAG-LMH pressure at the end of the run

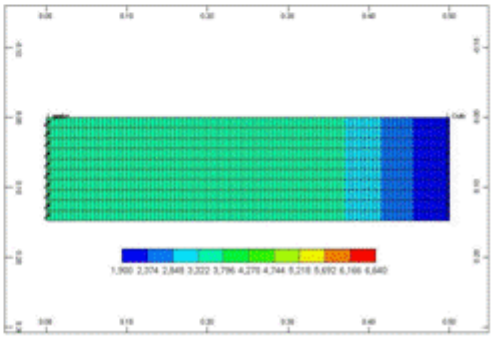

Fig. 5.86—SWAG-HML pressure at the end of the run

### 5.3.2 WAG Ratio

During WAG, the injection of each fluid is considered half-cycle. The half-cycle volume is referred to as slug size whereas the number of fluid-to-fluid half-cycles is referred to as WAG ratio. For example, a WAG ratio of 1:2 refers to one slug of water to two slugs of gas. WAG ratio is considered one of the most important parameters that define the economics of field development during $CO_2$ injection (Jarrell et al. 2002). Most researchers have found the ratio of 1:1 to be the optimum case (Christensen et al. 2001); however, different ratios have been reported in both research studies and field applications. In this study, different WAG ratios have been numerically investigated including both increasing water and gas ratios. Also, WAG ratio studies were carried out on homogenous and layered reservoirs. The slug size was kept constant at 0.33 PV during all WAG ratios and the first slug is always gas.

#### 5.3.2.1 WAG Ratio for Homogenous Cores

**Fig. 5.87** shows the cumulative oil recovery comparison during all WAG ratios. The simulation shows that increasing gas ($CO_2$) ratio results in higher oil recovery at 1:2 but then, the oil recovery decreases with increasing gas ratio. Also, the increase in oil recovery during the 1:2 WAG ratio is very small (2.6%) and does not justify the increase in the amount of injected $CO_2$. On the other hand, increasing water ratios decreases oil recovery significantly because it decreases the amount of injected $CO_2$.

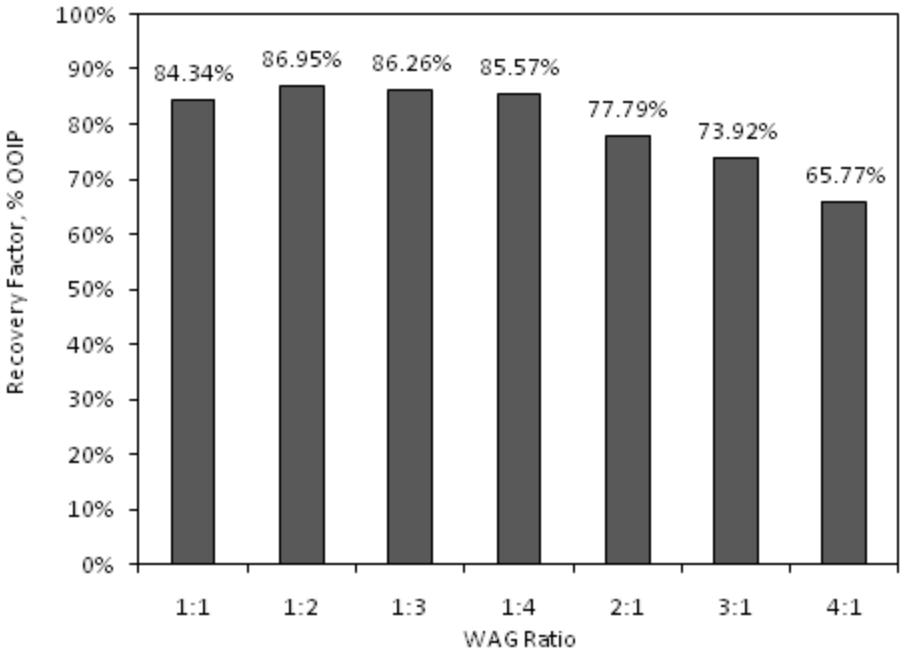


Fig. 5.87— Cumulative oil recovery sensitivity to WAG ratio

### 5.3.2.2 WAG Ratio for Layered Reservoirs

WAG ratio sensitivity was carried out on the layered reservoirs in a similar manner to that used in the homogenous case. For each permeability arrangement in layered reservoirs, a number of WAG ratios were tested including increasing water and gas ratios. It was found that for each permeability arrangement pair which resulted in a similar cumulative oil recovery (found in layered reservoirs), there is a certain WAG ratio that results in a higher oil recovery. The cumulative oil recovery figures for these entire WAG ratios and permeability arrangements are included in Appendix D. A summary of the results is shown in **Table 5.1**.

| TABLE 5.1 SUMMARY OF WAG RATIO STUDIES IN LAYERED RESERVOIRS | | | | | |
|---|---|---|---|---|---|
| **Case** | **1:1 RF,%** | **Highest Recovery** | | **Recovery Factor Response to WAG Ratio** | |
| | | **%** | **Ratio** | **Increasing Gas Ratio** | **Increasing Water Ratio** |
| **Homogeneous** | 84.34 | 86.95 | 1:2 | increases until 1:2, then decreases | Decreases |
| **MLH** | 56.25 | 57.26 | 1:4 | constant, low at 1:3, then increases | Decreases |
| **HLM** | 55.44 | 57.51 | 1:4 | constant, low at 1:3, then increases | Decreases |
| **LMH** | 49.10 | 49.21 | 1:2 | constant, decreases at 1:4 | constant, decreases at 4:1 |
| **MHL** | 48.87 | 48.87 | 1:1 | constant, decreases at 1:4 | constant, decreases at 4:1 |
| **LHM** | 44.44 | 44.44 | 1:1 | Decreases | Decreases, but higher oil recovery than increasing gas ratio |
| **HML** | 43.42 | 43.42 | 1:1 | Decreases | Decreases, but higher oil recovery than increasing gas ratio |

The results show that WAG ratio of 1:1 is the optimum ratio for most cases. Although some cases have shown higher oil recovery during different WAG ratios (e.g. MLH), the increase in oil recovery in these cases is very small that does not justify the increase in the amount of injected $CO_2$. The results also show that WAG ratio is sensitive to the location of the low permeability layer (flow barrier). Permeability arrangements that resulted in similar oil recoveries (pairs) have shown similar preference to WAG ratios.

However, two cases (LHM and HML) have shown different results and indicated that further WAG ratio optimization is very feasible. Both cases have shown that highest oil recovery is obtained during 1:1 WAG ratio but the cumulative oil recovery response to increasing water ratio is very promising. Those two cases are ranked the worst cases in terms of oil recovery among all layered reservoirs. This indicates that they have the highest degree of heterogeneity. Therefore, the increase in water ratio resulted in oil recoveries that are very close to those with higher gas ratios, yet the amount of injected $CO_2$ is reduced significantly. **Figs. 5.88** and **5.89** show a detailed look into the cumulative oil recovery and amount of injected $CO_2$, respectively, for the case of HML permeability arrangement. The figures show that during the increasing water ratios, the cumulative oil recovery is within 1-2 % difference to the 1:1 WAG ratio. However, the amount of injected $CO_2$ is about 53% less than 1:1 WAG ratio. Therefore, considering the overall economics of these cases, 3:1 WAG ratio would be the optimum ratio for this case.

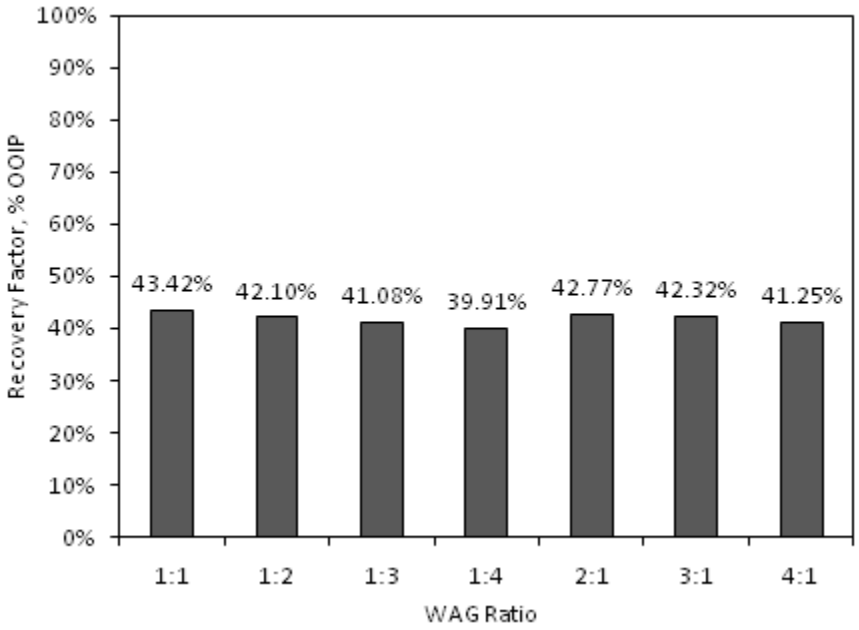


Fig. 5.88— HML: cumulative oil recovery during different WAG ratios

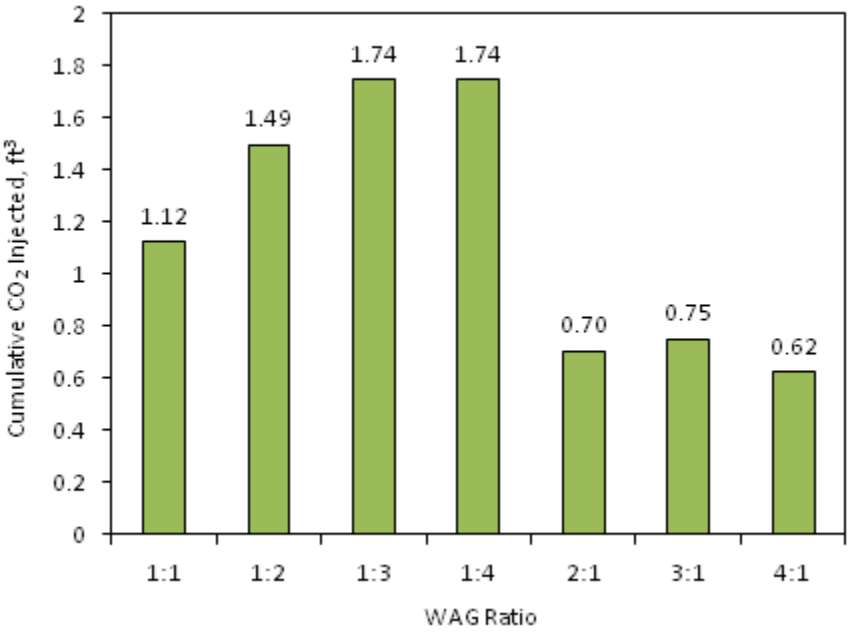


Fig. 5.89— HML: cumulative $CO_2$ injected during different WAG ratios

**Fig. 5.90** shows a traditional cumulative oil recovery versus pore volume injected graph for the HML case during three different WAG ratios: the common 1:1, increasing water ratio of 3:1, and increasing gas ratio of 1:3. During all cases, an increase in oil recovery is realized when water is injected after $CO_2$. For this case, this shows the reason why increasing water ratio results in oil recoveries close to those ratios that use higher amounts of injected $CO_2$.

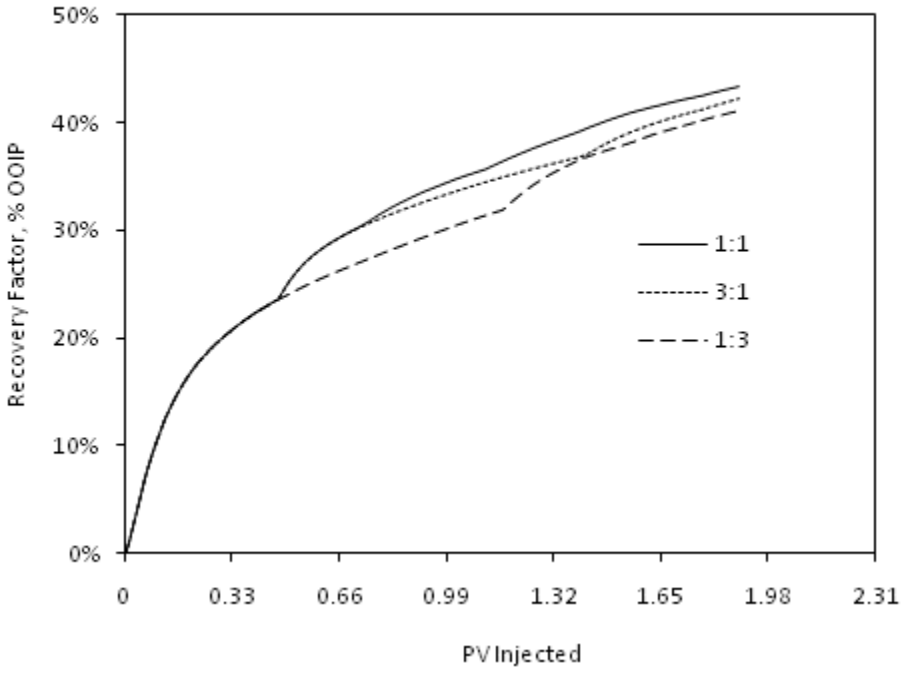


Fig. 5.90— HML: cumulative oil recovery versus PV injected during different WAG ratios

### 5.3.3 WAG Slug Size

In this study, different volumes of gas (slug sizes) have been investigated while keeping WAG ratio constant at 1:1 and gas is always the first slug. **Fig. 5.91** shows the cumulative oil recovery during the different $CO_2$ slug sizes. The simulation shows that slug size effect on oil recovery depends on the amount of injected $CO_2$ and the resulted number of $CO_2$ cycles. The results show that smaller $CO_2$ slug size allows for higher number of cycles and more mobility control by the water cycles. Therefore, smaller $CO_2$ cycles resulted in higher oil recovery.

In practice, WAG slug size depends greatly on operational flexibility to switch wells from one fluid to another. It has been reported in the literature that one week is the minimum practical time for manual switching; however, some fields with remote switching capability have reported one day switching (Jarrell et al. 2002).

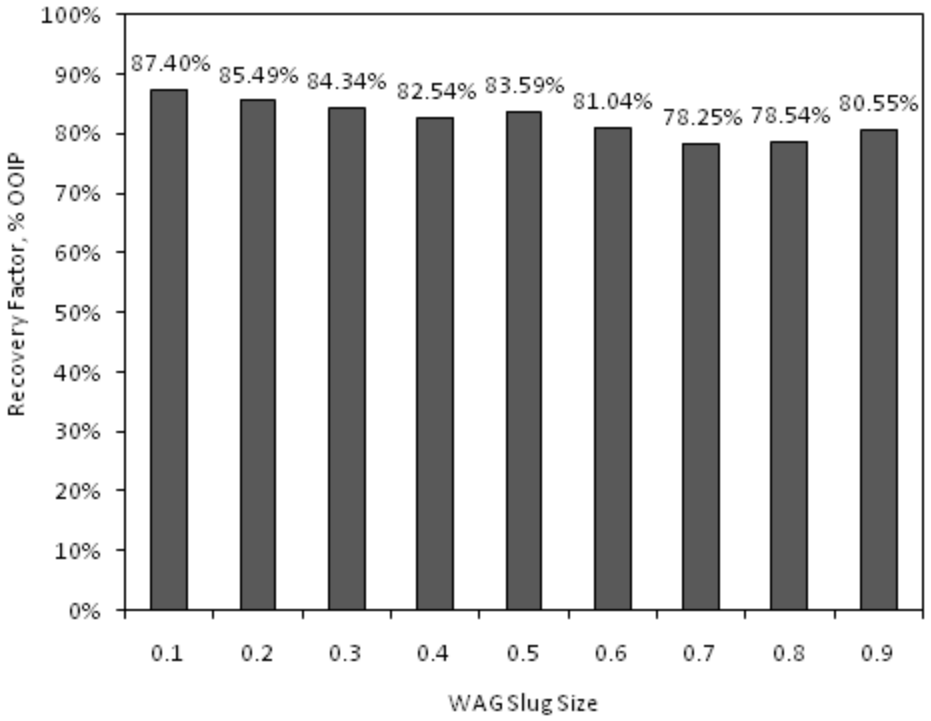


Fig. 5.91— Cumulative oil recovery sensitivity to WAG slug size

### 5.3.4 SWAG Volume Ratio

SWAG volume ratio refers to the injection rate of each fluid, water and $CO_2$. Caudle and Dyes (1958) were the first to study SWAG and they found that the optimum ratio is 1:1 based on fluids velocities. At this ratio, the displacement ensures a slug of solvent ($CO_2$) ahead of the displacement front, because of the gas high velocity, followed by a mixture of water and solvent. In this study, the ratio of each fluid was changed to investigate its effect on oil recovery. Each fluid injection rate was changed

while keeping the total fluid injection constant at 0.5 $cm^3$/min. For example, at a ratio of 1:3, water is injected at a rate of 0.125 $cm^3$/min while $CO_2$ is injected at a rate of 0.375 $cm^3$/min. **Fig. 5.92** shows the change in cumulative oil recovery during different SWAG ratios while 1:1 ratio was kept as the base case. The simulation shows that increasing water ratio will decrease the cumulative oil recovery whereas increasing $CO_2$ ratio increases oil recovery. However, the increase in oil recovery when increasing the $CO_2$ ratio is not significant and further increase in its ratio will result in no incremental recovery. On the other hand, the sensitivity to water ratio is more pronounced and further increase in water ratio will deteriorate the oil recovery. Therefore, it was concluded that the base case (1:1 ratio), which was used during the experimental part of this study, is the optimum case.

For layered reservoirs, a similar trend was observed for all permeability arrangements. A summary of the layered reservoirs' response to changing SWAG ratio is shown in **Table 5.2**.

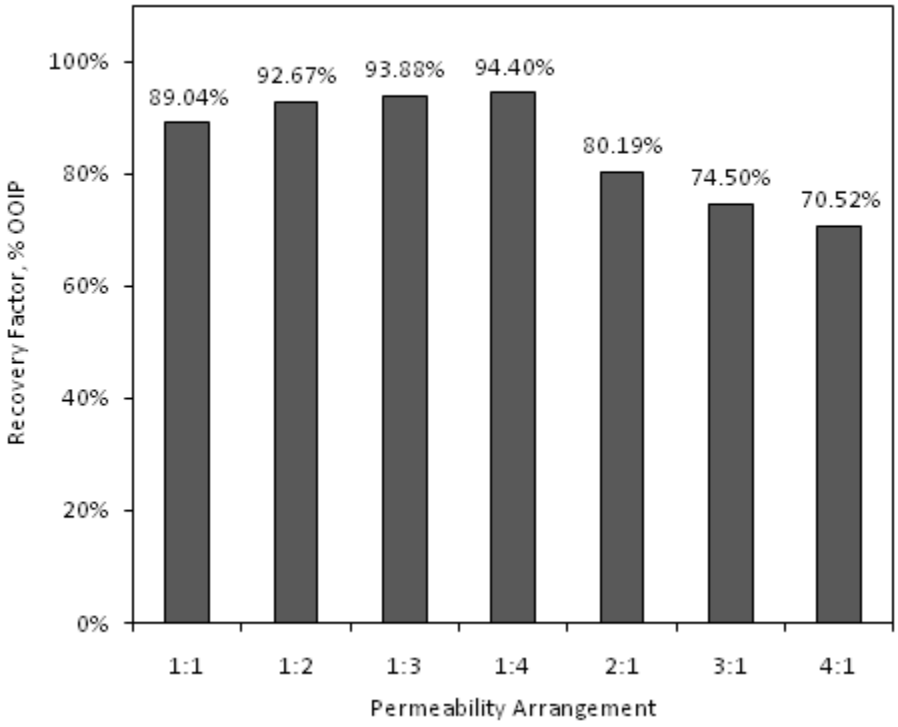


Fig. 5.92— Cumulative oil recovery sensitivity to SWAG volume ratio

| TABLE 5.2 SUMMARY OF SWAG VOLUME RATIO STUDIES IN LAYERED RESERVOIRS | | | | | |
|---|---|---|---|---|---|
| **Case** | **1:1 RF,%** | **Highest Recovery** | | **Recovery Factor Response to WAG Ratio** | |
| | | **%** | **Ratio** | **Increasing Gas Ratio** | **Increasing Water Ratio** |
| **Homogeneous** | 89.04 | 94.40 | 1:4 | increase | Decrease |
| **MLH** | 64.89 | 69.55 | 1:4 | increase | Decrease |
| **HLM** | 64.29 | 68.48 | 1:4 | increase | Decrease |
| **LMH** | 57.61 | 66.51 | 1:4 | increase | Decrease |
| **MHL** | 57.24 | 65.88 | 1:4 | increase | Decrease |
| **LHM** | 54.95 | 60.55 | 1:4 | increase | Decrease |
| **HML** | 53.82 | 60.05 | 1:4 | increase | Decrease |

# CHAPTER VI

# SUMMARY, CONCLUSIONS, AND RECOMMENDATIONS

## 6.1 Summary

The oil recovery from carbonate cores during $CO_2$ injection was investigated using coreflood experiments and numerical simulation. $CO_2$ was injected under miscible conditions where the MMP was measured using the industry standard method, slimtube apparatus. Then, the effects of the displacement length and core particle size distribution on oil recovery were studied by combining the slimtube coil to the core and CT scanning the core. During coreflood experiments, different modes of injection were studied including CGI, WF, WAG, and SWAG and the results were then compared. Different parameters were investigated for each injection mode such as: injected water salinity and two different fracture shapes.

Based on the experimental results, a numerical simulation model was constructed to match the main experiments and conduct a sensitivity study. The experiments were simulated with the Computer Modeling Group's (CMG) commercial reservoir simulator IMEX. The matched simulation model was used to study the effect of permeability variations in the core, WAG ratio and slug size, and SWAG volume ratio.

## 6.2 Conclusions

Based on both the experimental and numerical studies, the following are the main conclusions:

1. Miscible displacement is independent of length. The lower oil recovery during CGI is a result of dispersive bypassing due to the rock's heterogeneity as shown by the CT scanner results. When the displacement length was increased, no additional oil recovery was obtained confirming this conclusion.
2. Injecting water with $CO_2$ either simultaneously (SWAG) or in alternating cycles (WAG) results in higher oil recovery and significant reduction in $CO_2$ requirements. The following are the main advantages of SWAG and WAG injections:
    - The increase in oil recovery during SWAG and WAG injections over CGI was measured to be 23% and 17%, respectively.
    - SWAG uses 50% less $CO_2$ than CGI while WAG uses 40% less $CO_2$.
    - The associated water reduces the $CO_2$ high mobility and creates a water-$CO_2$ mixture that follows the displacement front and recovers the bypassed oil.
3. All $CO_2$ injection modes resulted in higher recovery than WF alone. WF resulted in 54% recovery of OOIP while SWAG injections resulted in 98.6% which is a 44% increase in recovery. This is because of the low IFT between the $CO_2$ and the oil during the miscible injection.

4. Injecting $CO_2$ in secondary mode results in higher recovery than tertiary mode (75.37% vs. 65.63% of OIP). However, if the WF recovery (prior to $CO_2$) is considered, the ultimate recovery of the tertiary mode is higher but at a later time. The combined recovery from WF and CGI (tertiary recovery) is measured to be 83% of OOIP.
5. For this system, changing water salinity has no effect on WF alone. Both salinity levels (6 wt. % and 0 wt. %) have shown identical results.
6. Changing water salinity during $CO_2$ injection in WAG and SWAG has a detrimental effect on oil recovery. The decrease in water salinity increases $CO_2$ solubility in water. Therefore, the experimental results show an increase in oil recovery when the salinity of the water is decreased. The increase in oil recovery because of lowering water salinity reaches 18% OOIP.
7. In a one-fracture core, CGI in secondary mode has resulted in very poor results. However, during tertiary recovery mode (because of the presence of water), the results are improved.
8. In a two-fracture core, all $CO_2$ injection modes showed better results than the one-fracture core because of the vertical fracture in the middle (at least 10% increase). This is because the middle vertical fracture caused fluids to diffuse upward and contact more matrix oil. This suggests injecting $CO_2$ perpendicular to the fractures in field applications.
9. WAG and SWAG injections have shown significantly higher recoveries than CGI in all fractured cores. The increase in oil recovery is estimated to be at least

17% of OOIP. This suggests that $CO_2$ should always be injected with water in fractured reservoirs.

10. WF oil recovery is much less affected by the fracture than all $CO_2$ injection modes because water is considered a wetting phase (only 7.5% decrease in recovery). This is the reason for the improvement in oil recovery during WAG and SWAG injections in fractured cores.
11. During the permeability variations, the simulation shows that the oil recovery is more affected by the change in permeability in k-direction (layered reservoirs) than the i-direction (sequenced reservoirs). This is because during layered reservoirs, the low permeability acts as a barrier and the injected fluids have an easier path to follow through the higher permeability layers. On the other hand, during sequenced reservoirs, injected fluids have to go through the low permeability layers and therefore, the differential pressure across the core increases significantly.
12. In layered reservoirs, higher oil recoveries are obtained when the low permeability (flow barrier) is in the middle during all injection modes. However, the oil recovery during all $CO_2$ injection modes shows higher results when the medium permeability is at the top while WF shows higher oil recovery when the high permeability is at the top. This is because of the difference between water and $CO_2$ densities which determines the segregation preference.
13. In sequenced reservoirs, each injection mode showed different preference to the arrangement of permeability values. CGI oil recovery is higher when the low

permeability is near the outlet. WF oil recovery is higher when the low permeability is near the inlet. WAG oil recovery is higher when the medium permeability is near the inlet. SWAG oil recovery is higher when the low permeability is near the outlet.

14. The optimum WAG and SWAG ratios are found to be 1:1 for the homogenous case. The increase in gas ratio had minor effect on recovery; however, when the water ratio increased, the oil recovery deteriorated during both WAG and SWAG. In layered reservoirs, higher oil recoveries were obtained at different WAG ratios depending on the location of the low permeability layer but the optimum was found to be 1:1. Unlike all cases, HML and LHM cases have shown higher oil recovery with increasing water ratio. SWAG volume ratio sensitivity in layered reservoirs has shown similar results to the homogenous case.
15. For WAG injection, smaller $CO_2$ slug size allows for higher number of $CO_2$ cycles and more mobility control by the water cycles. Therefore, smaller $CO_2$ slug size resulted in higher oil recovery.

## 6.3 Recommendations

The following are recommendations for field applications:

1. In EOR, $CO_2$ should always be injected in WAG or SWAG modes, unless operationally difficult. Both WAG and SWAG have shown higher oil recoveries and significant reduction in $CO_2$ requirements which will positively affect the project economics.
2. When oil bypassing is expected during $CO_2$ injection in the field, decreasing the injected water salinity will increase the $CO_2$ solubility in the water. As a result, the water-$CO_2$ mixture will better sweep the bypassed oil and increase oil recovery.
3. CGI should not be implemented in NFR. In this case, WAG and SWAG injections become essential. If for operational difficulties water cannot be injected, $CO_2$ should be injected perpendicular to the fractures and if possible in tertiary mode.
4. In reservoirs with heterogeneity in the form of permeability variations, prior assessment and meticulous reservoir management become more essential. For example, injection locations should be optimized to take advantage of flow barriers and $CO_2$ tendency to segregate to the top.

The following are the main recommendations for future studies:

1. Consider conducting similar research on a 3-D model to study the sweep efficiency.
2. Replace the carbonate cores with sandstones and study their effect on oil recovery.
3. Use “live” oil instead of dead oil. During “live” oil experiments, compositional analysis of the produced oil will provide essential data.
4. Use compositional simulation to match the “live” oil experimental results and study the changes in oil composition during $CO_2$ injection.

# NOMENCLATURE

| | |
|---|---|
| 1D | One Dimensional |
| 2D | Two Dimensional |
| 3D | Three Dimensional |
| API | American Petroleum Institute |
| ADSA | Axisymmetric Drop Shape Analysis |
| BPR | Back Pressure Regulator |
| BHP | Bottom Hole Pressure |
| $CO_2$ | Carbon Dioxide |
| CMG | Computer Modeling Group |
| CT | Computer Tomography |
| $CT_{x,y}^{100\%\ water}$ | CT Number for Core Saturated with 100% Water at x, y Position |
| $CT_{x,y}^{Dry}$ | CT Number for Dry Core at x, y Position |
| $CT_{water}$ | CT Number for Water |
| $CT_{air}$ | CT Number for Air |
| CGI | Continuous Gas Injection |
| DP | Differential Pressure |
| $D_o$ | Effective Molecular Diffusion Coefficient |
| $d_p$ | Particle Diameter |
| EOR | Enhanced Oil Recovery |

| | |
|---|---|
| EOS | Equation of State |
| FAWAG | Foam Assisted Water Alternating Gas |
| $F$ | Formation Factor |
| GOR | Gas Oil Ratio |
| HP-HI | Horizontal Producer-Horizontal Injector |
| HCPV | Hydrocarbon Pore Volume |
| HP/HT | High Pressure/High Temperature |
| IOR | Improved Oil Recovery |
| IMEX | Black Oil Simulator from CMG |
| IWAG | Immiscible Water Alternating Gas |
| $K_v$ | Vertical Permeability |
| $K_h$ | Horizontal Permeability |
| $K_l$ | Longitudinal Dispersivity Coefficient |
| LPG | Liquefied Petroleum Gas |
| MCM | Multiple Contact Miscible |
| MMP | Minimum Miscibility Pressure |
| MSCF | Thousand Standard Cubic Foot |
| mD | Millidarcy |
| NMR | Nuclear Magnetic Resonance |
| NFR | Naturally Fractured Reservoirs |
| NaCl | Sodium Chloride |
| NaI | Sodium Iodide |

| | |
|---|---|
| $N_c$ | Capillary Number |
| $N_{pc}$ | Dimensionless Peclet Number |
| $N_2$ | Nitrogen |
| OOIP | Original Oil In Place |
| OIIP | Oil Initially In Place |
| OIP | Oil In Place |
| PV | Pore Volume |
| PVT | Pressure, Volume, Temperature |
| ppm | Parts Per Million |
| RB | Reservoir Barrels |
| SWAG | Simultaneous Water and Gas |
| SSWAG | Selective Simultaneous Water and Gas |
| SEM | Scanning Electron Microscope |
| STB | Stock Tank Barrel |
| SAG | Surfactant Alternating Gas |
| $SO_4^{-2}$ | Sulphate Ion |
| VP-VI | Vertical Producer-Vertical Injector |
| WAG | Water Alternating Gas |
| WF | Waterflood |
| XRD | X-ray Diffraction |
| $\phi$ | Porosity |
| $\sigma$ | Inhomogeneity Factor |

# REFERENCES


Aguilera, M.E. and de Ramos, A.L. 2004. Effect of $CO_2$ Diffusion on Wettability for Hydrocarbon-Water-$CO_2$ Systems in Capillaries. *International Communications in Heat and Mass Transfer* **31** (8): 1115-1122. WOS:000224716700009.

Ahr, W.M. 2008. *Geology of Carbonate Reservoirs*. Hoboken, New Jersey: Wiley & Sons, Inc.

Akin, S. 2001. Estimation of Fracture Relative Permeabilities from Unsteady State Corefloods. *Journal of Petroleum Science and Engineering* **30** (1): 1-14. WOS:000169317700001.

Algharaib, M.K., Gharbi, R.B., and Al-Ghanim, W. 2007a. The Performance of a SWAG Process in Oil Recovery Operations. Paper presented at the Saudi Arabia Technical Symposium, Dhahran, Saudi Arabia. 110962-MS.

Algharaib, M.K., Gharbi, R.B., Malallah, A. et al. 2007b. Parametric Investigations of a Modified SWAG Injection Technique. Paper presented at the SPE Middle East Oil and Gas Show and Conference, Kingdom of Bahrain. 105071-MS.

Alston, R.B., Kokolis, G.P., and James, C.F. 1985. $CO_2$ Minimum Miscibility Pressure - a Correlation for Impure $CO_2$ Streams and Live Oil Systems. *SPE Journal* **25** (2): 268-274. WOS:A1985AGX1700011.

Attanucci, V., Aslesen, K.S., Hejl, K.A. et al. 1993. WAG Process Optimization in the Rangely $CO_2$ Miscible Flood. Paper presented at the SPE Annual Technical Conference and Exhibition, Houston, Texas. 26622-MS.

Bagci, S. and Tuzunoglu, E. 1998. 3D Model Studies of the Immiscible $CO_2$ Process Using Horizontal Wells for Heavy Oil Recovery. Paper presented at the 49th Annual Technical Meeting of the Petroleum Society, Calgary, Alberta, Canada. 98-74.

Barnawi, M. 2008. A Simulation Study to Verify Stone's Simultaneous Water and Gas Injection Performance in a 5-Spot Pattern. MS thesis, Texas A&M University.

Benham, A.L., Dowden, W.E., and Kunzman, W.J. 1960. Miscible Fluid Displacement - Prediction of Miscibility. *Transactions of the American Institute of Mining and Metallurgical Engineers* **219** (10): 229-237. WOS:A1960WY74400002.

Berge, L.I., Stensen, J.ï.g., Crapez, B. et al. 2002. SWAG Injectivity Behavior Based on Siri Field Data. Paper presented at the SPE/DOE Improved Oil Recovery Symposium, Tulsa, Oklahoma. 75126-MS.

Blackwell, R.J., Terry, W.M., Rayne, J.R. et al. 1960. Recovery of Oil by Displacements with Water-Solvent Mixtures. *Transactions of the American Institute of Mining and Metallurgical Engineers* **219** (12): 293-300. ISI:A1960WY74600002.

Caudle, B.H. and Dyes, A.B. 1958. Improving Miscible Displacement by Gas-Water Injection. *Transactions of the American Institute of Mining and Metallurgical Engineers* **213** (11): 281-284. ISI:A1958WY73300005.

Chakravarthy, D., Muralidharan, V., Putra, E. et al. 2006. Mitigating Oil Bypassed in Fractured Cores During $CO_2$ Flooding Using WAG and Polymer Gel Injections. Paper presented at the SPE/DOE Symposium on Improved Oil Recovery, Tulsa, Oklahoma. 97228-MS.

Christensen, J.R., Stenby, E.H., and Skauge, A. 2001. Review of WAG Field Experience. *SPE Reservoir Evaluation & Engineering* **4** (2): 97-106. ISI:000168663600003.

Cronquist, C. 1978. Carbon Dioxide Dynamic Miscibility with Light Reservoir Oils. In *Fourth Annual U.S. DOE Symposium*, 1. Tulsa, Oklahoma.

DB Robinson Design & Manufacturing Ltd. 2000. *Jefri Slim Tube Miscibility Apparatus Operating and Maintenance Manual*. Calgary, Alberta, Canada.

Eakin, B.E. and Mitch, F.J. 1988. Measurement and Correlation of Miscibility Pressures of Reservoir Oils. Paper presented at the SPE Annual Technical Conference and Exhibition, Houston, Texas. 18065-MS.

Egermann, P., Bazin, B., and Vizika, O. 2005. An Experimental Investigation of Reaction-Transport Phenomena During $CO_2$ Injection. Paper presented at the SPE Middle East Oil and Gas Show and Conference, Kingdom of Bahrain. 93674-MS.

Fathi, S.J., Austad, T., and Strand, S. 2010. "Smart Water" As a Wettability Modifier in Chalk: The Effect of Salinity and Ionic Composition. *Energy & Fuels* **24**: 2514-2519. ISI:000276563300040.

Fjelde, I., Zuta, J., and Duyilemi, O.V. 2008. Oil Recovery from Matrix During $CO_2$-Foam Flooding of Fractured Carbonate Oil Reservoirs. Paper presented at the EUROPEC/EAGE Conference and Exhibition, Rome, Italy. 113880-MS.

Gharbi, R.B.C. 2003. Integrated Reservoir Simulation Studies to Optimize Recovery from a Carbonate Reservoir. Paper presented at the SPE Asia Pacific Oil and Gas Conference and Exhibition, Jakarta, Indonesia. 80437-MS.

Glasø, Ø. 1985. Generalized Minimum Miscibility Pressure Correlation (Includes Associated Papers 15845 and 16287 ). **25** (6): 927-934. 12893-PA.

Guzman, R.E. and Aziz, K. 1992. Fine Grid Simulation of Two-Phase Flow in Fractured Porous Media. Paper presented at the SPE Annual Technical Conference and Exhibition, Washington, D.C. 24916-MS.

Harjadiwinangun, R. 1984. Feasibility Study: Pressure Maintenance of E-22 Reservoir, Ardjuna Field - Offshore Northwest Java. Paper presented at the Southeast Asia Show, Singapore. 12409-MS.

Holm, L.W. 1963. $CO_2$ Slug and Carbonated Water Oil Recovery Process. *Prod. Monthly* **6**.

Holm, L.W. and Josendal, V.A. 1974. Mechanisms of Oil Displacement by Carbon Dioxide. *SPE Journal of Petroleum Technology* **26** (12): 1427-1438. 4736-PA.

Holm, L.W. and Josendal, V.A. 1982. Effect of Oil Composition on Miscible-Type Displacement by Carbon Dioxide. **22** (1): 87-98. 8814-PA.

Hudgins, D.A., Llave, F.M., and Chung, F.T.H. 1990. Nitrogen Miscible Displacement of Light Crude Oil: A Laboratory Study. *SPE Reservoir Engineering* **5** (1): 100-106. 17372-PA.

Jarrell, M.J., Fox, C.E., Stein, M.H. et al. 2002. *Practical Aspects of $CO_2$ Flooding*. SPE Monograph 22. Richardson, Texas.

Johnson, J.P. and Pollin, J.S. 1981. Measurement and Correlation of $CO_2$ Miscibility Pressures. Paper presented at the SPE/DOE Enhanced Oil Recovery Symposium, Tulsa, Oklahoma. 9790-MS.

Kocurek Industries. www.kocurekindustries.com. Accessed June 1, 2008.

Kulkarni, M.M. and Rao, D.N. 2005. Experimental Investigation of Miscible and Immiscible Water-Alternating-Gas (WAG) Process Performance. *Journal of Petroleum Science and Engineering* **48** (1-2): 1-20. WOS:000231275000001.

Ma, T.D. and Youngren, G.K. 1994. Performance of Immiscible Water-Alternating-Gas (IWAG) Injection at Kuparuk River Unit, North Slope, Alaska. Paper presented at the SPE Annual Technical Conference and Exhibition, New Orleans, Louisiana. 28602-MS.

Ma, T.D., Rugen, J.A., Stoisits, R.F. et al. 1995. Simultaneous Water and Gas Injection Pilot at the Kuparuk River Field, Reservoir Impact. Paper presented at the SPE Annual Technical Conference and Exhibition, Dallas, Texas. 30726-MS.

Muralidharan, V., Putra, E., and Schechter, D.S. 2004. Experimental and Simulation Analysis of Fractured Reservoir Experiencing Different Stress Conditions. Paper presented at the Canadian International Petroleum Conference, Calgary, Alberta, Canada. 2004-229.

Nasir, F.M. and Amiruddin, N.A. 2008. Miscible $CO_2$ Injection: Sensitivity to Fluid Properties. Paper presented at the SPE Asia Pacific Oil and Gas Conference and Exhibition, Perth, Australia. 115314-MS.

Negahban, S., Shiralkar, G.S., and Gupta, S.P. 1990. Simulation of the Effects of Mixing in Gasdrive Core Tests of Reservoir Fluids. *SPE Reservoir Engineering* **5** (3): 402-408. 17377-PA.

Nezhad, S.A.R.T., Mojarad, M.R., Oskouei, S.J.P. et al. 2006. Experimental Study on Applicability of Water-Alternating-$CO_2$ Injection in the Secondary and Tertiary Recovery. Paper presented at the First International Oil Conference and Exhibition in Mexico, Cancun, Mexico. 103988-MS.

Orr Jr., F.M. and Silva, M.K. 1987. Effect of Oil Composition on Minimum Miscibility Pressure-Part 2: Correlation. *SPE Reservoir Engineering* **2** (4): 479-491. 14150-PA.

Potter, G.F. 1987. The Effects of $CO_2$ Flooding on Wettability of West Texas Dolomitic Formations. Paper presented at the SPE Annual Technical Conference and Exhibition, Dallas, Texas. 16716-MS.

Pu, H., Xie, X., Yin, P. et al. 2008. Application of Coalbed Methane Water to Oil Recovery from Tensleep Sandstone by Low Salinity Waterflooding. Paper presented at the SPE/DOE Symposium on Improved Oil Recovery, Tulsa, Oklahoma. 11341-MS.

Quale, E.A., Crapez, B., Stensen, J.A. et al. 2000. SWAG Injection on the Siri Field - an Optimized Injection System for Less Cost. Paper presented at the SPE European Petroleum Conference, Paris, France. 65165-MS.

Quraini, A.A., Sohrabi, M., and Jamiolahmady, M. 2007. Heavy Oil Recovery by Liquid $CO_2$/Water Injection. Paper presented at the EUROPEC/EAGE Conference and Exhibition, London, U.K. 107163-MS.

Robie, J., D.R., Roedell, J.W., and Wackowski, R.K. 1995. Field Trial of Simultaneous Injection of $CO_2$ and Water, Rangely Weber Sand Unit, Colorado. Paper presented at the SPE Production Operations Symposium, Oklahoma City, Oklahoma. 29521-MS.

Romm, E.S. 1966. *Fluid Flow in Fractured Rocks (in Russian)*. Nedra Publishing House. Moscow.

Sharma, M.M. and Filoco, P.R. 2000. Effect of Brine Salinity and Crude-Oil Properties on Oil Recovery and Residual Saturations. *SPE Journal* **5** (3): 293-300. 65402-PA.

Shedid, S.A. 2009. Influences of Different Modes of Reservoir Heterogeneity on Performance and Oil Recovery of Carbon Dioxide Miscible Flooding. *Journal of Canadian Petroleum Technology* **48** (2): 29-36. WOS:000263246100006.

Shelton, J.L. and Schneider, F.N. 1975. The Effects of Water Injection on Miscible Flooding Methods Using Hydrocarbons and Carbon Dioxide. **15** (3): 217-226. 4580-PA.

Shyeh-Yung, J.-G.J. 1991. Mechanisms of Miscible Oil Recovery: Effects of Pressure on Miscible and Near-Miscible Displacements of Oil by Carbon Dioxide. Paper presented at the SPE Annual Technical Conference and Exhibition, Dallas, Texas. 22651-MS.

Siregar, S., Mardisewojo, P., Kristanto, D., and Tjahyadi, R. 1999. Dynamic Interaction between $CO_2$ Gas and Crude Oil in Porous Medium. Paper presented at the SPE Asia Pacific Improved Oil Recovery Conference, Kuala Lumpur, Malaysia. 57300-MS.

Skrettingland, K., Holt, T., Tweheyo, M.T. et al. 2010. Snorre Low Salinity Water Injection-Core Flooding Experiments and Single Well Field Pilot. Paper presented at the SPE Improved Oil Recovery Symposium, Tulsa, Oklahoma. 129877-MS.

Slack, W.W. and Ehrlich, R. 1981. Immiscible Displacement of Oil by Simultaneous Injection of Water and Nitrogen. Paper presented at the SPE/DOE Enhanced Oil Recovery Symposium, Tulsa, Oklahoma. 9807-MS.

Sohrabi, M., Danesh, A., and Tehrani, D.H. 2005. Oil Recovery by Near-Miscible SWAG Injection. Paper presented at the SPE EUROPEC/EAGE Annual Conference, Madrid, Spain. 94073-MS.

Stalkup, F.I. 1992. *Miscible Displacement*. SPE Monograph 8. Richardson, Texas.

Stephenson, D.J., Graham, A.G., and Luhning, R.W. 1993. Mobility Control Experience in the Joffre Viking Miscible $CO_2$ Flood. *SPE Reservoir Engineering* **8** (3): 183-188. 23598-PA.

Stern, D. 1991. Mechanisms of Miscible Oil Recovery: Effects of Pore-Level Fluid Distribution. Paper presented at the SPE Annual Technical Conference and Exhibition, Dallas, Texas. 22652-MS.

Stoisits, R.F., Krist, G.J., Ma, T.D. et al. 1995. Simultaneous Water and Gas Injection Pilot at the Kuparuk River Field, Surface Line Impact. Paper presented at the SPE Annual Technical Conference and Exhibition, Dallas, Texas. 30645-MS.

Stone, H.L. 2004. A Simultaneous Water and Gas Flood Design with Extraordinary Vertical Gas Sweep. Paper presented at the SPE International Petroleum Conference in Mexico, Puebla Pue., Mexico. 91724-MS.

Surguchev, L.M., Hanssen, J.E., Johannessen, H.M. et al. 1996. Modelling Injection Strategies for a Reservoir with an Extreme Permeability Contrast: IOR Qualification. Paper presented at the European 3-D Reservoir Modelling Conference, Stavanger, Norway. 35504-MS.

Svec, R.K. and Grigg, R.B. 2001. Physical Effects of WAG Fluids on Carbonate Core Plugs. Paper presented at the SPE Annual Technical Conference and Exhibition, New Orleans, Louisiana. 71496-MS.

Van Lingen, P.P., Barzanji, O.H.M., and van Kruijsdijk, C.P.J.W. 1996. WAG Injection to Reduce Capillary Entrapment in Small-Scale Heterogeneities. Paper presented at the SPE Annual Technical Conference and Exhibition, Denver, Colorado. 36662-MS.

Walker, J.W. and Turner, J.L. 1968. Performance of Seeligson Zone 20B-07 Enriched-Gas-Drive Project. *SPE Journal of Petroleum Technology* **20** (4): 369-373. 1884-PA.

Warner Jr., H.R. 1977. An Evaluation of Miscible $CO_2$ Flooding in Waterflooded Sandstone Reservoirs. *SPE Journal of Petroleum Technology* **29** (10): 1339-1347. 6117-P.

Wu, R.S. and Batycky, J.P. 1990. Evaluation of Miscibility from Slim Tube Tests. *Journal of Canadian Petroleum Technology* **29** (6): 63-70. WOS:A1990ET56100009.

Yang, D.Y., Tontiwachwuthikul, P., and Gu, Y.G. 2005. Interfacial Interactions between Reservoir Brine and $CO_2$ at High Pressures and Elevated Temperatures. *Energy & Fuels* **19** (1): 216-223. WOS:000226471300027.

Yellig, W.F. and Metcalfe, R.S. 1980. Determination and Prediction of $CO_2$ Minimum Miscibility Pressures. *Journal of Petroleum Technology* **32** (1): 160-168. WOS:A1980JA92700017.

Yellig, W.F. 1982. Carbon-Dioxide Displacement of a West Texas Reservoir Oil. *SPE Journal* **22** (6): 805-815. WOS:A1982PX00700002.

Yildiz, H.O., Valat, M., and Morrow, N.R. 1999. Effect of Brine Composition on Wettability and Oil Recovery of a Prudhoe Bay Crude Oil. **38** (1). 99-01-02.

Yuan, H., Johns, R.T., Egwuenu, A.M. et al. 2005. Improved MMP Correlations for $CO_2$ Floods Using Analytical Gasflooding Theory. *SPE Reservoir Evaluation & Engineering* **8** (5): pp. 418-425. 89359-PA.

Zekri, A.Y., Shedid, S.A., and Almehaideb, R.A. 2007. Possible Alteration of Tight Limestone Rocks Properties and the Effect of Water Shielding on the Performance of Supercritical $CO_2$ Flooding for Carbonate Formation. Paper presented at the SPE Middle East Oil and Gas Show and Conference, Kingdom of Bahrain. 104630-MS.

# APPENDIX A

## EQUATIONS FOR PUBLISHED MMP CORRELATIONS

Holm and Josendal:

*Graphical*

Cronquist:

$$MMP_{pure} = 15.988T^{0.744206+0.0011038M_{C5+}+0.0015279C_1}$$

Glaso (no $C_2$-$C_6$):

$$MMP_{pure} = 810 - 3.404M_{C7+} + 1.7\times10^{-9}M_{C7+}^{3.730}e^{7868M_{C7+}^{-1.058}}T$$

Glaso (with $C_2$-$C_6$):

$$MMP_{pure} = 2947.9 - 3.404M_{C7+} + 1.7\times10^{-9}M_{C7+}^{3.730}e^{7868M_{C7+}^{-1.058}}T - 121.2C_{2-6}$$

Johnson and Pollin:

$$P_{MDMP} - P_c, inj = \alpha_{inj}\left(T_{res} - T_c, inj\right) + I\left(\beta - M_{inj}\right)^2$$

Alston:

$$p_{CO_2-STO} = 8.78\times10^{-4}\left(T_R\right)^{1.06}\left(M_{C5+}\right)^{1.78}$$

Yellig and Metcalfe:

$$MMP_{pure} = 1833.717 + 2.2518055T + 0.01800674T^2 - \frac{103949.93}{T}$$

Orr and Silva:

$$\rho_{MMP} = -0.524F + 1.189$$

Eakin and Mitch:

$$InP_r = In\left(MMP / P_c^{'}\right) = 0.01221 M_{C7+} - 0.0005899 M_{C7+}^{3/2} / T_r$$

Yuan:

$$MMP_{pure} = a_1 + a_2 M_{C_{7+}} + a_3 P_{C_{2-6}} + \left( a_4 + a_5 M_{C_{7+}} + a_6 \frac{P_{C_{2-6}}}{M_{C_{7+}}^{\ 2}} \right) T + \left( a_7 + a_8 M_{C_{7+}} + a_9 M_{C_{7+}}^{\ 2} + a_{10} P_{C_{2-6}} \right) T^2$$

After regressing the data, the best fit was found to be within an error of 15.7% and can be obtained with the following coeficients:

$a_1$ = - 1.4364 E-03

$a_2$ =0.6612 E=+01

$a_3$= -4.4979 E+01

$a_4$=0.2139 E+01

$a_5$=1.1667 E-01

$a_6$=8.1661 E+03

$a_7$=-1.2258 E-01

$a_8$=1.2883 E-03

$a_9$= -4.0152 E-06

$a_{10}$= -9.2577 E-04

# APPENDIX B

## SAMPLE SIMULATION DATA FILE: SWAG INJECTION

```
INUNIT FIELD
WSRF WELL 1
WSRF GRID TIME
WSRF SECTOR TIME
OUTSRF WELL LAYER NONE
OUTSRF RES ALL
OUTSRF GRID SO SG SW PRES OILPOT BPP SSPRES WINFLUX
WPRN GRID 0
OUTPRN GRID NONE
OUTPRN RES NONE
**$  Distance units: ft
RESULTS XOFFSET          0.0000
RESULTS YOFFSET          0.0000
RESULTS ROTATION          0.0000  **$  (DEGREES)
RESULTS AXES-DIRECTIONS 1.0 -1.0 1.0
**$ *****************************************************************************
**$ Definition of fundamental cartesian grid
**$ *****************************************************************************

GRID VARI 100 1 10
KDIR DOWN
DI IVAR
 100*0.005
DJ JVAR
 0.147704
DK ALL
 1000*0.0147704
DTOP
 100*0
**$ Property: NULL Blocks  Max: 1  Min: 1
**$  0 = null block, 1 = active block
NULL CON           1
**$ Property: Porosity  Max: 0.29  Min: 0.29
POR CON         0.29
**$ Property: Permeability I (md)   Max: 90  Min: 90
PERMI CON          90
**$ Property: Permeability J (md)   Max: 90  Min: 90
PERMJ CON          90
**$ Property: Permeability K (md)   Max: 90  Min: 90
PERMK CON          90
**$ Property: Pinchout Array  Max: 1  Min: 1
**$  0 = pinched block, 1 = active block
PINCHOUTARRAY CON           1
CPOR 12e-6
MODEL MISNCG
TRES 120
PVT BG 1

**$        p       Rs       Bo       Bg      viso       visg        co
      14.696     0.01        1    0.001   5.59877  0.0110266  3.00E-05
     120.383     5.01  1.00001  0.000999   4.89124   0.011146  3.00E-05
      226.07    10.01 1.000022  0.000998   4.26262  0.0113086  3.00E-05
     331.757    15.01 1.000036  0.000997   3.74273  0.0115033  3.00E-05
     437.444    20.01 1.000052  0.000996   3.31768   0.011728  3.00E-05
     543.131    25.01  1.00007  0.000995   2.96888  0.0119827  3.00E-05
     648.818    30.01  1.00009  0.000994   2.68017  0.0122686  3.00E-05
     754.505    35.01 1.000112  0.000993   2.43874  0.0125876  3.00E-05
```

```
     860.191     40.01  1.000136  0.000992   2.23475  0.0129418  3.00E-05
     965.878     45.01  1.000162  0.000991    2.0607  0.0133333  3.00E-05
     1071.57     50.01   1.00019   0.00099   1.91081  0.0137645  3.00E-05
     1177.25     55.01   1.00022  0.000989   1.78063  0.0142371  3.00E-05
     1282.94     60.01  1.000252  0.000988   1.66668  0.0147523  3.00E-05
     1388.63     65.01  1.000286  0.000987   1.56622  0.0153104  3.00E-05
     1494.31     70.01  1.000322  0.000986   1.47709  0.0159107  3.00E-05
       1600      75.01   1.00036  0.000985   1.39753  0.0165512  3.00E-05
       1680      80.01    1.0004  0.000984    1.3428  0.0170608  3.00E-05
       1760      85.01  1.000442  0.000983   1.29222  0.0175899  3.00E-05
       1840      90.01  1.000486  0.000982   1.24535  0.0181365  3.00E-05
       1920      95.01  1.000532  0.000981   1.20181  0.0186984  3.00E-05
       2000     100.01   1.00058   0.00098   1.16127  0.0192733  3.00E-05
BWI 1.01056
CVW 0.0
CW 3.15633e-006
DENSITY OIL 54.4
DENSITY WATER 62.1797
DRSDT 0
REFPW 14.696
VWI 0.62582
GRAVITY GAS .65
PVTS ZS
**$        p       Rss       zs      viss  omega_os
       1800       0.0    0.3261  0.047696       .55
       1900       0.0    0.3285  0.050929       .55
MINSS 0.2 SMOOTHEND OFF
OMEGASG 0.1
DENSITY SOLVENT 0.1258
**$ Property: PVT Type  Max: 1  Min: 1
PTYPE CON            1
ROCKFLUID
RPT 1 SCALING-OLD
SWT
**$        Sw          krw          krow
         0.2            0           0.2
      0.23125  4.57764e-006       0.154495
       0.2625  7.32422e-005       0.117236
      0.29375   0.000370789      0.0871613
        0.325    0.00117188      0.0632812
      0.35625    0.00286102      0.0446808
       0.3875    0.00593262      0.0305176
      0.41875     0.0109909      0.0200226
         0.45       0.01875         0.0125
      0.48125     0.0300339     0.00732727
       0.5125     0.0457764     0.00395508
      0.54375     0.0670212     0.00190735
        0.575     0.0949219     0.00078125
      0.60625      0.130742   0.000247192
       0.6375      0.175854  4.88281e-005
      0.66875      0.231743  3.05176e-006
          0.7           0.3             0
SGT
**$        Sg          krg          krog
         0.01            0           0.2
     0.040625  1.52588e-005       0.154495
      0.07125   0.000244141       0.117236
     0.101875    0.00123596      0.0871613
       0.1325    0.00390625      0.0632812
     0.163125    0.00953674      0.0446808
      0.19375     0.0197754      0.0305176
     0.224375     0.0366364      0.0200226
        0.255        0.0625         0.0125
     0.285625      0.100113     0.00732727
      0.31625      0.152588     0.00395508
     0.346875      0.223404     0.00190735
```

```
      0.3775      0.316406    0.00078125
    0.408125      0.435806   0.000247192
     0.43875      0.586182  4.88281e-005
    0.469375      0.772476  3.05176e-006
         0.5             1             0
INITIAL
VERTICAL DEPTH_AVE WATER_OIL_GAS EQUIL

REFDEPTH 0.074
REFPRES 1900
DWOC 2
DGOC .001

DATUMDEPTH 0.074 INITIAL
**$ Property: Bubble Point Pressure (psi)   Max: 0  Min: 0
PB CON           0
**$ Property: Solvent Sat Pressure (psi)   Max: 1900  Min: 1900
PBS CON        1900
NUMERICAL
DTMAX 0.005
DTMIN 0.0000001
RUN
DATE 2010 1 22
DTWELL 1e-005
**$
WELL  'Outlet'
PRODUCER 'Outlet'
OPERATE  MIN  BHP  1900.  CONT
PERF  WI  'Outlet'
**$ UBA       wi    Status  Connection
   100 1 1   1.  OPEN    FLOW-TO  'SURFACE'  REFLAYER
   100 1 2   1.    OPEN    FLOW-TO  1
   100 1 3   1.    OPEN    FLOW-TO  2
   100 1 4   1.    OPEN    FLOW-TO  3
   100 1 5   1.    OPEN    FLOW-TO  4
   100 1 6   1.    OPEN    FLOW-TO  5
   100 1 7   1.    OPEN    FLOW-TO  6
   100 1 8   1.    OPEN    FLOW-TO  7
   100 1 9   1.    OPEN    FLOW-TO  8
   100 1 10  1.    OPEN    FLOW-TO  9
OPEN 'Outlet'
**$
WELL  'water'
INJECTOR MOBWEIGHT 'water'
INCOMP  WATER
OPERATE  MAX  BHW  0.002264  CONT
PERF  WI  'water'
**$ UBA     wi    Status  Connection
   1 1 1   1.  OPEN    FLOW-FROM  'SURFACE'  REFLAYER
   1 1 2   1.    OPEN    FLOW-FROM  1
   1 1 3   1.    OPEN    FLOW-FROM  2
   1 1 4   1.    OPEN    FLOW-FROM  3
   1 1 5   1.    OPEN    FLOW-FROM  4
   1 1 6   1.    OPEN    FLOW-FROM  5
   1 1 7   1.    OPEN    FLOW-FROM  6
   1 1 8   1.    OPEN    FLOW-FROM  7
   1 1 9   1.    OPEN    FLOW-FROM  8
   1 1 10  1.    OPEN    FLOW-FROM  9
OPEN 'water'
**$
WELL  'gas'
INJECTOR MOBWEIGHT 'gas'
INCOMP  SOLVENT
OPERATE  MAX  BHS  0.0127  CONT
PERF  WI  'gas'
**$ UBA     wi    Status  Connection
```

```
   1 1 1   1.  OPEN    FLOW-FROM  'SURFACE'  REFLAYER
   1 1 2   1.    OPEN    FLOW-FROM  1
   1 1 3   1.    OPEN    FLOW-FROM  2
   1 1 4   1.    OPEN    FLOW-FROM  3
   1 1 5   1.    OPEN    FLOW-FROM  4
   1 1 6   1.    OPEN    FLOW-FROM  5
   1 1 7   1.    OPEN    FLOW-FROM  6
   1 1 8   1.    OPEN    FLOW-FROM  7
   1 1 9   1.    OPEN    FLOW-FROM  8
   1 1 10  1.    OPEN    FLOW-FROM  9
OPEN 'gas'
DATE 2010 1 22.01389
DATE 2010 1 22.02778
DATE 2010 1 22.04167
DATE 2010 1 22.05556
DATE 2010 1 22.06944
DATE 2010 1 22.08333
DATE 2010 1 22.09722
DATE 2010 1 22.11111
DATE 2010 1 22.12500
DATE 2010 1 22.13889
DATE 2010 1 22.15278
DATE 2010 1 22.16667
DATE 2010 1 22.18056
DATE 2010 1 22.19444
DATE 2010 1 22.20833
STOP
DATE 2010 1 22.22222
DATE 2010 1 22.23611
DATE 2010 1 22.25000
DATE 2010 1 22.26389
DATE 2010 1 22.27778
DATE 2010 1 22.29167
DATE 2010 1 22.30556
DATE 2010 1 22.31944
DATE 2010 1 22.33333
DATE 2010 1 22.34722
DATE 2010 1 22.36111
DATE 2010 1 22.37500
STOP
RESULTS RELPERMCORR NUMROCKTYPE 1
RESULTS RELPERMCORR CORRVALS 0.2 0.2 0.3 0.3 0.3 0.3 0.01 0.01
RESULTS RELPERMCORR CORRVALS 0.2 0.3 1 0.2 4 4 4 4
RESULTS RELPERMCORR CORRVALS_HONARPOUR 0.2 0.2 0.46 0.23 0.5 1 0.29 90
RESULTS RELPERMCORR STOP

RESULTS SPEC 'Bubble Point Pressure'
RESULTS SPEC SPECNOTCALCVAL -99999
RESULTS SPEC REGION 'PVT Type 1'
RESULTS SPEC REGIONTYPE 'REGION_TABLE'
RESULTS SPEC LAYERNUMB 1
RESULTS SPEC PORTYPE 1
RESULTS SPEC CON 0
RESULTS SPEC STOP


RESULTS SPEC 'Permeability K'
RESULTS SPEC SPECNOTCALCVAL -99999
RESULTS SPEC REGION 'All Layers (Whole Grid)'
RESULTS SPEC REGIONTYPE 'REGION_WHOLEGRID'
RESULTS SPEC LAYERNUMB 0
RESULTS SPEC PORTYPE 1
RESULTS SPEC CON 90
RESULTS SPEC STOP
```

```
RESULTS SPEC 'Solvent Sat Pressure'
RESULTS SPEC SPECNOTCALCVAL -99999
RESULTS SPEC REGION 'All Layers (Whole Grid)'
RESULTS SPEC REGIONTYPE 'REGION_WHOLEGRID'
RESULTS SPEC LAYERNUMB 0
RESULTS SPEC PORTYPE 1
RESULTS SPEC CON 1900
RESULTS SPEC STOP


RESULTS SPEC 'Permeability J'
RESULTS SPEC SPECNOTCALCVAL -99999
RESULTS SPEC REGION 'All Layers (Whole Grid)'
RESULTS SPEC REGIONTYPE 'REGION_WHOLEGRID'
RESULTS SPEC LAYERNUMB 0
RESULTS SPEC PORTYPE 1
RESULTS SPEC CON 90
RESULTS SPEC STOP


RESULTS SPEC 'Permeability I'
RESULTS SPEC SPECNOTCALCVAL -99999
RESULTS SPEC REGION 'All Layers (Whole Grid)'
RESULTS SPEC REGIONTYPE 'REGION_WHOLEGRID'
RESULTS SPEC LAYERNUMB 0
RESULTS SPEC PORTYPE 1
RESULTS SPEC CON 90
RESULTS SPEC STOP


RESULTS SPEC 'Porosity'
RESULTS SPEC SPECNOTCALCVAL -99999
RESULTS SPEC REGION 'All Layers (Whole Grid)'
RESULTS SPEC REGIONTYPE 'REGION_WHOLEGRID'
RESULTS SPEC LAYERNUMB 0
RESULTS SPEC PORTYPE 1
RESULTS SPEC CON 0.29
RESULTS SPEC STOP


RESULTS SPEC 'PVT Type'
RESULTS SPEC SPECNOTCALCVAL -99999
RESULTS SPEC REGION 'All Layers (Whole Grid)'
RESULTS SPEC REGIONTYPE 'REGION_WHOLEGRID'
RESULTS SPEC LAYERNUMB 0
RESULTS SPEC PORTYPE 1
RESULTS SPEC CON 1
RESULTS SPEC STOP


RESULTS SPEC 'Grid Thickness'
RESULTS SPEC SPECNOTCALCVAL -99999
RESULTS SPEC REGION 'All Layers (Whole Grid)'
RESULTS SPEC REGIONTYPE 'REGION_WHOLEGRID'
RESULTS SPEC LAYERNUMB 0
RESULTS SPEC PORTYPE 1
RESULTS SPEC CON 0.147704
RESULTS SPEC REGION 'Layer 1 - Whole layer'
RESULTS SPEC REGIONTYPE 'REGION_LAYER'
RESULTS SPEC LAYERNUMB 1
RESULTS SPEC PORTYPE 1
RESULTS SPEC CON 0.0147704
RESULTS SPEC REGION 'Layer 2 - Whole layer'
RESULTS SPEC REGIONTYPE 'REGION_LAYER'
RESULTS SPEC LAYERNUMB 2
RESULTS SPEC PORTYPE 1
```

```
RESULTS SPEC CON 0.0147704
RESULTS SPEC REGION 'Layer 3 - Whole layer'
RESULTS SPEC REGIONTYPE 'REGION_LAYER'
RESULTS SPEC LAYERNUMB 3
RESULTS SPEC PORTYPE 1
RESULTS SPEC CON 0.0147704
RESULTS SPEC REGION 'Layer 4 - Whole layer'
RESULTS SPEC REGIONTYPE 'REGION_LAYER'
RESULTS SPEC LAYERNUMB 4
RESULTS SPEC PORTYPE 1
RESULTS SPEC CON 0.0147704
RESULTS SPEC REGION 'Layer 5 - Whole layer'
RESULTS SPEC REGIONTYPE 'REGION_LAYER'
RESULTS SPEC LAYERNUMB 5
RESULTS SPEC PORTYPE 1
RESULTS SPEC CON 0.0147704
RESULTS SPEC REGION 'Layer 6 - Whole layer'
RESULTS SPEC REGIONTYPE 'REGION_LAYER'
RESULTS SPEC LAYERNUMB 6
RESULTS SPEC PORTYPE 1
RESULTS SPEC CON 0.0147704
RESULTS SPEC REGION 'Layer 7 - Whole layer'
RESULTS SPEC REGIONTYPE 'REGION_LAYER'
RESULTS SPEC LAYERNUMB 7
RESULTS SPEC PORTYPE 1
RESULTS SPEC CON 0.0147704
RESULTS SPEC REGION 'Layer 8 - Whole layer'
RESULTS SPEC REGIONTYPE 'REGION_LAYER'
RESULTS SPEC LAYERNUMB 8
RESULTS SPEC PORTYPE 1
RESULTS SPEC CON 0.0147704
RESULTS SPEC REGION 'Layer 9 - Whole layer'
RESULTS SPEC REGIONTYPE 'REGION_LAYER'
RESULTS SPEC LAYERNUMB 9
RESULTS SPEC PORTYPE 1
RESULTS SPEC CON 0.0147704
RESULTS SPEC REGION 'Layer 10 - Whole layer'
RESULTS SPEC REGIONTYPE 'REGION_LAYER'
RESULTS SPEC LAYERNUMB 10
RESULTS SPEC PORTYPE 1
RESULTS SPEC CON 0.0147704
RESULTS SPEC STOP
```

# APPENDIX C

## SAMPLE SIMULATION DATA FILE: SWAG INJECTION IN LAYERED RESERVOIRS (MHL)

```
INUNIT FIELD
WSRF WELL 1
WSRF GRID TIME
WSRF SECTOR TIME
OUTSRF WELL LAYER NONE
OUTSRF RES ALL
OUTSRF GRID SO SG SW PRES OILPOT BPP SSPRES WINFLUX
WPRN GRID 0
OUTPRN GRID NONE
OUTPRN RES NONE
**$  Distance units: ft
RESULTS XOFFSET          0.0000
RESULTS YOFFSET          0.0000
RESULTS ROTATION          0.0000  **$  (DEGREES)
RESULTS AXES-DIRECTIONS 1.0 -1.0 1.0
**$ *****************************************************************************
**$ Definition of fundamental cartesian grid
**$ *****************************************************************************
GRID VARI 100 1 10
KDIR DOWN
DI IVAR
 100*0.005
DJ JVAR
 0.147704
DK ALL
 1000*0.0147704
DTOP
 100*0
**$ Property: NULL Blocks  Max: 1  Min: 1
**$  0 = null block, 1 = active block
NULL CON           1
**$ Property: Porosity  Max: 0.29  Min: 0.29
POR CON         0.29


**$ Property: Permeability I (md)   Max: 90  Min: 90
PERMI CON           90

mod
1:100 1 1:4 = 100
1:100 1 5:7 = 1000
1:100 1 8:10 = 0.100


**$ Property: Permeability J (md)   Max: 90  Min: 90
PERMJ CON           90


mod
1:100 1 1:4 = 100
1:100 1 5:7 = 1000
1:100 1 8:10 = 0.100
```

```
**$ Property: Permeability K (md)   Max: 90  Min: 90
PERMK CON           90

mod
1:100 1 1:4 = 100
1:100 1 5:7 = 1000
1:100 1 8:10 = 0.100

**$ Property: Pinchout Array  Max: 1  Min: 1
**$  0 = pinched block, 1 = active block
PINCHOUTARRAY CON           1
CPOR 12e-6
MODEL MISNCG
TRES 120
PVT BG 1

**$        p       Rs       Bo       Bg      viso       visg        co
      14.696     0.01        1    0.001   5.59877  0.0110266  3.00E-05
     120.383     5.01  1.00001  0.000999   4.89124   0.011146  3.00E-05
      226.07    10.01 1.000022  0.000998   4.26262  0.0113086  3.00E-05
     331.757    15.01 1.000036  0.000997   3.74273  0.0115033  3.00E-05
     437.444    20.01 1.000052  0.000996   3.31768   0.011728  3.00E-05
     543.131    25.01  1.00007  0.000995   2.96888  0.0119827  3.00E-05
     648.818    30.01  1.00009  0.000994   2.68017  0.0122686  3.00E-05
     754.505    35.01 1.000112  0.000993   2.43874  0.0125876  3.00E-05
     860.191    40.01 1.000136  0.000992   2.23475  0.0129418  3.00E-05
     965.878    45.01 1.000162  0.000991    2.0607  0.0133333  3.00E-05
     1071.57    50.01  1.00019   0.00099   1.91081  0.0137645  3.00E-05
     1177.25    55.01  1.00022  0.000989   1.78063  0.0142371  3.00E-05
     1282.94    60.01 1.000252  0.000988   1.66668  0.0147523  3.00E-05
     1388.63    65.01 1.000286  0.000987   1.56622  0.0153104  3.00E-05
     1494.31    70.01 1.000322  0.000986   1.47709  0.0159107  3.00E-05
       1600    75.01  1.00036  0.000985   1.39753  0.0165512  3.00E-05
       1680    80.01   1.0004  0.000984    1.3428  0.0170608  3.00E-05
       1760    85.01 1.000442  0.000983   1.29222  0.0175899  3.00E-05
       1840    90.01 1.000486  0.000982   1.24535  0.0181365  3.00E-05
       1920    95.01 1.000532  0.000981   1.20181  0.0186984  3.00E-05
       2000   100.01  1.00058   0.00098   1.16127  0.0192733  3.00E-05
BWI 1.01056
CVW 0.0
CW 3.15633e-006
DENSITY OIL 54.4
DENSITY WATER 62.1797
DRSDT 0
REFPW 14.696
VWI 0.62582
GRAVITY GAS .65
PVTS ZS
**$        p      Rss       zs      viss  omega_os
       1800      0.0   0.3261  0.047696       .55
       1900      0.0   0.3285  0.050929       .55
MINSS 0.2 SMOOTHEND OFF
OMEGASG 0.1
DENSITY SOLVENT 0.1258
**$ Property: PVT Type  Max: 1  Min: 1
PTYPE CON           1
ROCKFLUID
RPT 1 SCALING-OLD
SWT
**$       Sw          krw         krow
        0.2            0          0.2
     0.23125  4.57764e-006      0.154495
      0.2625  7.32422e-005      0.117236
     0.29375   0.000370789     0.0871613
       0.325    0.00117188     0.0632812
     0.35625    0.00286102     0.0446808
```

```
      0.3875    0.00593262     0.0305176
     0.41875     0.0109909     0.0200226
        0.45       0.01875        0.0125
     0.48125     0.0300339    0.00732727
      0.5125     0.0457764    0.00395508
     0.54375     0.0670212    0.00190735
       0.575     0.0949219    0.00078125
     0.60625      0.130742   0.000247192
      0.6375      0.175854  4.88281e-005
     0.66875      0.231743  3.05176e-006
         0.7           0.3             0
SGT
**$        Sg           krg          krog
        0.01             0           0.2
    0.040625  1.52588e-005      0.154495
     0.07125  0.000244141      0.117236
    0.101875   0.00123596     0.0871613
      0.1325   0.00390625     0.0632812
    0.163125   0.00953674     0.0446808
     0.19375    0.0197754     0.0305176
    0.224375    0.0366364     0.0200226
       0.255       0.0625        0.0125
    0.285625     0.100113    0.00732727
     0.31625     0.152588    0.00395508
    0.346875     0.223404    0.00190735
      0.3775     0.316406    0.00078125
    0.408125     0.435806   0.000247192
     0.43875     0.586182  4.88281e-005
    0.469375     0.772476  3.05176e-006
         0.5            1             0
INITIAL
VERTICAL DEPTH_AVE WATER_OIL_GAS EQUIL

REFDEPTH 0.074
REFPRES 1900
DWOC 2
DGOC .001

DATUMDEPTH 0.074 INITIAL
**$ Property: Bubble Point Pressure (psi)   Max: 0  Min: 0
PB CON           0
**$ Property: Solvent Sat Pressure (psi)   Max: 1900  Min: 1900
PBS CON        1900
NUMERICAL
DTMAX 0.00005
DTMIN 0.0000001
RUN
DATE 2010 1 22
DTWELL 1e-005
**$
WELL  'Outlet'
PRODUCER 'Outlet'
OPERATE  MIN  BHP  1900.  CONT
PERF  WI  'Outlet'
**$ UBA       wi    Status  Connection
   100 1 1   1.  OPEN    FLOW-TO  'SURFACE'  REFLAYER
   100 1 2   1.    OPEN    FLOW-TO  1
   100 1 3   1.    OPEN    FLOW-TO  2
   100 1 4   1.    OPEN    FLOW-TO  3
   100 1 5   1.    OPEN    FLOW-TO  4
   100 1 6   1.    OPEN    FLOW-TO  5
   100 1 7   1.    OPEN    FLOW-TO  6
   100 1 8   1.    OPEN    FLOW-TO  7
   100 1 9   1.    OPEN    FLOW-TO  8
   100 1 10  1.    OPEN    FLOW-TO  9
OPEN 'Outlet'
```

```
**$
WELL  'water'
INJECTOR MOBWEIGHT 'water'
INCOMP  WATER
OPERATE  MAX  BHW  0.002264  CONT
PERF  WI  'water'
**$ UBA     wi    Status  Connection
   1 1 1   1.  OPEN    FLOW-FROM  'SURFACE'  REFLAYER
   1 1 2   1.    OPEN    FLOW-FROM  1
   1 1 3   1.    OPEN    FLOW-FROM  2
   1 1 4   1.    OPEN    FLOW-FROM  3
   1 1 5   1.    OPEN    FLOW-FROM  4
   1 1 6   1.    OPEN    FLOW-FROM  5
   1 1 7   1.    OPEN    FLOW-FROM  6
   1 1 8   1.    OPEN    FLOW-FROM  7
   1 1 9   1.    OPEN    FLOW-FROM  8
   1 1 10  1.    OPEN    FLOW-FROM  9
OPEN 'water'
**$
WELL  'gas'
INJECTOR MOBWEIGHT 'gas'
INCOMP  SOLVENT
OPERATE  MAX  BHS  0.0127  CONT
PERF  WI  'gas'
**$ UBA     wi    Status  Connection
   1 1 1   1.  OPEN    FLOW-FROM  'SURFACE'  REFLAYER
   1 1 2   1.    OPEN    FLOW-FROM  1
   1 1 3   1.    OPEN    FLOW-FROM  2
   1 1 4   1.    OPEN    FLOW-FROM  3
   1 1 5   1.    OPEN    FLOW-FROM  4
   1 1 6   1.    OPEN    FLOW-FROM  5
   1 1 7   1.    OPEN    FLOW-FROM  6
   1 1 8   1.    OPEN    FLOW-FROM  7
   1 1 9   1.    OPEN    FLOW-FROM  8
   1 1 10  1.    OPEN    FLOW-FROM  9
OPEN 'gas'
DATE 2010 1 22.01389
DATE 2010 1 22.02778
DATE 2010 1 22.04167
DATE 2010 1 22.05556
DATE 2010 1 22.06944
DATE 2010 1 22.08333
DATE 2010 1 22.09722
DATE 2010 1 22.11111
DATE 2010 1 22.12500
DATE 2010 1 22.13889
DATE 2010 1 22.15278
DATE 2010 1 22.16667
DATE 2010 1 22.18056
DATE 2010 1 22.19444
DATE 2010 1 22.20833
STOP
DATE 2010 1 22.22222
DATE 2010 1 22.23611
DATE 2010 1 22.25000
DATE 2010 1 22.26389
DATE 2010 1 22.27778
DATE 2010 1 22.29167
DATE 2010 1 22.30556
DATE 2010 1 22.31944
DATE 2010 1 22.33333
DATE 2010 1 22.34722
DATE 2010 1 22.36111
DATE 2010 1 22.37500
STOP
RESULTS RELPERMCORR NUMROCKTYPE 1
```

```
RESULTS RELPERMCORR CORRVALS 0.2 0.2 0.3 0.3 0.3 0.3 0.01 0.01
RESULTS RELPERMCORR CORRVALS 0.2 0.3 1 0.2 4 4 4 4
RESULTS RELPERMCORR CORRVALS_HONARPOUR 0.2 0.2 0.46 0.23 0.5 1 0.29 90
RESULTS RELPERMCORR STOP

RESULTS SPEC 'Permeability I'
RESULTS SPEC SPECNOTCALCVAL -99999
RESULTS SPEC REGION 'All Layers (Whole Grid)'
RESULTS SPEC REGIONTYPE 'REGION_WHOLEGRID'
RESULTS SPEC LAYERNUMB 0
RESULTS SPEC PORTYPE 1
RESULTS SPEC CON 90
RESULTS SPEC STOP


RESULTS SPEC 'Permeability J'
RESULTS SPEC SPECNOTCALCVAL -99999
RESULTS SPEC REGION 'All Layers (Whole Grid)'
RESULTS SPEC REGIONTYPE 'REGION_WHOLEGRID'
RESULTS SPEC LAYERNUMB 0
RESULTS SPEC PORTYPE 1
RESULTS SPEC CON 90
RESULTS SPEC STOP


RESULTS SPEC 'Permeability K'
RESULTS SPEC SPECNOTCALCVAL -99999
RESULTS SPEC REGION 'All Layers (Whole Grid)'
RESULTS SPEC REGIONTYPE 'REGION_WHOLEGRID'
RESULTS SPEC LAYERNUMB 0
RESULTS SPEC PORTYPE 1
RESULTS SPEC CON 90
RESULTS SPEC STOP


RESULTS SPEC 'Porosity'
RESULTS SPEC SPECNOTCALCVAL -99999
RESULTS SPEC REGION 'All Layers (Whole Grid)'
RESULTS SPEC REGIONTYPE 'REGION_WHOLEGRID'
RESULTS SPEC LAYERNUMB 0
RESULTS SPEC PORTYPE 1
RESULTS SPEC CON 0.29
RESULTS SPEC STOP


RESULTS SPEC 'PVT Type'
RESULTS SPEC SPECNOTCALCVAL -99999
RESULTS SPEC REGION 'All Layers (Whole Grid)'
RESULTS SPEC REGIONTYPE 'REGION_WHOLEGRID'
RESULTS SPEC LAYERNUMB 0
RESULTS SPEC PORTYPE 1
RESULTS SPEC CON 1
RESULTS SPEC STOP

RESULTS SPEC 'Bubble Point Pressure'
RESULTS SPEC SPECNOTCALCVAL -99999
RESULTS SPEC REGION 'PVT Type 1'
RESULTS SPEC REGIONTYPE 'REGION_TABLE'
RESULTS SPEC LAYERNUMB 1
RESULTS SPEC PORTYPE 1
RESULTS SPEC CON 0
RESULTS SPEC STOP

RESULTS SPEC 'Solvent Sat Pressure'
RESULTS SPEC SPECNOTCALCVAL -99999
RESULTS SPEC REGION 'All Layers (Whole Grid)'
```

```
RESULTS SPEC REGIONTYPE 'REGION_WHOLEGRID'
RESULTS SPEC LAYERNUMB 0
RESULTS SPEC PORTYPE 1
RESULTS SPEC CON 1900
RESULTS SPEC STOP


RESULTS SPEC 'Grid Thickness'
RESULTS SPEC SPECNOTCALCVAL -99999
RESULTS SPEC REGION 'All Layers (Whole Grid)'
RESULTS SPEC REGIONTYPE 'REGION_WHOLEGRID'
RESULTS SPEC LAYERNUMB 0
RESULTS SPEC PORTYPE 1
RESULTS SPEC CON 0.147704
RESULTS SPEC REGION 'Layer 1 - Whole layer'
RESULTS SPEC REGIONTYPE 'REGION_LAYER'
RESULTS SPEC LAYERNUMB 1
RESULTS SPEC PORTYPE 1
RESULTS SPEC CON 0.0147704
RESULTS SPEC REGION 'Layer 2 - Whole layer'
RESULTS SPEC REGIONTYPE 'REGION_LAYER'
RESULTS SPEC LAYERNUMB 2
RESULTS SPEC PORTYPE 1
RESULTS SPEC CON 0.0147704
RESULTS SPEC REGION 'Layer 3 - Whole layer'
RESULTS SPEC REGIONTYPE 'REGION_LAYER'
RESULTS SPEC LAYERNUMB 3
RESULTS SPEC PORTYPE 1
RESULTS SPEC CON 0.0147704
RESULTS SPEC REGION 'Layer 4 - Whole layer'
RESULTS SPEC REGIONTYPE 'REGION_LAYER'
RESULTS SPEC LAYERNUMB 4
RESULTS SPEC PORTYPE 1
RESULTS SPEC CON 0.0147704
RESULTS SPEC REGION 'Layer 5 - Whole layer'
RESULTS SPEC REGIONTYPE 'REGION_LAYER'
RESULTS SPEC LAYERNUMB 5
RESULTS SPEC PORTYPE 1
RESULTS SPEC CON 0.0147704
RESULTS SPEC REGION 'Layer 6 - Whole layer'
RESULTS SPEC REGIONTYPE 'REGION_LAYER'
RESULTS SPEC LAYERNUMB 6
RESULTS SPEC PORTYPE 1
RESULTS SPEC CON 0.0147704
RESULTS SPEC REGION 'Layer 7 - Whole layer'
RESULTS SPEC REGIONTYPE 'REGION_LAYER'
RESULTS SPEC LAYERNUMB 7
RESULTS SPEC PORTYPE 1
RESULTS SPEC CON 0.0147704
RESULTS SPEC REGION 'Layer 8 - Whole layer'
RESULTS SPEC REGIONTYPE 'REGION_LAYER'
RESULTS SPEC LAYERNUMB 8
RESULTS SPEC PORTYPE 1
RESULTS SPEC CON 0.0147704
RESULTS SPEC REGION 'Layer 9 - Whole layer'
RESULTS SPEC REGIONTYPE 'REGION_LAYER'
RESULTS SPEC LAYERNUMB 9
RESULTS SPEC PORTYPE 1
RESULTS SPEC CON 0.0147704
RESULTS SPEC REGION 'Layer 10 - Whole layer'
RESULTS SPEC REGIONTYPE 'REGION_LAYER'
RESULTS SPEC LAYERNUMB 10
RESULTS SPEC PORTYPE 1
RESULTS SPEC CON 0.0147704
RESULTS SPEC STOP
```

# APPENDIX D

# CUMULATIVE OIL RECOVERY FIGURES FOR WAG RATIO STUDY IN LAYERED RESERVOIRS

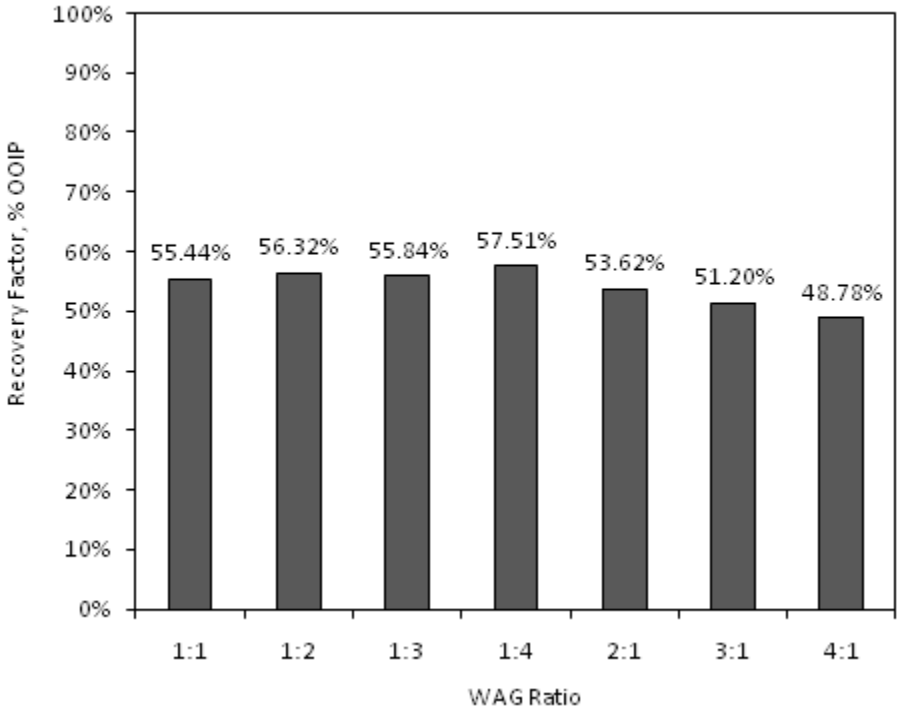


D.1— HML: cumulative oil recovery during different WAG ratios

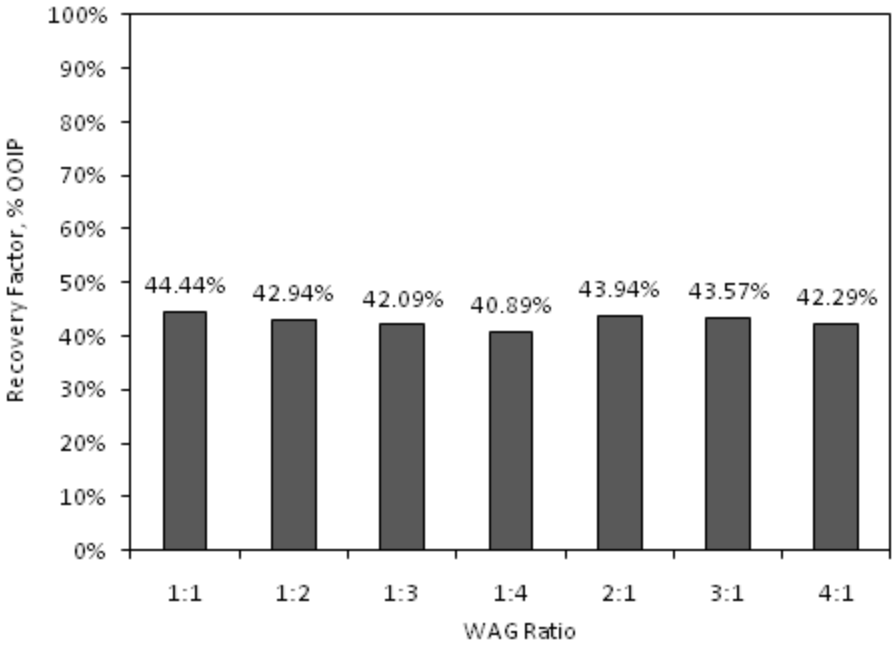


D.2— LHM: cumulative oil recovery during different WAG ratios

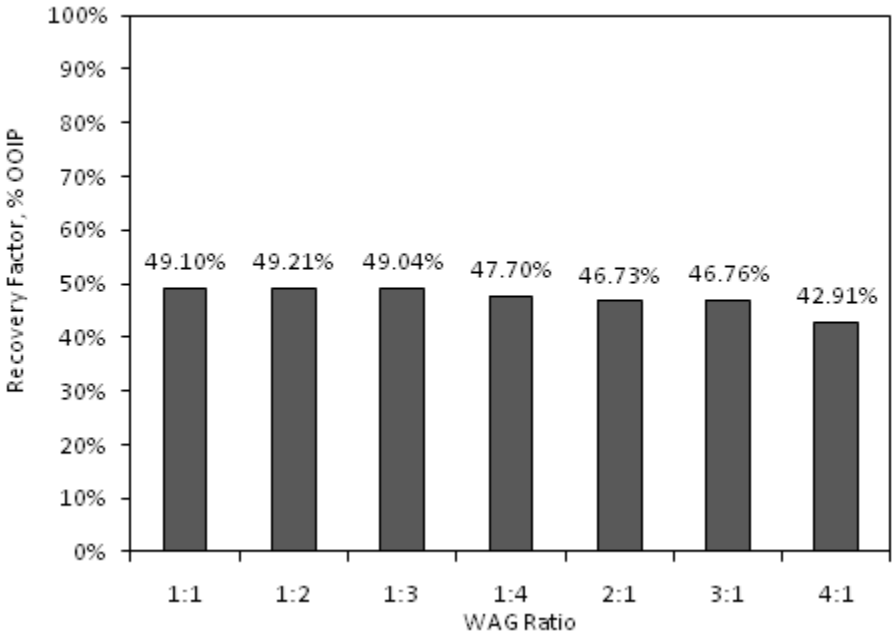


D.3— LMH: cumulative oil recovery during different WAG ratios

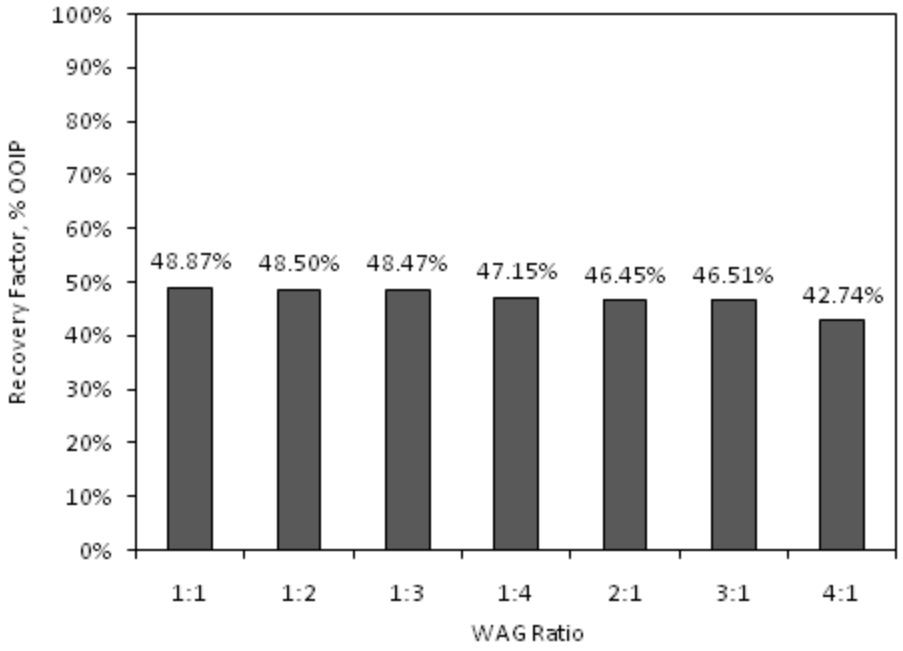


D.4— MHL: cumulative oil recovery during different WAG ratios

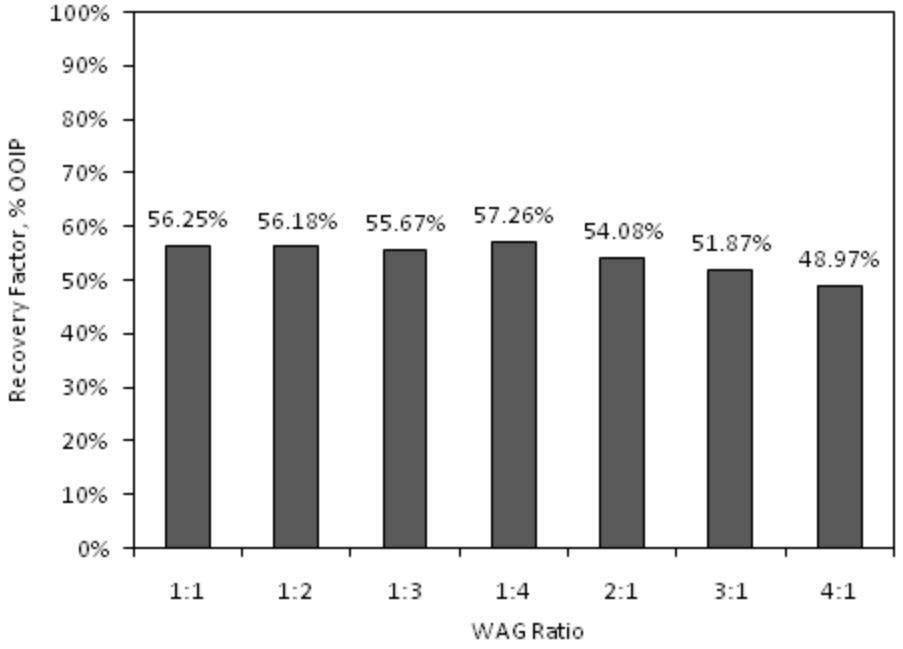


D.5— MLH: cumulative oil recovery during different WAG ratios

# VITA


Name: Ahmed Abdulaziz S. Aleidan

Address: P.O Box 1189
Dhahran, 31311
Saudi Arabia

Email Address: eidan55@hotmail.com
aidanaa@aramco.com


Education: B.S., Petroleum Engineering
Louisiana State University
May 2002

M.Eng., Petroleum Engineering
The University of Adelaide
August 2005

Ph.D., Petroleum Engineering
Texas A&M University
December 2010